NUMERICAL INVESTIGATION OF CONSTANT PRESSURE FILTRATION

RONALD MAINA WAIRAGU

A THESIS SUBMITTED

FOR A MPhil DEGREE

DEPARTMENT OF CHEMICAL ENGINEERING

LOUGBOROUGH UNIVERSITY

2012

A bend in the road is not the end of the road

... unless you fail to make the turn

Dedicated to my dearest Parents,

The lost loved ones,

And the helpless

Constantly loving

Always understanding

ACKNOWLEDGEMENTS

First of all, I wish to thank my academic supervisors, Dr E S Tarleton and Professor R J Wakeman for their invaluable guidance, advice and help throughout the course of this research study. The constant challenges have made me be a different person and have opened my thoughts to a newer way of thinking and performing tasks and I will forever be thankful. I express my sincere gratitude to the Department of Chemical Engineering Loughborough University for not only providing an opportunity to carry out the research but partially funding it. I extend my thanks to the Head of Department, Professor Chris Rielly and all the staff members in the Department of Chemical Engineering, Loughborough University. Without their kind and helpful support, I would not have been able to carry out my work smoothly and in good order.

Special thanks to Mr Paul Izzard., the IT manager for ensuring that my computer had the necessary software and always being ready to help with computing hardware problems, Yasmin Kosar for ensuring constant supply of tea bags and general encouragement, Rupert and Mathew for the encouragement and belief in me and Kuhan Chellappah for not only being a colleague but being a friend who constantly challenges me to be a better person in all aspects of life.

To my parents and my family, I am most grateful for their love, patience, encouragement, and support that enabled me to complete this thesis. Last but not least, in the memory of all the loved ones I lost through my research period, I wish to take this opportunity to express my sincere gratitude for giving me encouragement at the initial stage of this course. May they rest in peace.

*** MANY THANKS TO ALL OF YOU ***

TABLE OF CONTENTS

ACKNOWLEDGEMENTS ..... **i**
TABLE OF CONTENTS ..... **ii**
SUMMARY ..... **v**
LIST OF FIGURES ..... **vi**
LIST OF TABLES ..... **ix**
NOTATION ..... **x**
Chapter 1 : INTRODUCTION **1**
1.2. AIMS AND OBJECTIVES 2
1.3. THESIS STRUCTURE 2
Chapter 2 : LITERATURE REVIEW **4**
2.1 INTRODUCTION 4
2.2 CAKE FILTRATION THEORY 4
2.3 FLOW IN POROUS MEDIA 7
2.3.1 Liquid pressure and solid compressive pressure 9
2.4 FILTER CAKE PERMEABILITY AND POROSITY 12
2.5 CAKE FILTRATION ANALYSIS 14
2.6 CAKE FILTRATION NUMERICAL SOLUTIONS 18
2.7 CLOSURE 20
Chapter 3 : EXPERIMENTAL DATA ACQUISITION **21**
3.1 INTRODUCTION 21
3.2 EXPERIMENTAL APPARATUS DESCRIPTION 21
3.3 EXPERIMENTAL METHOD AND MATERIALS 24
3.4 RESULTS AND DISCUSSIONS 25
3.5 CONCLUSIONS 29
Chapter 4 : GOVERNING EQUATIONS **30**
4.1 INRODUCTION 30
4.2 COMPRESSIBLE CAKE FILRATION EQUATIONS 30
4.2.1 Force momentum balance 30
4.3 MATHEMATICAL MODEL 32
4.4 SOLUTIONS OF FILTRATION EQUATIONS 34
4.4.1 Solution of a dimensionless filtration equation 34
4.5 CLOSURE 39
Chapter 5 : NUMERICAL METHOD **40**

5.1 INTRODUCTION 40
5.2 CALCULATION OF LOCAL PROPERTIES 40
5.2.1 Calculation of local porosity 40
5.2.2 Relating cake permeability and specific cake resistance to porosity 43
5.2.3 Relating porosity to liquid pressure 44
5.3 FOURTH ORDER RUNGE KUTTA NYSTROM DISCRITISATION OF EQUATION 5.1 45
5.4 STRUCTURE OF THE SIMULATION PROCESS 47
5.5 INITIAL ESTIMATION OF VARIABLES 49
5.6 GENERAL SEQUENCE OF CALCULATIONS 50
5.6.1 Calcite experimental data analysis 51
5.7 CONCLUSIONS 53
Chapter 6 : RESULTS AND DISCUSSIONS 54
6.1 INTRODUCTION 54
6.2 VALIDATION OF THE USE OF THE SIMILARITY VARIABLE 54
6.3 FITTING OF MODEL TO EXPERIMENTAL DATA 55
6.3.1 Minimisation results for talc suspension at 400 kPa 56
6.3.2 Predicted internal cake properties 63
6.4 EFFECTS OF TIME ON THE PREDICTION OF LIQUID PRESSURE PROFILES OF TALC AT 400 kPa 68
6.4.1 Predicted liquid pressure profiles with ε_m constant for talc at 400 kPa ... 68
6.4.2 Predicted liquid pressure profiles by varying ε_m for talc at 400 kPa 72
6.4.3 Local filter cake properties 75
6.5 EFFECT OF PARTICLE SHAPE IN CALCULATION OF INTERNAL PROPERTIES 78
6.5.1 Predicted local values of compressibility, n 85
6.6 PREDICTION OF CAKE HEIGHT FOR TALC 86
6.6.1 Prediction of cake height with ε_i as calculated from the model 88
6.6.2 Prediction of cake height with using four different approaches 90
6.7 FILTRATION PRESSURE DISTRIBUTION IN A TALC FILTER CAKE .. 94
6.8 CONCLUSIONS 97
Chapter 7 : CONCLUSIONS AND RECOMMENDATIONS FOR FUTURE WORK 98
REFERENCES 102

Appendix I: MODEL FLOW DIAGRAM **109**
Appendix II: MODEL WORKSHEET **113**
Appendix III: SAMPLE VALIDATION FOR VALIDATION **125**
Appendix IV: COMPUTER CODE **131**
Appendix V: LIQUID PRESSURE PROFILE HISTORY **135**
Appendix VI: PLOTS OF MINIMISATION **139**
Appendix VII: **145**
Appendix VIII: DERIVATION OF EQUATION 6.4 ..... **151**
Appendix IX: PREDICTED LIQUID PRESSURE AND POROSITY PROFILES, POROSITY AT MEDIUM CONSTANT **153**
Appendix X: PREDICTED LIQUID PRESSURE AND POROSITY PROFILES, POROSITY VARYING AT THE MEDIUM **173**
Appendix XI: PREDICTED CAKE HEIGHTS **186**

SUMMARY

The objective of this research was to perform studies on cake filtration through a modelling approach. Cake filtration is an important process in solid liquid separation. A computer code was written with the aid of Runge Kutta numerical scheme to be able to analyse existing filtration data. The first instance of the study was to compare model predictions of liquid pressure profiles to experimentally measured liquid pressure profiles and this were found to be in agreement. Internal cake properties, average porosity, permeability and specific resistance, were obtained from the model and the average values compared to those obtained from the experiment. It was found that using the Happel cell model led to the over prediction of permeability and under prediction of specific cake resistance by an order of magnitude of 2. This was then corrected by a shape factor being used to account for the different shape of talc particle as the Happel cell model assumes all particles are spheres whereas in reality very few particulate systems are spherical in nature.

The effects of time and pressure on local cake properties were also investigated. It was seen that the porosity at the medium of a talc cake decreases rapidly as filtration pressure increases which was due to the compressible nature of talc suspensions. The porosity at the medium also changed very rapidly in the initial periods of filtration further highlighting the compressible nature of talc suspensions.

Filter cake height is an important parameter in filter design. However it was found to be arbitrary in nature. Four different approaches of obtaining a filter cake height namely mass balance equation, modern filtration theory, experimentally measured transient liquid pressure profiles and the model in the current work were used in order to obtain and compare filter cake heights. The model over predicted filter cake height as compared to the other methods however this was deduced to be a different physical interpretation of a filter cake height and was investigated. It was found that the model over predicted cake height. The distribution of filtration pressure within the filter cake was also studied. The over prediction of filter cake height using the model was shown to be as a consequence of buffer layer which was the region between the model prediction and mass balance equation prediction. It was shown that constant pressure filtration referred to the total pressure loss across the slurry, filter cake and filter medium as opposed to it being just the forming pressure.

LIST OF FIGURES

Figure 2.1: Schematic showing the two filtration modes, deadend and crossflow. 5
Figure 2.2: Mechanisms of filtration. Depth filtration occurs by the standard blocking law while most cake filtrations occur by a combination of blocking and bridging. (Wakeman and Tarleton, 1999) 6
Figure 2.3: Schematic diagram depicting cake formation and growth (Wakeman, 1978). 8
Figure 2.4: Schematic diagram of a filter cake pressure profiles (Tiller 1980). 10
Figure 3.1: Photograph of the experimental apparatus (Tarleton, 2008). 22
Figure 3.2: Schematic of pressure filtration apparatus without the compressed air circuitry (Tarleton, 2008). 23
Figure 3.3: Micro-pressure transducer arrangement of the mechatronic pressure filtration apparatus (Tarleton, 2008). 24
Figure 3.4: Plot of *V* against *t* for constant pressure filtrations of a 5 % w/w talc suspension at different filtration pressures. 25
Figure 3.5: Plot of *V* against *t* for three repeat constant pressure filtrations of a 5 % w/w talc suspension. 26
Figure 3.6: Hydraulic pressure history in a forming talc cake/suspension at a constant filtration pressure of 400 kPa. 27
Figure 3.7: Hydraulic pressure history in a forming talc cake/suspension at a constant filtration pressure of 400 kPa. 28
Figure 4.1: Schematic diagram of growing filter cake, (Wakeman, 1978). 32
Figure 4.2: Forces acting on the solids in an element of thickness dx 32
Figure 4.3: Schematic illustrating layer by layer cake deposit. 35
Figure 5.1: Flow diagram of simulation procedure for constant pressure filtration. 48
Figure 5.2: Liquid pressure history in a forming calcite cake at a constant filtration pressure of 300 kPa. 52
Figure 5.3: Predicted liquid pressure history in a forming calcite cake at a constant filtration pressure of 300 kPa. 52
Figure 5.4: Predicted porosity profile in a forming calcite cake at a constant filtration pressure of 300 kPa. 53
Figure 6.1: Plot of P_l vs. $x/\sqrt{t}$ at different times for 400 kPa filtration pressure. 55
Figure 6.2: Minimisation of variance between calculated and experimental liquid pressure through the increment of variable, a 57

Figure 6.3: Minimisation of variance between calculated and experimental average porosity through the increment of variable, $d\varepsilon^*/d\lambda\big|_{\lambda=0}$ 57

Figure 6.4: Calculated and experimental liquid pressure profiles after minimisation of variance at 400 kPa at end of filtration 185 s. For the experiment the cake height is 15.3 mm, for the model the values of a, $d\varepsilon^*/d\lambda\big|_{\lambda=0}$ and ε_m are 3.79, 0.31 and 0.57.....58

Figure 6.5: A comparison between the calculated and the measured liquid pressure profiles in a talc cake at 400 kPa.....59

Figure 6.6: Graph of a, $d\varepsilon^*/d\lambda\big|_{\lambda=0}$, ε_m and ε_{av} against filtration pressure. 61

Figure 6.7: Predicted porosity profile at different filtration pressures.....62

Figure 6.8: Graph of a, $d\varepsilon^*/d\lambda\big|_{\lambda=0}$, ε_m and ε_{av} against filtration pressure 62

Figure 6.9: Porosity distribution for ignition plug cakes (Wakeman ,1978). 63

Figure 6.9: Predicted porosity profile after minimisation of variance, talc 400 kPa. 64

Figure 6.10: Predicted internal permeability and specific resistance after minimisation of variance, talc 400 kPa. 65

Figure 6.11: Permeability comparisons using cell model and experimental calculation. 67

Figure 6.13: Predicted liquid pressure profile, talc at 400 kPa. 68

Figure 6.14: Predicted porosity profile, talc at 400 kPa.....69

Figure 6.15: Predicted liquid pressure profile, talc at 400 kPa , 5s.....69

Figure 6.16: Predicted liquid pressure profile, talc at 400 kPa, 20s.....70

Figure 6.17: Predicted liquid pressure profile, talc at 400 kPa, 60s.....70

Figure 6.18: Predicted liquid pressure profile, talc at 400 kPa, 150s.....71

Figure 6.19: Predicted liquid pressure profile, talc at 400 kPa. 73

Figure 6.20: Predicted porosity profile, talc at 400 kPa.....73

Figure 6.21: Predicted liquid pressure profile, talc at 400 kPa , 5s.....74

Figure 6.22: Predicted liquid pressure profile, talc at 400 kPa, 20s.....74

Figure 6.23: Change of ε_m with time as predicted by the model, talc 75

Figure 6.24: Transient porosity profile within a talc filter cake at 400 kPa.....77

Figure 6.25: Transient liquid pressure profile within a talc filter cake at 400 kPa 78

Figure 6.26: SEM micrograph of talc particles, (Tarleton, 1997).....79

Figure 6.27: Predicted and experimental permeability against filtration pressure, talc filtration.....80

Figure 6.28: Predicted and experimental specific resistance against filtration pressure, talc filtration. 81
Figure 6.29: Effect of particle shape on specific surface (Wakeman and Tarleton, 2005). 81
Figure 6.30: Permeability against filtration pressure using shape factor, talc filtration. 83
Figure 6.31: Corrected permeability against filtration pressure, talc filtration 84
Figure 6.32: Corrected specific resistance against filtration pressure, talc filtration 84
Figure 6.31: Predicted compressibility index values for talc at different filtration pressures 85
Figure 6.34: Predicted and theoretical cake heights with time, ... 89
Figure 6.35: Schematic of a filter cake 89
Figure 6.36: Predicted, theoretical and experimental cake heights with time, ... 90
Figure 6.37: Filter cake growth as determined from four different approaches with filtrations at 400 kPa. 91
Figure 6.38: Filter cake growth as determined from four different approaches with filtrations at 600 kPa. 92
Figure 6.39: Porosity values at the surface of a cake as defined by the different cake height approaches at 400 kPa. 94
Figure 6.40: Distribution of filtration pressure during cake formation of a talc suspension 96

LIST OF TABLES

Table 2.1:Summary of different constant pressure modelling approaches 19
Table 3.1: Results of cake properties from constant pressure experiments. 27
Table 5.1 Characteristic properties of calcite powder dispersed in distilled water..... 51
Table 6.1: Results of constant pressure analysis. 60
Table 6.2: Results of internal properties from constant pressure analysis, Talc using experimental average porosity. 66
Table 6.3: Results of internal properties from constant pressure analysis, Talc using average porosity as that closest to the medium. 66
Table 6.4: Results of prediction of ε_{av}, ε_m , a, and $d\varepsilon^* / d\lambda \big|_{\lambda=0}$ for talc suspension at 400 kPa 75

NOTATION

a	Constant in the definition of $F\left(\varepsilon^*\right)$
A	Filtration Area (m^2)
b	Dimensionless distance, Equation (3.31)
c	Volume fraction of solids in the solid-liquid mixture
d	Particle diameter (m)
E	Compressibility coefficient ($m^2\ s^{-1}$)
F_D	Interfacial drag force per unit volume of solids ($N\ m^{-3}$)
g	Acceleration due to gravity ($m\ s^{-2}$)
$h_{\exp}$	Filter cake height determined experimentally using pressure probes
h_{mb}	Filter cake height determined by mass balance
h_{mft}	Filter cake height determined by modern filtration theory
h_{mod}	Filter cake height determined by model
k	Permeability (m^2)
L	Thickness of filter cake (m)
m_{av}	mass of wet cake/dry cake
$\overline{P}$	Dynamic pressure ($N\ m^{-2}$)
p_l	Liquid pressure (Pa)
p_s	Solids pressure
Δp	Filtration pressure (Pa)
Q	Filtrate flowrate
R_m	Medium resistance (m^{-1})
s	Mass fraction of solids in a feed suspension
S_0	Specific surface of particles ($m^2\ m^{-3}$)
t	Time (s)
v	Velocity ($m^2\ s^{-1}$)
V	Filtrate volume (m^3)
x	Coordinate distance (m)

Greek Letters

α	Specific cake resistance, (m kg^{-1})
ε	Porosity
$\varepsilon *$	Dimensionless porosity
λ	a similarity variable
μ	Viscosity (Pa s)
ρ	Density (kg m^{-3})
θ	Dimensionless time, Equation (3.30)
κ	Shape factor

Subscripts

av	Average
i	Value at cake/slurry interface.
l	of liquid.
m	value at cake/medium interface.
o	of slurry .
s	of liquid.
x	Value at distance x from filter cloth.

Chapter 1 : INTRODUCTION

1.1. MOTIVATION FOR RESEARCH

Cake filtration is a process widely used in numerous industrial applications such as chemical, medical, agriculture, food manufacture, process, minerals treatment and water treatment industries. Matters pertaining to key environmental issues have led to more stringent demands on industries and as a result more emphasis has been placed towards better understanding of filtration processes. The principle underlying filtration basically involves the separation of a solid from the liquid in which it is suspended by passing the liquid through a porous medium with pore sizes too small to allow the passage of the solid particles.

The total pressure which varies through the cake and filter medium affects the cake structure, local porosity and permeability, and influences the filtration performance. Rigorous models describing cake formation have been published which use the equations of continuity, an equation to relate liquid flow rate through the cake to pressure drop and constitutive equations that relate cake structure and local permeability to solid compressive pressure. The data required for establishing these relationships can be obtained from filtration experiments A lot of high quality experimental data exists on cake filtration including data obtained according to constant pressure. This data needs careful analysis through the development of models in order to fully understand the process of initial cake formation based on cake characteristics and pressure.

This work deals with the modelling of cake filtration. A variety of mathematical models have been previously used to simulate cake filtration. As pointed out by Olivier *et al*. (2007), the differences between all this modelling approaches are the material and momentum balance equations for both the liquid and solid phases and material property parameters

In the present work the similarity analysis is presented in the context of a single ordinary differential equation applicable throughout the filter cake, a similarity variable based on position and time as the independent variable, and employing material property functions. Numerical solutions based on this formulation are obtained and a representative sample of results is presented graphically to illustrate interesting aspects of the approach.

1.2. AIMS AND OBJECTIVES

The main objective of this research was to perform studies on cake filtration through a modelling approach. Cake filtration is an important process in solid liquid separation. In the present work a computer code was written with the aid of Runge Kutta Nystrom numerical scheme to be able to analyse existing filtration data.

The stages involved in achieving the desired aims are outlined as follows:

1. Write a computer code to aid in the solution of the governing equation
2. Obtain experimental data for a calcite suspension and verify the model predictions with experimental ones.
3. Once model verification is done analyse talc suspension data and highlight findings
4. Analyse predicted local internal porosity, permeability and specific cake resistance with regards to how time and pressure affect.

1.3. THESIS STRUCTURE

This thesis consists of seven chapters, with this chapter intended to put the thesis into general context in terms of the flow and where it fits into the present field of knowledge. Chapter 2 reviews relevant literature, including past modelling approaches by various researchers relevant to the present work. Chapter 3 shows how the experimental data was obtained with a brief description of the apparatus used as well as the materials used in obtaining the experimental data Chapter 4 describes the governing equations used for the particular model. Chapters 5 discuss the numerical technique used in solving the problem as well as some initial model verification results. Chapter 6 discusses some interesting observations from the analysis done using the model. Chapter 7 concludes the thesis by suggesting potential future investigations.

Chapter 2 : LITERATURE REVIEW

2.1 INTRODUCTION

This chapter reviews previously published literature that is relevant to the present work. The theory of cake filtration is explained, and then flow through porous media explained and relevant filtration equations explained. The important parameters of permeability and porosity are also explained and finally previous modelling approaches are also explained.

2.2 CAKE FILTRATION THEORY

Filtration can be classified according to the mode of operation, namely dead end or cross flow modes (Wakeman and Tarleton, 1999). In dead end filtration, the feed flow is perpendicular to the filter surface whereas in cross flow filtration the feed flow is tangential to the filter surface. These two process modes are shown schematically in Figure 2.1. For this particular study, investigations will be carried out on data from dead-end filtration experiments. The filter medium, denoted by the dotted lines in Figure 2.1, is that critical component which determines whether or not a filter will perform adequately and can be defined as any permeable material upon or within which particles are deposited by the process of filtration (Purchas, 1996). The filter medium is the most important component in a filter as it facilitates the clean separation of particulate solids from a fluid. It is of paramount importance to choose the right specification of filter medium as it greatly influences the economic viability of a filtration process in order to get the desired output such as clean filtrate, economic filtrate times and desired cake properties.

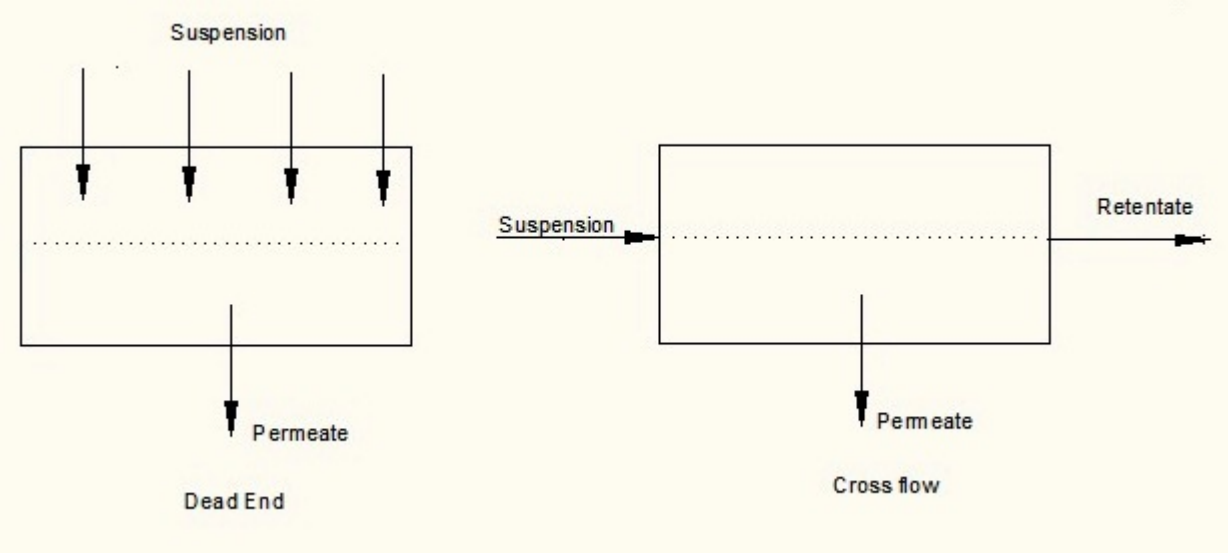

Figure 2.1: Schematic showing the two filtration modes, deadend and crossflow.

Dead-end filtration gives rise to both cake filtration and depth filtration. In depth filtration, the particles are generally smaller than the filter pores and particle deposition is predominantly inside the filter medium. The particles either get trapped or lodged in the tortuous filter pores or get adsorbed onto active sites within the depth of the filter medium. The adsorption of these particles is dependent on the electrostatic interaction between the particles and the surface, which in turn depends on the pore surface and particle's repulsive electrical double layer forces and attractive van der Waals forces.

Cake filtration occurs when the solids concentration is sufficiently high and the particles are larger than the filter pores whereby these particles bridge over the entrance of the filter medium pores, forming a deposit on the filter surface known as 'filter cake'. This filter cake brings about an additional resistance to flow and takes on the role of the being the main filter medium.

Cake filtration is used for separating two phases, solid and liquid, of a suspension from each other. The purpose of separation varies from case to case, including the recovery of solid, clarifying the liquid or recovering both. It has been an engineering principle for a long time and is widely used in the chemical, process, mineral, food and water treatment industries.

The so-called laws of filtration inferred by the mechanisms described by Figure 2.2 (taken from Wakeman and Tarleton, 1999) have been studied by Grace (1956), Hermia (1982) amongst others. Their origins stem from a stochastic modelling of filtration and

the behaviour of a particle arriving at the surface of a filter medium. The characteristic form of the filtration laws is:

$$\frac{d^2t}{dV^2} = k_1\left(\frac{dt}{dV}\right)^{k_2} \tag{2.1}$$

for constant pressure filtration, where k_1 and k_2 are constant. k_1 is dependent on the initial flow rate of slurry reaching the medium, and k_2 = 2, 1.5, 1 and 0 for complete blocking, standard blocking, intermediate blocking and cake filtration respectively. These 'laws' are convenient for visualising and giving an understanding to the microscopic phenomena that may take place at the filter medium surface, but they do not describe the physics of particle deposition beyond the initial few moments of filtration (Wakeman and Tarleton, 1999).

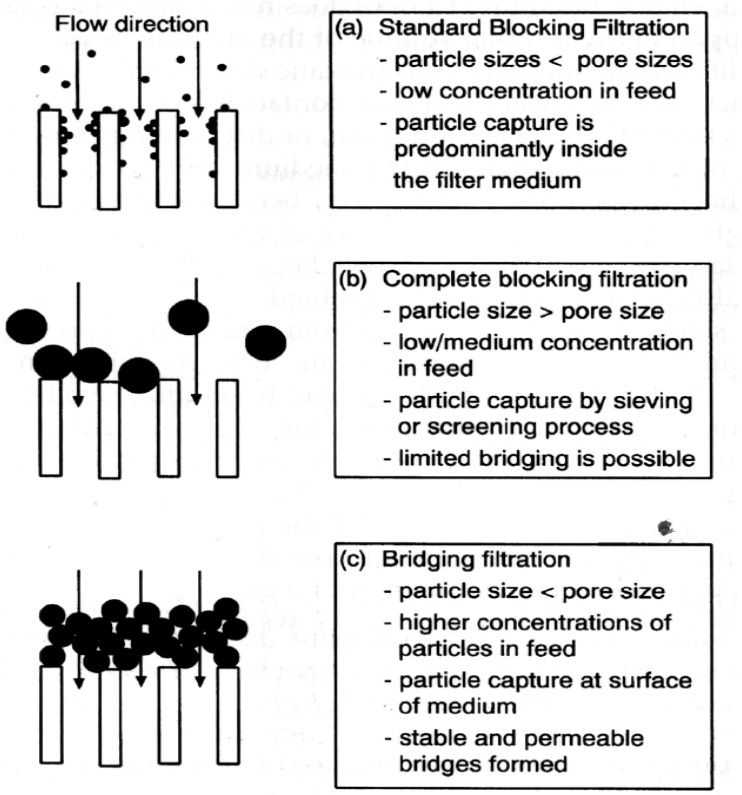

Figure 2.2: Mechanisms of filtration. Depth filtration occurs by the standard blocking law while most cake filtrations occur by a combination of blocking and bridging. (Wakeman and Tarleton, 1999).

More often, filtration processes may be classified according to the variation of the pressure and flow rate with time. The pumping mechanism determines the flow characteristics and gives rise to the various modes of filtration which include constant pressure, constant rate, variable rate-variable pressure and stepped pressure filtration.

2.3 FLOW IN POROUS MEDIA

Filtration theory has evolved from the classical law governing fluid flow through porous media, Darcy's law (Wakeman, 1979(a)). Darcy (1856) carried out experiments which passed water through beds of sand and was thus able to develop an equation for fluid flow through a porous medium. A schematic diagram depicting cake filtration is shown in Figure 2.3. Darcy's law for one dimensional flow is written in the form:

$$\frac{dp_L}{dx} = -\frac{\mu q}{k} \tag{2.2}$$

where k is the permeability; dp_l/dx the hydraulic gradient and q the superficial liquid velocity. Viscosity is included in Equation (2.1) because flow is generally assumed to be laminar. In filtration it is more conventional to use the Ruth (1946) modification of Equation (2.1) in the form:

$$\frac{dp_L}{dw} = \mu \alpha q \tag{2.3}$$

where w is the mass of dry solid deposited per unit area and α is the specific flow or filtration resistance. The mass of dry solids is related to thickness by:

$$dw = \rho_s (1 - \varepsilon) dx \tag{2.4}$$

where ρ_s is the true solid density and ε the local porosity. Integrating over the entire cake yields:

$$w = \rho_s (1 - \varepsilon_{av}) L \tag{2.5}$$

where L is the cake thickness.

By substituting Equation (2.3) into Equation (2.2) it is possible to show that α and k are related by

$$\alpha = \frac{1}{k\rho_s (1 - \varepsilon)} \tag{2.6}$$

Darcy's law interprets the pressure drop in a porous medium, which is strictly valid in an isotropic, stationary porous matrix (Jonsson and Jonssen, 1992a, b).For a more accurate analysis of filtration the Darcy-Shirato equation (1969) should be used. This equation takes into account the velocity of the liquid relative to the solids and is expressed in the form:

$$\frac{dp_L}{dx} = -\mu\alpha (q - eq_s) \tag{2.7}$$

where $e = \varepsilon/(1 - \varepsilon)$ is the void ratio and q_s the superficial velocity of the solids.

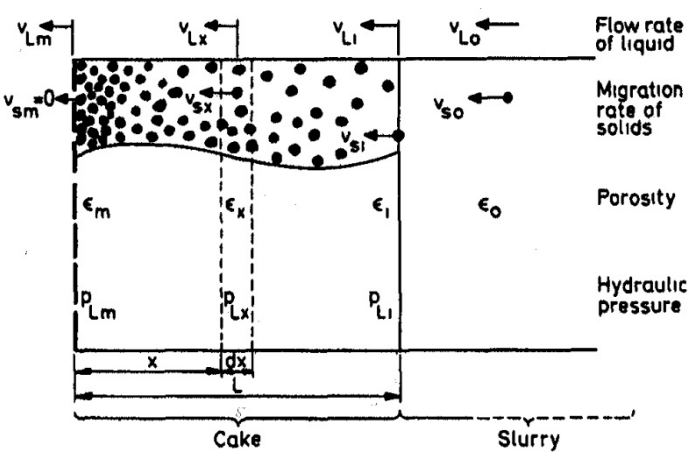

Figure 2.3: Schematic diagram depicting cake formation and growth (Wakeman, 1978).

2.3.1 Liquid pressure and solid compressive pressure

The origin of the cake compressive stress in cake filtration may be explained as follows (Walker *et al.*, 1937): The flow of liquid through a filter cake imparts fluid drag on particles constituting the cake. Since these particles are contiguous, the drag forces experienced by individual particles are transmitted and accumulated along the direction of the liquid flow, giving rise to a compressive stress in the cake phase. Liquid flows through the interstices of the compressible cake in the direction of decreasing hydraulic pressure. The solids forming the cake are compact and relatively dry at the medium surface, whereas the interface layer of incoming slurry and cake is in a wet and soupy condition. As such, the cake porosity changes from its maximum value at the cake-slurry interface ($x = L$) to its minimum value at the cake-septum interface ($x = 0$) (Figure 2.3). The particles are assumed to be in point contact and the liquid completely surrounds each particle. The drag on each particle is transmitted to the next particle. Consequently, the net solid compressive pressure increases as the medium is approached, thereby accounting for the decreasing porosity (Tiller, 1953; Tiller *et al.*, 1987). Instances of a minimum porosity at some distance from the filter medium have been reported when a filter cake collapses after deposition of a critical amount of solids (Rietema, 1953; Baird and Perry, 1967). Solid particles in the slurry flow stream are subjected to both skin drag (from fluid-particle interface) and form drag (from fluid pressure) caused by the friction developed at the surface of the particles. Surface forces on the particles generate internal forces which are communicated from particle to particle at points of contact. As the solid particles are in point instead of area contact, the hydraulic pressure, p_L is effective over the entire cross-sectional area, A. By neglecting inertia forces, a force balance over the filter cake from x to L is written as

$$F_s(x,t) + Ap_L(x,t) = Ap(t) \tag{2.8}$$

where F_s is the accumulated frictional drag on the particles and p the applied pressure which is a function of time only. Dividing by A yields

$$p_s(x,t) + p_L(x,t) = p_{app}(t) \tag{2.9}$$

where a pseudo-solid compressive or drag pressure defined as $p_s = F_s / A$. The internal pressures p_s and p_l are functions of both position and time. The effective pressure is not a physical quantity. The true pressure at the points of contact would be the local F, divided by the local contact area, a, which is assumed to be negligible in filtration theory. The effective pressure is then simply the drag on all the particles in the distance from x to L divided by the cross-sectional area. By taking the differential of Equation (2.9) with respect to x at a constant time, one obtains

$$dp_s + dp_L = 0 \tag{2.10}$$

this implies that the drop in hydraulic pressure is exactly equal to the rise in solid compressive pressure. Typical curves illustrating variations of hydraulic and effective pressures within a filter cake is presented in Figure 2.4

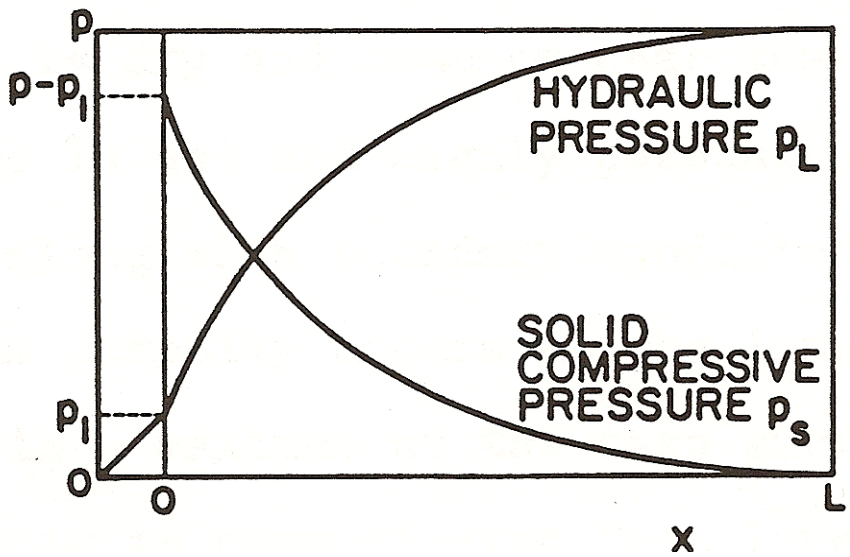

Figure 2.4: Schematic diagram of a filter cake pressure profiles (Tiller 1980).

Differentiating Equation (2.10) with respect to material coordinates yields:

$$\left(\frac{dp_s}{dw}\right)_t + \left(\frac{dp_L}{dw}\right)_t = 0 \tag{2.11}$$

Substituting Equation (2.10) into Equation (2.3) and integrating over the entire cake depth at a given time with respect to $p_s(0, \Delta p - \Delta p_m)$ and $w(w_c, 0)$ gives

$$\mu q w_c = \frac{\Delta p - \Delta p_m}{\alpha} = \frac{\Delta p - \mu q R_m}{\alpha} = \frac{\Delta P_c}{\alpha} \tag{2.12}$$

where $\mu q R_m$ represents the pressure (p_m) required to overcome the resistance of the filter, ΔP_c is the pressure drop across the cake and is given by:

$$\Delta P_c = P - P_l = P - \mu q R_m \tag{2.13}$$

where P is the filtration pressure, P_l the liquid pressure at the cake medium interface and R_m the medium resistance $= L_m / k_m$, that is the medium thickness divided by the permeability. Integration of Equation (2.7) over the entire filter cake yields:

$$q = \frac{1}{A}\frac{dV}{dt} = \frac{\Delta P}{\mu(\alpha_{av} w + R_m)} \tag{2.14}$$

The above is true if q is a constant at any instant throughout the cake and α is a unique function of cumulative drag stress. The average specific resistance, α_{av}, is defined as:

$$\frac{1}{\alpha_{av}} = \frac{1}{\Delta P_c}\int_0^{\Delta P_c} \frac{1}{\alpha} dP_s \tag{2.15}$$

A limitation of Equation (2.14) is that for α_{av} to remain constant then ΔP_c must be constant, from this it is very clear that average specific cake resistance is dependent on the pressure drop across the cake, for constant pressure filtration, in the initial stages the pressure drop is as a result of the medium, thus as medium resistance increases the cake builds up on the surface of the medium, therefore as ΔP_c increases the value of α_{av} will also change.

2.4 FILTER CAKE PERMEABILITY AND POROSITY

Many researchers have investigated flow through porous media in terms of cake permeability and porosity. Besides the earliest work performed by Carman (1937) for packed beds, Sullivan (1942), Brownell and Katz (1947), Brown (1950), Davies (1952), Chen (1955) and Ingmanson *et al.* (1959) have made valuable contributions to permeability measurements using a wide variety of porous media. Poiseuille (1840) and Darcy (1856) discussed theoretical approaches to the permeability of porous media. Further advancement of knowledge in this field have been carried out by Muskat and Wyckoff (1946), Happel and Brenner (1965), Philip (1970), Payatakes *et al.* (1973), Scheidegger (1974), Rajagopalan and Tien (1976), Jackson and James (1986) and Dullien (1992).

The key properties of a filter cake are the cake porosity and permeability. The cake porosity (ε) is a measure of the fluid capacity of the formed cake or the fraction of a porous medium available for fluid flow. The cake permeability (k) is an indication of how easily the fluid can pass through its voids under an applied pressure gradient. That is, the extent of permeability is determined by the porosity of the medium and also the sizes of pores in its internal structure. However, the complexity of the internal pore structure and geometry render it virtually impossible to be described with mathematical rigour. Therefore, simplified models relating permeability to the porosity of a filter cake and to the mean size of the particles forming the cake have been developed. The earliest theoretical concept of porous media was attributed to the work of Kozeny (1927) and Carman (1938).

The average specific resistance has been analysed from a basic viewpoint in the study of viscous flow through packed beds of particulate materials by several workers such as Carman (1937; 1938), Fair (1951) Fair and Hatch (1933) and Coulson (1949). Perhaps the most significant outcome of this host of work is the development of the Kozeny Carman equation which was derived for viscous flow in granular beds by the assumption of perfectly random packing of discrete particles and through the use of a mean hydraulic pore diameter expressed in terms of the void fraction and particle specific surface. Comparing the Kozeny Carman equation to Darcy's equation yields an

expression for the specific resistance in terms of the porosity, specific surface, solid density and permeability. The Kozeny Carman model is a useful tool for correlating resistance data for fluid flow through porous media and for determining the specific surface of powder samples from permeability data.

Instead of viewing a packed bed as a bundle of tortuous channels as the Kozeny Carman theory does, the Happel cell model (Happel and Brenner, 1965) views the bed grains as an assemblage of interacting, but essentially individual spheres, with the flow field about an average sphere being described more realistically and in more detail. The expression for the permeability derived from the cell model is:

$$k = \frac{x^2}{36} \frac{6 - 9(1-\varepsilon)^{0.33} + 9(1-\varepsilon)^{1.67} - 6(1-\varepsilon)^2}{(1-\varepsilon)\left(3 + 2(1-\varepsilon)^{1.67}\right)} \tag{2.16}$$

Shirato and Aragaki (1972) argued that the determination of an average specific resistance dud not shed any light on the internal mechanism of cake filtration operations nor on some particular problems which were encountered in industry. Kelsey (1965) found that the specific cake resistance decreased with higher suspension concentrations and attributed this to a reduction in the time available for particles to orientate themselves. The arrival rate of the particles at the filter medium is also thought to influence cake properties as has been reported by Rushton (1973; 1976) and Wakeman (1979). Particle size distribution is known to affect the cake resistance as the fine particles may pass through the cake along with the suspending liquid and lodge themselves at various locations within the cake depth, producing a non homogenous cake (Tien, 1991). Wakeman (2007a) discussed the influence of particle properties on filtration. He pointed out that the particle properties with the most profound effects on the specific resistance are the particle size, size distribution, shape and interaction with the surrounding fluid. Furthermore, if the particle properties could be specified for a filtration, the target properties would be for the particles to have as large a size as possible, be as near to spherical as possible and have a monosize distribution.

Tiller and Crump (1977) acknowledged the fact that, generally, the porosity is minimum at the filter medium surface and a maximum at the cake-suspension interface (refer to Figure 2.3 for example). This is due to the nature of the drag exerted by the fluid.

2.5 CAKE FILTRATION ANALYSIS

To be able to analyse cake filtration one may consider the problem as one concerned with the motions of a large number of particles and a fluid stream. By satisfying the Navier-Stokes equation at each point of the fluid and equations of motion for each particle it is possible to analyse a multiphase system. However owing to the complication of this method it would be impractical to carry it out hence an alternative would be to derive a set of equations by replacing the relevant point variables with their local mean variables over a region containing many particles but smaller than the macroscopic scale of the intended problem. The equations to be obtained where there are two phases present may be viewed as the continuity equations of two interpenetrating continua, and there solutions constitute the analysis of the problem.

A study on mechanisms of cake formation and growth in filtration processes requires information on filtrate flow rate and cake thickness against filtration time (v *vs* t and L *vs* t). Volume against time data can be obtained by performing constant pressure filtration tests or C-P test in order to collect the flow rate of the filtrate as a function of time.

Compression-Permeability (C-P) cell would provide an appropriate method for characterising compressible cake filtration as envisaged by Ruth (1946). This would be done by carrying out a range of filtration experiments over a range of constant pressures. Although the methodology has proven successful through investigations performed by Ingmanson (1953), Kottwitz and Boylan (1958) and Grace (1953 (a), 1953 (b)), several researchers highlighted problems with this. Shirato *et al* (1986) questioned the applicability and principles of the C-P cell by pointing out that the influences of side-wall friction had been ignored. Tiller (1955, 1958) found that there were significant interactions between the cell wall and compressed cake, ant that all the experimental data should have been adjusted accordingly to account for non-uniform stress distribution profiles. Tiller further elaborated on this in his papers of (Tiller *et al.* 1972(a), Tiller and Leu 1972 (b)). Inherent within C-P cell data generation is the

assumption that measured porosity and/or specific cake resistances are comparable to those obtained in filters. For suspension demonstrating time dependency i.e. an ageing effect, this does not hold. Wakeman (1978) attributed little confidence to C-P cell data estimation of filtration times; he was supported by Shirato *et al* (1985) who also questioned the applicability of C-P cell data to industrial applications. The time taken to generate C-P cell data was deemed to be excessive in light of the limitations of the technique. C-P cells have been used to generate data from which scale-up methodologies are based.

Most filter cakes show some degree of compressibility whereby the porosity varies from a maximum at the cake surface to the filter medium (Baird and Perry, 1967). As a filter cake develops, a new surface layer deposits on the previously compressed layer this causes liquid to be quashed out of the already formed cake. As filtration proceeds, the cake permeability reduces and this aids in the retention of solids.

Wakeman (1985), deduced that once a compressible cake has been deposited, its characteristics are time dependent and are affected by a number of factors such as

i. Re-alignment of the particles. By assuming that the particles are not compressible, particle re-arrangement may occur, leading to a lower porosity arrangement. The drag on each particle is communicated to the next particle which consequently increases the net solid compressive pressure towards the medium (Shirato *et al.* 1985) and is dependent on particle shape, size distribution and arrangement (Tiller and Crump, 1985).
ii. Deformation of particles under high pressures.
iii. A gradual increase in medium resistance throughout the filtration as finer particles from the cake penetrate the cloth pores.
iv. The migration of the finest particles within the cake in the direction of flow, leading to the entrapment within the cake and interstices and an increase in the specific resistance

Various methods have been proposed to determine the cake thickness history. Some investigators used conductive electrodes to measure cake conductivity at different positions in the filtration chamber and indirectly calculated the local cake porosity (Baird and Perry, 1967; Shirato *et al.*,1971 and Wakeman, 1981). Others placed

pressure sensors along the surface of experimental cell at various heights to record the hydraulic pressure histories and determine *L* vs. *t (*Okamura and Shirato, 1955; Willis *et al.* 1983; Fathi-Najafi and Theliander, 1995). These methods are basically costly and the limited number of measuring points employed causes incomplete porosity or pressure profiles. The intrusive measuring device placed within the filter cake also affects the cake growth and cake internal structure. Based on the principle of sudden flow area reduction in an orifice, Murase *et al.* (1987) showed that by placing a plate with a small opening at different heights in the filtration cell, the results of cake height against time could be established as a sharp decrease in filtration rate was observed when the growth of cake reached the plate. However, Tarleton and co-workers (1997; 1998; 1999b) proposed the use of mechatronics principles, with integrated electronics, computers, process control and mechanical systems, to investigate the local properties of filter cakes during filtration. Ten micro-pressure transducers (for hydraulic pressure measurements) were fixed in a spiral arrangement around the inner circumference of the filter cell and ranged from heights of 0.5 mm to 15.3 mm from the filter medium and protrude ~2 mm into the cell. This essentially allows non-intrusive measurements of cake properties to be made close to the filter medium. Moreover, the pneumatic valves are computer controlled and the relevant filtration data semi-continuously transmitted and displayed on the personal computer. Tarleton (1999b) pointed out that this allows filtration data to be acquired in a repeatable and reliable manner with a minimum of operator interference for either constant or variable pressure conditions. The on-line measurement of experimental parameters also allowed a real time display of results on the computer screen as an experiment proceeded.

After obtaining the local filter cake porosity, several studies that analyse the simulation of filter cake formation and growth arose, some of these analyses included (Wakeman, 1978, 1981; Stamatakis and Tien, 1991; Lu and Hwang, 1993; Theliander and Fathi-Najafi, 1996). Most of these analyses were based on the solutions of the volume averaged continuity equations for the fluid and particle phases. Wakeman (1981) proposed the model of filter cake growth layer by layer, followed by compression by upper cake layer to simulate the cake growth. He used porosity vs. time data determined from electrode measurements; porosity and specific cake resistance relationship obtained using the Happel cell model, Equation (2.12), volume against time and cake height against time data to simulate the local cake properties by way of computer

programming. Theliander and Fathi-Najafi (1996) improved his method by using least-square regression to obtain porosity as a function of solids pressure, p_s, thus avoiding the measurement of porosity as a function of time and position within a forming cake.

The modelling approach used by Tiller *et al* (1953,1961,1973,1977) used a Darcian approach which was based on two parameters that is the specific cake resistance and the solids pressure that described flow through the filter cake. The specific cake resistance came from the work of Ruth *et al* (1933, 1935) and the solids stress concept from soil mechanics. The solids pressure is referred to as compressive stress (Tiller *et al*, 1961, Shirato *et al*, 1969, Stamatakis *et al*, 1991, Wu, 1994), compressive drag pressure (Tiller *et al*, 1973), accumulative drag pressure (Tiller *et al*, 1977, Tiller et al, 1981), contact pressure (Sorensen *et al*,1996), and structure stress (Sorensen *et al*, 1997). A force due to liquid flow through the filter cake is transmitted by friction with the solid particles. The force being transmitted by the liquid to the solids builds up from particle to particle with a maximum being attained at the filter medium. The liquid loses its energy and thus its pressure reduces toward the filter medium.

The modelling approach of Buscall and White (1987) considered the quantities that defined liquid flow through the cake and consolidation stages as material properties than parameter dependent thus the material was considered as networked material possessing a compressive yield , P_y. The stress was assumed to be an indirect function of the bonding between the particles and a direct function of the volume fraction of the solids phase. As a result it was seen that it only appeared in a system above a certain volume fraction ϕ_G commonly referred to as the gel point. This corresponded to a fully networked system. During filtration when the solids stress exceeded the pressure P_y, the filter cake restructured itself forming a different filter cake structure which porosity permitted $P_y = P_s$. This was also demonstrated in the work of Landman *et al* (1991, 1993, and 1994).

Smiles *et al* (1970, 1987, and 2000) used the piezometric potential of liquid instead of the liquid pore pressure in Darcy's law thus deriving the filtration equation in the form of a diffusion equation. As a result of the complexities of its development it is scarcely used in modern filtration.

Willis *et al* (1980, 1983, 1992, 1995) used the concept of multiphase theory. They derived the filtration equations in 3D in continuous phases. To overcome the limited

knowledge of cake structure they used volume averaging equations proposed by Gray (1975) and Whitaker (1977).

As pointed out by Olivier *et al*. (2007), the differences between all this modelling approaches are the material and momentum balance equations for both the liquid and solid phases and material property parameters

2.6 CAKE FILTRATION NUMERICAL SOLUTIONS

In recent cases of constant pressure filtration, numerical modelling methods have been deemed necessary in order avoid assumptions needed in solving analytical solutions. Numerical models have been suggested for constant pressure filtration, where medium resistance and sedimentation of solids on the filter cake surface are disregarded. With these assumptions, the partial differential equations are easily transformed into ordinary differential equations in two ways. The first method is using the similarity variable where by the average voids ratio in the cake is assumed to be constant and therefore the filtrate volume is proportional to $t^{\frac{1}{2}}$. Atsumi and Akiyama (1975), solved numerical filtration models by utilising the similarity variable and using material coordinates. They solved the resulting ordinary differential equations using the method of moments. Wakeman (1978) solved the same problem by using the similarity variable and using absolute coordinates, he solved the resulting equation using a Runge-Kutta-Nystrom algorithm. Yeh (1985) transformed the partial differential equation to an ordinary differential equation by assuming that the void ratio in the filter cake during filtration was a unique function of cake thickness. He formulated the numerical method into material coordinates and solved the ordinary differential equation using weighted residuals method. Tosun (1986) claimed that the transformation of the partial differential equation to ordinary differential one used by earlier researchers was a laborious, time consuming method, he instead formulated the partial differential equation using material coordinates and solved the partial differential equation by using kehoes method. Theliander and Fathi-Najafi (1996) used the layer by layer model presented by Wakeman (1981), he divided his filtration process into a number of time intervals, and this is a usual approach when the transient behaviour of a process is

studied. However Tosun (1986) claimed that this was not the best way of discretising the process because the amount of deposited solid material per unit time decreases during filtration. A summary of the various constant pressure filtration modelling approaches is shown in Table 2.1

Table 2.1:Summary of different constant pressure modelling approaches

RESEARCHER	**COORDINATE SYSTEM**	**INITIAL CONDITIONS**	**SOLUTION METHOD**
Atsumi *et al*, 1975	Material	Suspension	Similarity variable transformation of governing equation. Method of moments used
Wakeman , 1978	Absolute	Suspension	Similarity variable transformation of governing equation. Runge-Kutta Nystrom method used
Yeh, 1985	Material	Suspension	Quasi stationary assumption used to transform governing equation. Weighted residuals method used
Tosun, 1986	Material	Suspension	Kehoes method used

2.7 CLOSURE

Cake filtration is an operation that normally is characterized by measuring average data of the filter cake formed. This is sufficient in many cases but it gives no relevant information about the local properties of the filter cake or of the build-up of the filter cake. The conventional theory has been discussed along with its aspects. Multiphase concept and derivations of fundamental cake filtration equations have been discussed. The relationships between cake characteristics and cake compressive stress have been discussed. An analysis of the different models and approaches has been discussed. It is apparent that more detailed work on the constitutive equations as well as more analysis of filtration data needs to be done to gain a further understanding on cake filtration and this will be subsequently carried out in the remainder of this work.

Chapter 3 : EXPERIMENTAL DATA ACQUISITION

3.1 INTRODUCTION

It should be noted that this work involved modelling of constant pressure filtration data. However there needed to be an appreciation of how this data was obtained. In this chapter, the sophisticated mechatronic filtration apparatus used to obtain constant pressure filtration data is described briefly as well as the results obtained from the constant pressure filtration experiments.

3.2 EXPERIMENTAL APPARATUS DESCRIPTION

A photograph of the mechatronic apparatus is seen in Figure 3.1. Figure 3.2 gives a schematic of the pressure filtration apparatus used in acquiring the experimental data. A stainless steel suspension feed vessel (1) capable of containing 2L of suspension was connected to a stainless steel filter cell (2). Although both vessels can withstand much higher pressures; the normal operating limit (relief valve setting) was 600 kPa. The feed was manually fed into a funnel located above the feed vessel inlet; the flow into the feed vessel was controlled by a manual valve. A stainless steel stirrer was employed in the feed vessel to keep the suspension well mixed and to prevent particle settling. Suspension flowed from the feed vessel to the filter cell though an automated ball valve which was sequenced by means of a personal computer.

The filter cell base rested on a detachable platform whose position could be adjusted by means of a pneumatic system to enable cleaning, insertion and removal of the filter medium as well as filter cake removal. The filter medium which was 120 cm^2 in area rested up on a sintered support, which in turn rested on a star shaped support to maintain the sinter's shape on a sloping filter cell base. The filter cell base was sloped to angle the filtrate flow directly to an electronic balance (3) with minimal hold up.

The personal computer attached to the filter and ancillaries contained a program created using QuickBasic which controlled the automated pneumatic ball valves via solenoid valves situated in the main control box. The program enabled the user to control the valve sequencing and also to carry out experiments at constant pressure. The filtrate was

collected and weighed by an electronic balance which sent its readings to the personal computer. Values of filtration pressure, filtrate volume, hydraulic pressure and time were then saved on the personal computer for further analysis.

Figure 3.1: Photograph of the experimental apparatus (Tarleton, 2008).

In order to determine the transient liquid pressure variations within the filter cake, titanium micro-pressure transducers were fixed in a spiral arrangement around the inner circumference of the wall of the filter cell. These transducers sent signals to the personal computer, enabling liquid pressure profiles to be measured, which in turn allowed further analysis into the cake characteristics and filtration behaviour. The transducers are attached to custom made stainless steel holders and micro-bore tubes (0.5 mm O.D.). As illustrated in Figure 3.3, the ten transducers ranged from heights of 0.5 mm to 15.3 mm from the filter medium (0.5, 0.8, 1.0, 1.3, 1.8, 2.3, 3.3, 5.3, 9.3 and 15.3 mm) and protruded ~2 mm into the cell. A liquid bridge was created between the cake and the tip of a transducer by injecting deionised water from a separate reservoir into each holder.

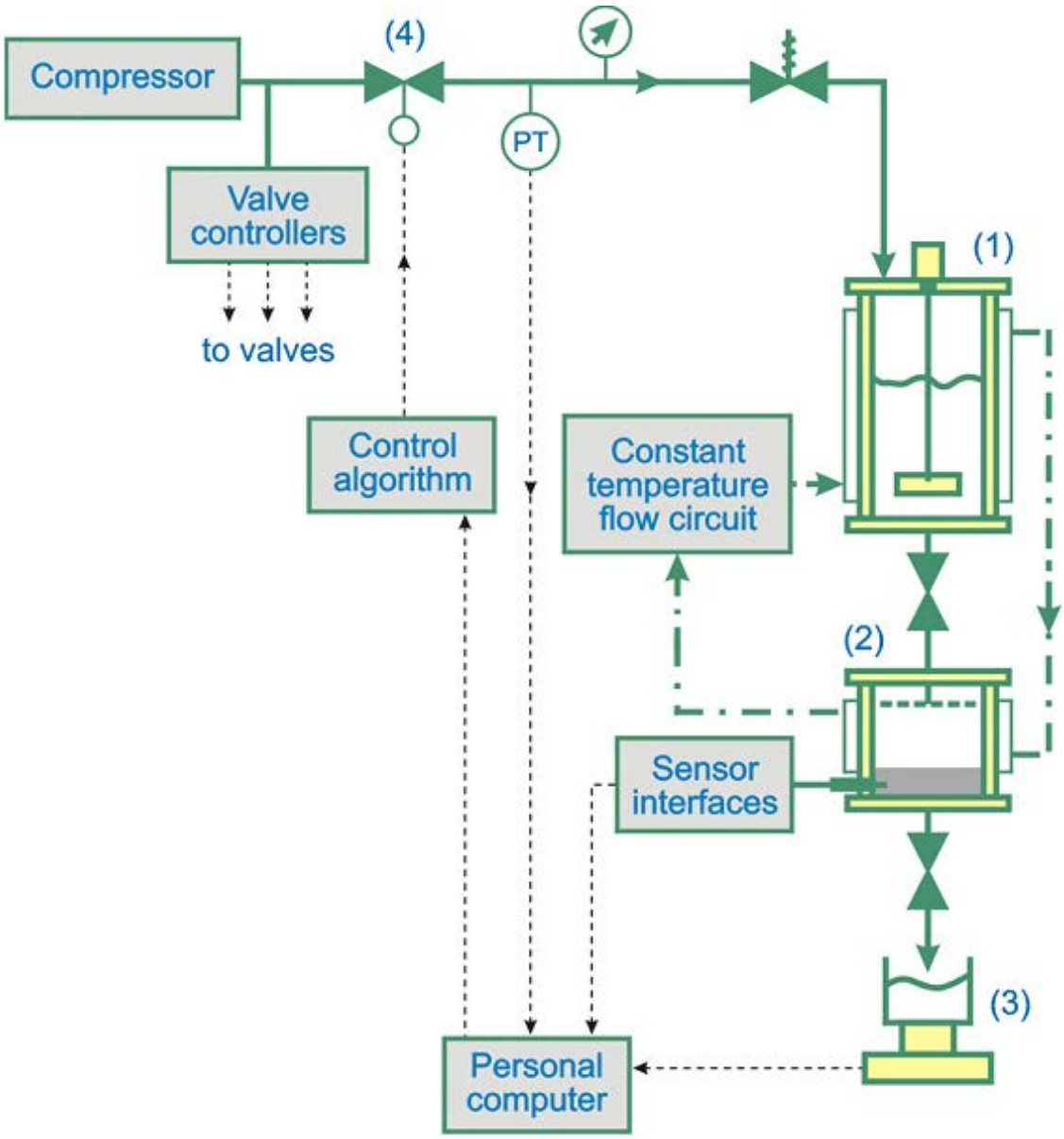

Figure 3.2: Schematic of pressure filtration apparatus without the compressed air circuitry (Tarleton, 2008).

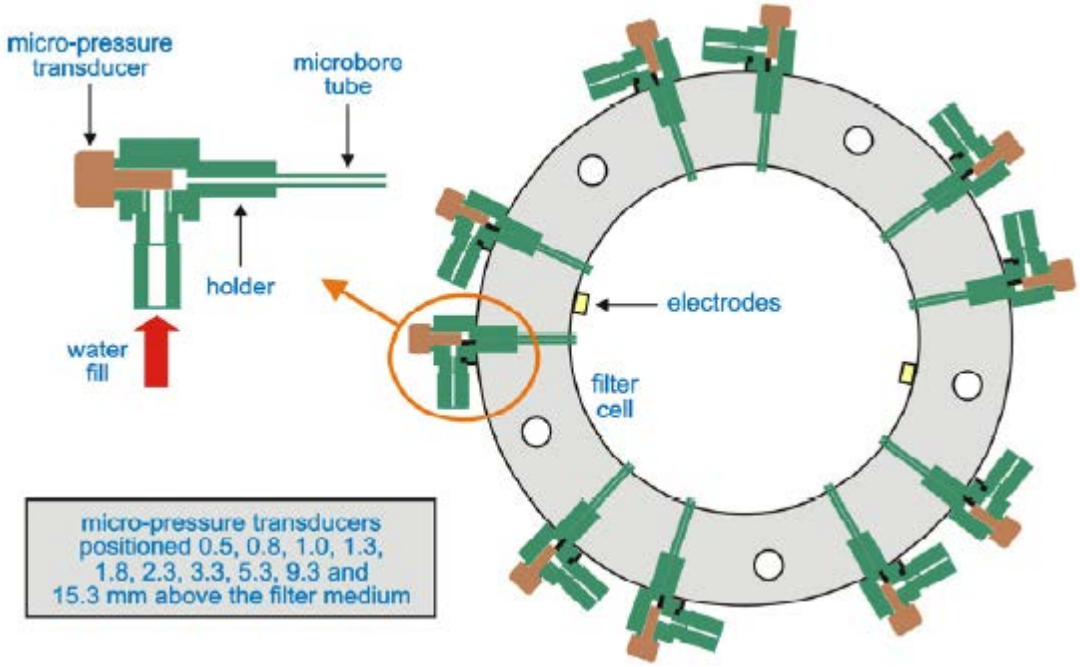

Figure 3.3: Micro-pressure transducer arrangement of the mechatronic pressure filtration apparatus (Tarleton, 2008).

3.3 EXPERIMENTAL METHOD AND MATERIALS

The apparatus used for experiments was the one previously described. Constant pressure filtration experiments were carried out on 5% solids concentration talc and calcite suspensions. The filtration pressure range investigated was between 100-600 *kPa* for the talc suspension and 300 kPa for the calcite suspension. Filtration was allowed to proceed and stopped once deliquoring, which was determined when the *t/V* against *V* plot experienced a sudden change in accordance to traditional filtration behaviour, was deemed to be beginning. On the conclusion of filtration the formed cake in the filter cell was removed and weighed when wet. It was then dried over a period of twenty four hours and reweighed.

3.4 RESULTS AND DISCUSSIONS

The volume against time plots for the talc suspension filtrations for the pressure ranges being investigated are shown in Figure 3.4.

With an increase in driving force, filtration rate was expected to increase, resulting in higher pressure filtrations taking a shorter time. It was also observed that at higher pressures the plots of *V* against *t* were closer together than at lower pressures. The *t/v* against *V* plots are shown in Figure 3.5. By using equation 3.1, the average specific cake resistance and medium resistance were determined from the gradients of Figure 3.5

$$\frac{t}{V} = \frac{\alpha_{av} c \mu}{2A^2 \Delta p} V + \frac{\mu R}{A \Delta p} = K_1 x + K_2 \tag{3.1}$$

At shorter filtration times observed at higher pressures resulted in a decrease in gradient as the applied pressure was increased.

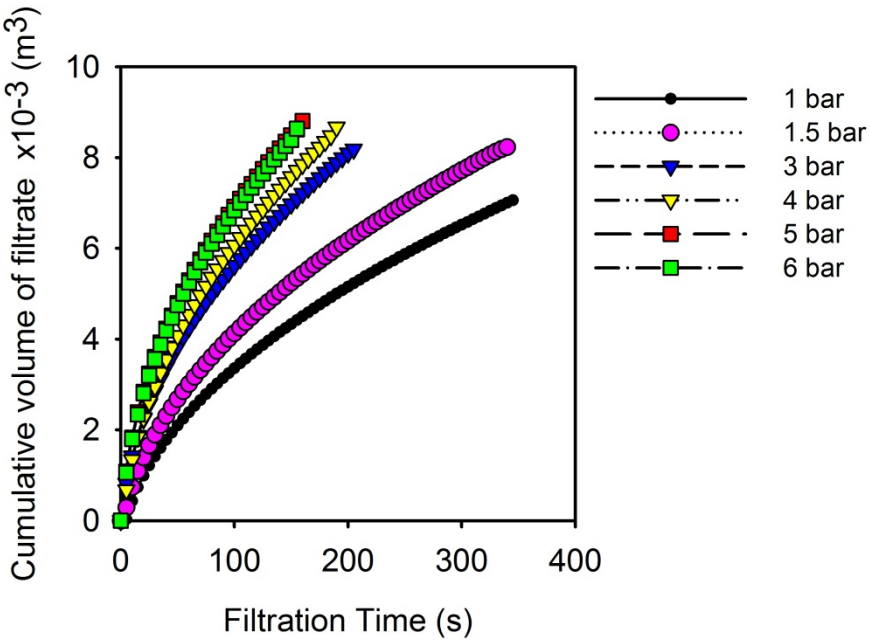

Figure 3.4: Plot of *V* against *t* for constant pressure filtrations of a 5 % w/w talc suspension at different filtration pressures.

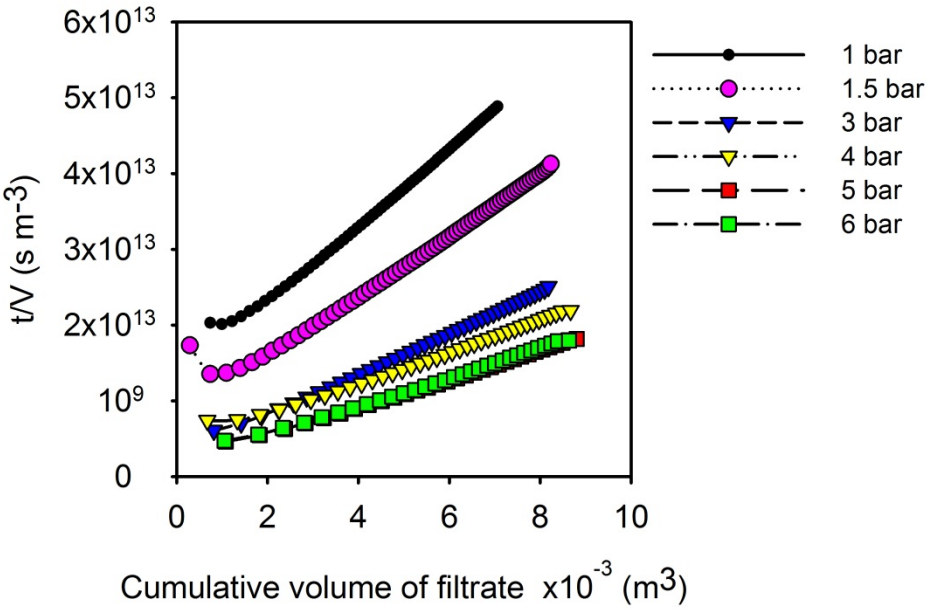

Figure 3.5: Plot of *V* against *t* for three repeat constant pressure filtrations of a 5 % w/w talc suspension.

By utilising Equation 3.2, the average porosity of the cake could be determined.

$$m_{av} = 1 + \frac{\rho_l \varepsilon_{av}}{\rho_s (1 - \varepsilon_{av})} \tag{3.2}$$

It was then possible to obtain cake properties at different filtration pressures. The cake properties were the average porosity, specific resistance and the cake permeability. The properties obtained are shown in Table 3.1.

At lower pressures one observes that the porosity is high, as at lower pressures compaction is at its lowest hence forming a more permeable structure and least resistance to flow of fluid. At higher pressures however the opposite effect is observed, the porosity decreases as more particles are forced towards the medium as the cake grows, this results in higher compaction which results in less permeability and hence higher resistance to flow of fluid through the particles.

Table 3.1: Results of cake properties from constant pressure experiments.

ΔP (kPa)	ε_{av}	k_{av} (m^2)	α_{av}($m\ kg^{1}$)
100	0.702	1.29×10^{-14}	9.84×10^{10}
150	0.685	1.09×10^{-14}	1.10×10^{11}
300	0.671	7.86×10^{-15}	1.46×10^{11}
400	0.666	7.63×10^{-15}	1.48×10^{11}
500	0.654	6.38×10^{-15}	1.71×10^{11}
600	0.639	5.03×10^{-15}	2.08×10^{11}

Figure 3.6 shows the liquid pressure history of a 400 kPa filtration at various times within the forming cake/suspension. At *t = 0s*, the start of filtration, the talc suspension was in its original homogenously mixed state and the measured liquid pressures were equal to the applied filtration pressure. At these time; as no cake had formed the talc particles in suspension were sufficiently far apart to carry zero compressive pressure. As filtration progressed, liquid pressure began to fall, this was a result of the particles forming a network and thus one was able to deduce that a cake was forming. As a result cake thickness increased with time thus reducing liquid pressure at the pressure probes positions above the filter medium.

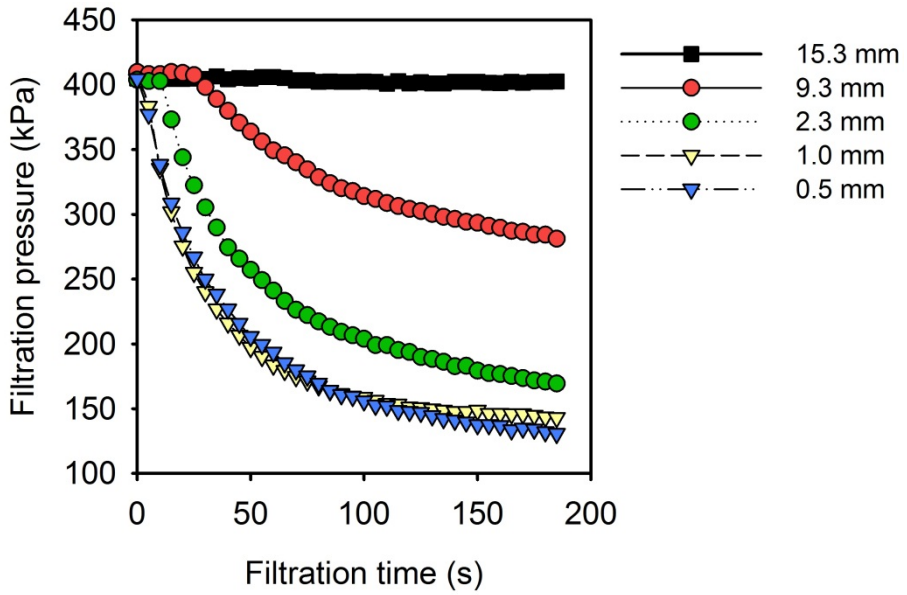

Figure 3.6: Hydraulic pressure history in a forming talc cake/suspension at a constant filtration pressure of 400 kPa.

Figure 3.7 shows liquid pressure profile against cake height at 400 kPa and will be the form used for the rest of the work because the model gives its output in the form of liquid pressure against cake height. The rest of the plots at different pressures can be seen in Appendix V.

It can be seen that as filtration progressed the liquid pressure decreased meaning a cake was growing. This is supported by looking at the curves say at 5 s and 185 s, one would deduce the cake heights of the developing cakes to be between 1 and 2 mm for the first case and 9.3 and 15.3 mm for the second case. As more solids deposited; regions of the cake closest to the medium became more compact due to the drag force as a result of liquid flow through the interstices of the cake and also as a result of the weight of the layers being deposited per unit time. This resulted in the liquid pressure at any given height decreasing with time, if one were to observe the pressure probe closest to the medium, it can be seen that the liquid pressure at the cake/medium falls up to the final value at the final filtration time at 185 s. This would be a clear indication that as filtration proceeds some particle rearrangement is occurring and such compression occurs as filtration proceeds.

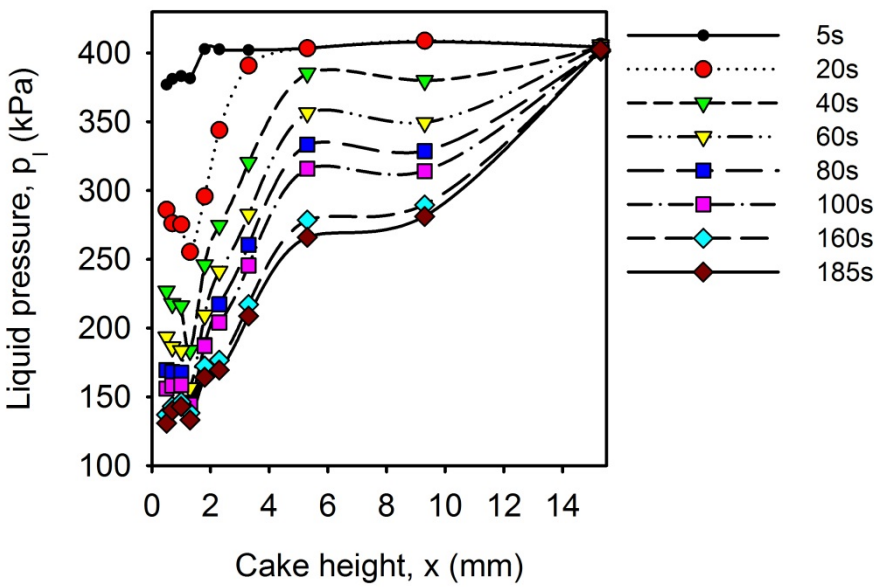

Figure 3.7: Hydraulic pressure history in a forming talc cake/suspension at a constant filtration pressure of 400 kPa.

3.5 CONCLUSIONS

The acquisition of the experimental data has been explained; the apparatus used has been briefly mentioned and shown. The experimental results for the constant pressure filtration of 5 % w/w talc suspensions between 100-600 kPa filtration pressures been explained and are in agreement with theory.

Chapter 4 : GOVERNING EQUATIONS

4.1 INRODUCTION

Mathematical modelling of a filtration system is based on the fundamental governing equations that reflect the physics of the system. A modelling process begins with the formulation of a mathematical model based on the laws of conservation of mass, energy and momentum. In this chapter the governing equations leading to the final mathematical model equation are presented.

4.2 COMPRESSIBLE CAKE FILRATION EQUATIONS

By considering Figure 4.1, a material balance on the particles either in the suspension or the cake yields:

$$\frac{\partial c}{\partial t} = -\frac{\partial (c v_S)}{\partial x} \tag{4.1}$$

where $c = 1 - \varepsilon$ is the volume fraction of the solids in the mixture.

The liquid material balance is written as:

$$\frac{\partial \varepsilon}{\partial t} = -\frac{\partial (\varepsilon v_L)}{\partial x} \tag{4.2}$$

where ε is the volume fraction of the liquid (porosity) in the mixture, v_S and v_L are the true velocities of the solid and liquid respectively and are written relative to the chamber in which the solid/liquid mixture is contained.

4.2.1 Force momentum balance

The force-momentum balance on the solids when their concentration is greater than the critical value is obtained by equating the net force on the particles. The critical concentration occurs when the solid compressive stress just begins to be felt through the

particulate structure and thus some strength starts to develop in the filter cake. The net force on the particles is the gravitational force minus the sum of the buoyancy and drag forces and the solid stress gradient, to the net rate of convection of momentum of the particles and the rate of change of particle momentum in a differential layer of the solid/liquid mixture of thickness dx. This is shown in Figure 4.2 and is formally written as:

$$c(\rho_S - \rho_L)g - cF_D - \frac{\partial P_S}{\partial x} = \rho_S \frac{\partial\left(cv_S{}^2\right)}{\partial x} + \rho_S \frac{\partial(cv_S)}{\partial t} \tag{4.3}$$

Similarly for the liquid phase the force momentum balance equates the hydraulic pressure gradient to the sum of gravity, buoyancy and drag forces:

$$cF_D - \frac{\partial \overline{P}_L}{\partial x} = \rho_L \frac{\partial\left(\varepsilon v_L{}^2\right)}{\partial x} + \rho_L \frac{\partial(\varepsilon v_L)}{\partial t} \tag{4.4}$$

where $\overline{P}_L = P_L - \rho g x$ with P_L being the pressure acting on the liquid phase. In filtration, the liquid flow is considered laminar and inertial terms are neglected, hence liquid flow is described by Darcy's law thus from Equation (4.4)

$$\frac{\partial \overline{P}_L}{\partial x} = cF_D = \frac{\partial P_L}{\partial x} - \rho g \tag{4.5}$$

where the drag force is given by

$$F_D = \frac{\mu}{k} \cdot \frac{1-c}{c}(v_L - v_S) \tag{4.6}$$

By neglecting inertial forces, Equation (4.3) simplifies to:

$$-\frac{\partial P_S}{\partial x} = c(\rho_S - \rho_L)g - cF_D \tag{4.7}$$

Equation (4.7) assumes that only liquid is displaced by the moving particles, which is only true approaching the limit where the cake is totally compressed.

Equations (4.1), (4.2), (4.5), (4.6) and (4.7) provide the basis for the mathematical formulation of compressible cake filtration. The model is based on a grown filter cake.

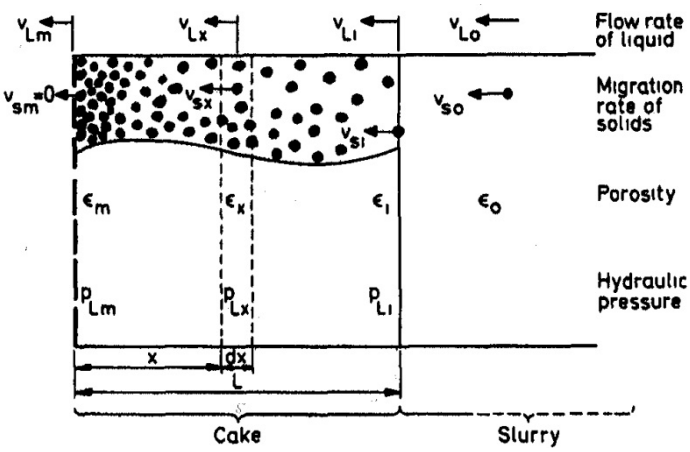

Figure 4.1: Schematic diagram of growing filter cake, (Wakeman, 1978).

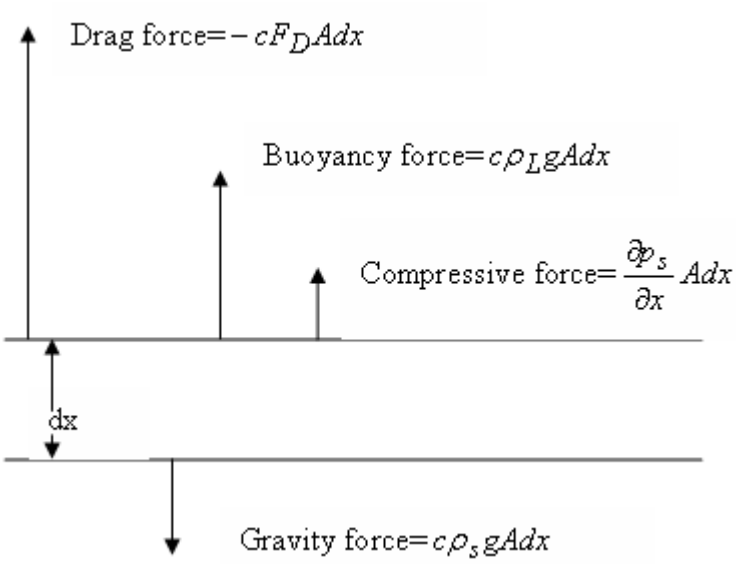

Figure 4.2: Forces acting on the solids in an element of thickness dx.

4.3 MATHEMATICAL MODEL

Equations (4.5) and (4.6) can be combined to express the volumetric flux density of the solids relative to the liquid in terms of the local hydraulic pressure gradient. By neglecting gravity effects and putting $P_L = \overline{P}_L$ and $P_s = P - P_L$ where P the liquid pressure at the cake surface is (pump pressure), Darcy's law becomes:

$$v_L - v_S = \frac{k}{\mu(1-c)}\frac{\partial P_L}{\partial x} \tag{4.8}$$

.

The solids velocity is obtained from the solids material balance as:

$$v_s = -\frac{1}{c}\int_0^x \frac{\partial c}{\partial t}dx \tag{4.9}$$

By substituting Equation (4.9) into Equation (4.8), an expression for the liquid velocity at any given distance from the filter cloth is given by:

$$v_L = \frac{k}{\mu(1-c)}\frac{\partial P_L}{\partial x} - \frac{1}{c}\int_0^x \frac{\partial c}{\partial t}dx \tag{4.10}$$

.

As a result of continuity, at all points within the cake,

$$\begin{aligned}(1-c)v_L + cv_S &= (1-c_m)v_{lm} \\ &= \left(\frac{k}{\mu}\frac{\partial P_L}{\partial x}\right)_{x=0}\end{aligned} \tag{4.11}$$

where c_m is the volume fraction of solids at the medium surface and v_{lm} is the liquid flux in the pores at that point. By assuming there is no loss of solids through bleeding $v_{sm} = 0$, the partial integro differential equation describing liquid movement and cake volume change can then be obtained by rewriting Equation (4.11) using Equations (4.9) and (4.10) as:

$$\frac{1}{c}\int_0^x \frac{\partial c}{\partial t}dx = \frac{k}{\mu}\frac{\partial P_L}{\partial x} - \left(\frac{k}{\mu}\frac{\partial P_L}{\partial x}\right)_{x=0} \tag{4.12}$$

An alternative form can be obtained by differentiating with respect to x:

$$\frac{\partial c}{\partial t} = \frac{\partial}{\partial x}\left(\frac{ck}{\mu}\frac{\partial P_L}{\partial x}\right) - \left(\frac{k}{\mu}\frac{\partial P_L}{\partial x}\right)_{x=0}\frac{\partial c}{\partial x} \tag{4.13}$$

or by differentiating Equation (4.11) with respect to x and using Equations (4.9) and (4.10):

$$\frac{\partial}{\partial x}\left(\frac{k}{\mu}\frac{\partial P_L}{\partial x}\right)=\frac{\partial}{\partial x}\left(\frac{1}{c}\int_0^x\frac{\partial c}{\partial x}dx\right) \tag{4.14}$$

Equation (4.14) assumes that the filter medium resistance is negligible compared with cake resistance. It avoids the entry conditions at the cake/filter medium interface and underlines the importance of any interfacial effects of the cloth structure on cake properties.

4.4 SOLUTIONS OF FILTRATION EQUATIONS

The solutions of the above equations depend on the quantity of measured information that is available. That is the average porosity as well as the liquid pressure profiles within the cake.

4.4.1 Solution of a dimensionless filtration equation

The suspended solids are initially considered to be evenly distributed throughout the liquid thus forming slurry with a volume fraction of solids $(1-\varepsilon_0)$. After the start of filtration, a cake deposits on the medium with a porosity that varies from ε_m at the filter medium surface to ε_0 at the cake/slurry interface. The initial and boundary conditions governing Equations (4.12) to (4.14) are:

$$\varepsilon=\varepsilon_0 \text{ at } t=0 \text{ for all } x \tag{4.15}$$

$$\varepsilon=\varepsilon(0,t)=\varepsilon_m \text{ at } x=0 \text{ for all } t \tag{4.16}$$

$$\varepsilon=\varepsilon(x(t),t)=\varepsilon_i \text{ at } x=x(t)=x_i \text{ for all } t \tag{4.17}$$

As the location of the moving cake/slurry is unknown a further condition is required. By denoting the flow rate of liquid reaching the cake surface accompanied by dw of solid mass by v_{l0}, where

$$\varepsilon_0 v_{l0} = \frac{1-s}{\rho_l s}\frac{dw}{dt}$$

$$= \frac{\varepsilon_0}{\rho_l(1-\varepsilon_0)}\frac{dw}{dt} \tag{4.18}$$

where s is the mass fraction of solids in the feed slurry. If the porosity of the cake surface is ε_i and dL is the increase of cake thickness in time dt, a part of the liquid volume reaching the cake surface stays in the surface layer $(\varepsilon_i dL')$ and the excess liquid flows into the cake, then :

$$\varepsilon_i v_{li} = \varepsilon_0 v_{l0} - \varepsilon_i \frac{dL'}{dt} \tag{4.19}$$

By assuming the flow to be Darcian, liquid leaving the surface will obey Darcy's law and liquid flow in the slurry is related to the mass rate of solids so that:

$$\frac{k_i}{\mu}\frac{\partial P_l}{\partial x}\bigg|_{x_i} - \frac{\varepsilon_i}{1-\varepsilon_i}\int_0^{x_i}\frac{\partial c}{\partial t}dx = \frac{\varepsilon_0}{\rho_s(1-\varepsilon_0)}\frac{dw}{dt}\bigg|_{x_i} - \varepsilon_i\frac{dL'}{dt} \tag{4.20}$$

To further understand the final term in Equations (4.19) and (4.20) consider Figure 4.3 which depicts the cake at times t and $t+dt$.

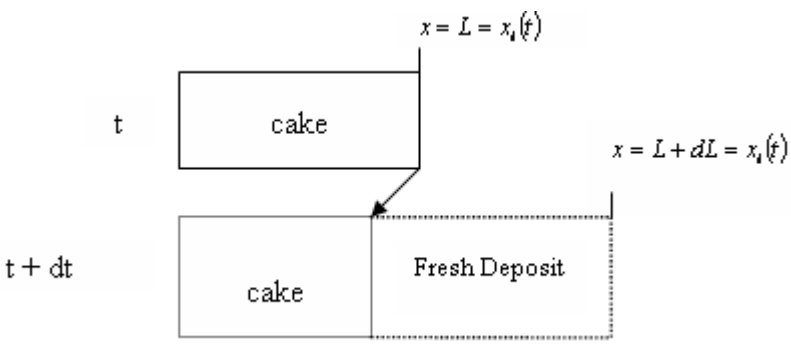

Figure 4.3: Schematic illustrating layer by layer cake deposit.

During dt the cake has compacted whilst further solids were being added, therefore the rate of volume deposit of cake (including both solids and liquid) is:

$$\frac{dL'}{dt} = \frac{dL}{dt} - \left(\frac{\partial x}{\partial t}\right)_{x=L} \tag{4.21}$$

$\partial x/\partial t$ is negative indicating the consolidation of the cake of depth L at time t. The left hand side of Equation (4.20) is the flux of liquid leaving the surface layer by Darcy's law and the first term on the right hand side is flux of liquid entering the layer from the slurry. $(dw/dt)_{x_i}$ is the mass of solids added to the cake. Rearranging Equation (4.20) gives:

$$\left.\frac{\partial P_l}{\partial x}\right|_{x_i} = \frac{\mu}{k_i}\left\{\frac{\varepsilon_i}{1-\varepsilon_i}\int_0^{x_i}\frac{\partial c}{\partial t}dx + \frac{\varepsilon_0}{\rho_s(1-\varepsilon_0)}\left.\frac{dw}{dt}\right|_{x_i} - \varepsilon_i\frac{dL'}{dt}\right\} \tag{4.22}$$

Using the chain rule with Equation (4.1) and substituting into Equation (4.21) gives:

$$\frac{dL'}{dt} = \frac{dL}{dt} + v_{si} + c_i\frac{\partial v_{si}}{\partial c} \tag{4.23}$$

Noting that

$$v_{si} = -\frac{1}{c_i}\int_0^{x_i}\frac{\partial c}{\partial t}dx \tag{4.24}$$

It follows that

$$\frac{dL'}{dt} = \frac{dL}{dt} - \frac{1}{c_i}\int_0^{x_i}\frac{\partial c}{\partial t}dx - \frac{\partial}{\partial c}\int_0^{x_i}\frac{\partial c}{\partial t}dx \tag{4.25}$$

For the freshly deposited cake we have

$$\left.\frac{dw}{dt}\right|_{x_i} = \rho_s\left(1-\varepsilon_i\right)\frac{dL'}{dt} \tag{4.26}$$

Using Equations (4.21), (4.23) and (4.26) in Equation (4.22) gives:

$$\left.\frac{\partial P_l}{\partial x}\right|_{x_i} = \frac{\mu}{k_i}\left\{\frac{\varepsilon_i}{1-\varepsilon_i}\int_0^{x_i}\frac{\partial c}{\partial t}dx + \frac{\varepsilon_0-\varepsilon_i}{1-\varepsilon_0}\frac{dL'}{dt}\right\}$$

$$= \frac{\mu}{k_i}\left\{\frac{\varepsilon_0-\varepsilon_i\left(2-\varepsilon_0\right)}{1-\varepsilon_0}v_{si} + \frac{\varepsilon_0-\varepsilon_i}{1-\varepsilon_0}\left(\frac{dL}{dt}+\left(1-\varepsilon_i\right)\frac{\partial v_{si}}{dc}\right)\right\} \tag{4.27}$$

Equation (4.27) is the moving boundary condition to be satisfied at the cake surface; it can be approximated when the term $\frac{\varepsilon_0-\varepsilon_i}{1-\varepsilon_0}\frac{dL'}{dt}$ is greater than the other two terms on the right hand side by:

$$\left.\frac{\partial P_l}{\partial x}\right|_{x_i} \approx \frac{\mu}{k_i}\frac{\varepsilon_0-\varepsilon_i}{1-\varepsilon_0}\frac{dL'}{dt} \tag{4.28}$$

as originally suggested by Wakeman (1978).

Using dimensionless porosity and time defined by:

$$\varepsilon^* = \frac{\varepsilon-\varepsilon_m}{\varepsilon_i-\varepsilon_m} \tag{4.29}$$

$$\theta = \frac{E_i t}{x_i^{\ 2}} \tag{4.30}$$

where E_i is the compressibility coefficient at the cake/slurry interface, a dimensionless distance from the filter cloth,

$$b = x/x_i \tag{4.31}$$

and introducing a similarity variable

$$\lambda = b/\sqrt{\theta} \tag{4.32}$$

equations (4.13), (4.16), (4.17) and (4.28) become

$$\frac{\partial^2 \varepsilon^*}{\partial \lambda^2} + \frac{\partial \ln F(\varepsilon^*)}{\partial \varepsilon^*}\left(\frac{\partial \varepsilon^*}{\partial \lambda}\right)^2 + \frac{1}{F(\varepsilon^*)}\left(\frac{E_m}{E_i}\cdot\frac{\varepsilon_i - \varepsilon_m}{1-\varepsilon_m}\cdot\left.\frac{\partial \varepsilon^*}{\partial \lambda}\right|_{\lambda=0} + \frac{\lambda}{2}\right)\frac{\partial \varepsilon^*}{\partial \lambda} = 0 \tag{4.33}$$

$$\lambda = 0\,,\, \varepsilon^* = 0 \tag{4.34}$$

$$\lambda = \lambda_i\,,\ \varepsilon^* = 1 \tag{4.35}$$

$$\left.\frac{\partial \varepsilon^*}{\partial \lambda}\right|_{\lambda_i} = \frac{\lambda_i}{2}\cdot\frac{\varepsilon_0 - \varepsilon_i}{\varepsilon_i - \varepsilon_m}\cdot\frac{1-\varepsilon_i}{1-\varepsilon_0} \tag{4.36}$$

respectively, where

$$E = \frac{k(1-\varepsilon)}{\mu}\frac{\partial p_L}{\partial \varepsilon} \tag{4.37}$$

and

$$F(\varepsilon^*) = E/E_I \tag{4.38}$$

E is a variable of compressibility coefficient used to express the behaviour of a cake formed from slurry of a particular solids concentration at a particular filtration pressure, and $F(\varepsilon^*)$ is the normalised compressibility coefficient. The compressibility coefficient can be expressed in terms of filtration resistance:

$$E = \frac{1}{\alpha \rho_s \mu}\frac{\partial p_l}{\partial \varepsilon} \tag{4.39}$$

from out of which

$$F\left(\varepsilon^{*}\right)=\frac{\alpha_i}{\alpha}\frac{\partial p_l/\partial\varepsilon}{\partial p_l/\partial\varepsilon\big|_{x_i}} \tag{4.40}$$

where α is the specific cake resistance.

4.5 CLOSURE

In this chapter, the governing equations used in this study have been discussed. The assumptions and boundary conditions were also discussed. The equations are now ready to be discretized. The discretization of the working equations will be discussed in the next chapter

.

Chapter 5 : NUMERICAL METHOD

5.1 INTRODUCTION

This chapter describes the numerical scheme employed to solve the differential equation describing constant pressure filtration. A computer program was written with the aid of a flow sheet and a calculation scheme. The calculation steps were divided into three sections; that is the calculation of porosity, relating specific cake resistance to porosity and finally relating calculated porosity to liquid pressure. Initial estimation of variables was done in order to validate the chosen solution scheme. Predicted results were compared to hand calculations and were found to be in agreement. This showed that the employed solution scheme was correct as they gave reliable initial predictions.

5.2 CALCULATION OF LOCAL PROPERTIES

5.2.1 Calculation of local porosity

The equation to be solved is stated below as Equation (5.1) with its necessary boundary conditions Equations (5.2)-(5.4).

$$\frac{d^2\varepsilon^*}{\partial\lambda^2}+\frac{d\ln F\left(\varepsilon^*\right)}{\partial\varepsilon^*}\left(\frac{d\varepsilon^*}{\partial\lambda}\right)^2+\frac{1}{F\left(\varepsilon^*\right)}\left(\frac{E_m}{E_i}\cdot\frac{\varepsilon_i-\varepsilon_m}{1-\varepsilon_m}\cdot\left.\frac{d\varepsilon^*}{\partial\lambda}\right|_{\lambda=0}+\frac{\lambda}{2}\right)\frac{d\varepsilon^*}{\partial\lambda}=0 \quad (5.1)$$

$$\lambda=0\,,\,\varepsilon^*=0 \quad (5.2)$$

$$\lambda=\lambda_i\,,\;\varepsilon^*=1 \quad (5.3)$$

$$\left.\frac{d\varepsilon^*}{\partial\lambda}\right|_{\lambda_i}=\frac{\lambda_i}{2}\cdot\frac{\varepsilon_0-\varepsilon_i}{\varepsilon_i-\varepsilon_m}\cdot\frac{1-\varepsilon_i}{1-\varepsilon_0} \quad (5.4)$$

where

$$E = \frac{k(1-\varepsilon)}{\mu}\frac{\partial p_l}{\partial \varepsilon} \tag{5.5}$$

and

$$F(\varepsilon^*) = E/E_I = \exp[a(1-\varepsilon^*)] \tag{5.6}$$

$$\varepsilon^* = \frac{\varepsilon - \varepsilon_m}{\varepsilon_i - \varepsilon_m} \tag{5.7}$$

E, is a variable of compressibility coefficient used to express the behaviour of a cake formed from a slurry of a particular solids concentration at a particular filtration pressure, and $F(\varepsilon^*)$ is the normalised compressibility coefficient. The compressibility coefficient can be expressed in terms of filtration resistance:

$$E = \frac{1}{\alpha \rho_s \mu}\frac{dp_l}{d\varepsilon} \tag{5.8}$$

from out of which

$$F(\varepsilon^*) = \frac{\alpha_i}{\alpha}\frac{dp_l/d\varepsilon}{dp_l/d\varepsilon|_{x_i}} \tag{5.9}$$

Equation (5.1) was to be solved using the fourth order Runge Kutta Nystrom method as suggested by Kreyszig (1993) subject to boundary conditions (5.2)-(5.4). To solve second order ODE problems of the form $y'' = f(x, y, y')$, the Runge Kutta Nystrom method was chosen as it offered a more accurate method as compared to other numerical integration methods such as Euler's method. In the general step, the $(n+1)^{th}$ step, of the method the auxiliary points are first calculated, that is

$$A_n = \frac{h}{2} f(x_n, y_n, y_n') \tag{5.10}$$

where the terms (x_n, y_n, y_n') are $(\lambda, \varepsilon^*, d\varepsilon^*/d\lambda)$respectively in Equation (5.1).

$$B_n = \frac{h}{2} f\left(x_n + \frac{h}{2}, y_n + \beta_n, y_n' + A_n \right) \tag{5.11}$$

where $\beta_n = \frac{h}{2}\left(y_n' + \frac{A_n}{2} \right)$ (5.12)

$$C_n = \frac{h}{2} f\left(x_n + \frac{h}{2}, y_n + \beta_n, y_n' + B_n \right) \tag{5.13}$$

$$D_n = \frac{h}{2} f\left(x_n + h, y_n + \delta_n, y_n' + 2C_n \right) \tag{5.14}$$

where $\delta_n = \frac{h}{2}\left(y_n' + C_n \right)$ (5.15)

After the above values were computed then the new values

$$y_{n+1} = y_n + h\left(y_n' + K_n \right) \tag{5.16}$$

where

$$K_n = \frac{1}{3}\left(A_n + B_n + C_n \right) \tag{5.17}$$

which is an approximation for $y(x_{n+1})$ and

$$y'_{n+1} = y_n' + K_n * \tag{5.18}$$

where

$$K_n* = \frac{1}{3}\left(A_n + 2B_n + 2C_n + D_n \right) \tag{5.19}$$

which is an approximation for $y'(x_{n+1})$ needed in the next step is obtained. It should be noted that $y_n' = d\varepsilon * / d\lambda$ and $y_n = \varepsilon *$ as previously stated.

5.2.2 Relating cake permeability and specific cake resistance to porosity

Noting that α is given by

$$\alpha = \frac{1}{\rho_s (1-\varepsilon) k} \tag{5.20}$$

Therefore

$$\frac{\alpha_i}{\alpha} = \frac{(1-\varepsilon)k}{(1-\varepsilon_i)k_i} \tag{5.21}$$

By introducing the cell model,

$$k = \frac{d^2}{36} \frac{6 - 9(1-\varepsilon)^{\frac{1}{3}} + 9(1-\varepsilon)^{\frac{5}{3}} - 6(1-\varepsilon)^2}{(1-\varepsilon)\left(3 + 2(1-\varepsilon)^{\frac{5}{3}}\right)} \tag{5.22}$$

and noting that d is constant for any suspension for all x, t, Equation (5.21) therefore becomes

$$\frac{\alpha_i}{\alpha} = \frac{6 - 9(1-\varepsilon)^{\frac{1}{3}} + 9(1-\varepsilon)^{\frac{5}{3}} - 6(1-\varepsilon)^2}{6 - 9(1-\varepsilon_i)^{\frac{1}{3}} + 9(1-\varepsilon_i)^{\frac{5}{3}} - 6(1-\varepsilon_i)^2} \cdot \frac{3 + 2(1-\varepsilon_i)^{\frac{5}{3}}}{3 + 2(1-\varepsilon)^{\frac{5}{3}}} \tag{5.23}$$

and cake permeability and cake resistance can hence be estimated. In the Happel-cell model it is assumed that the filter cake can be divided into a number of cells, each of which contains two concentric spheres. The inner one is solid and the outer is fluid, furthermore, the particle sizes are considered to be uniform in the slurry, (Happel & Brenner 1965).

5.2.3 Relating porosity to liquid pressure

From the solution of Equation (5.1), the average porosity, ε_{av} was determined as

$$\varepsilon_{av} = \frac{1}{L}\int_0^L \varepsilon dx \tag{5.24}$$

Then from Equation (5.24), average solidosity, c_{av},

$$c_{av} = 1 - \varepsilon_{av} = 1 - \frac{1}{L}\int_0^L \varepsilon dx \tag{5.25}$$

It was also possible to calculate the value of , *x*, from

$$\lambda = \frac{x}{L} \tag{5.26}$$

therefore $x = L\lambda$, L can be estimated with the help of Equation (5.27) (Wakeman and Tarleton, 2005).

$$V = \frac{\rho_s\left[1-\left(m_{av}s\right)\right]}{s\left[\rho_s\left(m_{av}-1\right)+\rho_l\right]}AL \tag{5.27}$$

The values of ε^*, x and c_{av} are now known. As previously stated, the data was in the form of $\left(P_l, x\right)_t$ and hence a further relationship between porosity and liquid pressure to relate the model to the experimental data needed to be obtained. By using a functional form of $F\left(\varepsilon^*\right)$ one obtained:

$$F\left(\varepsilon^*\right) = \exp\left[a\left(1-\varepsilon^*\right)\right] = \frac{E}{E_i} = \frac{k_x}{k_i}\frac{1-\varepsilon_x}{1-\varepsilon_i}\frac{dP_L/d\varepsilon\big|_x}{dP_L/d\varepsilon\big|_i} \tag{5.28}$$

Rearranging Equation (5.28) with the use of Equation (5.7) one obtained:

$$a\left(1-\frac{\varepsilon-\varepsilon_m}{\varepsilon_i-\varepsilon_m}\right)=\ln\left(\frac{k_x}{k_i}\frac{1-\varepsilon_x}{1-\varepsilon_i}\frac{dP_l/\partial\varepsilon\big|_x}{dP_l/d\varepsilon\big|_i}\right) \tag{5.29}$$

From Equation (5.29) the only unknown was $dP_l/d\varepsilon\big|_x$. On rearrangement of Equation (5.29) one obtained:

$$\frac{dP_l}{d\varepsilon}\bigg|_x=\frac{k_i}{k_x}\frac{1-\varepsilon_i}{1-\varepsilon_x}dP_L/d\varepsilon\big|_i\exp\left[a\left(1-\varepsilon^*\right)\right]=\frac{\Delta P}{\Delta\varepsilon}=\frac{P_{l_{x+1}}-P_{l_x}}{\varepsilon_{x+1}-\varepsilon_x} \tag{5.30}$$

and from this it was then possible to get a value of liquid pressure from the model and compare it to experimental data. The criteria for comparison was by minimising the variance between the experimental and theoretical liquid pressures, that is

$$\frac{1}{n-1}\sum_{i=1}^{n}\left(P_{l_x(\exp erimental)}-P_{l_x(theoretical)}\right)^2 \tag{5.31}$$

and thus it was assumed that the correct combination of $F\left(\varepsilon^*\right)$ and $d\varepsilon^*/d\lambda$ had been obtained.

5.3 FOURTH ORDER RUNGE KUTTA NYSTROM DISCRITISATION OF EQUATION 5.1

For the following procedures, it should be noted that $\varepsilon^*=y$ and $\lambda=x$ respectively. In Equation (5.1), the term $\frac{d\ln F\left(\varepsilon^*\right)}{d\varepsilon^*}$ was simplified further to yield $\frac{d\ln e^{[a(1-y)]}}{d\varepsilon^*}$ and on further elimination yielded $\frac{d\left[a\left(1-y\right)\right]}{dy}=-a$. $\frac{E_m}{E_I}$ in Equation (5.1) was approximated to be e^a at the medium.

Rearranging of Equation (5.1) yielded,

$$\frac{d^2y}{dx^2} = \left[\frac{dy}{dx}\right]\left[a\frac{dy}{dx} - e^{ay}\frac{\varepsilon_i - \varepsilon_m}{1-\varepsilon_m}\left.\frac{dy}{dx}\right|_{x=0} - \frac{x}{2e^{[a(1-y)]}}\right] \tag{5.32}$$

Equation (5.32) was further discretised into the Runge Kutta Nystrom steps as follows,

$$A_n = \frac{h}{2}\left[\frac{dy}{dx}\right]\left[a\frac{dy}{dx} - e^{ay}\frac{\varepsilon_i - \varepsilon_m}{1-\varepsilon_m}\left.\frac{dy}{dx}\right|_{x=0} - \frac{x_n}{2e^{[a(1-y)]}}\right] \tag{5.33}$$

$$\beta_n = \frac{h}{2}\left[\frac{dy}{dx} + \frac{A_n}{2}\right] \tag{5.34}$$

$$B_n = \frac{h}{2}\left[\frac{dy}{dx} + A_n\right]\left[\begin{array}{c}\left(a\left(\frac{dy}{dx} + A_n\right)\right) - e^{a(y+\beta_n)}\frac{\varepsilon_i - \varepsilon_m}{1-\varepsilon_m}\left.\frac{dy}{dx}\right|_{x=0} \\ -\frac{x_n + \frac{h}{2}}{2e^{[a(1-(y+\beta_n))]}}\end{array}\right] \tag{5.35}$$

$$C_n = \frac{h}{2}\left[\frac{dy}{dx} + B_n\right]\left[\begin{array}{c}\left(a\left(\frac{dy}{dx} + B_n\right)\right) - e^{a(y+\beta_n)}\frac{\varepsilon_i - \varepsilon_m}{1-\varepsilon_m}\left.\frac{dy}{dx}\right|_{x=0} \\ -\frac{x_n + \frac{h}{2}}{2e^{[a(1-(y+\beta_n))]}}\end{array}\right] \tag{5.36}$$

$$\delta_n = \frac{h}{2}\left[\frac{dy}{dx} + C_n\right] \tag{5.37}$$

$$D_n = \frac{h}{2}\left[\frac{dy}{dx} + 2C_n\right]\left[\begin{array}{l}\left(a\left(\frac{dy}{dx} + 2C_n\right)\right) - e^{a(y+\delta_n)}\,\frac{\varepsilon_i - \varepsilon_m}{1-\varepsilon_m}\,\frac{dy}{dx}\Big|_{x=0} \\ -\frac{x_n + h}{2e^{[a(1-(y+\delta_n))]}}\end{array}\right] \quad (5.38)$$

$$K_n = \frac{1}{3}\left(A_n + B_n + C_n\right) \quad (5.39)$$

$$y_{n+1} = y_n + h\left(y_n' + K_n\right) \quad (5.40)$$

$$K_n^* = \frac{1}{3}\left(A_n + 2B_n + 2C_n + D_n\right) \quad (5.41)$$

$$y'_{n+1} = y_n' + K_n^* \quad (5.42)$$

5.4 STRUCTURE OF THE SIMULATION PROCESS

A computer algorithm was written to aid in the automation of the model. A simplified flowchart is shown in Figure 5.1. The full version of the flow chart is shown in Appendix I. The model worksheet is shown in Appendix II and the written computer algorithm is shown in Appendix IV.

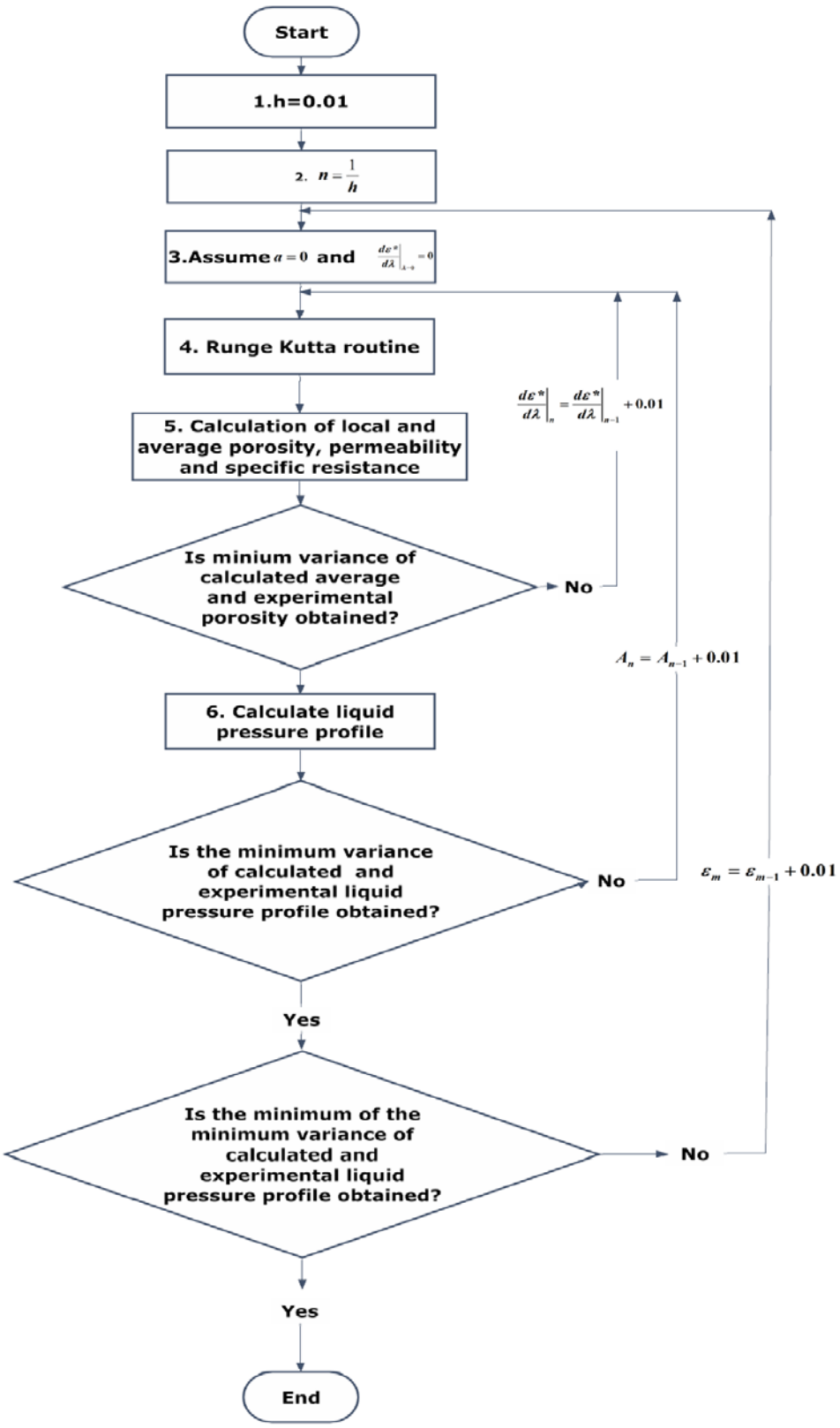

Figure 5.1: Flow diagram of simulation procedure for constant pressure filtration.

5.5 INITIAL ESTIMATION OF VARIABLES

To be able to run the model initially in order to verify that the chosen methodology worked some variables had to be estimated. The variable a was set at 3.076 and $d\varepsilon^*/d\lambda\big|_{\lambda=0}$ at 0.14 obtained from Wakeman (1978). The value of ε_m at $t=0$ was assumed to be 0.4 and constant throughout the filtration. Randomly packed spheres have a porosity of 0.40~0.50 hence it would be safe to assume a value of 0.40 for porosity at the medium. The value of ε_i at $t=0$ is the porosity of the suspension in the first iteration. In Equation (5.28) the values of k_i and k_x can be calculated from Equation (5.22). The values for α_i and α were calculated using Equations (5.20) and (5.23) respectively. The gradient $dP_l/d\varepsilon\big|_i$ was calculated by using Equation (5.43)

$$dP_l/d\varepsilon\Big|_i = \frac{P_{l_x} - P_{l_i}}{\varepsilon - \varepsilon_i} \tag{5.43}$$

Initial results showed that the liquid pressure dropped from the top of the cake towards the bottom of the cake with lowest being observed closest to the filter medium which was expected. Also a porosity gradient was formed with the lowest value of porosity observed at the bottom and highest at the top of the cake. The cake permeability and specific resistance were also what was expected according to theory. A sample calculation is shown using the initial estimates described earlier in Appendix III.

A number of initial simulations were done with *n*, the number of steps, set at *10*, 100 and 1000. It was observed beforehand that when *n* was set at a value of *10* the model was unable to fit the experimental data at the end of filtration as it was deemed to be too coarse. When *n* was set to 1000, the fitting of experimental data was not achieved due to the over fitting which caused the computer to often hang or crash; hence an acceptable value of *n* at 100 was used and this gave acceptable initial results and was thus employed for all simulations.

5.6 GENERAL SEQUENCE OF CALCULATIONS

In section 5.5 initial variables were assumed to be of a certain context. However, as described, this was for verification purposes. Having established that the solution scheme developed worked; the variables a, $d\varepsilon^*/d\lambda\big|_{\lambda=0}$ and ε_m were set at 0-5, 0 and 0.5-0.6 with intervals of 0.01 respectively. These ranges of values were chosen by looking at typical values obtained from the analysis done by Wakeman (1978). His values were found to be in the range of 1.9-3.08 for a and 0.14-0.5 for $d\varepsilon^*/d\lambda\big|_{\lambda=0}$. As a result the values used were deemed to be within a reasonable range. The values of ε_m were set between 0.75 and 0.25 solidosity.

The first step of the solution method was to set the value of a, $d\varepsilon^*/d\lambda\big|_{\lambda=0}$ as 0 and ε_m as 0.25 respectively. These variables were increased at intervals of 0.01 and local values within the cake were calculated at each interval. The second step was to match calculated average porosity values to experimentally obtained ones. The variances between experimental and calculated average porosities were computed. $d\varepsilon^*/d\lambda\big|_{\lambda=0}$ was increased in incremental steps of 0.01 until a minimum in variance was achieved.

Once the calculated porosity values were validated, these values were then used to calculate liquid pressure thus obtaining a liquid pressure profile. The second step was to match calculated liquid pressure profiles to the experimentally determined ones. This was done by computing the variance between the experimental and calculated liquid pressure profiles. The variable a was increased in incremental steps of 0.01 until a minimum of variance between the experimental and calculated liquid pressure profiles was obtained. Once this was achieved, a and $d\varepsilon^*/d\lambda\big|_{\lambda=0}$ were zeroed and ε_m was increased in incremental steps of 0.01 and another combination of a, $d\varepsilon^*/d\lambda\big|_{\lambda=0}$ and ε_m computed. Unique combinations of a, $d\varepsilon^*/d\lambda\big|_{\lambda=0}$ and ε_m that gave the least variance were then obtained as well as the predicted liquid pressure profiles and the local cake properties at different filtration pressures.

The numerical technique employed was the fourth order Runge-Kutta-Nystrom method. The nature of the simulation process was that first the local porosity values were calculated, and then the local cake permeability and specific resistance were related to the calculated local porosity.

5.6.1 Calcite experimental data analysis

Calcite experimental data was analysed initially in order to make sure that the numerical method employed gave reasonable results as compared to the experimental values. The calcite experimental data was such that one was able to have transient values of liquid pressure and volume during cake formation. The calcite properties are shown in Table 5.1.

Table 5.1 Characteristic properties of calcite powder dispersed in distilled water

Parameter	Calcite
50% by Volume particle size (μm)	12.8
Particle shape	Rhomboid
Solids density	2710 kg m^{-3}

The particle size and solids density were used as inputs in the model. The model predictions were then compared to the experimental data and were deemed to be acceptable based on Figure 5.2 which shows the model predictions of liquid pressure history of the forming calcite cake and the experimental data.

The predicted pressure and porosity profiles of a calcite forming cake at 300 kPa were obtained and are shown in Figures 5.3 and 5.4.

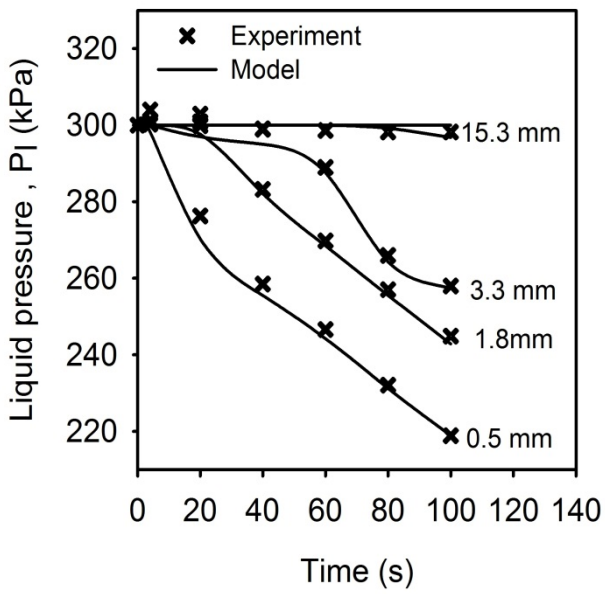

Figure 5.2: Liquid pressure history in a forming calcite cake at a constant filtration pressure of 300 kPa.

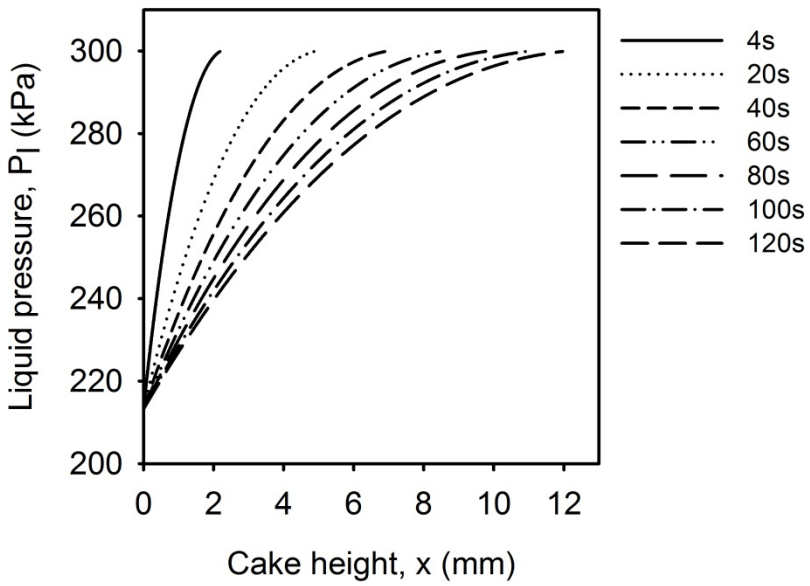

Figure 5.3: Predicted liquid pressure history in a forming calcite cake at a constant filtration pressure of 300 kPa.

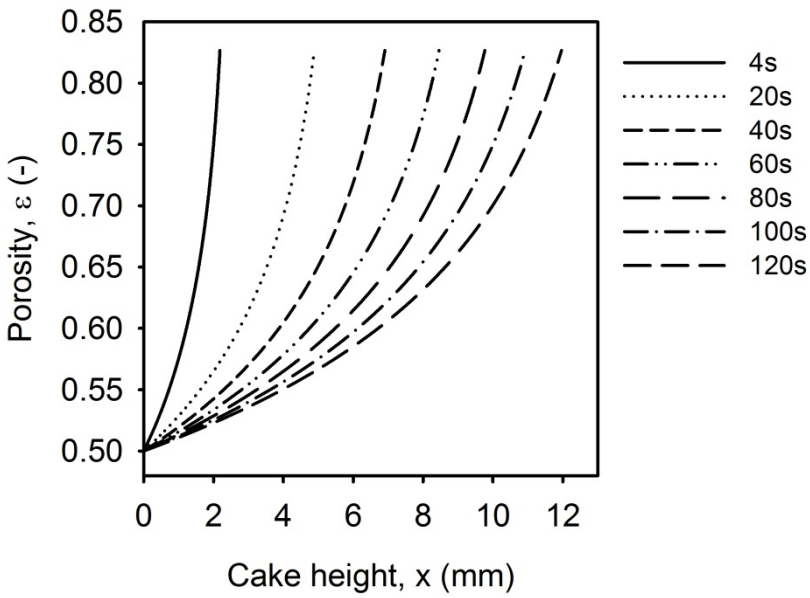

Figure 5.4: Predicted porosity profile in a forming calcite cake at a constant filtration pressure of 300 kPa.

An obvious advantage of having experimental liquid pressure profile history data was that one was then able to analyse the experimental data at different times of the filtration process which would give an insight into the finer details of cake formation.

5.7 CONCLUSIONS

The main governing equations have been described in detail and discretised according to the solution scheme employed, and some model inputs determined. A flow sheet showing how the computer code works has also been described in detail. The general sequence of calculations has been explained in detail. The written computer code with the aid of Microsoft excel was then used in the next chapter to aid in the analysis of constant pressure filtration data.

Chapter 6 : RESULTS AND DISCUSSIONS

6.1 INTRODUCTION

The results obtained from the constant pressure filtration discussed in Chapter 4 will be analysed using the model developed in Chapter 5. The theory of the model has been discussed in detail previously; the calculated filter cake properties are obtained and compared to experimental ones. The liquid pressure profiles are obtained from the model and are compared to the experimentally obtained values. A computer code written in visual basic has been developed and modified at different stages to help better understand the constant pressure filtration. The experimental data used was that of constant pressure filtration of talc and calcite suspensions. The concentration of solids in the feed suspension was 5% V/V at 400 kPa applied pressure. The experimental data was in the form of liquid pressure against time.

6.2 VALIDATION OF THE USE OF THE SIMILARITY VARIABLE

To verify the validity of using the similarity variable λ, Equation 4.32 was expanded and a final form obtained as Equation 6.1

$$\lambda = x \big/ \sqrt{E_i t} \tag{6.1}$$

For different times, the liquid pressure profiles were plotted against $x \big/ \sqrt{t}$ as shown in Figure 6.1.

It can be seen that the use of the similarity variable on the experimental data shows that for different times the internal liquid pressure profiles follow a similar trend bar the initial periods of filtration ~ 5 s which would seem to support the notion that filtration propertied change in the initial periods of filtration as compared to the later ones; hence the use of the similarity variable is valid. The same was observed for different experimental data at different filtration pressures.

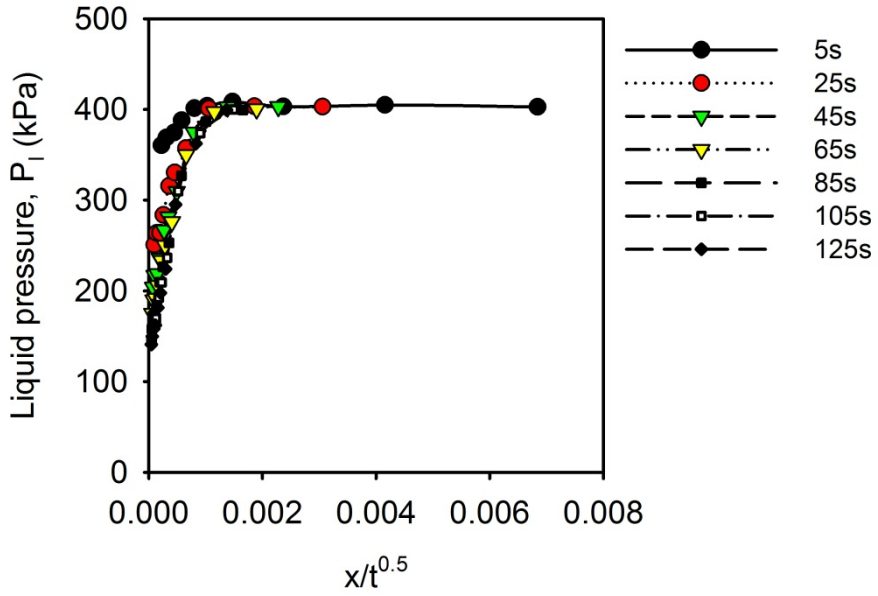

Figure 6.1: Plot of P_l vs. $x/\sqrt{t}$ at different times for 400 kPa filtration pressure.

6.3 FITTING OF MODEL TO EXPERIMENTAL DATA

The objective of the on-going work was to analyse existing constant pressure filtration experimental data using the written code. This would be done by comparing predicted liquid pressure profiles to experimental ones by a technique of minimisation of variance and in so doing one would be able to determine the exact values of the changing parameters, a, $d\varepsilon^*/d\lambda|_{\lambda=0}$ and ε_m which are variables in Equations 5.1, 5.2 and 5.3 and establish trends with varying pressures.

The calculation process as previously described was divided into three parts which helped in providing greater insight as to what is happening within the formed cake. The first part was to obtain porosity distribution within the cake, the second part was to obtain internal cake properties that is; the local porosity, specific cake resistance and permeability profiles. The third part was to obtain the liquid pressure from the calculated porosity. This was done by solving Equation 5.1 subject to conditions 5.2-5.4 and utilising the Runge Kutta Nystrom method of solving second order differential equations.

The criteria for comparison of the experimental data and model data was the minimisation of variances between the experimental average porosity and calculated

average porosity as well as experimental and theoretical liquid pressures, that is; once a minimum had been obtained it was assumed that the correct combination of $F(\varepsilon^*)$ and $d\varepsilon^*/d\lambda\big|_{\lambda=0}$ had been obtained.

6.3.1 Minimisation results for talc suspension at 400 kPa

Experimental data for the constant pressure filtration of a talc suspension was analysed. The calculation criteria was employed as described above and typical results are observed in Figures 6.2 and 6.3 which show the minimisation of variances obtained by running the simulation at 400 kPa. Figure 6.2 shows the ranges of variable a and the values of variance obtained. It can be seen a minimum of the variance does occur at a value of 3.8. It should be noted that for each respective value of a in Figure 6.2, a plot similar to Figure 6.3 was obtained. It would be cumbersome to show all the minimisations of variance for $d\varepsilon^*/d\lambda\big|_{\lambda=0}$ hence Figure 6.3 is the minimisation of variance with the correct combination of a and predicted ε_m. It can be seen from the Figures 6.2 and 6.3 that a global minimum for the variance is obtained.

This trend was generally observed for all the pressure ranges investigated. A global minima was observed and thus the minimisation of variances showed unique combinations for both a and $d\varepsilon^*/d\lambda\big|_{\lambda=0}$. The results of minimisation and best fit data for all the filtration pressure ranges investigated are shown in Appendix VI.

It is important to remember that the criteria of obtaining what was deemed to be a suitable model fit was done through the minimisation of variance. With the minimisation of variances achieved one was then able to obtain a predicted liquid pressure profile which was matched to an experimental profile and the results are shown in Figure 6.4.

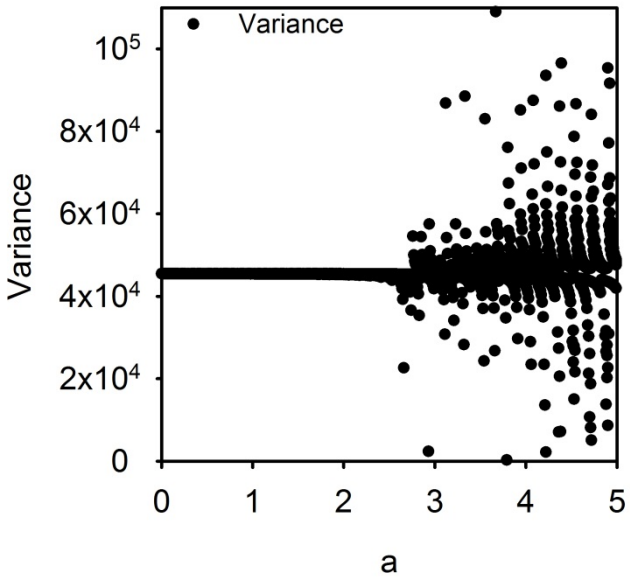

Figure 6.2: Minimisation of variance between calculated and experimental liquid pressure through the increment of variable, a.

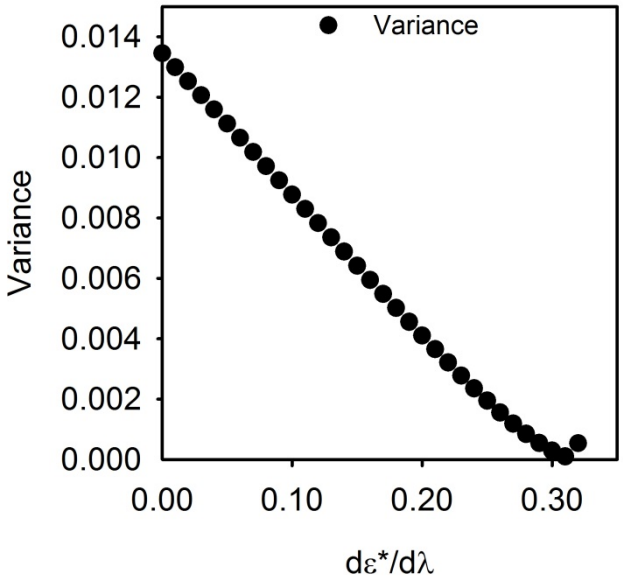

Figure 6.3: Minimisation of variance between calculated and experimental average porosity through the increment of variable, $d\varepsilon^* / d\lambda \big|_{\lambda=0}$.

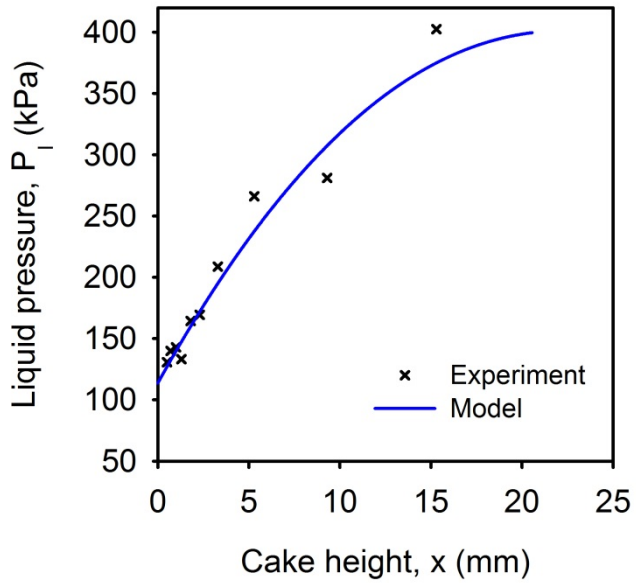

Figure 6.4: Calculated and experimental liquid pressure profiles after minimisation of variance at 400 kPa at end of filtration 185 s. For the experiment the cake height is 15.3 mm, for the model the values of a, $d\varepsilon^* / d\lambda\big|_{\lambda=0}$ and ε_m are 3.79, 0.31 and 0.57.

A comparison between the calculated and the measured liquid pressure profile history is shown in Figure 6.5.

It can be seen from Figure 6.5 that the form of calculated pressure profile is similar to the measured one. The average deviation between the calculated and the measured liquid pressure profiles was $\pm 1\%$. At low applied pressures the deviation was slightly greater than at higher applied pressures.

The experimental data used to initially get the best fit data was at the end of filtration; that is the liquid pressure profiles and the average cake porosity; this was because the model initially required average porosity data as an input for the criteria for minimisation of variance. For average porosity this was only obtainable at the end of filtration. This is important because in later stages of the thesis, the model was continuously updated in order to give more detail in regards to effects of time and those findings discussed.

Initial indications are that the numerical technique employed gave reasonably good fits of the model to experimental data throughout the filtration pressures investigated. This is evident when one looks at Figure 6.4 and 6.5.

Similar trends were observed for the different pressures investigated. It was also worth noting that one obtained best fits at higher pressures. Najafi and Theliander (1995) also observed this trend. A plausible explanation for this is that at higher filtration pressures, the particles tend to form a more rigid compact structure whereas in low filtration pressures the particles form a looser form of packing. One ought to remember that if one had a densely packed structure, the particles would be in their positions; there is no randomness in particle arrangement. However if one had a loosely packed structure the particle arrangement would be random. This is quite evident in Table 6.1 where the average porosity decreases with increase in filtration pressure. At low filtration pressures particles tend to be arranged randomly, as filtration pressure increases more dense closely packed structures tend to be formed. Table 6.1 shows a summary of the results of calculated variables that give the best fit to experimental data after the minimisation criteria.

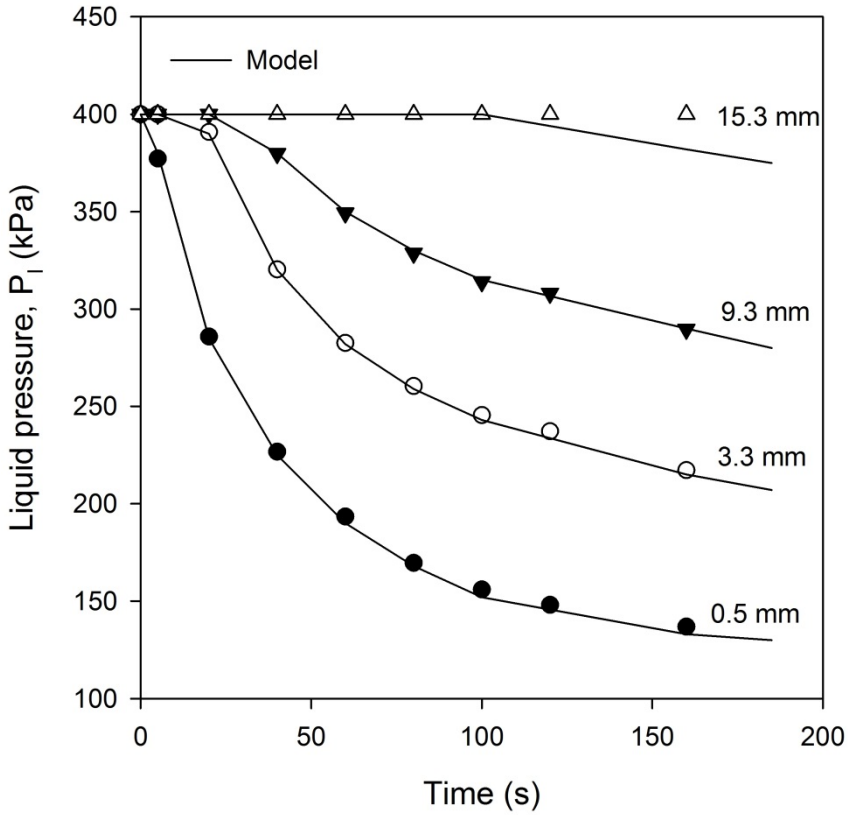

Figure 6.5: A comparison between the calculated and the measured liquid pressure profiles in a talc cake at 400 kPa.

Table 6.1: Results of constant pressure analysis.

ΔP (kPa)	ε_0	ε_{av} Exp	ε_{av} Calc	ε_m Calc	ε_i Calc	a	$d\varepsilon^*/d\lambda\big\|_{\lambda=0}$
100	0.95	0.702	0.704	0.59	0.859	2.22	0.47
150	0.95	0.685	0.689	0.58	0.866	2.90	0.39
300	0.95	0.671	0.677	0.58	0.875	3.78	0.31
400	0.95	0.666	0.670	0.57	0.874	3.79	0.31
500	0.95	0.654	0.663	0.56	0.873	3.80	0.31
600	0.95	0.639	0.647	0.53	0.865	3.46	0.34

A representative graph of the results is shown in Figure 6.6.

It can be seen that in general an increase in filtration pressure has an effect on ε_m, ε_{av}, a and $d\varepsilon^*/d\lambda\big|_{\lambda=0}$. At low pressures, 100-300 kPa, ε_m remains fairly constant at a value of 0.59-0.58, but as pressure gets high, 400-600 kPa, there is a decrease; this could be attributed to some form of particle rearrangement as a result of pressure thus more particles are packed closest to the medium thus changing the nature of packing towards the medium. Regions of cake closest to the medium became more compact due to the drag imparted by the continual flow of liquid through the cake interstices as well as the increasing weight of particles above those already constituting the cake. An increase in filtration pressure also leads to an increase in a and a decrease in $d\varepsilon^*/d\lambda\big|_{\lambda=0}$ generally. The greatest effects of compressibility appear to be at the highest filtration pressure. This is further shown in Figure 6.7 which shows the porosity profiles against normalised cake height. It can be seen in Figure 6.7 that an increase in filtration pressure leads to a reduction in porosity at the medium. It should be noted that this reduction is greatest at the highest filtration pressure if one were to compare between two filtration pressures. It can also be seen that curvature is more pronounced at the highest filtration pressure. This shows the degree of compressibility. With the highest degree of compressibility experienced at the highest filtration pressure.

One would deduce by looking at Figure 6.6 that the plots of a and $d\varepsilon^*/d\lambda\big|_{\lambda=0}$ are mirror images which would infer that they have a relationship in Equation 5.1, thus reducing the number of variables. However in the formulation of Equation 5.1, these two variables are completely independent of each other Wakeman (1978) investigated Hutto's (1965) data of ignition plug cakes, and though he minimised the average porosities and then calculated liquid pressure profiles, it would appear that he obtained a similar trend in plots of a and $d\varepsilon^*/d\lambda\big|_{\lambda=0}$ as can be seen in Figure 6.8. However on closer inspection the values of a decreased with pressure and $d\varepsilon^*/d\lambda\big|_{\lambda=0}$ increased with pressure which was the opposite effect to what was observed in the results obtained from the on-going analysis.

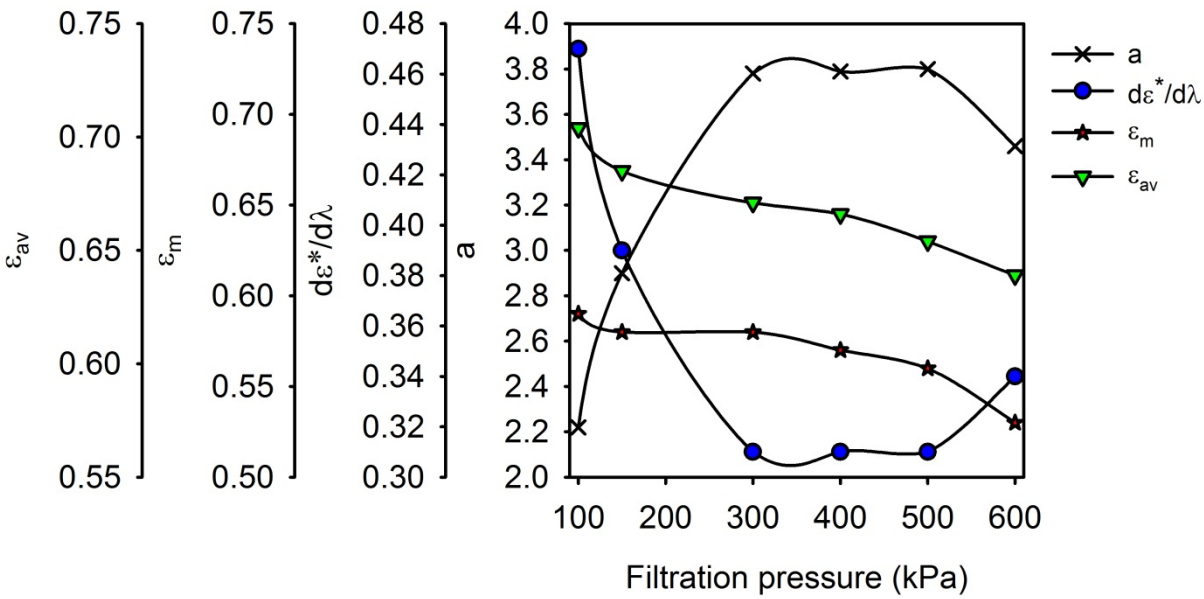

Figure 6.6: Graph of a, $d\varepsilon^*/d\lambda\big|_{\lambda=0}$, ε_m and ε_{av} against filtration pressure.

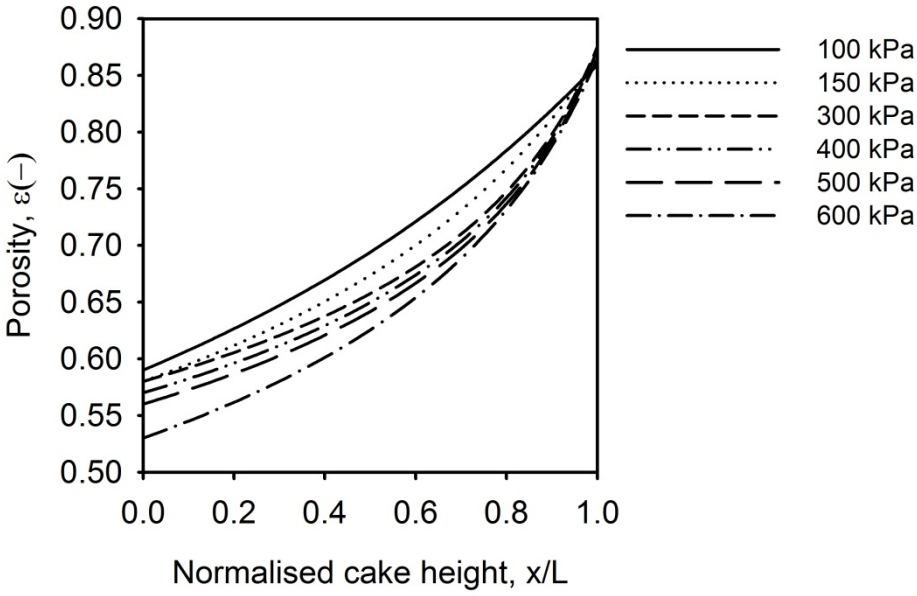

Figure 6.7: Predicted porosity profile at different filtration pressures.

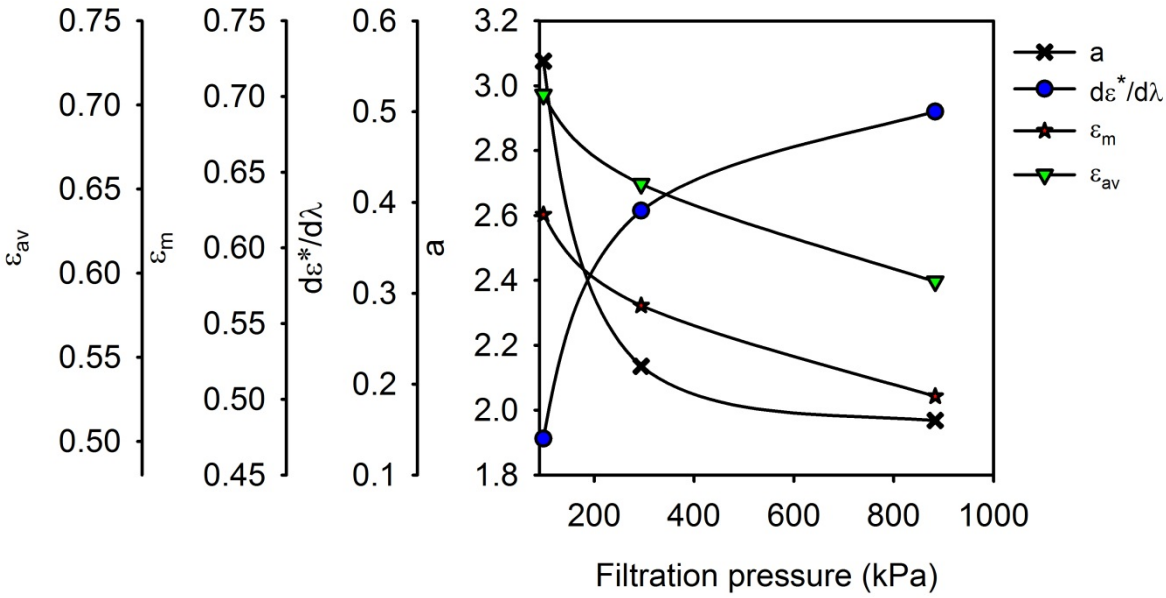

Figure 6.8: Graph of a, $d\varepsilon^{*}/d\lambda\big|_{\lambda=0}$, ε_m and ε_{av} against filtration pressure (Wakeman ,1978).

A closer look at the predicted porosity profiles gave a clue as to why this was occurring. Figure 6.9 shows predicted porosity profiles obtained by Wakeman (1978). On closer observation it can be seen that closest to the medium, the porosity gradients increase

with increase of filtration pressure. Furthermore it can be seen that the effect of compression are great with increase of filtration pressure. This suggests that ignition plug cakes are more compressible as compared to filter cakes formed from a talc suspension. If one looked at Figure 6.7, the increase in porosity gradients closest to the medium for talc are not as pronounced as those of ignition plug cakes except when at high filtration pressures.

Although some initial discussions are given in Wakeman (1978) on a and $d\varepsilon^* / d\lambda\big|_{\lambda=0}$, more experimental data from different particulate systems needs to be accompanied by rigorous analysis in order to under the physical significance of the mentioned variables.

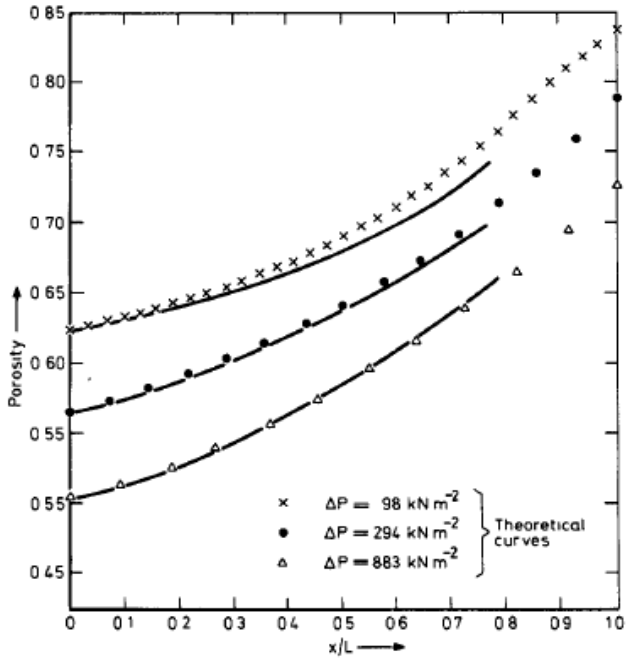

Figure 6.9: Porosity distribution for ignition plug cakes (Wakeman ,1978).

6.3.2 Predicted internal cake properties

With the best fit data obtained it was then deemed necessary to compare model predictions of the cake properties, that is; the specific resistance and permeability. The criterion for obtaining the experimental values has been discussed in an earlier chapter. However for the predicted results from the model, one had to first obtain the cake permeability from the Happel cell model as can be seen in Equation 6.2 and then use Equation 6.3 to obtain the specific resistance

$$k = \frac{d^2}{36} \frac{6 - 9(1-\varepsilon)^{\frac{1}{3}} + 9(1-\varepsilon)^{\frac{5}{3}} - 6(1-\varepsilon)^2}{(1-\varepsilon)\left(3 + 2(1-\varepsilon)^{\frac{5}{3}}\right)} \tag{6.2}$$

$$\alpha = \frac{1}{k(1-\varepsilon)\rho_s} \tag{6.3}$$

The predicted internal cake profiles obtained for Figure 6.4 are shown in Figures 6.9 and 6.10 respectively. Similar results were obtained for the rest of the filtration pressure ranges investigated and this are seen in Appendix VII. The average internal properties obtained from the model were then compared to the experimental data and are seen in Table 6.2.

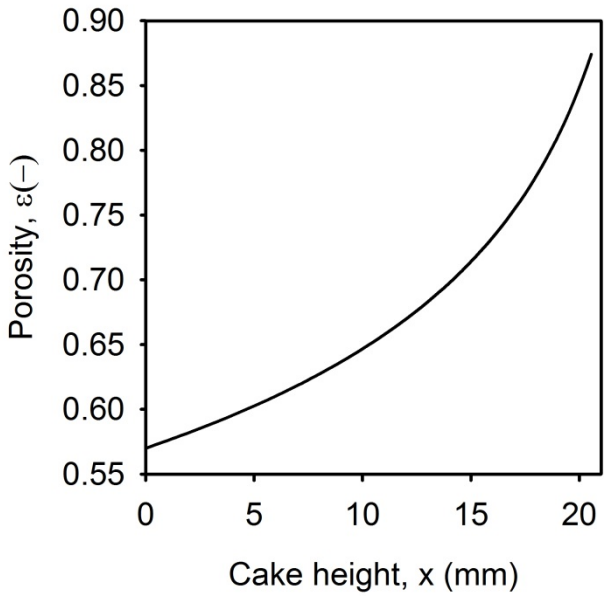

Figure 6.10: Predicted porosity profile after minimisation of variance, talc 400 kPa.

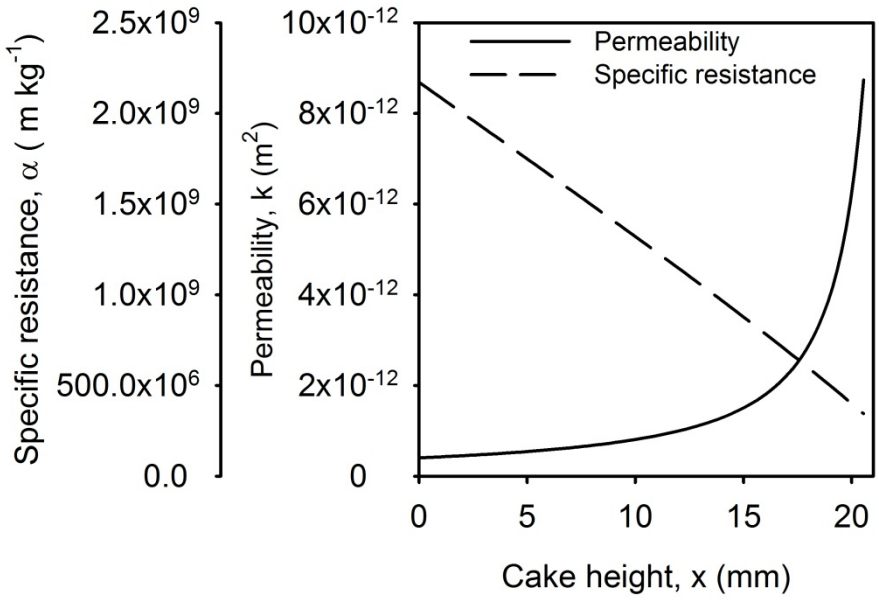

Figure 6.11: Predicted internal permeability and specific resistance after minimisation of variance, talc 400 kPa.

As can be seen in Table 6.2, an increase in pressure leads to a general decrease in average porosity as the cake gets more compact, subsequently the specific cake resistance is seen to increase as permeability decreases as seen above. The calculated internal profiles conform to theory however on closer inspection it was observed that there was a trend emerging where by the prediction of permeability by the model seemed to overestimate permeability by a magnitude of two and as a consequence underestimated the predicted specific cake resistance.

It was rather puzzling as to why this was happening. An initial thought was that the use of experimental average value for porosity was wrong and it was thought that this led to the difference of two orders of magnitude between calculated and experimental specific resistance and permeability hence a value of porosity close to the medium, which would take into account compression effects, was then used to check the effect of using the value of porosity closest to the medium on the specific resistance and permeability as seen in Table 6.3.

Table 6.2: Results of internal properties from constant pressure analysis, Talc using experimental average porosity.

ΔP (kPa)	ε_{av}		α_{av} (m kg^{1})		k_{av} (m^2)	
	Exp	Calc	Exp	Calc	Exp	Calc
100	0.702	0.704	9.84×10^{10}	1.04×10^{9}	1.29×10^{-14}	1.37×10^{-12}
150	0.685	0.689	1.10×10^{11}	1.14×10^{9}	1.09×10^{-14}	1.19×10^{-12}
300	0.671	0.677	1.46×10^{11}	1.22×10^{9}	7.86×10^{-15}	1.07×10^{-12}
400	0.666	0.669	1.48×10^{11}	1.28×10^{9}	7.63×10^{-15}	9.92×10^{-13}
500	0.654	0.663	1.71×10^{11}	1.35×10^{9}	6.38×10^{-15}	9.39×10^{-13}
600	0.639	0.647	2.08×10^{11}	1.54×10^{9}	5.03×10^{-15}	8.12×10^{-13}

Table 6.3: Results of internal properties from constant pressure analysis, Talc using average porosity as that closest to the medium.

ΔP (kPa)	ε_{av}	α_{av} (m kg^{1})		k_{av} (m^2)	
		Exp	Calc	Exp	Calc
100	0.591	9.84×10^{10}	1.89×10^{9}	1.29×10^{-14}	4.90×10^{-13}
150	0.583	1.10×10^{11}	1.99×10^{9}	1.09×10^{-14}	$4..55\times10^{-13}$
300	0.581	1.46×10^{11}	2.02×10^{9}	7.86×10^{-15}	4.47×10^{-13}
400	0.571	1.48×10^{11}	2.16×10^{9}	7.63×10^{-15}	4.08×10^{-13}
500	0.561	1.71×10^{11}	2.31×10^{9}	6.38×10^{-15}	3.72×10^{-13}
600	0.531	2.08×10^{11}	2.84×10^{9}	5.03×10^{-15}	8.12×10^{-13}

Using the porosity value closest to the filter medium did increase the calculated values of specific resistance slightly however specific resistance and permeability were still two orders of magnitude different as is observed in Figure 6.11. To obtain a liquid pressure profile from the model one needs to calculate a value of permeability using Equation 6.2 and thereafter a value of specific resistance was obtained using Equation

6.3. It would appear that the use of Happel cell model over predicts permeability and consequently the values of calculated specific resistance are under predicted.

The calculation of cake height was done by using Equation 6.4 which is derived in Appendix VIII,

$$x = \sqrt{E_i t}\lambda \tag{6.4}$$

where

$$E_i = \frac{k_i(1-\varepsilon_i)}{\mu}\left.\frac{dp_l}{d\varepsilon}\right|_i \tag{6.5}$$

$$\left.\frac{dp_l}{d\varepsilon}\right|_i = \frac{\Delta p - p_{li}}{\varepsilon_i - \varepsilon_x} \tag{6.6}$$

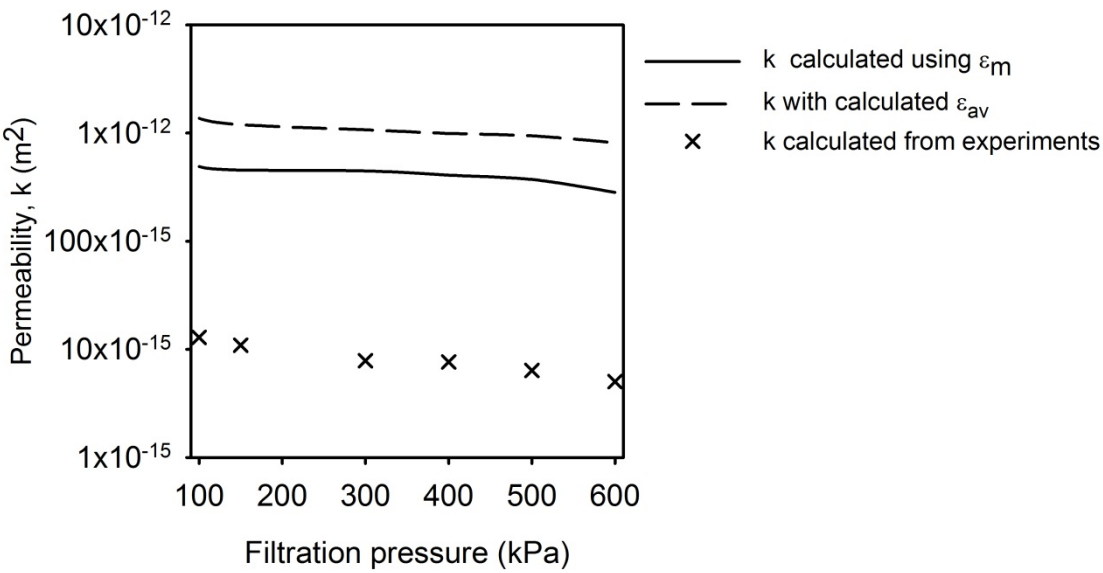

Figure 6.12: Permeability comparisons using cell model and experimental calculation.

Generally the calculated cake heights from the model were past the last point in the experimental data which was the probe at 15.3mm as can be seen in Figure 6.4, it then raised the question of what a cake height is and will be discussed later.

6.4 EFFECTS OF TIME ON THE PREDICTION OF LIQUID PRESSURE PROFILES OF TALC AT 400 kPa

It has been claimed by many researchers that the variables a and $d\varepsilon^* / d\lambda \big|_{\lambda=0}$ are material specific. For this theory to hold, it suggests that these variables do not change with time.

6.4.1 Predicted liquid pressure profiles with ε_m constant for talc at 400 kPa

In order to investigate this theory the variables where kept constant as well as the variable ε_m and time was varied in order to see whether the predicted profiles at different times would match experimental profiles. The predicted liquid pressure and porosity profiles are shown in Figures 6.13 and 6.14 respectively.

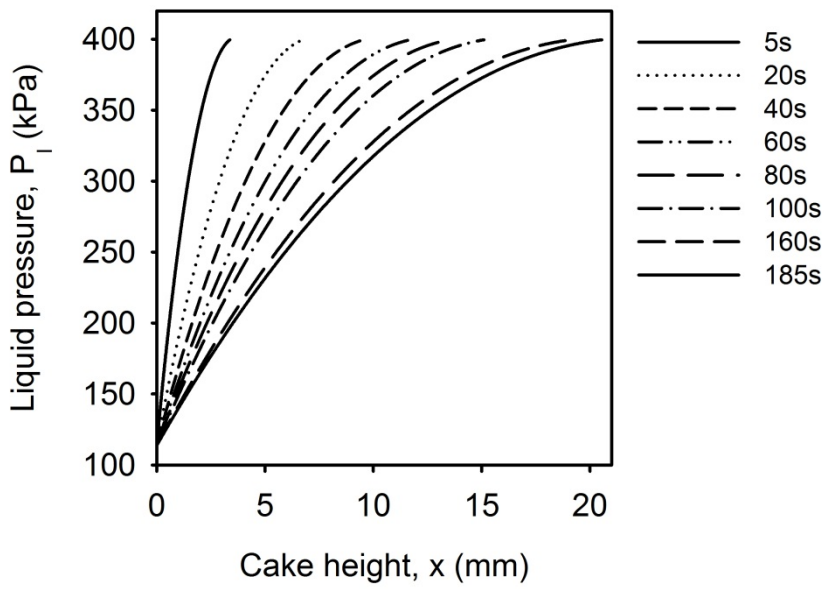

Figure 6.13: Predicted liquid pressure profile, talc at 400 kPa.

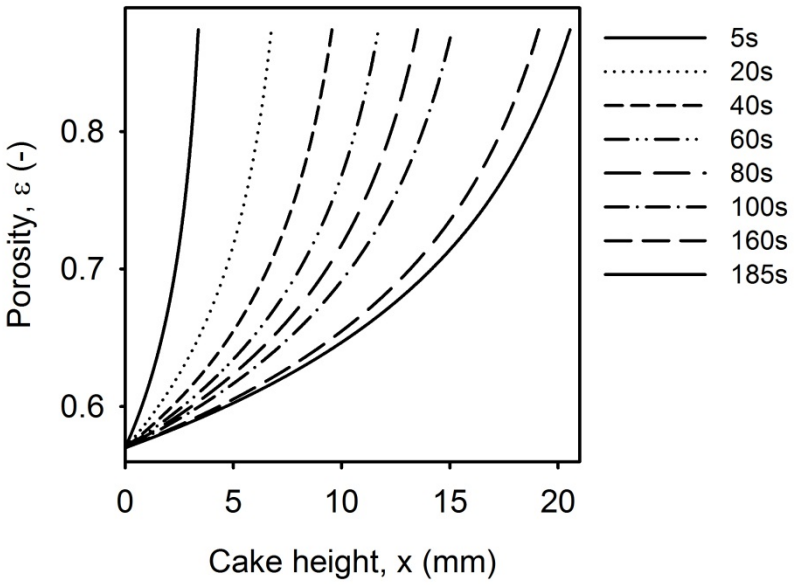

Figure 6.14: Predicted porosity profile, talc at 400 kPa.

In order to confirm if the predicted profiles were similar to experimental ones, the experimental and predicted pressure profiles were plotted at the different times, the plots at 5, 20, 60 and 150 seconds are shown in Figures 6.15-6.18.

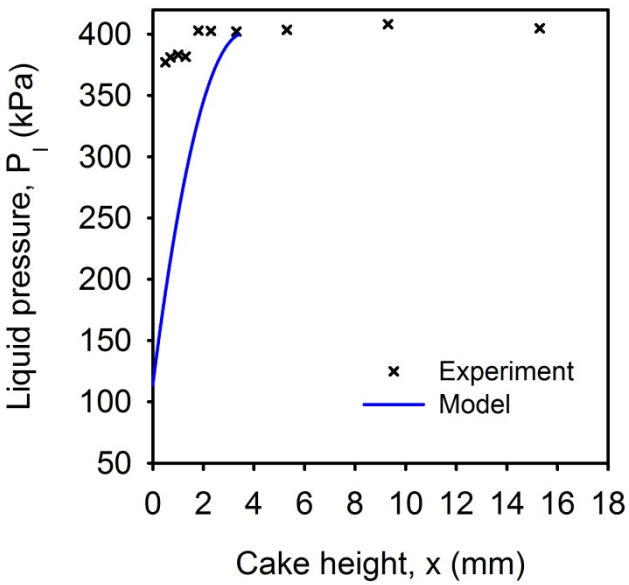

Figure 6.15: Predicted liquid pressure profile, talc at 400 kPa , 5s.

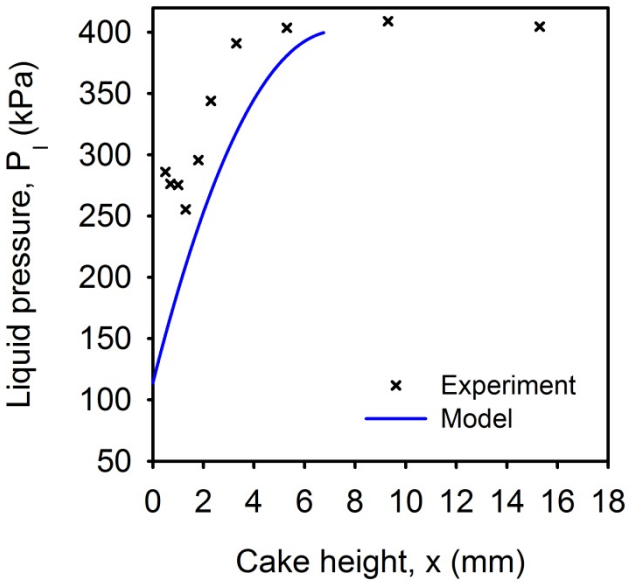

Figure 6.16: Predicted liquid pressure profile, talc at 400 kPa, 20s.

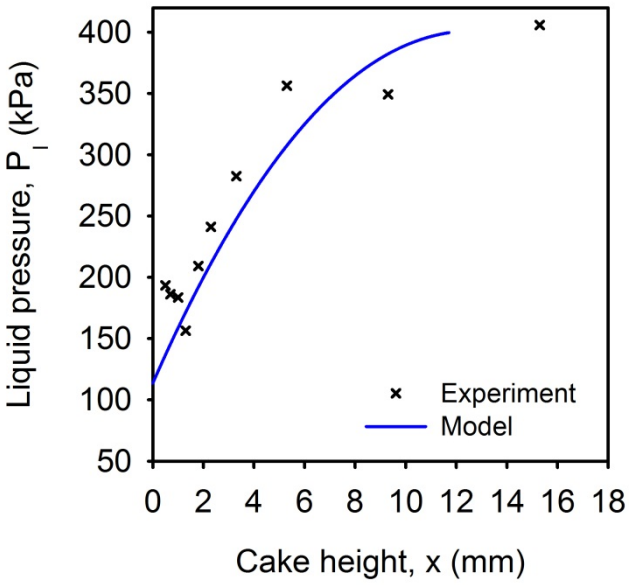

Figure 6.17: Predicted liquid pressure profile, talc at 400 kPa, 60s.

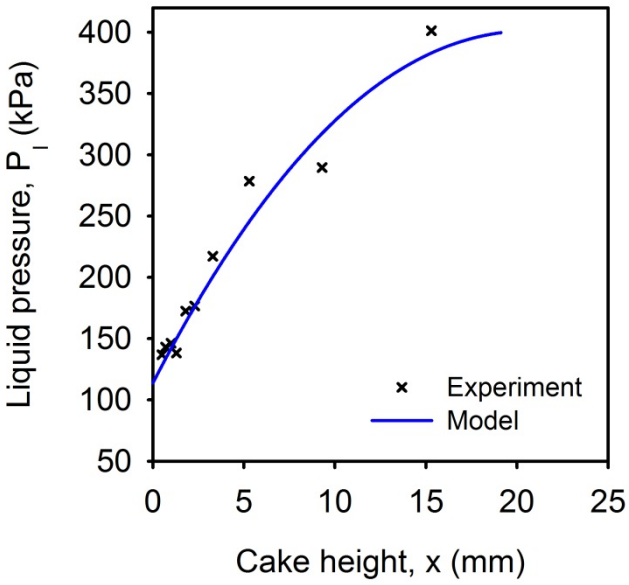

Figure 6.18: Predicted liquid pressure profile, talc at 400 kPa, 150s.

When the variables a, $d\varepsilon^*/d\lambda\big|_{\lambda=0}$ are fixed and ε_m fixed, then for a compressible cake it becomes completely impossible in the initial stages of filtration 5 -20 seconds for one to obtain a reasonable fit as can be seen in Figures 6.15 and 6.16. At the start of a filtration at constant pressure the only resistance to flow is that that is offered by the filter medium. The difference in pressure between the suspension and the filtrate is purely over the medium. When filtration time exceeds zero a deposit of solids occurs on the filter medium. In the initial stages of filtration, the particles at the medium are loosely packed hence one would expect the value of ε_m to be significantly higher than the assumed one at the end of filtration. Also this suggests that the average porosity changes rapidly during this initial phase as rapid deposition of particles on the medium occurs. This was also seen by Koenders and Wakeman (1996) who developed a model to examine the behaviour of the initial stages of cake formation.

At later times, from 60 seconds onwards, the model predictions give a reasonable fit which suggests that at the medium the cake is fully compact, no particle rearrangement is occurring, thus ε_m changes very rapidly in the initial stages at the latter stages it remains fairly constant. Similar trends were observed for the rest of the filtration pressure investigated and can be seen in Appendix IX.

6.4.2 Predicted liquid pressure profiles by varying ε_m for talc at 400 kPa

At this stage the code was modified slightly to account for varying ε_m and simulations were carried out with time changing. Talc suspensions form a slightly compressible cake meaning that the average porosity changes with time. With this in mind the average porosity values were set between 0.50 – 0.95 and ε_m set between 0.25-0.75 and the simulation process was carried out. The predicted pressure and porosity profiles are observed in Figures 6.19 and 6.20 respectively.

In order to confirm if the predicted profiles were similar to experimental ones, the experimental and predicted pressure profiles were plotted at the different times, the plots at 5 and 20seconds are shown in Figures 6.21-6.22.

It can be seen from Figures 6.18-6.19 that the liquid pressure profile when varying ε_m seems to give best fits at initial periods of deposition this shows that indeed during this period there is a rapid change in cake structure as described before. The change in ε_m with time is best seen in Figure 6.23. Similar trends were observed for the other filtration pressure ranges investigated and can be seen in Appendix IX. It was also observed that at low filtration pressures, the fits of the model obtained although deemed to be okay were not as perfect as those at higher pressures. At lower filtration pressures it would appear that the particle arrival rate is slow as compared to higher filtration pressures subsequently it was deduced that at low filtration pressure the effects of thickening are more pronounced whilst in higher filtrations the effects of filtration are more pronounced.

It can be seen that at higher pressures the changes of ε_m seem to be more pronounced last longer. This is due to the higher driving force acting on the particles thus changing the structure of the filter cake as it grows as compared to lower filtration pressures.

The computer code was modified to account for the fact that in the initial stages of filtration the average porosity changes; consequently it was deemed necessary to investigate if the variables a, $d\varepsilon^* / d\lambda\big|_{\lambda=0}$ changed with filtration time or remained material specific. The results of this are observed in Table 6.4. From the results obtained it can be seen that for the initial periods of filtration, 5-40 s, the average porosity and porosity at the medium change as filtration proceeds. It can also be seen that the

predicted variables a, and $d\varepsilon^*/d\lambda\big|_{\lambda=0}$ remain constant and the notion that they are material specific holds.

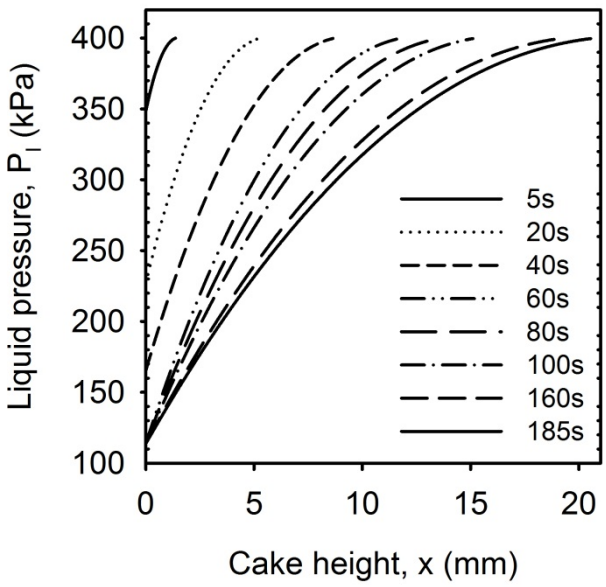

Figure 6.19: Predicted liquid pressure profile, talc at 400 kPa.

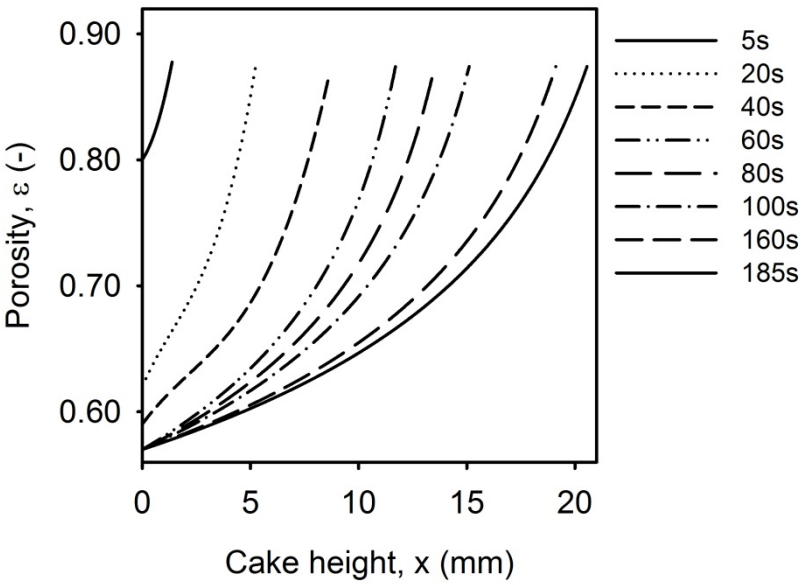

Figure 6.20: Predicted porosity profile, talc at 400 kPa.

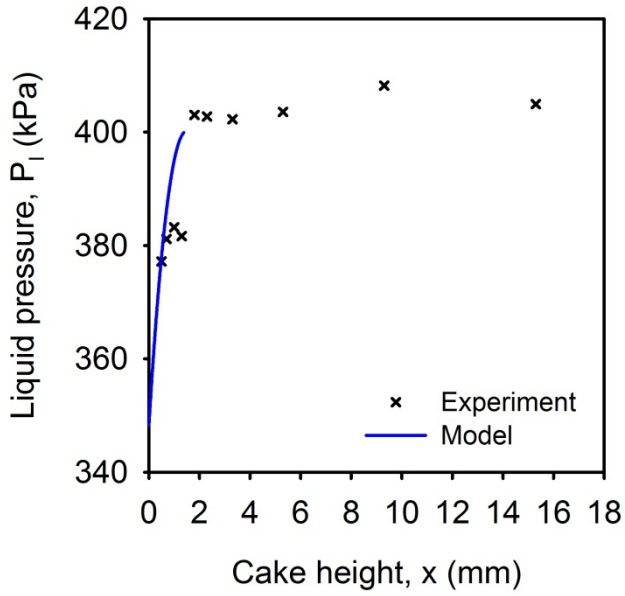

Figure 6.21: Predicted liquid pressure profile, talc at 400 kPa , 5s.

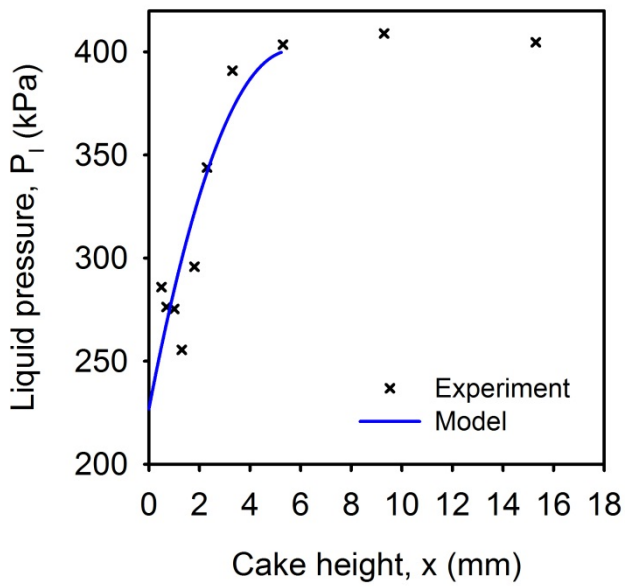

Figure 6.22: Predicted liquid pressure profile, talc at 400 kPa, 20s.

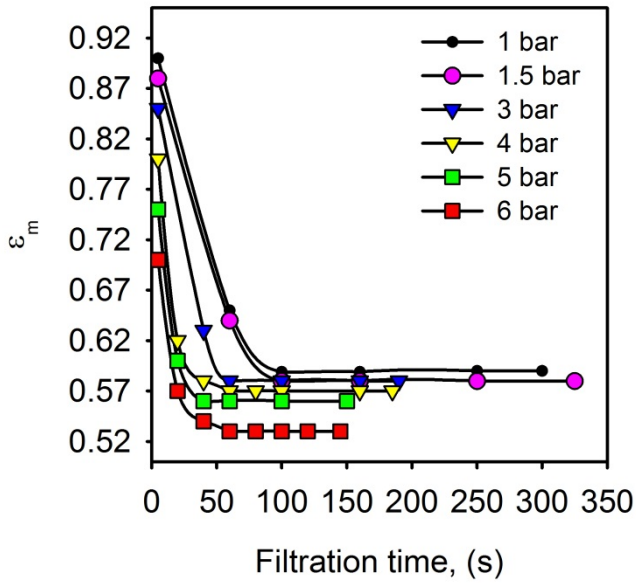

Figure 6.23: Change of ε_m with time as predicted by the model, talc

Table 6.4: Results of prediction of ε_{av}, ε_m, a, and $d\varepsilon^*/d\lambda\big|_{\lambda=0}$ for talc suspension at 400 kPa

Time (s)	ε_{av} Calc	ε_m Calc	a	$d\varepsilon^*/d\lambda\big\|_{\lambda=0}$
5	0.84	0.80	3.79	0.31
20	0.72	0.62	3.79	0.31
40	0.68	0.58	3.79	0.31
80	0.67	0.57	3.79	0.31
100	0.67	0.57	3.79	0.31

6.4.3 Local filter cake properties

The transient liquid pressure and porosity profiles of a filter cake formed at 400 kPa are shown in Figures 6.24 and 6.25 respectively. As a filter cake forms, the hydraulic pressure gradient causes an interfacial momentum transfer in the form of viscous drag at the particle-fluid interfaces. This drag force, along with the weight of subsequent layers

of filter cake, exerts a compressive force on a given layer of filter cake. Hence, particle rearrangement tends to occur, particularly at the initial stages of filtration. This rearrangement results in a decrease in porosity with time at any given distance from the filter medium, as seen in Figure 6.24. When the solids concentration is sufficiently high to communicate solids compressive pressure, then the liquid pressure decreases according to Equation 2.9. This decrease in liquid pressure is seen in Figure 6.25. It is further noted that the rate of porosity decrease was most pronounced at the initial periods of filtration at all heights. As the porosity decreases, the increase in solids concentration tends to make it more difficult for particles to further rearrange towards an even more dense packing. The packing arrangement in the bed is such that it can now sustain the experienced drag force without further movement, and equilibrium is reached between the compaction forces and those resisting closer particle packing. This is illustrated in Figure 6.24 which shows that after the initial decrease in porosity, a time is reached (~60 s) at a given height after which the porosity remained approximately constant. Similarly, after approximately 60 s the liquid pressure closest to the medium remained approximately constant. Figure 6.24 and Figure 6.25 also show that the porosity and liquid pressure decreased to a lower value close to the medium, resulting in a distribution throughout the depth of the cake. This is another manifestation of compressibility. If the drag on each filter cake layer is communicated to the previous one, then the net solids compressive pressure increases as the medium is approached, accounting for the decreasing porosity and liquid pressure.

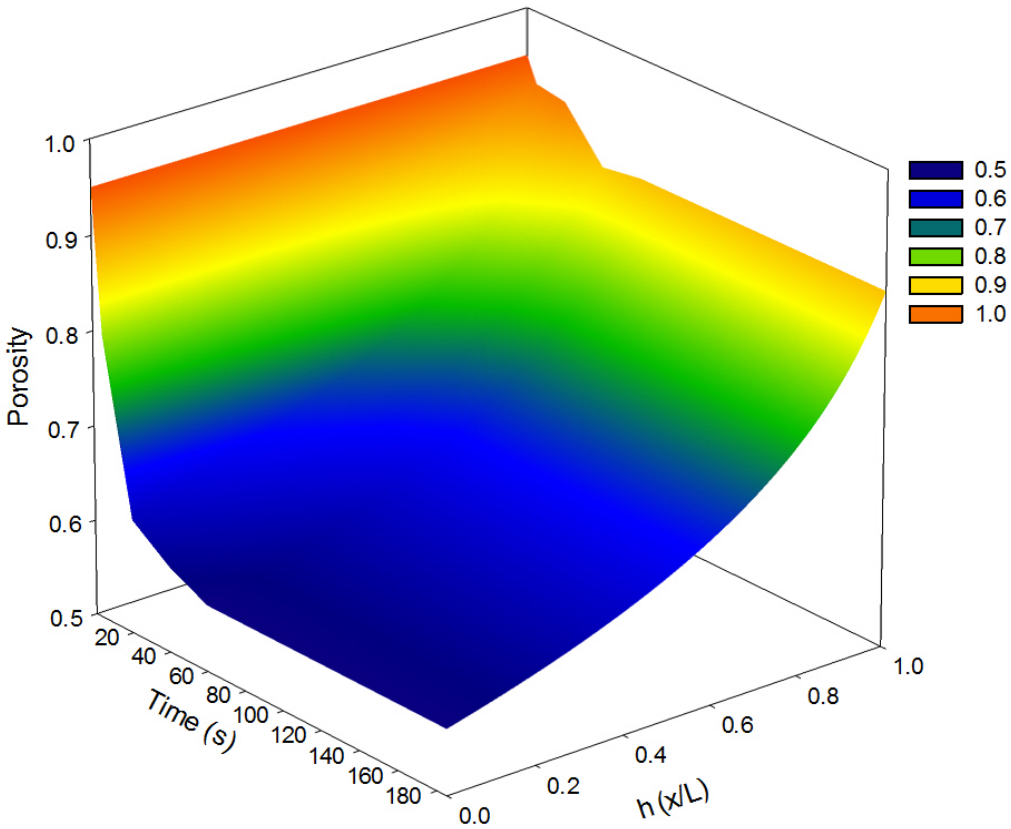

Figure 6.24: Transient porosity profile within a talc filter cake at 400 kPa.

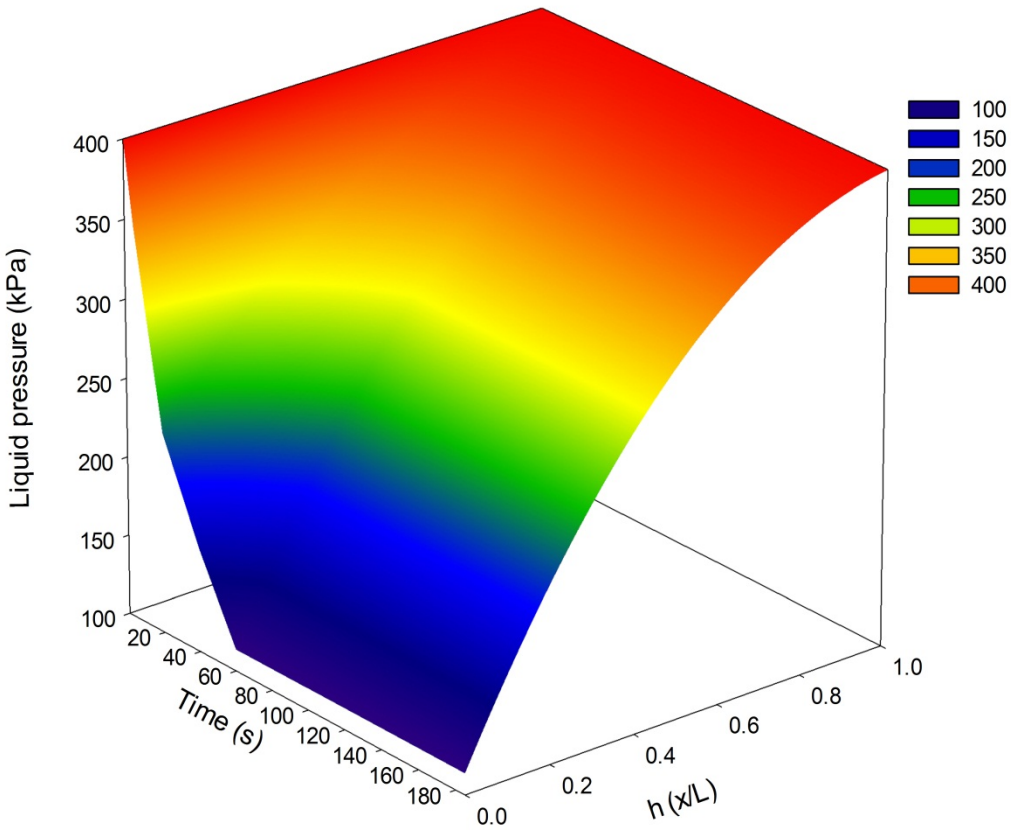

Figure 6.25: Transient liquid pressure profile within a talc filter cake at 400 kPa

6.5 EFFECT OF PARTICLE SHAPE IN CALCULATION OF INTERNAL PROPERTIES

When particles are suspended in a fluid, the drag force on a non spherical particle is generally greater than that on a sphere of the same volume moving with the same velocity. Thus, the settling velocity and other dynamic behaviours of a particle are determined by both particle size and shape. The shape factor, defined as ratio of drag forces for a non spherical particle and a sphere of equal volume moving at the same velocity, is often used. Spheres have a shape factor of 1, and larger values indicate a higher degree of deviation from a spherical shape. The drag force and the shape factor depended on both the aspect ratio of the particle and the orientation of the particle with respect to the flow direction.

As discussed previously it was observed that when using the Happel cell model to predict permeability it seemed to over predict permeability and consequently the specific cake resistance was under predicted. Fathi (1995) observed something similar however he argued that the Happel cell model could not be able to take the effect of compression for the material, calcite, in his study however, calcite is fairly incompressible so the argument on the compressibility effect does not hold. On further investigation it was deduced that the Happel cell model was derived for purely spherical particles. For a sphere the specific surface is determined as,

S_0 = surface area of particle/ volume of particle

For a sphere, $S_0 = \frac{6}{x}$.

A talc particle is generally flakey spherical in shape as can be seen in Figure 6.26

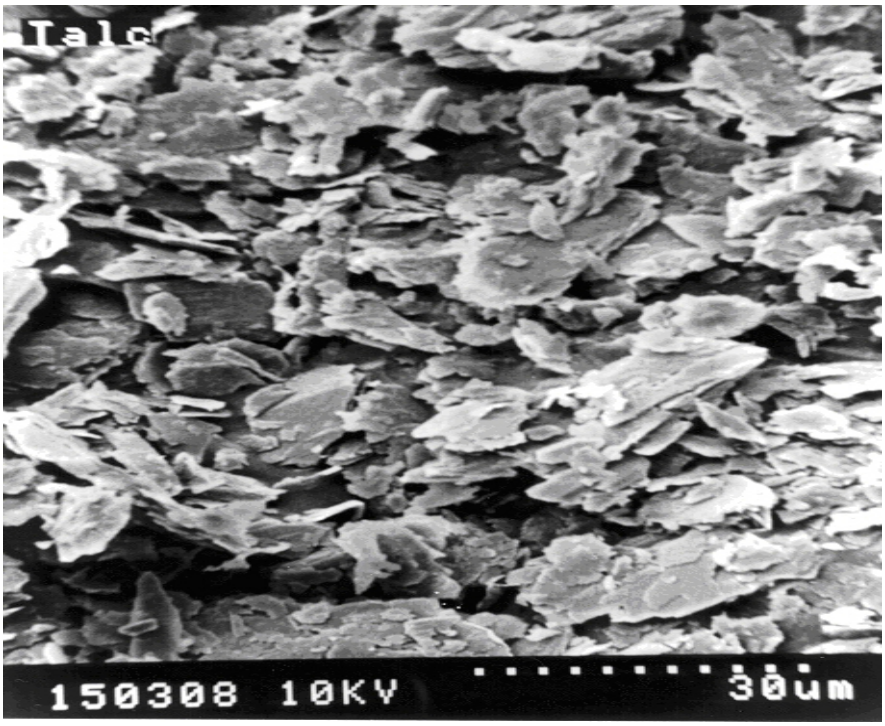

Figure 6.26: SEM micrograph of talc particles, (Tarleton, 1997).

The plots of cake permeability and specific resistance can be seen in Figures 6.27-6.28. As previously discussed, it can be seen that there is an over prediction and under prediction of permeability and specific resistance.

The properties of a filter cake at any given time during a filtration depend, to a large extent, on the packing behaviour of its constituent particles. Many researchers have investigated the packing of assemblies of equal spheres because of its simplicity and its convenience in theoretical work. Furthermore, regular packing is the easiest to use to describe internal structure as a set of unit cells. Regular packing of equal spheres are seldom encountered in filter cakes. Irregular shaped particles of wide size distributions often add to the complexity of random packing structures where porosities and coordination numbers vary with filtration time and spatially within a filter cake. Figure 6.29 (Wakeman and Tarleton, 2005) illustrate the typical effects of some common, regular, particle shapes on the specific surface.

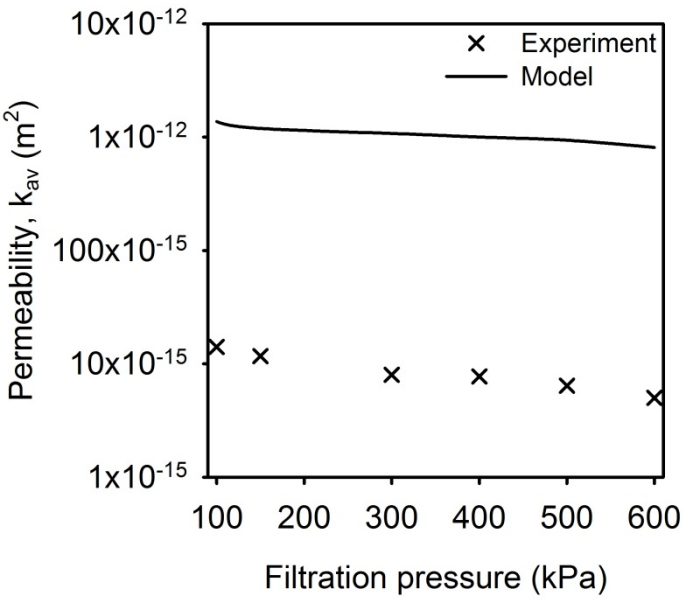

Figure 6.27: Predicted and experimental permeability against filtration pressure, talc filtration

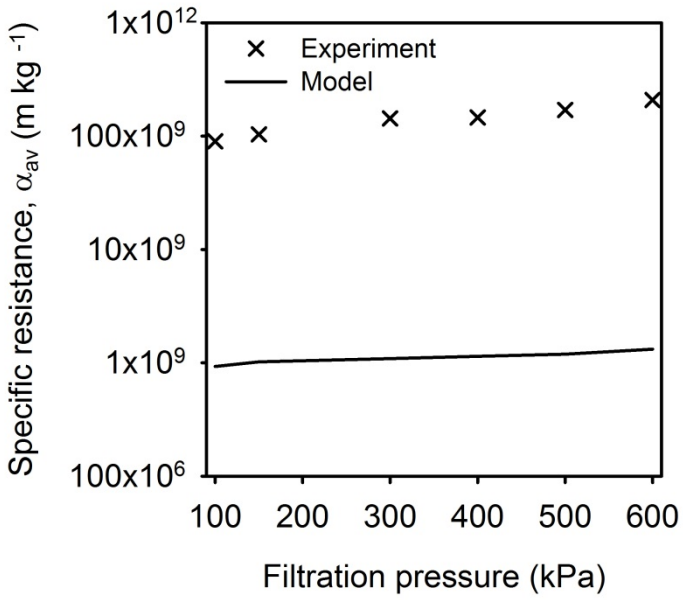

Figure 6.28: Predicted and experimental specific resistance against filtration pressure, talc filtration.

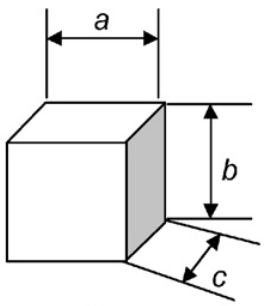	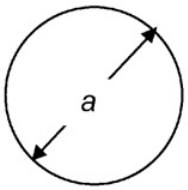	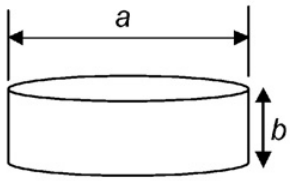
Cubic $b=c=a$ **Rectangular** $b=a$; $c=10a$ (say)	**Spherical**	**Fibrous** $b=10000a$ (say) **Cylindrical** $b=10a$ (say) **Flakey** $b=0.01a$ (say)
Surface $2(ab+ac+bc)$	πa^2	$\frac{\pi}{4}a^2+\pi ab$
Volume abc	$\frac{\pi}{6}a^3$	$\frac{\pi}{4}a^2 b$
Specific surface $\frac{2(ab+ac+bc)}{abc}$	$\frac{6}{a}$	$\frac{1}{b}+\frac{4}{a}$

Figure 6.29: Effect of particle shape on specific surface (Wakeman and Tarleton, 2005).

As can be seen in Figure 6.29, the specific surface of a flaky particle, talc, can be determined using the terms,

$$S_0 = \frac{1}{b} + \frac{4}{a}.$$

This then emphasised that in the Happel cell model there had to be a term that affected the specific surface in order for its use in the prediction of permeability which is inverse of specific resistance. This term was best defined as a shape factor.

It was then decided to introduce a shape factor, κ, into the Happel cell model specifically the specific surface, the new cell model used was then of the form

$$k = \left(\frac{d}{6\kappa}\right)^2 \frac{6 - 9\left(1-\varepsilon\right)^{\frac{1}{3}} + 9\left(1-\varepsilon\right)^{\frac{5}{3}} - 6\left(1-\varepsilon\right)^2}{\left(1-\varepsilon\right)\left(3 + 2\left(1-\varepsilon\right)^{\frac{5}{3}}\right)} \tag{6.7}$$

Different shape factors were obtained at different filtration pressures to try and minimise the predicted permeability to experimental permeability. The particle size does not change with filtration pressure hence resulting in the different shape factors. An average shape factor $\kappa = 11.29$ was then determined to give the lest worst fit to the data as can be seen in Figure 6.30.

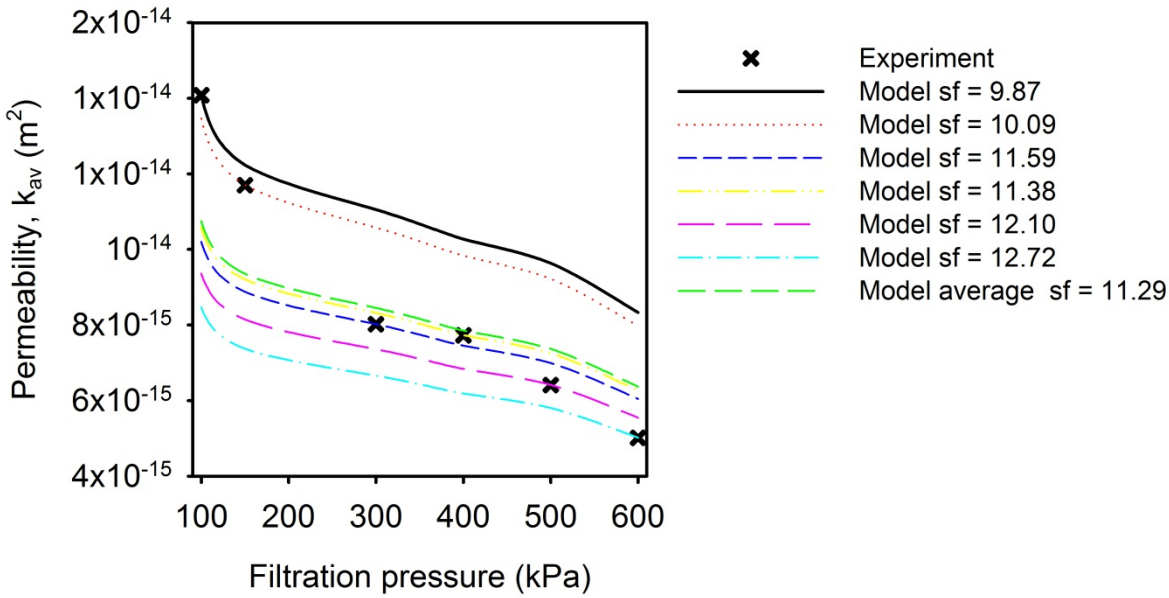

Figure 6.30: Permeability against filtration pressure using shape factor, talc filtration.

The corrected Permeability and specific cake resistance plots are shown in Figures 6.31-6.32 The use of the shape factor did indeed enable the predictions given by the model for permeability to be similar to those of the experimental data and us a result the specific cake resistances were similar. As pointed out by Donohue and Wensrich (2009), although a shape factor can be used to account for irregular particles, it must be found empirically.

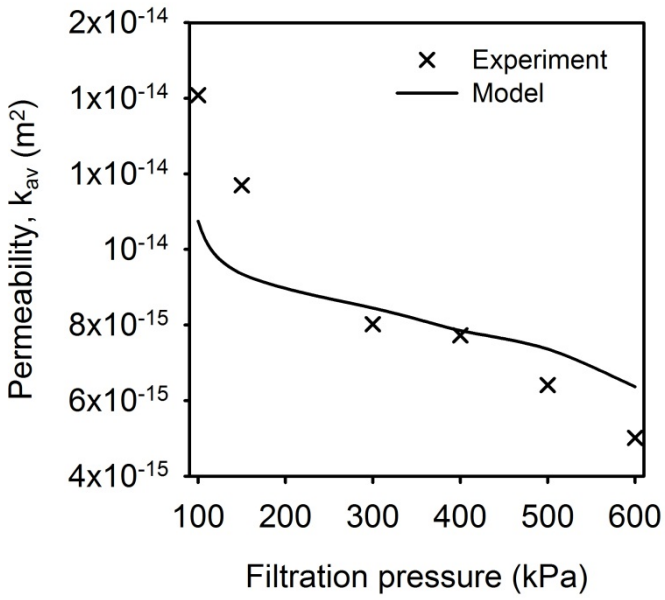

Figure 6.31: Corrected permeability against filtration pressure, talc filtration

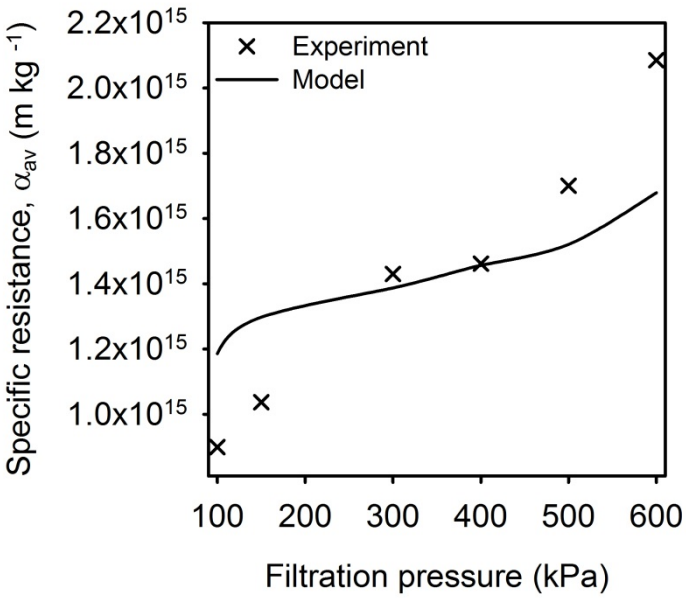

Figure 6.32: Corrected specific resistance against filtration pressure, talc filtration

6.5.1 Predicted local values of compressibility, n

By using Equation 6.8, local values of compressibility were plotted for different pressure and are seen in Figure 6.31

$$\alpha = \alpha_0 (1 + p_s)^n \tag{6.8}$$

At low pressures local compressibility increased with time, however at higher filtration pressures the layer of the cake compressed at a faster rate as can be seen. The maximum compressibility was seen at 600 kPa at a value of 0.45. In all cases after maximum compressibility the compressibility evened out with subsequent layer formation reducing this to about 0.4. The average values of specific filtration were plotted against filtration pressure and Equation 6.8 was used with average values. The value of compressibility coefficient obtained was 0.37.

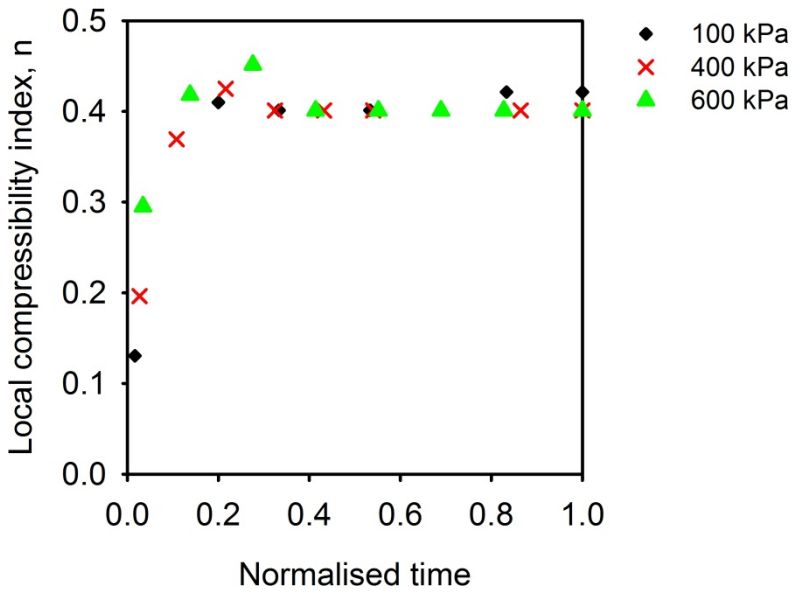

Figure 6.33: Predicted compressibility index values for talc at different filtration pressures

6.6 PREDICTION OF CAKE HEIGHT FOR TALC

The prediction of cake height formed during a filtration is essential for accurate filter design there have been different approaches used in elucidating the rate of growth of a filter cake. Thus the determination of cake height is a rather complicated task, since the condition of the cake/suspension interface is not well defined for most materials. Murase *et al.* (1987 placed a horizontal plate with a small opening at a specific height in the cell. A sharp change in filtrate rate was observed when the filter cake reached this height. Tarleton and Hancock (1997) placed electrode pairs at various heights above the filter medium. Electrical resistance measurements were then used in the determination of solids concentration within a filter cake at a given height. However the method was not without fault. It was observed that deviations in electrical current pathway led to false readings especially close to the filter medium. Less time consuming methods have been suggested. Chase and Willis (1982) visually inspected the cake/suspension interface. Fathi-Najafi and Theliander (1995) used pressure probes at various heights, when the hydrostatic pressure dropped from a value corresponding to the applied pressure, the cake was deemed to have reached this height. A common disadvantage of all these methods is that the properties of the determined cake surface are unknown.

Industrially the most common method used to determine filter cake height is the conventional filtration theory that uses the mass balance equation (Ruth 1935, Wakeman and Tarleton, 1999). A common disadvantage of this method is that in theory it is valid only when dealing with incompressible filter cakes. As is the case in industry compressible filter cakes are more common. An improvement to this theory in order to be able to deal with compressibility is the ‘Modern’ filtration theory which uses averages in the calculation of solids concentration profiles by using characteristic empirical constants obtained from a series of constant pressure filtrations (Tarleton and Hancock, 1997). The use of this method was seen to be an improvement on the previous method however it was deemed that the averaging procedure would result in inaccurate filter cake height predictions at particular filtration pressure.

It thus can be seen that without going into too much detail the determination of filter cake height involves a lot of complexities. These are further compounded by the fact that the filter cake/suspension interface is arbitrary in nature. As a result, even without errors arising from experimental and modelling techniques, the various methods are

actually capture different physical interpretations of a filter cake/suspension interface. Discussions of the various methods as well as their comparisons are not dense in literature.

Filter cake heights determined from five different approaches are compared and discussed. These approaches are:

- Setting the value of the interface to be at porosity of 0.7
- The mass balance equation (Wakeman and Tarleton, 1999)
- Modern filtration theory (Holdich, 1994)
- Model presented in the current work
- Experimentally determined transient liquid pressure profiles (Tarleton and Headley (2003), Shirato (1969), Johanson and Theliander (2007)).

Using experimentally measured liquid pressure profiles, the filter cake height was obtained when a pressure probe first registered a decrease in liquid pressure from the filtration pressure. The Equations used for the first three aforementioned methods are given as Equations (6.9), (6.11) and (6.12) respectively.

Mass balance equation used in the prediction of filter cake height

$$L = \frac{s\rho_l V\left(\varepsilon_{av} - 1\right)}{\rho_s\left[1 - \left(\left(1 + \frac{\rho_l \varepsilon_{av}}{\rho_s\left(1 - \varepsilon_{av}\right)}\right)s\right)\right]A} \tag{6.9}$$

where ε_{av} was determined from Equation (6.10).

$$\varepsilon_{av} = \frac{1}{L}\int_0^L \varepsilon dx \tag{6.10}$$

Modern filtration theory equation:

$$L = \frac{\Delta P_{cake}^{(1-m-n)}}{\mu\alpha_0 C_0 \rho_s\left(1 - m - n\right)}\frac{A}{Q} \tag{6.11}$$

where *m* and *n* are empirical constitutive coefficients (Holdich, 1994)

The current model equation for predicting filter cake height is given as:

$$x = \sqrt{E_i t \lambda} \tag{6.12}$$

6.6.1 Prediction of cake height with ε_i as calculated from the model

The model calculated cake height using Equation 6.11 which utilised the porosity at was determined as a cake height by the model. With the calculated local values of porosity obtained, one was able to obtain average porosities by using Equation 6.10. With these values and with volume *vs.* time data, cake heights were calculated using Equation 6.9 and the theoretical cake heights were compared to the predicted cake heights and it was observed that in general the model over predicted the results of filter cake height as can be seen in Figure 6.34.

A possible cause of the problem would have been the moving boundary condition aids in estimating the value of the porosity at the cake/slurry interface. Tien (2001) raised issues with the moving boundary condition used by (Wakeman, 1978) and used in this work. He mentioned the addition of an extra term in the right hand side of the moving boundary equation, Equation (5.4). however based on the results of the minimisation of variances and the fits of experimental and model liquid pressure profiles, it is possible to say that the results obtained are credible and the addition of an extra term in the right hand side of the moving boundary equation, Equation (5.4) would not aid in the reduction of over prediction of cake height.

In literature at a solidosity of 0.3, the particles are said to be networked and thus a cake has formed. Johanson and Thelieander (2005) used their model to predict cake heights and did this by altering the solidosity at the surface of the cake. They were able to show that at solidosity of 0.25-0.30 the profiles of the model compared well to the theoretical ones. With this in mind porosity at the surface of the cake was set at 0.7 , ε_{i_c} , which corresponds to 0.30 solidosity. A schematic diagram showing this is shown in Figure 6.35.

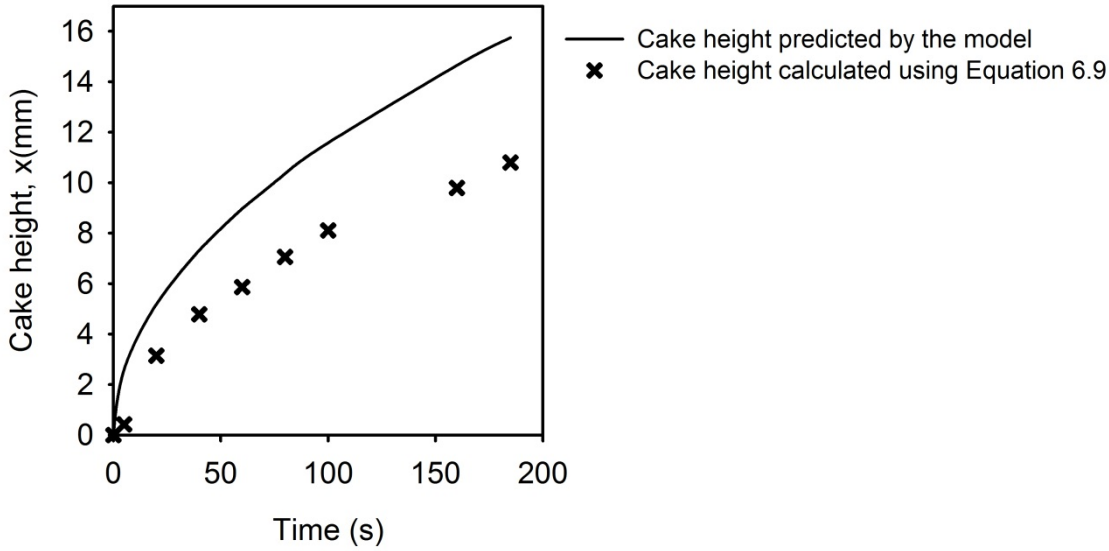

Figure 6.34: Predicted and theoretical cake heights with time, talc at 400 kPa.

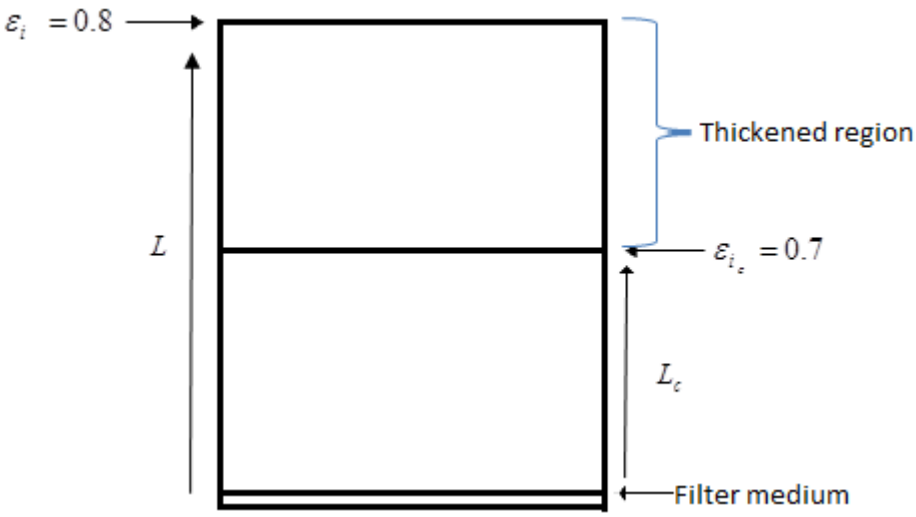

Figure 6.35: Schematic of a filter cake

At each time interval the porosity profile was investigated and at each point which corresponded to 0.7 porosity the value of cake height, L_c, recorded. This was now determined to be the new cake height. $L - L_c$, was then considered to be a thickened layer. Average porosity was recalculated for the new cake height and was then used together with volume *vs.* time data to calculate new theoretical heights. The new

predicted and model cake heights are shown in Figure 6.36. It can be seen that when solidosity is set at 0.7 the predicted and theoretical cake heights are almost similar. Similar trends were observed with the different filtration pressures investigated and can be seen in Appendix XI.

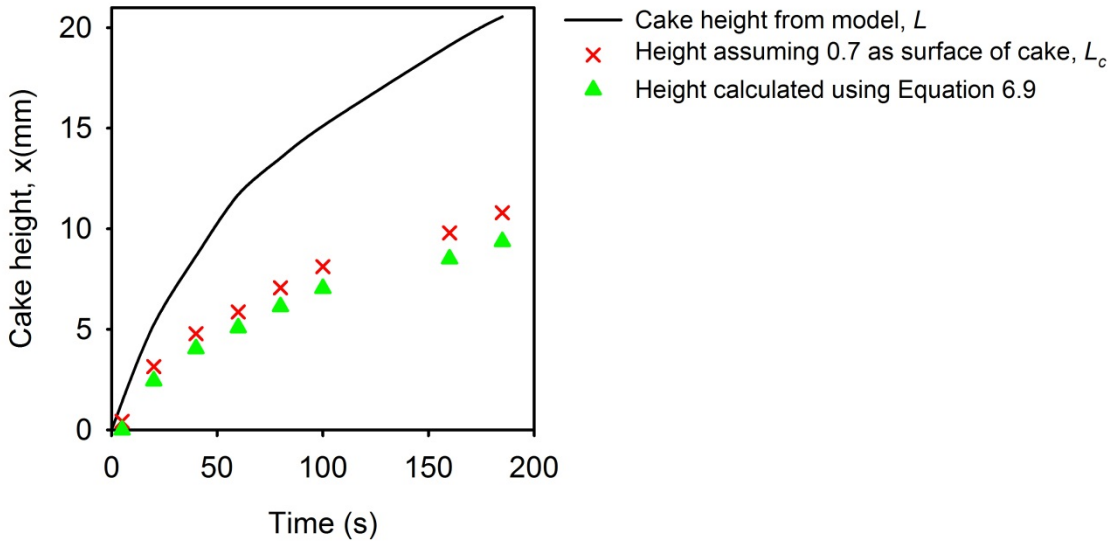

Figure 6.36: Predicted, theoretical and experimental cake heights with time, talc at 400 kPa.

6.6.2 Prediction of cake height with using four different approaches

Filter cake height predictions using the last four previously methods are plotted in Figures 6.37 and 6.38 for 400 and 600 kPa filtration pressures, respectively. Before going into further discussions the following terms of filter cake/suspension interface are defined to ease in clarity of discussions: h_{mft} is the cake height as determined by modern filtration theory, h_{mb} as determined by the mass balance equation, h_{mod} by the current model, and h_{exp} by the experimental approach using pressure probes.

It was generally seen that at all trialled filtration pressures the filter cake heights $h_{mod} > h_{mft} > h_{exp} > h_{mb}$ respectively. The current model seems to suggest a thicker cake at a given time relative to the other approaches. It may seem curious that the model's liquid pressure predictions were validated on experimental liquid pressure data, yet the model suggests thicker cakes than the experimental method with about a 30% difference. As previously described a possible cause of this apparent discrepancy could

have been the moving boundary condition, which plays a role in estimating the value of porosity at the cake/slurry interface. Tien (2001) raised issues with the moving boundary condition used by Wakeman (1978), and hence that used in this work, and proposed an additional term for this boundary condition. However, the model as it was used in this work represented experimental behaviour in such a way that suggests it to be a valid approach. It is perhaps more likely that the experimental resolution is a more significant contributor to this discrepancy. Generally, when using the experimental transient liquid pressure measurement approach, relatively infrequent measurement times and distance between consecutive probes can result in a delayed recording of a filter cake height.

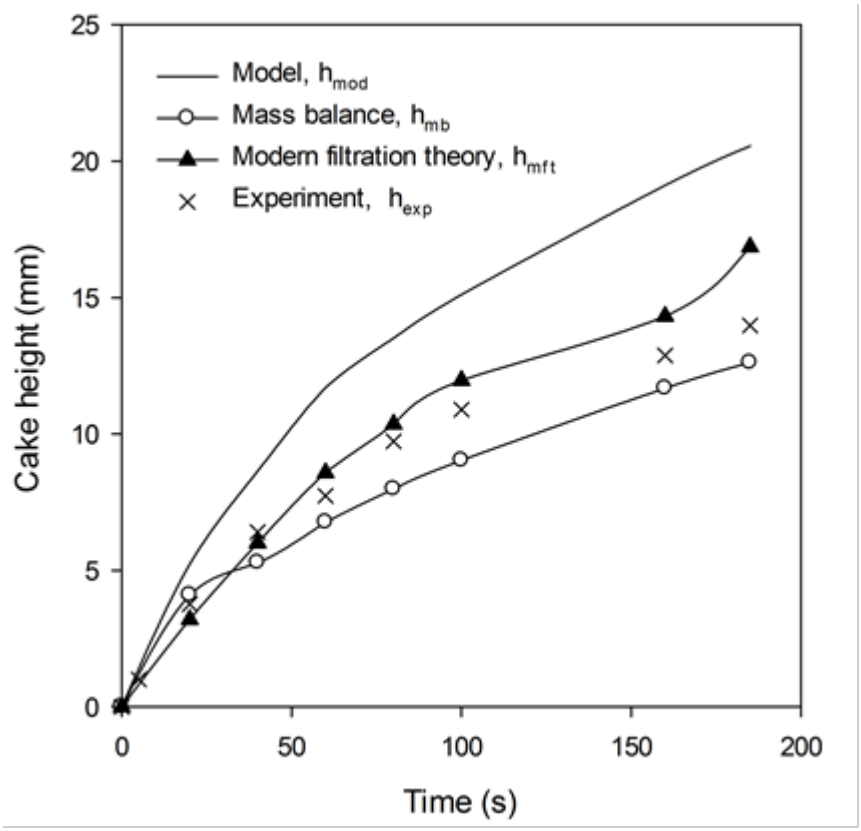

Figure 6.37: Filter cake growth as determined from four different approaches with filtrations at 400 kPa.

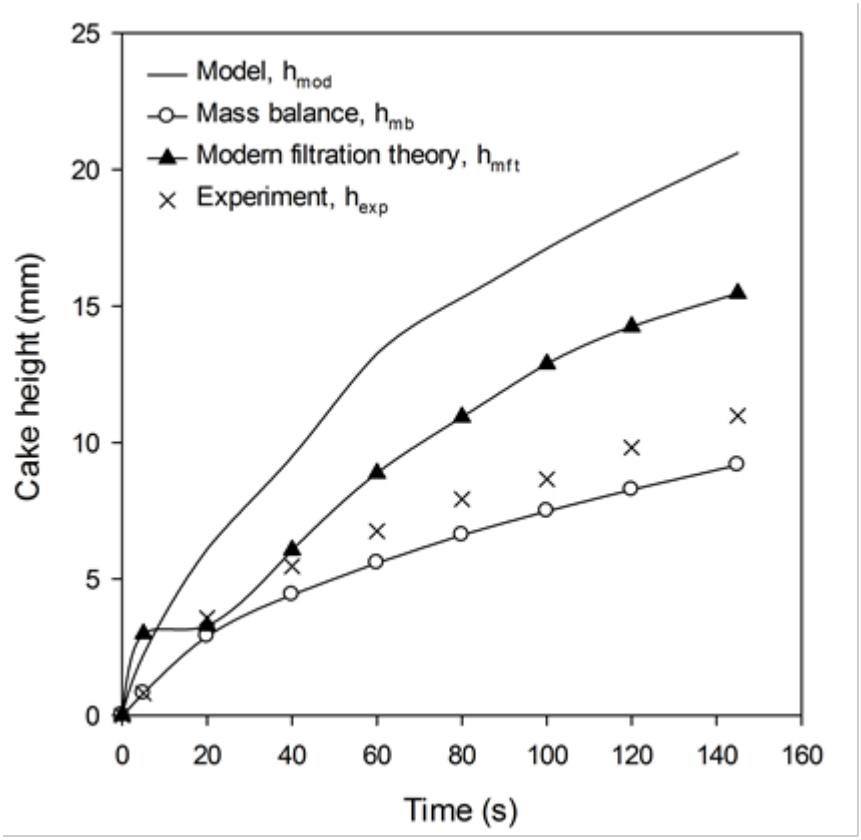

Figure 6.38: Filter cake growth as determined from four different approaches with filtrations at 600 kPa.

At 400 kPa, values of h_{mft}, h_{exp}, and h_{mb} are comparable to within ± 20 %), whereas disagreements were generally exaggerated at 600 kPa. Modern filtration theory seemed to predict thicker cakes than the experimental approach, which in turn predicted thicker cakes than the mass balance equation. A similar trend was obtained by Tarleton and Hancock (1997) with filtrations of zinc sulphide. They pointed out that from a design view-point; the modern filtration theory actually performed worse in that it over-predicted filter cake height. Their experimental approach was to determine solids concentration using electrical resistance measurements and not liquid pressure using pressure probes. In their paper, Tarleton and Hancock also presented results of calcite and talc filtrations. They claimed that it was more difficult to determine the position of a talc filter cake surface than it was with calcite. Furthermore, they were able to make cake height predictions using conventional filtration theory with calcite suspensions, but struggled with talc suspensions.

The current model was used to calculate the porosity at the filter cake surface, assuming cake height values of h_{mft}, h_{mb}, h_{mod} and h_{exp}. The results obtained are plotted in Figure 6.39. As expected, it is seen that the surface porosity with h_{mod} is greater than the surface porosities with h_{mft} and h_{mb}. The surface porosities at h_{mft} and h_{mb} initially decrease with filtration time before reaching a plateau, consistent with the porosity trends at other heights within the cake. The porosity at h_{mod} seems less prone to this initial decrease, and generally remains in the relatively high region of 0.85 to 0.9. Though quite subjective, these values of porosity intuitively seem quite high for a particulate filter cake. The porosities at h_{mft} and h_{mb}, however, remain in the region of 0.65 to 0.75 after the initial decline. These values agree with those suggested by Johanson and Theliander (2007) using kaolin suspensions. Johanson and Theliander used γ-ray attenuation measurements to determine transient solidosity profiles within their filter cakes which generally showed that there was a pronounced porosity gradient, decreasing porosity, towards the filter medium, up to a porosity of about 0.7. A sharp change in porosity gradient was observed at a porosity of roughly 0.7 and a more gradual decrease in porosity was observed from 0.7 to approximately 0.5 at the filter medium. Although they recognised in their paper the arbitrary nature of what a filter cake/suspension interface is, the results mentioned suggested this interface to have a porosity of approximately 0.7. Tarleton and Hancock, as previously mentioned, found it difficult to identify the filter cake/slurry interface due to the compressible nature of their talc suspensions. They found that their model which was based on conventional filtration theory best fit their 50 kPa data assuming a porosity value higher than 0.7, but best fit their 600 kPa data assuming a porosity value lower than 0.7.

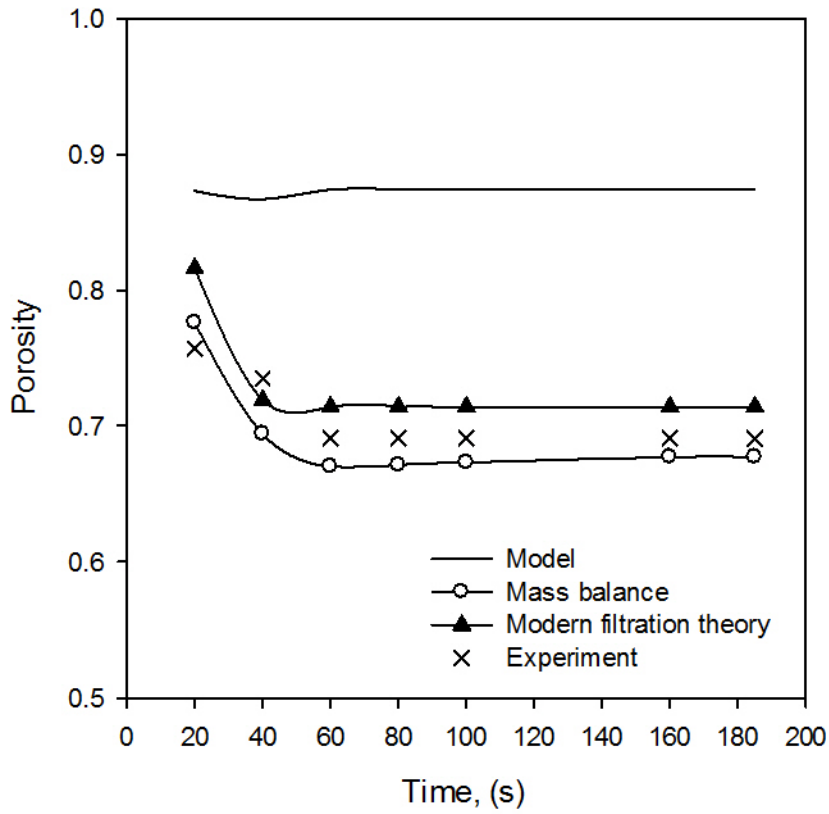

Figure 6.39: Porosity values at the surface of a cake as defined by the different cake height approaches at 400 kPa.

6.7 FILTRATION PRESSURE DISTRIBUTION IN A TALC FILTER CAKE

Having decided to address the issue of the arbitrary nature of the filter cake height/suspensions interface in the previous section, the next step was to try and obtain a pressure distribution profile during cake filtration of the formed talc cake.

Inconsistencies between the current model and conventional filtration theory, mass balance equation, interpretations of filter cake height may be reconciled to a certain extent by considering the arbitrary nature of a cake/suspension interface, and hence what a cake height really is. For example, using the talc filtrations in this work, conventional filtration theory uses as an input the average cake porosity as measured on a compact cake at the end of a filtration. On the other hand, the current model registers a filter cake as soon as a solids compressive pressure is experienced. The porosity at the surface of this filter cake, as suggested by the current model, is only marginally less

than that of the feed suspension. The layer between h_{mod} and h_{mb} is hereby termed a "buffer layer". This approach is similar to one taken by Wakeman (1981, 1985) who defined a "buffer layer" as that part of the slurry just forming the cake, or about to be deposited. Although in the present work a filter cake/suspension interface has not been defined, this "buffer layer" can be considered to be a region of solids concentration greater than that of the feed suspension, but located a layer above a bed of more compact solids packing, h_{mb}.

The pressure drop across the filter medium, as well as across h_{mb} and the "buffer layer", were calculated for the various filtration times. Example pressure distribution trends during filtrations at 400, 500 and 600 kPa are shown in Figure 6.40. It is seen that with all filtrations, the percentage pressure loss across the medium initially decreases with time. As a filter cake grows, so does the pressure loss across it and less is available to cause particle deposition. This may be offset by the reducing pressure loss over the medium as the filtrate rate decreases. The distribution of pressure appears to remain reasonably constant after the initial stages of filtration. As a proportion of the total pressure drop, the "buffer layer" was always less than 20%. Wakeman (1981, 1985) found the "buffer layer" as defined by him to generally contribute less than ~10% to the total pressure drop.

Figure 6.40 also serves as a reminder that a "constant pressure filtration" refers to the total pressure loss across the slurry, cake and medium, and not just the cake forming pressure. Furthermore, in certain aspects of filtration analysis the pressure drop across the filter medium is sometimes neglected. In Figure 6.40, it is seen that the pressure drop across the medium can be a substantial portion (~40%) of the total pressure drop, and deserves due recognition. The substantial pressure drop across the filter medium also highlights the importance of medium selection for a given filtration.

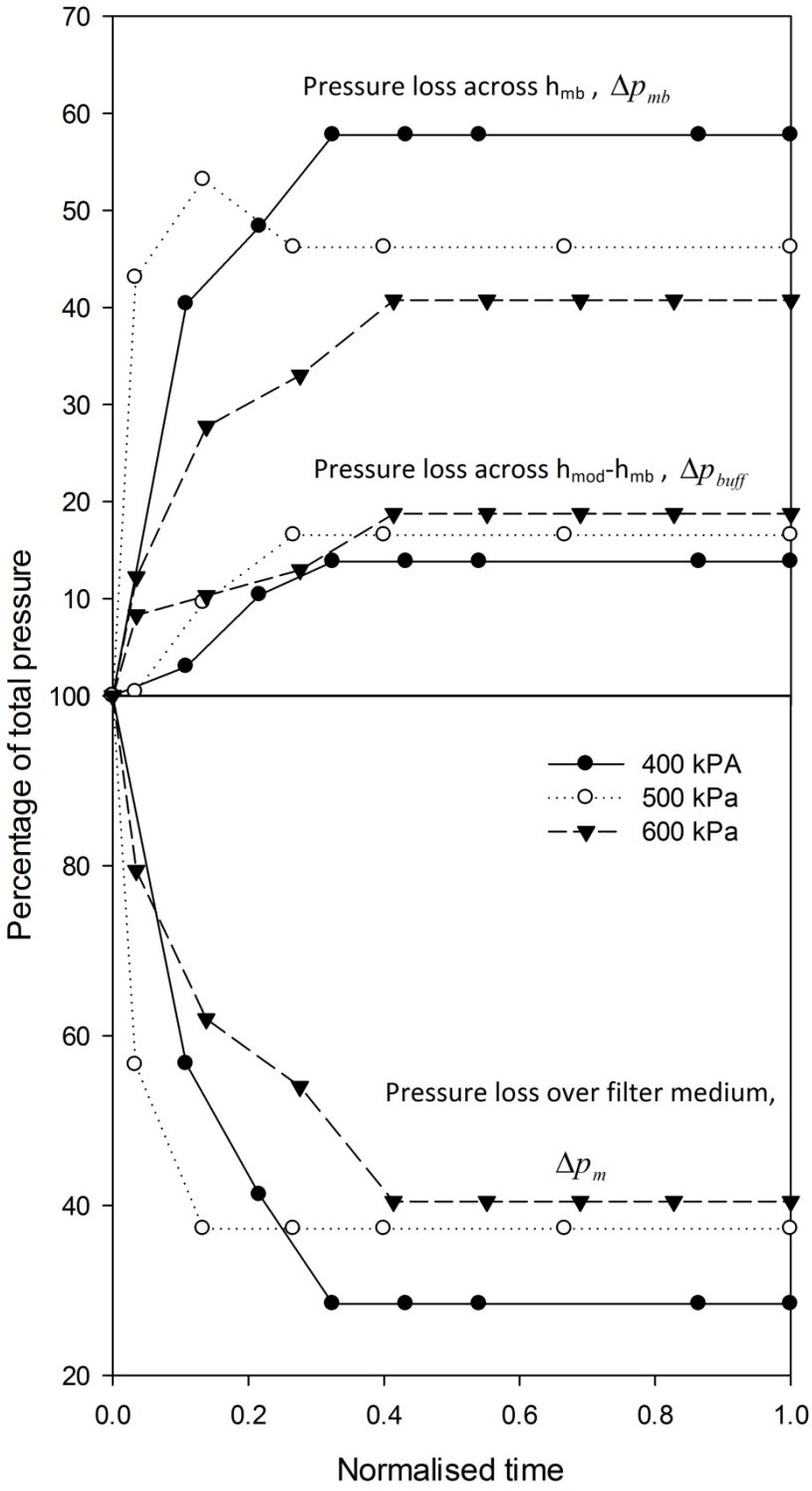

Figure 6.40: Distribution of filtration pressure during cake formation of a talc suspension

6.8 CONCLUSIONS

Experimental data has been studied and analysed using the developed model. The predictions from the model gave reasonably good fits of data for the liquid pressure when compared to experimental values. The numerical procedure employed has been shown to give the desired results with evidence of global minima been obtained for the required variables. This suggested unique values of a, $d\varepsilon^{*}/d\lambda\big|_{\lambda=0}$ at different filtration pressures.

The results obtained have shown that during the initial stages of filtration, the value of the calculated porosity at the medium changes rapidly especially at higher pressures which was shown to be caused by the nature of compression of talc suspensions. The use of the Happel cell model to estimate internal cake properties has to be done with caution when dealing with non spherical particles as has been shown.

An attempt was made to explain the reason for over prediction of cake height by the model. The arbitrary nature of the filter cake/slurry interface was shown to be significant. This resulted in different physical meanings of cake heights based on the methods used to determine. Subsequently distribution of filtration pressure was studied and the findings helped in the better understanding of compressible cake filtration of a talc suspension.

Chapter 7 : CONCLUSIONS AND RECOMMENDATIONS FOR FUTURE WORK

Chapter 1 served as an introductory chapter for this thesis, attempting to put the main body into context.

In Chapter 2 filtration theory was discussed and various mechanisms of filtration described. Flow in porous media was discussed and the governing equations derived. The concept of liquids and solids compressive pressure was discussed in great detail and the various forms of compressive stress used by various researchers described. Filter cake porosity and permeability were discussed and identified to be key parameters in filter cake formation. The Carmen Kozeny equation and Happel cell model were compared and it was seen that the Happel cell model gave better predictions of permeability when faced with porosity values >0.6. This was particularly important given that in the current work porosity values greater than 0.6 were registered thus rendering the use of Carman Kozeny equation null and void. In the analysis of filter cake formation different methods of analysis utilised by different researchers were identified and comparison drawn. The differences between all these methods was determined to be the way the derivation of the material and momentum balances for both the liquids and solids phases were carried out as well as the material property parameters. Different numerical solutions of the governing filtration equations were also compared. It was deduced that it was rather difficult to describe the definition of a filter cake height owing to the arbitrary nature of the filter cake/slurry interface. It was also shown that not much information is available in literature thus the physical significance of the filter cake/slurry interface using the different methods exists and is open to debate and there is no universal definition.

In chapter three, the acquisition of the experimental data used in this work was discussed by briefly and accurately describing the filtration equipment in use. The formation of a cake by interpreting liquid pressure profiles was also discussed. It should be noted that no experiments were carried out in the context of the present work.

The derivation of the governing equations used in this modelling approach was described in Chapter 4. The assumptions as well as the boundary conditions used were highlighted.

In Chapter five the numerical method employed in the discretisation and solution of the governing equations was introduced. It was shown that the general sequence of liquid pressure profile calculation involved calculation of local porosity, relation of filter cake permeability and specific cake resistance to porosity and finally relating the porosity to the liquid pressure. The fourth order Runge Kutta Nystrom method was used to discretise the governing equations. It was generally chosen as compared to other numerical techniques as it was the most stable and gave the best solutions for second order differential equations. Initial tests were carried out in order to find a range for the input variables a, $d\varepsilon^*/d\lambda\big|_{\lambda=0}$ and ε_m. In general it is assumed that randomly packed spheres have porosity ranges between 0.4 and 0.5 and as such it was deemed safe to set the value of ε_m for talc as 0.4. However it would be interesting to study other particulate systems to determine if this theory holds or if indeed other values may be obtained. One would expect the latter as different particulate systems would be of different shapes and thus the nature of packing would be different. The number of subdivisions of the physical domain was quite a daunting task. Initially, n, was set at 10, 100 and 1000 subdivisions and simulations carried out. It was observed that when $n = 10$ under fitting occurred and poor results were obtained which was caused by the coarse nature of the subdivisions. At $n = 1000$ the simulation hangs as a result of over fitting due to the fineness of the subdivisions. The optimal subdivisions were obtained when $n = 100$ which resulted in the best fits of experimental data to model data. It should be noted as a result of this the porosity values obtained from the model were of three significant figures. For example porosity values of 0.870 and 0.871 would be deduced to be 0.87, however as a result of the subdivision this gave porosity values in three significant values and cannot be altered. Furthermore the alteration of these values would lead to inaccurate liquid pressure profiles being obtained from the model. One cannot manipulate the porosity values as the process is automated.

In Chapter six, the validation of using the similarity variable was shown in Figure 6.1 where it was seen that all the liquid pressure profiles at different time intervals followed a similar trend bar the one at five seconds. The use of the similarity variable was thus adjudged to be reasonable. The results of the fitting of experimental data to the model showed good promise with matching fits of liquid pressure profiles obtained. This led to retrieval of transient porosity profiles. Similar results were obtained in all filtration

ranges investigated that is 400, 500 and 600 kPa which gave the best fits as compared to lower filtration pressures. Figure 6.6 resulted in quite a unique trend of a, $d\varepsilon^*/d\lambda\big|_{\lambda=0}$ and ε_m against filtration pressure. The physical significance of a and $d\varepsilon^*/d\lambda\big|_{\lambda=0}$ is rather difficult to ascertain owing to lack of more experimental data of different particulate systems. It would be interesting to obtain experimental data of different particulate systems in order to carry out a rigorous analysis of these data in order to elucidate the physical significance of the aforementioned parameters. It was also observed that initially the specific cake resistance was being overestimated and thus the specific cake resistance being underestimated. This complication arose due to the Happel cell model not taking into account the specific surface of a talc particle. One ought to remember that this model assumes particles to be spherical in nature which is often not the case in reality. This required the addition of a term, κ, termed as a shape factor. One would argue that this is just a fitting parameter, but as shown in the current work it would seem to have a physical meaning which has not been explored fully and would be an interesting study to carry out for different particulate systems. The arbitrary nature of the filter cake/slurry interface was also explored. Four methods were used to analyse this in the present context of this work. The four methods were the; the mass balance equation, modern filtration theory, experimentally determined transient liquid pressure profiles and the use of the current model. It was generally seen that the current model over predicted the filter cake height as compared to the other methods. That is not to say that the model prediction was wrong. All is signifies is that each different approach meant that the filter cake/slurry interface heralded a different physical significance. It was highlighted that there is scarcity in literature on research on the filter cake/slurry interface. This is puzzling as it has been shown that filter cake height determination is of significance in the design of filtration process. The distribution of filtration pressure within the filter cake was also studied. It was shown that the inconsistencies arising in the difference of the filter cake/slurry interface using the model and mass balance could be attributed to a buffer layer. The buffer layer is a region of solids concentration greater than the feed suspension which is located above a bed of more compact layers. It was shown that the percentage pressure loss across the filter medium decreases with time. The distribution of pressure remained constant after the initial periods of filtration. It was shown that the real meaning of constant pressure

filtration referred to the total pressure loss across the slurry, filter cake and filter medium and not just the cake forming pressure.

REFERENCES

Atsumi K. and Akiyama T. (1975) A study of cake filtration- formulation as a Stefan problem. *Journal of Chemical Engineering Japan* **8**, 487-492.

Baird R.L. and Perry M.G. (1967) The distribution of porosity in filter cakes. *Filtration and Separation* **4**, 471-476.

Brown, J. C. Jr. Determination of Exposed Specific Surface of Pulp Fibers from Air Permeability Measurements, *TAPPI*, **33**, pp. 130, 1950.

Brownell, L. E. and D. L Katz. Flow of Fluids through Porous Media, I. Single Homogeneous Fluids, *Chem. Eng. Prog*., **43**, No. 10, pp. 537-548. 1947.

Buscall, R. and White, L.R. (1987) The consolidation of concentrated suspensions. Part I. -The theory of sedimentation. *J. Chem. Soc. Faraday Trans*.,**83**: 873.

Carman P.C. (1937) Fluid flow through granular beds. *Trans IChemE* **15**, 150-166.

Carman P.C. (1938) The determination of the specific surface of powders. *Journal of the Society of Chemical Industry* **57**,225-234.

Chase G.G. and Willis M.S. (1992) Compressive cake filtration. *Chemical Engineering Science* **47**, 1373-1381.

Chen, C. Y. Filtration of Aerosols by Fibrous Media, *Chem. Rev*., **55**, pp. 595. 1955.

Darcy H. P. G. Les Fontaines Publiques de la Ville de Dijon. Dalamont, Paris. 1856.

Donohue T.J. and Wensrich C.M. (2009) Improving permeability prediction for fibrous materials through a numerical investigation into pore size and pore connectivity. *Powder Technology* **195**, 57-62.

Coulson J.M. (1949) The flow of fluids through granular beds: effect of particle shape and voids in streamline flow. *Trans IChemE* **27**, 237-257.

Davies, C. N. The Separation of Airborne Dust and Particles, *Proc. Inst. Mech. Eng*. (London), ***B1***, pp. 185. 1952.

Fair G.M. (1951) The hydraulics of rapid sand filters. *Journal of the Institution of Water Engineers* **5**, 171-213.

Fair G.M. and Hatch L.P. (1933) Fundamental factors governing the streamline flow of water through sand. *Journal of the American Water Works Association* **25**, 1551-1565.

Fathi-Najafi M. and Theliander H. (1995) Determination of local filtration properties at constant pressure. *Separation Technology* **5**, 165-178.

Grace H.P. (1953) Resistance and compressibility of filter cakes. *Chemical Engineering Progress* **49**, 303-318.

Grace H.P. (1956) Structure and performance of filter media. *AIChE Journal* **2**, 307-336.

Gray, W.G. (1975) A derivation of the equations for multi-phase transport. *Chem. Eng. Sci*., **30**: 229.

Whitaker, S. (1977) Simultaneous heat, mass and momentum transfer in porous media: a theory of drying. *Advances in Heat Transfer*; Academic Press: New York, 119–203.

Hadley R. (2002) *A Mechatronic Investigation of Thin Cake Filtration*. MEng Dissertation, Loughborough University.

Happel J. and Brenner H. (1965) *Low Reynolds Number Hydrodynamics*. Prentice-Hall, Englewood Cliffs, N.J.

Heertjes P.M. (1964) Filtration. *Trans IChemE* **42**, T266.

Hermia J. (1982) Constant pressure blocking filtration laws- application to power law non-Newtonian fluids. *Trans IChemE* **60**, 183-187.

Holdich R.G. (1990) Solids concentration and pressure profiles during compressible cake filtration. *Chemical Engineering Communications* **91**, 255-268.

Ingmanson, W. L., B. D. Andrews and R. C. Johnson. Internal Pressure Distribution in Compressible Mats under Fluid Stress. *TAPP*I, **42**, pp. 840. 1959.

Jackson, G. W. and D. F. James. The Permeability of Fibrous Porous Media, *Can. J. Chem. Eng*., **64**, pp. 364-372. 1986.

Johansson C. and Theliander H., (2007) Validation of predicted local profiles in cake filtration, *Chem. Eng. Res. Des*., **85** (A2) 220-228.

Jonsson K. A. and Jonssen B. T. L. (1992a), Fluid flow incompressible porous media: I: steady-state conditions. *AIChE J*. **38**, 1340-1348.

Jonsson K. A. and Jonssen B. T. L. (1992b), Fluid flow incompressible porous media: I: dynamic behavior. *AIChE J*. **38**, 1349-1356.

Koenders M.A. and Wakeman R.J. (1997a) Filter cake formation from structured suspensions. *Trans IChemE* **75**, 309-320.

Koenders M.A. and Wakeman R.J. (1997b) Initial deposition of interacting particles by filtration of dilute suspensions. *AIChE Journal* **43**, 946-958.

Lee, D.J., Ju, S.P., Kwon, J.H., and Tiller, F.M. (2000) Filtration of highly compactible filter cake: variable internal flow rate. *AIChE J*., **46** (1): 110.

Landman, K.A., Sirakoff, C., and White, L.R. (1991) Dewatering of flocculated suspensions by pressure filtration. *Phys. Fluids A*., **3** (6): 1495.

Landman, K.A. and Russel, W.B. (1993) Filtration at large pressure for strongly flocculated suspensions. *Phys. Fluids A*., **5** (3): 550.

Landman, K.A. and White, L.R. (1994) Solid/liquid separation of flocculated suspensions. *Adv. Colloid Interface Sci*., **51**: 175.

Landman, K.A., White, L.R., and Eberl, M. (1995) Pressure filtration of flocculated suspensions. *AIChE J*., **41** (7): 1687.

Lu W. M. and Hwang K. J. (1993) Mechanism of cake formation in constant pressure filtrations. Sep. Tech. **3**, 122-132.

Murase, T., E. Iritani, J. H. Cho, S. Nakanomori and M. Shirato. Determination of Filtration Characteristics Due To Sudden Reduction in Filtration Area of Filter Cake Surface, J. Chem. Eng. (Japan), **20**, No. 3, pp. 246-251. 1987.

Muskat, M and R. D. Wyckoff. The Flow of Homogeneous Fluid through Porous Media. *In International Series in Physics*, New York: McGraw-Hill, 1946.

Olivier J., Vaxelaire J. and Vorobiev E. (2007) Modelling of cake filtration: an overview. *Separation Science and Technology* **42**, 1667-1700.

Payatakes, A. C., C. Tien and R. Turian. A New Model for Granular Porous Media: I. Model Formulation. *AIChE J*., **19**, No. 1, pp. 58. 1973.

Purchas D.B. (1996) *Handbook of Filter Media*. Elsevier, Oxford.

Rajagopalan, R. and C. Tien. Trajectory Analysis of Deep-bed Filtration with the Sphere In-Cell Porous Media Model. *AIChE J.*, **22**, No.3, pp. 523. 1976.

Rietema K. (1953) Stabilizing effects in compressible filter cakes. *Chemical Engineering Science* **2**, 88-94.

Rushton A., (1973) Sedimentation effects in filtration. *Filtration and Separation* **10**, 267-272.

Rushton A. (1976) Liquid-solid separation, recent research evaluated. *Filtration and Separation* **13**, 573-578.

Ruth, B.F., Montillon, G.H., and Montonna, R.E. (1933) Studies in filtration II.Fundamental axiom of constant pressure filtration. *Ind. Eng. Chem*., **25** (2): 153.

Ruth, B.F. (1935) Studies in Filtration III. Derivation of general filtration equation. *Ind. Eng. Chem*., **27** (6): 708.

Shirato, M., Sambuichi, M., Kato, H., and Aragaki, T. (1969) Internal flow mechanism in filter cakes. *AIChE J*., **15** (3): 405.

Shirato M., Aragaki T., Ichimura K. and Ootsuti N. (1971) Porosity variation in filter cakes under constant pressure filtration. *Journal of Chemical Engineering of Japan* **2**, 172-177.

Shirato M. T., Aragaki T., Ichimura K. and Ootsuti N.(1986), Principles of expression and design of membranecompression-type filter press operation. In ed. N. P. *Cheremisinoff, Encyclopedia of Fluid Mechanics, Vol. 5*. Gulf Pub, Houston.

Sorensen, P.B., Moldrup, P., and Hansen, J.Aa. (1996) Filtration and expression of compressible cakes. *Chem. Eng. Sci*., **51** (6): 967.

Smiles, D.E. (1970) A theory of constant pressure filtration. *Chem. Eng. Sci*., **25**: 985.

Smiles, D.E. and Kirby, J.M. (1987) Aspects of one-dimensional filtration. *Sep. Sci. Tech*., **22**: 1405.

Smiles, D.E. (2000) Use of material coordinates in porous media solute and water flow. *Chem. Eng. J*., **80** (1–3): 215.

Sorensen, B.L. and Sorensen, P.B. (1997) Structure compression in cake filtration. *J. Environ. Eng*., **123** (4): 345.

Stamatakis, K. and Tien, C. (1991) Cake formation and growth in cake filtration. *Chem. Eng. Sci.*, **46** (8): 1917.

Sullivan, R. R. Specific Surface Measurements on Compact Bundles of Parallel Fibers. *J. Appl. Phy*., **13**, pp. 725. 1942.

Tarleton E.S. and Hadley R.C., 2003, The application of mechatronic principles in pressure filtration and its impact on filter simulation, *Filtration*, **3**(1), 40-47.

Tarleton E.S. and Hancock D.L. (1997) Using mechatronics for the interpretation and modelling of the pressure filter cycle. *Trans IChemE* **75**, 298-308.

Tarleton E.S. and Willmer S.A. (1997) The effects of scale and process parameters in cake filtration. *Trans IChemE* **75(A)**, 497-507.

Tarleton E.S. (1999a) The use of electrode probes in determinations of filter cake formation and batch filter scale-up. *Mineral Engineering* **12**, 1263-1274.

Tarleton E.S. (1999b) Using mechatronics technology to assess pressure filtration. *Powder Technology* **104**, 121-129.

Tarleton E.S., 2008 Cake filter scale-up, simulation and data acquisition, *J. Chinese Institute Chemical Engineers*, **39**, 151-160

Theliander H. and Fathi-Najafi M. (1996) Simulation of the build up of a filter cake. *Filtration and Separation* **33**, 417-420.

Tien C. (1991) Penetration of fine particles within filter cakes in cake filtration. *Journal of the Chinese Institute of Chemical Engineers* **22**, 385-391.

Tien C., Teoh S.K. and Tan R.B.H. (2001) Cake filtration analysis- the effect of the relationship between the pore liquid pressure and the cake compressive stress. *Chemical Engineering Science* **56**, 5361-5369.

Tiller F.M. (1953) The role of porosity in filtration I: numerical methods. *Chemical Engineering Progress* **49**, 467-479.

Tiller, F.M. and Huang, C.J. (1961) Filtration equipment. Theory. *Ind. Eng. Chem.*, **53** (7): 529.

Tiller F.M. and Green T.C. (1973) Role of porosity in filtration IX: skin effect with highly compressible materials. *AIChE Journal* **19**, 1266-1269.

Tiller F.M. and Crump J.R. (1977) Solid-liquid separation: an overview. *Chemical Engineering Progress* **73**, 65-75.

Tiller F.M., Crump J.R. and Ville F. (1979) Filtration theory in its historical perspective, a revised approach with surprises. *World Filtration Congress II*, 1-13.

Tiller F.M. and Leu W.F. (1980) Basic data fitting in filtration. *Journal of the Chinese Institute of Chemical Engineers* **11**, 61-70.

Tiller, F.M., Chow, R., Weber, W., and Davies, O. (1981) Clogging phenomena in the filtration of liquefied coal. *Chem. Eng. Prog*., **77**: 61.

Tiller F.M. and Yeh C.S. (1987) The role of porosity in filtration. Part XI: filtration followed by expression. *AIChE Journal* **33**, 1241-1255.

Tiller F.M., Hsyung N.B. and Cong D.Z. (1995) The role of porosity in filtration: XII. filtration with sedimentation. *AIChemE Journal* **41**, 1153-1164.

Tosun, I., Willis, M.S., Desai, F., and Chase, G.G. (1995) Analysis of drag and particulate stress in porous media flows. *Chem. Eng. Sci*., **50** (12): 1961.

Tosun I. (1986) Formulation of cake filtration. *Chemical Engineering Science* **41**, 2563-2568.

Wakeman R.J. (1978) A numerical integration of the differential equations describing the formation of and flow in compressible filter cakes. *Trans IChemE* **56**, 258-265.

Wakeman R.J. (1981a) Thickening and filtration: a review and evaluation of recent research. *Trans IChemE* **59**, 147-160.

Wakeman R.J. (1981b) The formation and properties of apparently incompressible filter cakes under vacuum on downward facing surfaces. *Trans IChemE* **59**, 260-270.

Wakeman R.J. (1985) Filtration theory: formation and structure of compressible filter cakes. In: *Mathematical Models and Design Methods in Solid-Liquid Separation.* Ed: A. Rushton. Martinus Nijhoffp, Dordrecht.

Wakeman R.J. and Tarleton E.S. (1999) *Filtration: equipment selection, modelling and process simulation*. Elsevier, Oxford.

Wakeman R.J. and Tarleton E.S. (2005) *Solid/Liquid Separation: Principles of Industrial Filtration*. Elsevier, Oxford.

Wakeman R.J. (2007a) The influence of particle properties on filtration. *Separation and Purification Technology* **58**, 234-241.

Willis, M.S. and Tosun, I. (1980) A rigorous cake filtration theory. *Chem. Eng. Sci*., 35: 2427.

Willis M. S., Collins R. M. and Bridges W. G. (1983), Complete analysis of non-parabolic filtration behavior.*Chem. Eng. Res. Des.* **61**, 96-109.

Wu, Y. (1994) An analysis of constant-pressure filtration. *Chem. Eng. Sci*., **49** (6):831.

Appendix I: MODEL FLOW DIAGRAM

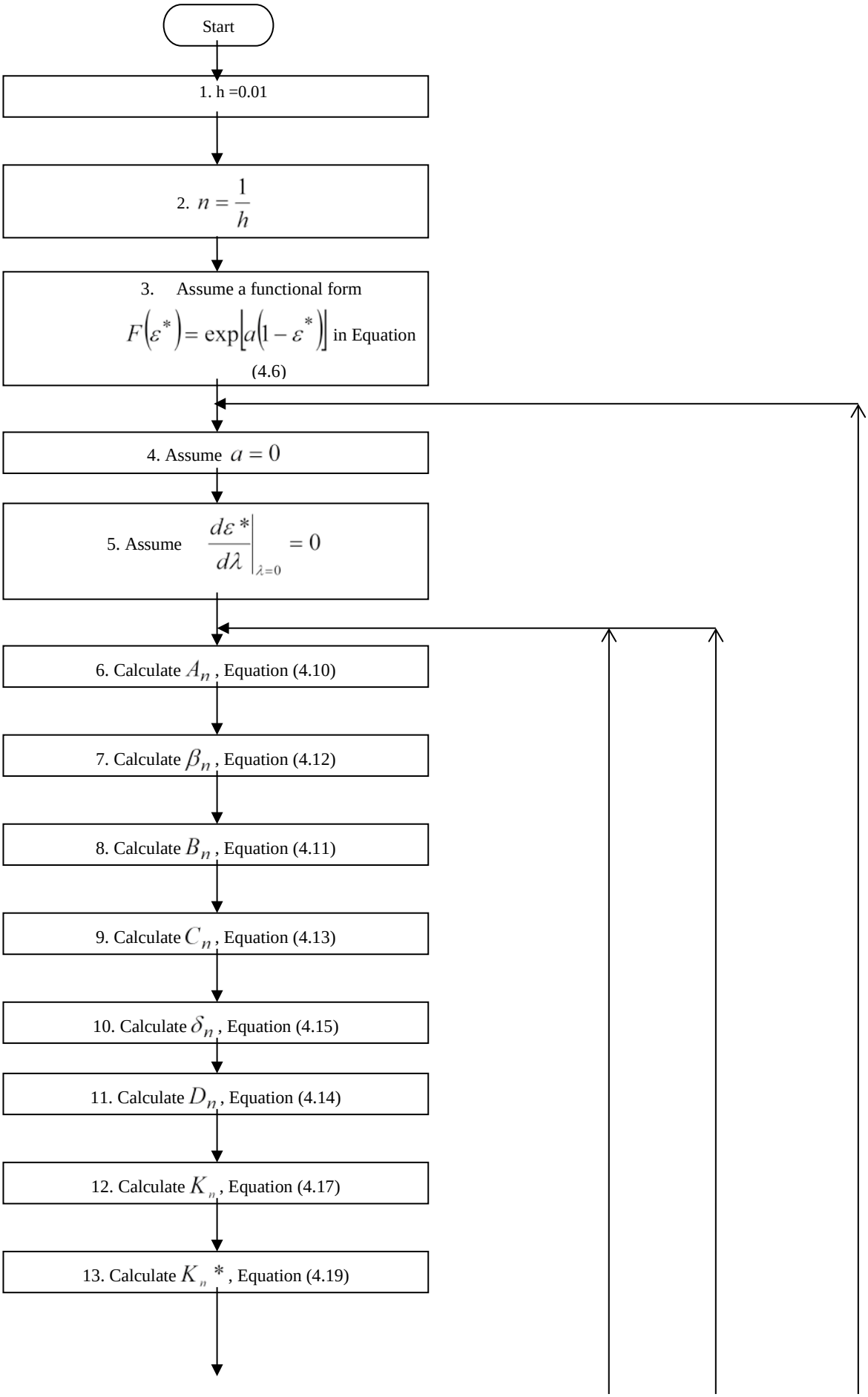
Start
1. h =0.01
2. $n = \frac{1}{h}$
3. Assume a functional form $F(\varepsilon^*) = \exp[a(1-\varepsilon^*)]$ in Equation (4.6)
4. Assume $a = 0$
5. Assume $\left.\frac{d\varepsilon^*}{d\lambda}\right|_{\lambda=0} = 0$
6. Calculate A_n, Equation (4.10)
7. Calculate β_n, Equation (4.12)
8. Calculate B_n, Equation (4.11)
9. Calculate C_n, Equation (4.13)
10. Calculate δ_n, Equation (4.15)
11. Calculate D_n, Equation (4.14)
12. Calculate K_n, Equation (4.17)
13. Calculate K_n^*, Equation (4.19)

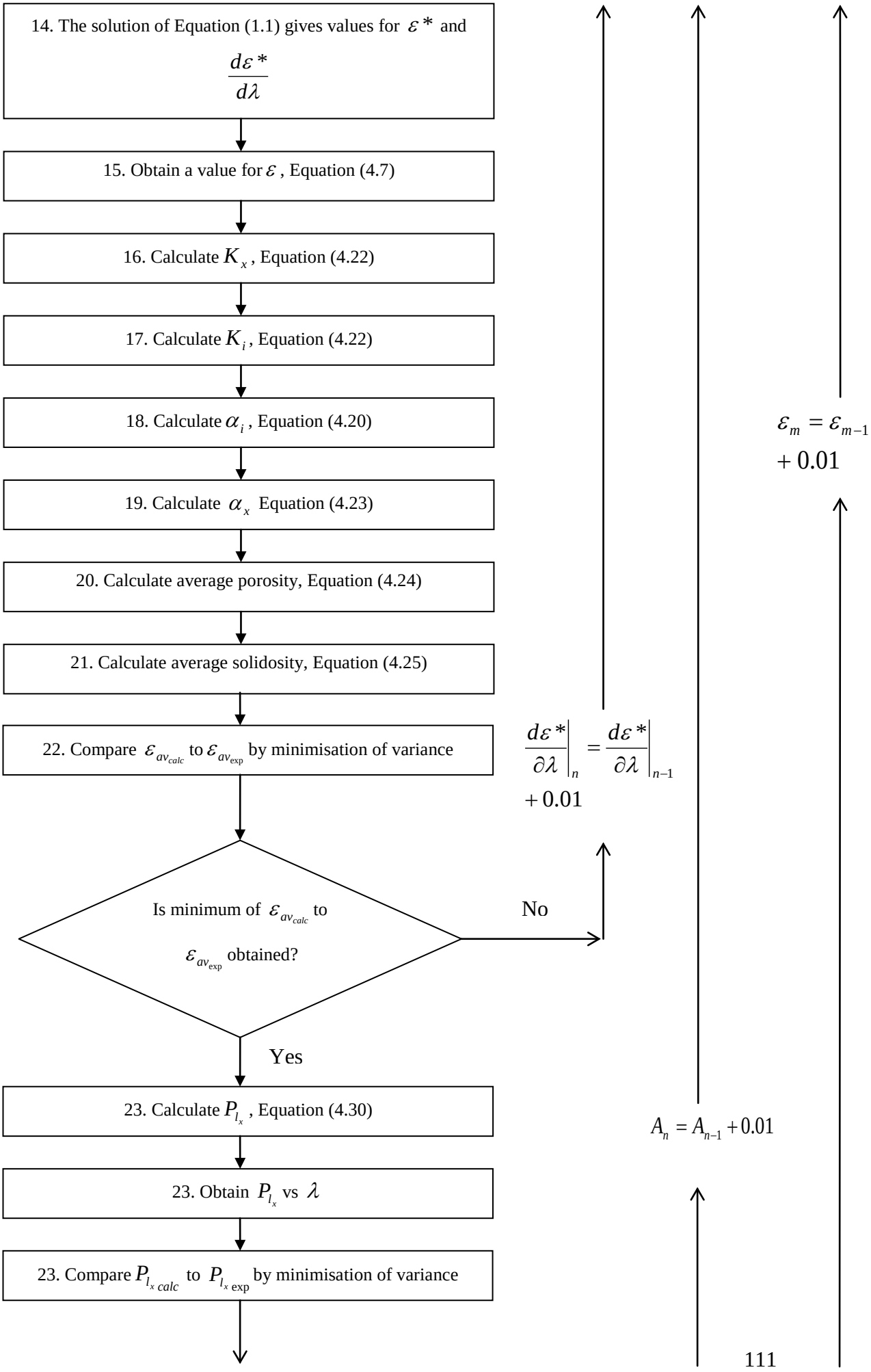
14. The solution of Equation (1.1) gives values for ε^* and $\frac{d\varepsilon^*}{d\lambda}$
15. Obtain a value for ε, Equation (4.7)
16. Calculate K_x, Equation (4.22)
17. Calculate K_i, Equation (4.22)
18. Calculate α_i, Equation (4.20)
19. Calculate α_x Equation (4.23)
20. Calculate average porosity, Equation (4.24)
21. Calculate average solidosity, Equation (4.25)
22. Compare $\varepsilon_{av_{calc}}$ to $\varepsilon_{av_{\exp}}$ by minimisation of variance
Is minimum of $\varepsilon_{av_{calc}}$ to $\varepsilon_{av_{\exp}}$ obtained?
No
Yes
23. Calculate P_{l_x}, Equation (4.30)
23. Obtain P_{l_x} vs λ
23. Compare $P_{l_x\,calc}$ to $P_{l_x\,\exp}$ by minimisation of variance
$\left.\frac{d\varepsilon^*}{\partial\lambda}\right|_n = \left.\frac{d\varepsilon^*}{\partial\lambda}\right|_{n-1} + 0.01$
$A_n = A_{n-1} + 0.01$
$\varepsilon_m = \varepsilon_{m-1} + 0.01$

AppendiX 1: Model flow diagram

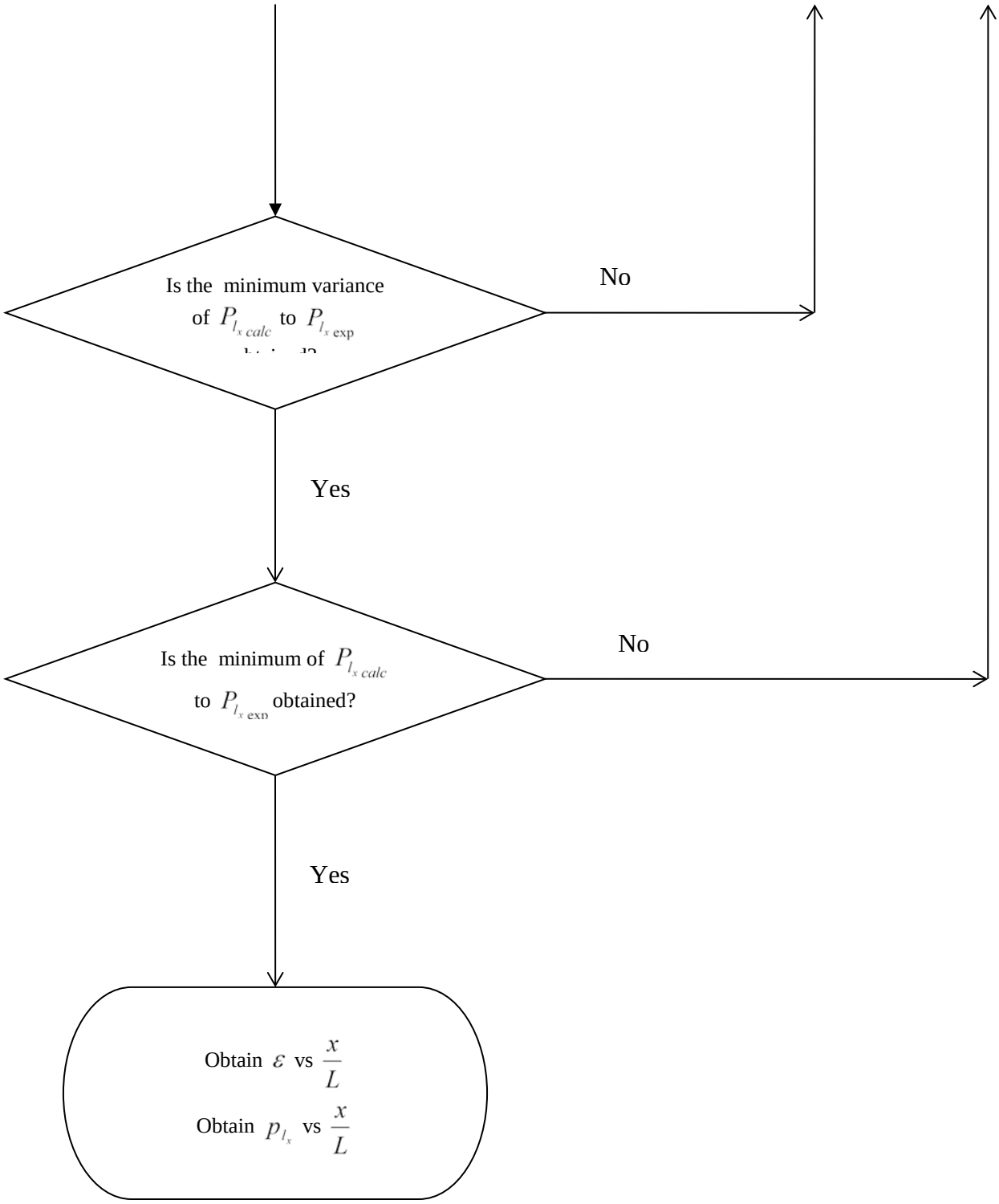

Appendix II: MODEL WORKSHEET

Material	Talc	
	Inputs	
	em	0.57
	e0	0.95
	solids density	2650
	viscosity	0.001
	Pressure	400000
	Particle diameter	0.0000085
	c/Vs	0.05
	Liquid Density	1000
	time	185
	eav exp	0.666
Assumed values	y'	0.31
In Main Equation	a	3.79
step size	h	0.01
	Output	
happel cell model	km	4.04255E-13
	ki	8.80126E-12
	alpha m	2.17E+09
	alpha i	3.42E+08
	D(ei-em/1-em)	0.88372093
	D(ei-em/1-em)	0.708444629
	dpl/de @m	701754.386
	dpl/de @i	2069.875852
	Em	0.000121986
	Ei	2.28391E-06

alpha av	1.28E+09
k av	1.47566E-12
e av	0.670

ei	**ex below interface**						
0.875	0.874						
pli							
4.00E+05							
mbc							
ei	lb/2	e0-ei	ei-em	1-ei	1-e0	**DE/DY CALC**	**DE/DY ASSUMED**
0.875	0.5	0.075	0.305	0.125	0.05	0.31	0.31
a	**b**	**c**					
1	-1.9810175	0.967679975					
		e_i +	1.106				
		e_i -	0.875				

Runge Kutta

n	e (POROSITY)	x	y (e*)	y'	A_n	beta $_n$	B_n	C_n	Sigma $_n$	D_n	K_n	K^*_n
0	0.570	0	0.0000	0.31018	0.00140	0.00155	0.00141	0.00141	0.00156	0.00142	0.00141	0.00282
1	0.571	0.01	0.0031	0.31300	0.00151	0.00157	0.00152	0.00152	0.00157	0.00154	0.00152	0.00305
2	0.572	0.02	0.0063	0.31604	0.00154	0.00158	0.00155	0.00155	0.00159	0.00157	0.00155	0.00310
3	0.574	0.03	0.0094	0.31915	0.00157	0.00160	0.00158	0.00158	0.00160	0.00160	0.00158	0.00316
4	0.575	0.04	0.0126	0.32231	0.00160	0.00162	0.00161	0.00161	0.00162	0.00163	0.00161	0.00322
5	0.576	0.05	0.0159	0.32553	0.00163	0.00163	0.00164	0.00164	0.00164	0.00166	0.00164	0.00329
6	0.577	0.06	0.0192	0.32882	0.00166	0.00165	0.00168	0.00168	0.00165	0.00169	0.00167	0.00335
7	0.579	0.07	0.0225	0.33217	0.00169	0.00167	0.00171	0.00171	0.00167	0.00173	0.00170	0.00342
8	0.580	0.08	0.0258	0.33559	0.00173	0.00168	0.00174	0.00174	0.00169	0.00176	0.00174	0.00349
9	0.581	0.09	0.0292	0.33908	0.00176	0.00170	0.00178	0.00178	0.00170	0.00180	0.00177	0.00356
10	0.582	0.1	0.0326	0.34264	0.00180	0.00172	0.00181	0.00182	0.00172	0.00184	0.00181	0.00363
11	0.584	0.11	0.0360	0.34627	0.00183	0.00174	0.00185	0.00185	0.00174	0.00187	0.00185	0.00371
12	0.585	0.12	0.0395	0.34997	0.00187	0.00175	0.00189	0.00189	0.00176	0.00191	0.00188	0.00378
13	0.586	0.13	0.0430	0.35376	0.00191	0.00177	0.00193	0.00193	0.00178	0.00195	0.00192	0.00386
14	0.588	0.14	0.0466	0.35762	0.00195	0.00179	0.00197	0.00197	0.00180	0.00200	0.00197	0.00395
15	0.589	0.15	0.0502	0.36156	0.00199	0.00181	0.00201	0.00201	0.00182	0.00204	0.00201	0.00403
16	0.590	0.16	0.0538	0.36559	0.00204	0.00183	0.00206	0.00206	0.00184	0.00208	0.00205	0.00412
17	0.592	0.17	0.0575	0.36971	0.00208	0.00185	0.00210	0.00210	0.00186	0.00213	0.00210	0.00421
18	0.593	0.18	0.0612	0.37392	0.00213	0.00187	0.00215	0.00215	0.00188	0.00218	0.00214	0.00430
19	0.595	0.19	0.0650	0.37822	0.00217	0.00190	0.00220	0.00220	0.00190	0.00223	0.00219	0.00440
20	0.596	0.2	0.0688	0.38262	0.00222	0.00192	0.00225	0.00225	0.00192	0.00228	0.00224	0.00450
21	0.598	0.21	0.0726	0.38712	0.00227	0.00194	0.00230	0.00230	0.00195	0.00233	0.00229	0.00460
22	0.599	0.22	0.0765	0.39172	0.00233	0.00196	0.00235	0.00235	0.00197	0.00238	0.00234	0.00471
23	0.601	0.23	0.0805	0.39643	0.00238	0.00199	0.00241	0.00241	0.00199	0.00244	0.00240	0.00482
24	0.602	0.24	0.0844	0.40124	0.00244	0.00201	0.00246	0.00247	0.00202	0.00250	0.00246	0.00493
25	0.604	0.25	0.0885	0.40618	0.00249	0.00204	0.00252	0.00252	0.00204	0.00256	0.00251	0.00505
26	0.605	0.26	0.0926	0.41123	0.00255	0.00206	0.00258	0.00259	0.00207	0.00262	0.00257	0.00517
27	0.607	0.27	0.0967	0.41640	0.00262	0.00209	0.00265	0.00265	0.00210	0.00269	0.00264	0.00530
28	0.608	0.28	0.1009	0.42170	0.00268	0.00212	0.00271	0.00271	0.00212	0.00275	0.00270	0.00543
29	0.610	0.29	0.1051	0.42713	0.00275	0.00214	0.00278	0.00278	0.00215	0.00282	0.00277	0.00557
30	0.612	0.3	0.1094	0.43269	0.00282	0.00217	0.00285	0.00285	0.00218	0.00290	0.00284	0.00571
31	0.613	0.31	0.1138	0.43840	0.00289	0.00220	0.00293	0.00293	0.00221	0.00297	0.00291	0.00585
32	0.615	0.32	0.1182	0.44426	0.00296	0.00223	0.00300	0.00300	0.00224	0.00305	0.00299	0.00601
33	0.617	0.33	0.1227	0.45026	0.00304	0.00226	0.00308	0.00308	0.00227	0.00313	0.00307	0.00616
34	0.618	0.34	0.1272	0.45643	0.00312	0.00229	0.00316	0.00316	0.00230	0.00321	0.00315	0.00633
35	0.620	0.35	0.1318	0.46275	0.00321	0.00232	0.00325	0.00325	0.00233	0.00330	0.00323	0.00650

33	0.617	0.33	0.1227	0.45026	0.00304	0.00226	0.00308	0.00308	0.00227	0.00313	0.00307	0.00616
34	0.618	0.34	0.1272	0.45643	0.00312	0.00229	0.00316	0.00316	0.00230	0.00321	0.00315	0.00633
35	0.620	0.35	0.1318	0.46275	0.00321	0.00232	0.00325	0.00325	0.00233	0.00330	0.00323	0.00650
36	0.622	0.36	0.1365	0.46925	0.00329	0.00235	0.00334	0.00334	0.00236	0.00339	0.00332	0.00668
37	0.624	0.37	0.1412	0.47593	0.00338	0.00239	0.00343	0.00343	0.00240	0.00349	0.00341	0.00686
38	0.625	0.38	0.1460	0.48279	0.00348	0.00242	0.00352	0.00353	0.00243	0.00358	0.00351	0.00705
39	0.627	0.39	0.1509	0.48984	0.00357	0.00246	0.00362	0.00363	0.00247	0.00369	0.00361	0.00725
40	0.629	0.4	0.1558	0.49710	0.00368	0.00249	0.00373	0.00373	0.00250	0.00379	0.00371	0.00746
41	0.631	0.41	0.1608	0.50456	0.00378	0.00253	0.00384	0.00384	0.00254	0.00390	0.00382	0.00768
42	0.633	0.42	0.1659	0.51224	0.00389	0.00257	0.00395	0.00395	0.00258	0.00402	0.00393	0.00791
43	0.635	0.43	0.1710	0.52015	0.00401	0.00261	0.00407	0.00407	0.00262	0.00414	0.00405	0.00814
44	0.637	0.44	0.1763	0.52829	0.00413	0.00265	0.00419	0.00419	0.00266	0.00427	0.00417	0.00839
45	0.639	0.45	0.1816	0.53668	0.00426	0.00269	0.00432	0.00432	0.00271	0.00440	0.00430	0.00865
46	0.641	0.46	0.1870	0.54533	0.00439	0.00274	0.00446	0.00446	0.00275	0.00454	0.00443	0.00892
47	0.643	0.47	0.1925	0.55425	0.00453	0.00278	0.00460	0.00460	0.00279	0.00469	0.00458	0.00920
48	0.645	0.48	0.1981	0.56346	0.00467	0.00283	0.00475	0.00475	0.00284	0.00484	0.00472	0.00950
49	0.647	0.49	0.2038	0.57296	0.00482	0.00288	0.00490	0.00490	0.00289	0.00500	0.00488	0.00981
50	0.650	0.5	0.2096	0.58277	0.00498	0.00293	0.00506	0.00507	0.00294	0.00517	0.00504	0.01014
51	0.652	0.51	0.2154	0.59290	0.00515	0.00298	0.00523	0.00524	0.00299	0.00534	0.00521	0.01048
52	0.654	0.52	0.2214	0.60338	0.00532	0.00303	0.00541	0.00542	0.00304	0.00553	0.00538	0.01084
53	0.656	0.53	0.2275	0.61421	0.00551	0.00308	0.00560	0.00560	0.00310	0.00572	0.00557	0.01121
54	0.659	0.54	0.2337	0.62543	0.00570	0.00314	0.00580	0.00580	0.00316	0.00592	0.00577	0.01161
55	0.661	0.55	0.2400	0.63703	0.00590	0.00320	0.00601	0.00601	0.00322	0.00614	0.00597	0.01202
56	0.664	0.56	0.2464	0.64906	0.00612	0.00326	0.00623	0.00623	0.00328	0.00637	0.00619	0.01246
57	0.666	0.57	0.2530	0.66152	0.00634	0.00332	0.00646	0.00646	0.00334	0.00660	0.00642	0.01293
58	0.669	0.58	0.2597	0.67445	0.00658	0.00339	0.00670	0.00670	0.00341	0.00686	0.00666	0.01341
59	0.671	0.59	0.2665	0.68786	0.00683	0.00346	0.00696	0.00696	0.00347	0.00712	0.00692	0.01393
60	0.674	0.6	0.2734	0.70179	0.00709	0.00353	0.00723	0.00723	0.00355	0.00740	0.00718	0.01447
61	0.677	0.61	0.2805	0.71626	0.00737	0.00360	0.00752	0.00752	0.00362	0.00770	0.00747	0.01505
62	0.679	0.62	0.2878	0.73131	0.00767	0.00368	0.00782	0.00782	0.00370	0.00802	0.00777	0.01566
63	0.682	0.63	0.2952	0.74696	0.00798	0.00375	0.00814	0.00815	0.00378	0.00835	0.00809	0.01630
64	0.685	0.64	0.3027	0.76326	0.00831	0.00384	0.00848	0.00849	0.00386	0.00870	0.00843	0.01699

65	0.688	0.65	0.3104	0.78025	0.00866	0.00392	0.00884	0.00885	0.00395	0.00908	0.00879	0.01771
66	0.691	0.66	0.3183	0.79796	0.00904	0.00401	0.00923	0.00924	0.00404	0.00948	0.00917	0.01848
67	0.694	0.67	0.3264	0.81644	0.00943	0.00411	0.00964	0.00965	0.00413	0.00991	0.00957	0.01931
68	0.697	0.68	0.3346	0.83575	0.00986	0.00420	0.01008	0.01008	0.00423	0.01037	0.01001	0.02018
69	0.700	0.69	0.3431	0.85593	0.01031	0.00431	0.01054	0.01055	0.00433	0.01085	0.01047	0.02111
70	0.704	0.7	0.3518	0.87704	0.01079	0.00441	0.01104	0.01105	0.00444	0.01137	0.01096	0.02211
71	0.707	0.71	0.3606	0.89915	0.01130	0.00452	0.01157	0.01158	0.00455	0.01193	0.01148	0.02317
72	0.711	0.72	0.3698	0.92233	0.01185	0.00464	0.01214	0.01215	0.00467	0.01252	0.01205	0.02431
73	0.714	0.73	0.3791	0.94664	0.01244	0.00476	0.01275	0.01276	0.00480	0.01316	0.01265	0.02553
74	0.718	0.74	0.3887	0.97217	0.01307	0.00489	0.01340	0.01341	0.00493	0.01384	0.01329	0.02685
75	0.721	0.75	0.3985	0.99902	0.01375	0.00503	0.01410	0.01411	0.00507	0.01458	0.01399	0.02825
76	0.725	0.76	0.4087	1.02727	0.01448	0.00517	0.01486	0.01487	0.00521	0.01538	0.01473	0.02977
77	0.729	0.77	0.4191	1.05704	0.01526	0.00532	0.01567	0.01568	0.00536	0.01623	0.01554	0.03140
78	0.733	0.78	0.4298	1.08844	0.01611	0.00548	0.01655	0.01656	0.00553	0.01716	0.01641	0.03316
79	0.738	0.79	0.4409	1.12160	0.01702	0.00565	0.01749	0.01751	0.00570	0.01816	0.01734	0.03507
80	0.742	0.8	0.4523	1.15667	0.01801	0.00583	0.01852	0.01854	0.00588	0.01925	0.01836	0.03713
81	0.746	0.81	0.4640	1.19380	0.01908	0.00602	0.01963	0.01965	0.00607	0.02043	0.01945	0.03936
82	0.751	0.82	0.4761	1.23316	0.02024	0.00622	0.02084	0.02086	0.00627	0.02171	0.02065	0.04178
83	0.756	0.83	0.4887	1.27494	0.02149	0.00643	0.02215	0.02218	0.00649	0.02311	0.02194	0.04442
84	0.761	0.84	0.5016	1.31935	0.02286	0.00665	0.02358	0.02361	0.00671	0.02463	0.02335	0.04728
85	0.766	0.85	0.5151	1.36664	0.02435	0.00689	0.02513	0.02516	0.00696	0.02629	0.02488	0.05041
86	0.771	0.86	0.5290	1.41705	0.02598	0.00715	0.02683	0.02687	0.00722	0.02811	0.02656	0.05382
87	0.777	0.87	0.5434	1.47088	0.02776	0.00742	0.02868	0.02872	0.00750	0.03010	0.02839	0.05756
88	0.782	0.88	0.5584	1.52843	0.02970	0.00772	0.03071	0.03076	0.00780	0.03228	0.03039	0.06164
89	0.788	0.89	0.5740	1.59007	0.03182	0.00803	0.03293	0.03298	0.00812	0.03468	0.03258	0.06611
90	0.794	0.9	0.5902	1.65617	0.03415	0.00837	0.03536	0.03542	0.00846	0.03731	0.03497	0.07100
91	0.801	0.91	0.6071	1.72718	0.03670	0.00873	0.03802	0.03809	0.00883	0.04020	0.03760	0.07637
92	0.807	0.92	0.6248	1.80355	0.03948	0.00912	0.04093	0.04101	0.00922	0.04338	0.04047	0.08224
93	0.814	0.93	0.6432	1.88579	0.04254	0.00954	0.04411	0.04420	0.00965	0.04685	0.04361	0.08867
94	0.822	0.94	0.6625	1.97446	0.04587	0.00999	0.04757	0.04768	0.01011	0.05066	0.04704	0.09568
95	0.829	0.95	0.6827	2.07014	0.04949	0.01047	0.05133	0.05145	0.01061	0.05480	0.05076	0.10329
96	0.838	0.96	0.7040	2.17342	0.05340	0.01100	0.05539	0.05552	0.01114	0.05928	0.05477	0.11150
97	0.846	0.97	0.7262	2.28492	0.05761	0.01157	0.05971	0.05985	0.01172	0.06408	0.05906	0.12027
98	0.855	0.98	0.7497	2.40519	0.06206	0.01218	0.06424	0.06440	0.01235	0.06914	0.06356	0.12949
99	0.864	0.99	0.7744	2.53468	0.06667	0.01284	0.06888	0.06905	0.01302	0.07433	0.06820	0.13895
100	0.874	1	0.8004	2.67363	0.07131	0.01355	0.07344	0.07361	0.01374	0.07946	0.07279	0.14829

		using the cell model									
		get k for different e				8		Ei			
n	exp(a(1-e*)	e*	e	kx	ki	alpha	1-ei/1-ex		dpl/de at i	E	dpl/de at x
0	44.2564	0	0.570	4.043E-13	8.801E-12	2.17E+09	0.291555371	2.3E-06	2069.875852	0.000101	581474.834
1	43.736854	0.00311581	0.571	4.086E-13	8.801E-12	2.15E+09	0.292360388	2.3E-06	2069.875852	9.99E-05	570067.378
2	43.218602	0.006260948	0.572	4.131E-13	8.801E-12	2.14E+09	0.293177502	2.3E-06	2069.875852	9.87E-05	558785.906
3	42.701516	0.00943683	0.574	4.176E-13	8.801E-12	2.12E+09	0.294007252	2.3E-06	2069.875852	9.75E-05	547627.044
4	42.185606	0.012644044	0.575	4.223E-13	8.801E-12	2.10E+09	0.294849968	2.3E-06	2069.875852	9.63E-05	536590.553
5	41.670886	0.015883193	0.576	4.27E-13	8.801E-12	2.08E+09	0.295705992	2.3E-06	2069.875852	9.52E-05	525676.193
6	41.157367	0.019154898	0.577	4.319E-13	8.801E-12	2.07E+09	0.296575681	2.3E-06	2069.875852	9.4E-05	514883.722
7	40.645063	0.022459797	0.579	4.368E-13	8.801E-12	2.05E+09	0.297459403	2.3E-06	2069.875852	9.28E-05	504212.899
8	40.133986	0.025798548	0.580	4.419E-13	8.801E-12	2.03E+09	0.29835754	2.3E-06	2069.875852	9.17E-05	493663.481
9	39.62415	0.029171827	0.581	4.47E-13	8.801E-12	2.01E+09	0.299270491	2.3E-06	2069.875852	9.05E-05	483235.224
10	39.115568	0.032580331	0.582	4.523E-13	8.801E-12	2.00E+09	0.300198667	2.3E-06	2069.875852	8.93E-05	472927.885
11	38.608254	0.036024777	0.584	4.577E-13	8.801E-12	1.98E+09	0.301142499	2.3E-06	2069.875852	8.82E-05	462741.219
12	38.102223	0.039505906	0.585	4.632E-13	8.801E-12	1.96E+09	0.302102431	2.3E-06	2069.875852	8.7E-05	452674.98
13	37.597487	0.04302448	0.586	4.689E-13	8.801E-12	1.95E+09	0.303078927	2.3E-06	2069.875852	8.59E-05	442728.921
14	37.094063	0.046581283	0.588	4.747E-13	8.801E-12	1.93E+09	0.30407247	2.3E-06	2069.875852	8.47E-05	432902.796
15	36.591965	0.050177127	0.589	4.806E-13	8.801E-12	1.91E+09	0.305083563	2.3E-06	2069.875852	8.36E-05	423196.356
16	36.091209	0.053812846	0.590	4.866E-13	8.801E-12	1.89E+09	0.306112727	2.3E-06	2069.875852	8.24E-05	413609.351
17	35.591809	0.057489304	0.592	4.928E-13	8.801E-12	1.88E+09	0.307160508	2.3E-06	2069.875852	8.13E-05	404141.532
18	35.093783	0.06120739	0.593	4.991E-13	8.801E-12	1.86E+09	0.308227473	2.3E-06	2069.875852	8.02E-05	394792.649
19	34.597146	0.064968024	0.595	5.056E-13	8.801E-12	1.84E+09	0.309314215	2.3E-06	2069.875852	7.9E-05	385562.447
20	34.101915	0.068772154	0.596	5.123E-13	8.801E-12	1.82E+09	0.310421351	2.3E-06	2069.875852	7.79E-05	376450.676
21	33.608107	0.072620762	0.598	5.191E-13	8.801E-12	1.81E+09	0.311549525	2.3E-06	2069.875852	7.68E-05	367457.081
22	33.115739	0.076514861	0.599	5.261E-13	8.801E-12	1.79E+09	0.312699413	2.3E-06	2069.875852	7.56E-05	358581.406
23	32.62483	0.080455498	0.601	5.333E-13	8.801E-12	1.77E+09	0.313871715	2.3E-06	2069.875852	7.45E-05	349823.395
24	32.135398	0.084443758	0.602	5.406E-13	8.801E-12	1.75E+09	0.31506717	2.3E-06	2069.875852	7.34E-05	341182.792
25	31.647461	0.088480763	0.604	5.482E-13	8.801E-12	1.74E+09	0.316286544	2.3E-06	2069.875852	7.23E-05	332659.336
26	31.161038	0.092567671	0.605	5.559E-13	8.801E-12	1.72E+09	0.317530644	2.3E-06	2069.875852	7.12E-05	324252.77
27	30.676149	0.096705687	0.607	5.639E-13	8.801E-12	1.70E+09	0.318800314	2.3E-06	2069.875852	7.01E-05	315962.831
28	30.192814	0.100896053	0.608	5.72E-13	8.801E-12	1.68E+09	0.320096435	2.3E-06	2069.875852	6.9E-05	307789.257
29	29.711054	0.10514006	0.610	5.804E-13	8.801E-12	1.67E+09	0.321419935	2.3E-06	2069.875852	6.79E-05	299731.785
30	29.23089	0.109439044	0.612	5.891E-13	8.801E-12	1.65E+09	0.322771784	2.3E-06	2069.875852	6.68E-05	291790.15
31	28.752343	0.113794393	0.613	5.979E-13	8.801E-12	1.63E+09	0.324153003	2.3E-06	2069.875852	6.57E-05	283964.085
32	28.275435	0.118207545	0.615	6.071E-13	8.801E-12	1.61E+09	0.325564664	2.3E-06	2069.875852	6.46E-05	276253.321

33	27.800189	0.122679992	0.617	6.164E-13	8.801E-12	1.60E+09	0.327007891	2.3E-06	2069.875852	6.35E-05	268657.591
34	27.326629	0.127213285	0.618	6.261E-13	8.801E-12	1.58E+09	0.32848387	2.3E-06	2069.875852	6.24E-05	261176.621
35	26.854778	0.131809034	0.620	6.361E-13	8.801E-12	1.56E+09	0.329993847	2.3E-06	2069.875852	6.13E-05	253810.141
36	26.384661	0.136468913	0.622	6.463E-13	8.801E-12	1.54E+09	0.331539135	2.3E-06	2069.875852	6.03E-05	246557.875
37	25.916303	0.141194663	0.624	6.569E-13	8.801E-12	1.53E+09	0.333121118	2.3E-06	2069.875852	5.92E-05	239419.546
38	25.44973	0.145988093	0.625	6.678E-13	8.801E-12	1.51E+09	0.334741256	2.3E-06	2069.875852	5.81E-05	232394.878
39	24.984968	0.150851089	0.627	6.791E-13	8.801E-12	1.49E+09	0.33640109	2.3E-06	2069.875852	5.71E-05	225483.589
40	24.522045	0.155785612	0.629	6.907E-13	8.801E-12	1.47E+09	0.338102248	2.3E-06	2069.875852	5.6E-05	218685.399
41	24.06099	0.160793707	0.631	7.027E-13	8.801E-12	1.46E+09	0.339846453	2.3E-06	2069.875852	5.5E-05	212000.022
42	23.60183	0.165877505	0.633	7.151E-13	8.801E-12	1.44E+09	0.341635526	2.3E-06	2069.875852	5.39E-05	205427.173
43	23.144596	0.171039228	0.635	7.279E-13	8.801E-12	1.42E+09	0.343471398	2.3E-06	2069.875852	5.29E-05	198966.563
44	22.689319	0.176281196	0.637	7.411E-13	8.801E-12	1.40E+09	0.345356115	2.3E-06	2069.875852	5.18E-05	192617.901
45	22.236029	0.18160583	0.639	7.548E-13	8.801E-12	1.38E+09	0.347291849	2.3E-06	2069.875852	5.08E-05	186380.895
46	21.78476	0.18701566	0.641	7.69E-13	8.801E-12	1.37E+09	0.349280905	2.3E-06	2069.875852	4.98E-05	180255.248
47	21.335545	0.192513333	0.643	7.837E-13	8.801E-12	1.35E+09	0.351325738	2.3E-06	2069.875852	4.87E-05	174240.662
48	20.888419	0.198101613	0.645	7.989E-13	8.801E-12	1.33E+09	0.353428956	2.3E-06	2069.875852	4.77E-05	168336.836
49	20.443417	0.203783396	0.647	8.148E-13	8.801E-12	1.31E+09	0.355593341	2.3E-06	2069.875852	4.67E-05	162543.465
50	20.000576	0.209561716	0.650	8.312E-13	8.801E-12	1.30E+09	0.357821859	2.3E-06	2069.875852	4.57E-05	156860.243
51	19.559935	0.215439751	0.652	8.482E-13	8.801E-12	1.28E+09	0.360117678	2.3E-06	2069.875852	4.47E-05	151286.859
52	19.121532	0.221420833	0.654	8.659E-13	8.801E-12	1.26E+09	0.362484183	2.3E-06	2069.875852	4.37E-05	145823
53	18.685409	0.227508462	0.656	8.843E-13	8.801E-12	1.24E+09	0.364924998	2.3E-06	2069.875852	4.27E-05	140468.349
54	18.251606	0.23370631	0.659	9.035E-13	8.801E-12	1.22E+09	0.367444008	2.3E-06	2069.875852	4.17E-05	135222.584
55	17.820168	0.24001824	0.661	9.235E-13	8.801E-12	1.21E+09	0.370045379	2.3E-06	2069.875852	4.07E-05	130085.382
56	17.39114	0.246448311	0.664	9.443E-13	8.801E-12	1.19E+09	0.372733591	2.3E-06	2069.875852	3.97E-05	125056.413
57	16.964569	0.2530008	0.666	9.66E-13	8.801E-12	1.17E+09	0.37551346	2.3E-06	2069.875852	3.87E-05	120135.344
58	16.540501	0.259680209	0.669	9.887E-13	8.801E-12	1.15E+09	0.378390179	2.3E-06	2069.875852	3.78E-05	115321.839
59	16.118989	0.266491286	0.671	1.012E-12	8.801E-12	1.13E+09	0.381369351	2.3E-06	2069.875852	3.68E-05	110615.555
60	15.700084	0.273439041	0.674	1.037E-12	8.801E-12	1.12E+09	0.38445703	2.3E-06	2069.875852	3.59E-05	106016.145
61	15.283839	0.280528765	0.677	1.063E-12	8.801E-12	1.10E+09	0.387659773	2.3E-06	2069.875852	3.49E-05	101523.256
62	14.870311	0.287766052	0.679	1.09E-12	8.801E-12	1.08E+09	0.390984686	2.3E-06	2069.875852	3.4E-05	97136.5315
63	14.459558	0.295156819	0.682	1.119E-12	8.801E-12	1.06E+09	0.394439493	2.3E-06	2069.875852	3.3E-05	92855.6061
64	14.051641	0.302707333	0.685	1.149E-12	8.801E-12	1.04E+09	0.398032596	2.3E-06	2069.875852	3.21E-05	88680.1101

65	13.646624	0.310424239	0.688	1.181E-12	8.801E-12	1.02E+09	0.401773158	2.3E-06	2069.875852	3.12E-05	84609.6668
66	13.244571	0.318314586	0.691	1.214E-12	8.801E-12	1.01E+09	0.405671189	2.3E-06	2069.875852	3.02E-05	80643.8922
67	12.845552	0.326385864	0.694	1.249E-12	8.801E-12	9.88E+08	0.409737648	2.3E-06	2069.875852	2.93E-05	76782.3947
68	12.449638	0.334646036	0.697	1.286E-12	8.801E-12	9.69E+08	0.413984559	2.3E-06	2069.875852	2.84E-05	73024.775
69	12.056904	0.343103581	0.700	1.325E-12	8.801E-12	9.51E+08	0.418425146	2.3E-06	2069.875852	2.75E-05	69370.6249
70	11.667428	0.351767533	0.704	1.366E-12	8.801E-12	9.32E+08	0.423073982	2.3E-06	2069.875852	2.66E-05	65819.5273
71	11.281293	0.360647533	0.707	1.41E-12	8.801E-12	9.13E+08	0.427947174	2.3E-06	2069.875852	2.58E-05	62371.055
72	10.898583	0.369753881	0.711	1.457E-12	8.801E-12	8.95E+08	0.433062569	2.3E-06	2069.875852	2.49E-05	59024.7704
73	10.519389	0.379097591	0.714	1.506E-12	8.801E-12	8.76E+08	0.438439992	2.3E-06	2069.875852	2.4E-05	55780.2249
74	10.143805	0.388690462	0.718	1.559E-12	8.801E-12	8.57E+08	0.44410154	2.3E-06	2069.875852	2.32E-05	52636.9572
75	9.7719292	0.398545143	0.721	1.616E-12	8.801E-12	8.39E+08	0.450071904	2.3E-06	2069.875852	2.23E-05	49594.4934
76	9.4038664	0.408675218	0.725	1.676E-12	8.801E-12	8.20E+08	0.456378777	2.3E-06	2069.875852	2.15E-05	46652.3452
77	9.0397258	0.419095293	0.729	1.741E-12	8.801E-12	8.01E+08	0.463053318	2.3E-06	2069.875852	2.06E-05	43810.0091
78	8.6796227	0.429821093	0.733	1.81E-12	8.801E-12	7.82E+08	0.470130712	2.3E-06	2069.875852	1.98E-05	41066.9651
79	8.3236787	0.440869575	0.738	1.885E-12	8.801E-12	7.63E+08	0.477650852	2.3E-06	2069.875852	1.9E-05	38422.6752
80	7.9720223	0.45225905	0.742	1.966E-12	8.801E-12	7.44E+08	0.485659144	2.3E-06	2069.875852	1.82E-05	35876.5818
81	7.6247892	0.464009319	0.746	2.054E-12	8.801E-12	7.24E+08	0.494207504	2.3E-06	2069.875852	1.74E-05	33428.106
82	7.2821233	0.476141827	0.751	2.149E-12	8.801E-12	7.05E+08	0.503355562	2.3E-06	2069.875852	1.66E-05	31076.6456
83	6.9441768	0.488679833	0.756	2.252E-12	8.801E-12	6.86E+08	0.513172149	2.3E-06	2069.875852	1.59E-05	28821.573
84	6.6111114	0.501648605	0.761	2.366E-12	8.801E-12	6.66E+08	0.523737147	2.3E-06	2069.875852	1.51E-05	26662.2325
85	6.2830992	0.515075629	0.766	2.49E-12	8.801E-12	6.47E+08	0.535143786	2.3E-06	2069.875852	1.44E-05	24597.9375
86	5.9603231	0.528990847	0.771	2.627E-12	8.801E-12	6.27E+08	0.547501552	2.3E-06	2069.875852	1.36E-05	22627.9675
87	5.6429781	0.543426926	0.777	2.779E-12	8.801E-12	6.08E+08	0.560939873	2.3E-06	2069.875852	1.29E-05	20751.5642
88	5.3312723	0.558419546	0.782	2.947E-12	8.801E-12	5.88E+08	0.575612856	2.3E-06	2069.875852	1.22E-05	18967.9276
89	5.0254285	0.574007724	0.788	3.136E-12	8.801E-12	5.68E+08	0.59170543	2.3E-06	2069.875852	1.15E-05	17276.2109
90	4.7256849	0.590234169	0.794	3.347E-12	8.801E-12	5.48E+08	0.609441401	2.3E-06	2069.875852	1.08E-05	15675.5154
91	4.432297	0.607145656	0.801	3.586E-12	8.801E-12	5.28E+08	0.629094158	2.3E-06	2069.875852	1.01E-05	14164.8841
92	4.1455393	0.624793434	0.807	3.858E-12	8.801E-12	5.08E+08	0.651001087	2.3E-06	2069.875852	9.47E-06	12743.2945
93	3.8657067	0.643233637	0.814	4.17E-12	8.801E-12	4.88E+08	0.675583266	2.3E-06	2069.875852	8.83E-06	11409.6498
94	3.5931169	0.66252769	0.822	4.53E-12	8.801E-12	4.67E+08	0.703372851	2.3E-06	2069.875852	8.21E-06	10162.7697
95	3.3281123	0.682742677	0.829	4.951E-12	8.801E-12	4.47E+08	0.735051827	2.3E-06	2069.875852	7.6E-06	9001.37839
96	3.0710619	0.703951613	0.838	5.447E-12	8.801E-12	4.26E+08	0.771508025	2.3E-06	2069.875852	7.01E-06	7924.09121
97	2.8223642	0.726233539	0.846	6.039E-12	8.801E-12	4.06E+08	0.813917991	2.3E-06	2069.875852	6.45E-06	6929.39888
98	2.582449	0.749673309	0.855	6.756E-12	8.801E-12	3.85E+08	0.86387287	2.3E-06	2069.875852	5.9E-06	6015.64847
99	2.3517797	0.77436086	0.864	7.637E-12	8.801E-12	3.64E+08	0.92357563	2.3E-06	2069.875852	5.37E-06	5181.02106
100	2.1308548	0.800389657	0.874	8.742E-12	8.801E-12	3.43E+08	0.996161197	2.3E-06	2069.875852	4.87E-06	4423.50488

n	lamda	ex	ki/kx	1-ei/1-ex	dpl/de ati	f(e*)	dpl/de atx	pl
100	1	0.874	1.00678965	7.945845541	2069.875852	2.130854772	35283.93463	399651.0086
99	0.99	0.864	1.1523966	7.366869259	2069.875852	2.351779654	41326.2364	399242.2532
98	0.98	0.855	1.30273646	6.890652251	2069.875852	2.582448963	47983.61317	398792.106
97	0.97	0.846	1.45732887	6.492188871	2069.875852	2.822364154	55272.1119	398299.7911
96	0.96	0.838	1.61575741	6.153907242	2069.875852	3.071061862	63206.24113	397764.6155
95	0.95	0.829	1.77766038	5.863115625	2069.875852	3.328112254	71799.18524	397185.9574
94	0.94	0.822	1.94272279	5.610429363	2069.875852	3.593116943	81062.98334	396563.2563
93	0.93	0.814	2.11066949	5.388766697	2069.875852	3.865706723	91008.67964	395896.0043
92	0.92	0.807	2.28125941	5.192687787	2069.875852	4.14553929	101646.4503	395183.7395
91	0.91	0.801	2.45428063	5.017947925	2069.875852	4.432297022	112985.7113	394426.0397
90	0.9	0.794	2.62954628	4.86118838	2069.875852	4.725684888	125035.2096	393622.5178
89	0.89	0.788	2.80689098	4.719718018	2069.875852	5.025428502	137803.102	392772.8171
88	0.88	0.782	2.98616796	4.591356159	2069.875852	5.331272329	151297.0222	391876.608
87	0.87	0.777	3.16724652	4.474317613	2069.875852	5.642978054	165524.1387	390933.5847
86	0.86	0.771	3.35000991	4.367127307	2069.875852	5.960323089	180491.205	389943.4623
85	0.85	0.766	3.53435355	4.268556012	2069.875852	6.283099232	196204.603	388905.9749
84	0.84	0.761	3.72018345	4.177571346	2069.875852	6.611111447	212670.3808	387820.8734
83	0.83	0.756	3.90741497	4.093300005	2069.875852	6.94417676	229894.2862	386687.9237
82	0.82	0.751	4.09597162	4.014998333	2069.875852	7.282123269	247881.7952	385506.9051
81	0.81	0.746	4.28578413	3.942029168	2069.875852	7.624789243	266638.1379	384277.6092
80	0.8	0.742	4.4767896	3.873843468	2069.875852	7.97202231	286168.3211	382999.8384
79	0.79	0.738	4.66893079	3.809965598	2069.875852	8.323678723	306477.1478	381673.4052
78	0.78	0.733	4.86215547	3.749981463	2069.875852	8.679622694	327569.2356	380298.1309
77	0.77	0.729	5.05641591	3.693528868	2069.875852	9.039725794	349449.0317	378873.8451
76	0.76	0.725	5.25166835	3.640289627	2069.875852	9.403866399	372120.8276	377400.3849
75	0.75	0.721	5.44787264	3.58998307	2069.875852	9.771929201	395588.7715	375877.5942
74	0.74	0.718	5.64499184	3.542360662	2069.875852	10.14380475	419856.8795	374305.3231
73	0.73	0.714	5.8429919	3.497201527	2069.875852	10.51938903	444929.0459	372683.4273
72	0.72	0.711	6.0418414	3.454308689	2069.875852	10.89858312	470809.0522	371011.768
71	0.71	0.707	6.24151125	3.413505921	2069.875852	11.2812928	497500.5756	369290.211
70	0.7	0.704	6.44197453	3.374635069	2069.875852	11.66742827	525007.1964	367518.6266
69	0.69	0.700	6.64320624	3.337553789	2069.875852	12.05690385	553332.4049	365696.8893
68	0.68	0.697	6.84518316	3.302133606	2069.875852	12.44963771	582479.6074	363824.8774
67	0.67	0.694	7.04788365	3.268258262	2069.875852	12.84555164	612452.1319	361902.4726
66	0.66	0.691	7.25128756	3.235822289	2069.875852	13.24457082	643253.2334	359929.5599
65	0.65	0.688	7.45537608	3.204729779	2069.875852	13.64662359	674886.0986	357906.0273

64	0.64	0.685	7.66013163	3.174893315	2069.875852	14.05164131	707353.8498	355831.7658
63	0.63	0.682	7.86553773	3.146233053	2069.875852	14.45955812	740659.5496	353706.6687
62	0.62	0.679	8.07157896	3.118675907	2069.875852	14.87031084	774806.2037	351530.6321
61	0.61	0.677	8.27824085	3.092154848	2069.875852	15.28383877	809796.765	349303.5542
60	0.6	0.674	8.4855098	3.066608285	2069.875852	15.70008357	845634.1361	347025.3353
59	0.59	0.671	8.69337302	3.041979517	2069.875852	16.11898915	882321.1727	344695.8778
58	0.58	0.669	8.90181846	3.018216257	2069.875852	16.54050149	919860.6856	342315.0859
57	0.57	0.666	9.11083478	2.995270204	2069.875852	16.96456859	958255.4438	339882.8655
56	0.56	0.664	9.32041127	2.973096671	2069.875852	17.39114033	997508.1763	337399.1244
55	0.55	0.661	9.5305378	2.951654245	2069.875852	17.8201684	1037621.574	334863.7715
54	0.54	0.659	9.74120483	2.930904494	2069.875852	18.25160615	1078598.293	332276.7177
53	0.53	0.656	9.95240329	2.9108117	2069.875852	18.68540859	1120440.955	329637.8749
52	0.52	0.654	10.1641246	2.891342621	2069.875852	19.12153223	1163152.148	326947.1564
51	0.51	0.652	10.3763607	2.872466277	2069.875852	19.55993506	1206734.432	324204.4767
50	0.5	0.650	10.5891038	2.85415376	2069.875852	20.00057645	1251190.336	321409.7515
49	0.49	0.647	10.8023466	2.836378062	2069.875852	20.4434171	1296522.361	318562.8975
48	0.48	0.645	11.0160821	2.819113919	2069.875852	20.88841896	1342732.982	315663.8325
47	0.47	0.643	11.2303037	2.80233767	2069.875852	21.33554518	1389824.649	312712.4754
46	0.46	0.641	11.4450052	2.786027134	2069.875852	21.78476009	1437799.788	309708.7457
45	0.45	0.639	11.6601805	2.77016149	2069.875852	22.23602909	1486660.801	306652.5641
44	0.44	0.637	11.8758238	2.754721177	2069.875852	22.68931863	1536410.068	303543.8519
43	0.43	0.635	12.0919297	2.739687796	2069.875852	23.14459616	1587049.949	300382.5314
42	0.42	0.633	12.3084931	2.725044027	2069.875852	23.60183012	1638582.782	297168.5255
41	0.41	0.631	12.5255088	2.710773546	2069.875852	24.06098982	1691010.887	293901.7577
40	0.4	0.629	12.7429722	2.696860957	2069.875852	24.52204549	1744336.565	290582.1526
39	0.39	0.627	12.9608787	2.683291726	2069.875852	24.98496819	1798562.098	287209.635
38	0.38	0.625	13.1792239	2.670052118	2069.875852	25.44972979	1853689.753	283784.1305
37	0.37	0.624	13.3980037	2.657129145	2069.875852	25.91630293	1909721.779	280305.5654
36	0.36	0.622	13.6172139	2.644510513	2069.875852	26.38466101	1966660.41	276773.8664
35	0.35	0.620	13.8368509	2.632184578	2069.875852	26.85477813	2024507.862	273188.9607
34	0.34	0.618	14.0569109	2.620140299	2069.875852	27.32662908	2083266.341	269550.7762
33	0.33	0.617	14.2773903	2.608367203	2069.875852	27.80018934	2142938.035	265859.2412

32	0.32	0.615	14.4982857	2.596855349	2069.875852	28.27543498	2203525.12	262114.2843
31	0.31	0.613	14.719594	2.585595288	2069.875852	28.75234272	2265029.758	258315.835
30	0.3	0.612	14.9413118	2.574578039	2069.875852	29.23088986	2327454.099	254463.8226
29	0.29	0.610	15.1634363	2.563795058	2069.875852	29.71105426	2390800.281	250558.1774
28	0.28	0.608	15.3859645	2.553238208	2069.875852	30.19281433	2455070.43	246598.8298
27	0.27	0.607	15.6088936	2.542899742	2069.875852	30.67614902	2520266.659	242585.7106
26	0.26	0.605	15.8322208	2.532772269	2069.875852	31.16103778	2586391.071	238518.7509
25	0.25	0.604	16.0559437	2.522848746	2069.875852	31.64746054	2653445.76	234397.8823
24	0.24	0.602	16.2800596	2.513122446	2069.875852	32.13539773	2721432.807	230223.0368
23	0.23	0.601	16.5045661	2.503586947	2069.875852	32.62483022	2790354.285	225994.1464
22	0.22	0.599	16.7294609	2.494236114	2069.875852	33.11573933	2860212.255	221711.1437
21	0.21	0.598	16.9547418	2.485064079	2069.875852	33.6081068	2931008.771	217373.9616
20	0.2	0.596	17.1804065	2.476065231	2069.875852	34.10191479	3002745.877	212982.533
19	0.19	0.595	17.4064529	2.467234199	2069.875852	34.59714585	3075425.607	208536.7915
18	0.18	0.593	17.632879	2.458565841	2069.875852	35.09378294	3149049.989	204036.6705
17	0.17	0.592	17.8596829	2.450055229	2069.875852	35.59180937	3223621.039	199482.1041
16	0.16	0.590	18.0868625	2.441697642	2069.875852	36.09120882	3299140.769	194873.0264
15	0.15	0.589	18.3144161	2.433488549	2069.875852	36.59196533	3375611.181	190209.3717
14	0.14	0.588	18.5423418	2.425423606	2069.875852	37.09406326	3453034.269	185491.0747
13	0.13	0.586	18.7706379	2.417498642	2069.875852	37.59748732	3531412.019	180718.0702
12	0.12	0.585	18.9993028	2.409709652	2069.875852	38.10222253	3610746.414	175890.2933
11	0.11	0.584	19.2283348	2.402052787	2069.875852	38.60825421	3691039.424	171007.6793
10	0.1	0.582	19.4577323	2.394524349	2069.875852	39.11556801	3772293.017	166070.1636
9	0.09	0.581	19.6874937	2.387120782	2069.875852	39.62414983	3854509.152	161077.6819
8	0.08	0.580	19.9176177	2.379838663	2069.875852	40.13398588	3937689.783	156030.17
7	0.07	0.579	20.1481027	2.3726747	2069.875852	40.64506265	4021836.855	150927.5641
6	0.06	0.577	20.3789473	2.365625725	2069.875852	41.15736687	4106952.31	145769.8002
5	0.05	0.576	20.6101502	2.358688682	2069.875852	41.67088555	4193038.083	140556.8149
4	0.04	0.575	20.84171	2.351860631	2069.875852	42.18560595	4280096.102	135288.5447
3	0.03	0.574	21.0736255	2.345138737	2069.875852	42.70151556	4368128.29	129964.9262
2	0.02	0.572	21.3058954	2.338520266	2069.875852	43.21860211	4457136.567	124585.8964
1	0.01	0.571	21.5385184	2.332002581	2069.875852	43.73685359	4547122.843	119151.3922
0	0	0.570	21.7715572	2.325581395	2069.875852	44.25640028	4638114.021	113659.8282

Appendix III: SAMPLE VALIDATION FOR VALIDATION

Some input data is required as shown in Table I.

Table I: Input parameters

Parameter	**Values**
Material	Talc
ε_m	0.57
ε_0	0.95
Filtration Pressure	400000 Pa
Filtrate Volume, V	0.00086 m^3
Particle Diameter	0.0000085 m
Solids density	2650 Kg m^{-3}
Liquid density	1000 Kg m^{-3}
Viscosity	0.001 Pa.s

Starting with $a = 3.79$ and $\left.\frac{dy}{dx}\right|_{x=0} = 0..31$, the Runge-Kutta-Nystrom calculation steps are initiated as follows,

At $n = 0$

$$A_0 = \frac{0.01}{2}[0.31]\left[(3.79 \times 0.31) - \left(e^{(3.79\times 0)} \times \frac{0.95-0.57}{1-0.57} \times 0.31\right) - \left(\frac{0}{2e^{[3.79(1-0)]}}\right)\right]$$

$$= 0.0014$$

$$\beta_0 = \frac{0.1}{2}\left[0.31 + \frac{0.0014}{2}\right] = 0.016$$

$$B_0 = \frac{0.01}{2}[0.31 + 0.0014]\left[(3.79 \times (0.31 + 0.0014)) - \left(e^{(3.79\times(0+0.016))} \times \frac{0.95-0.57}{1-0.57} \times 0.31\right) - \left(\frac{0 + \frac{0.1}{2}}{2e^{[3.79(1-(0+0.016))]}}\right)\right]$$

$$= 0.00138$$

$$C_0 = \frac{0.01}{2}[0.31 + 0.00138]\left[\begin{array}{l}(3.79 \times (0.31 + 0.00138)) - \left(\begin{array}{l} e^{(3.79\times(0+0.016))} \\ \times \dfrac{0.95 - 0.57}{1 - 0.57} \times 0.31 \end{array}\right) \\ - \left(\dfrac{0 + \dfrac{0.1}{2}}{2e^{[3.79(1-(0+0.016))]}}\right)\end{array}\right]$$

$$= 0.00138$$

$$\delta_0 = \frac{0.01}{2}[0.31 + 0.00138] = 0.0016$$

$$D_0 = \frac{0.01}{2}[0.31 + (2 \times 0.00138)]\left[\begin{array}{l}(3.79 \times [0.31 + (2 \times 0.00138)]) - \\ \left(\begin{array}{l} e^{(3.79\times(0+0.0016))} \\ \times \dfrac{0.95 - 0.4}{1 - 0.4} \times 0.31 \end{array}\right) \\ - \left(\dfrac{0 + 0.1}{2e^{[3.79(1-(0+0.0016))]}}\right)\end{array}\right]$$

$$= 0.00142$$

$$K_0 = \frac{1}{3}(0.0014 + 0.00138 + 0.00138) = 0.00139$$

$$y_1 = 0 + 0.01(0.31 + 0.00139) = 0.00031$$

$$K_0 * = \frac{1}{3}(0.0014 + (2 \times 0.00138) + (2 \times 0.00138) + 0.00142) = 0.0028$$

$$y'_1 = 0.31 + 0.0028 = 0.3128$$

At $n = 1$

Introducing the moving boundary condition,

$0.31 = \frac{1}{2} \cdot \frac{0.95 - \varepsilon_i}{\varepsilon_i - 0.4} \cdot \frac{1 - \varepsilon_i}{1 - 0.95}$, the value of ε_i calculated for the remaining steps becomes 0.875 and the value of suspension porosity $\varepsilon_0 = 0.95$

$$A_1 = \frac{0.01}{2}[0.3128]\left[\begin{array}{l}(3.79 \times 0.3128) - \left(e^{(3.76\times 0.00031)} \times \dfrac{0.875 - 0.57}{1 - 0.57} \times 0.31\right) \\ - \left(\dfrac{0.01}{2e^{[3.79(1-0.00031)]}}\right)\end{array}\right]$$

$$= 0.00151$$

$$\beta_1 = \frac{0.01}{2}\left[0.3128 + \frac{0.00151}{2}\right] = 0.00157$$

$$B_1 = \frac{0.01}{2}[0.3128 + 0.00151]\left[\begin{array}{l}(3.79 \times (0.3128 + 0.00151)) - \\ \left(\begin{array}{l} e^{(3.79\times(0.00031+0.00157))} \\ \times \dfrac{0.875 - 0.57}{1 - 0.57} \times 0.31 \end{array}\right) - \\ \left(\dfrac{0.01 + \dfrac{0.01}{2}}{2e^{[3.79(1-(0.00031+0.00157))]}}\right)\end{array}\right]$$

$$= 0.00152$$

$$C_1 = \frac{0.01}{2}[0.3128 + 0.00152]\left[\begin{array}{l}(3.79 \times (0.3128 + 0.00152)) - \\ \left(\begin{array}{l} e^{(3.79\times(0.00031+0.00157))} \\ \times \dfrac{0.875 - 0.57}{1 - 0.57} \times 0.31 \end{array}\right) - \\ \left(\dfrac{0.01 + \dfrac{0.01}{2}}{2e^{[3.79(1-(0.00031+0.00157))]}}\right)\end{array}\right]$$

$$= 0.00152$$

$$\delta_1 = \frac{0.01}{2}[0.3128 + 0.00152] = 0.00157$$

$$D_1 = \frac{0.01}{2}[0.3128 + (2 \times 0.00152)]\left[\begin{array}{l}(3.79 \times [0.3128 + (2 \times 0.00152)]) - \\ \left(\begin{array}{l} e^{(3.79\times(0.00031+0.00157))} \\ \times \dfrac{0.875 - 0.57}{1 - 0.57} \times 0.31 \end{array}\right) \\ -\left(\dfrac{0.01 + 0.01}{2e^{[3.79(1-(0.00031+0.00157))]}}\right)\end{array}\right]$$

$$= 0.00154$$

$$K_1 = \frac{1}{3}(0.00151 + 0.00152 + 0.00152) = 0.00152$$

$$y_2 = 0.00031 + 0.01(0.3128 + 0.00152) = 0.0035$$

$$K_1* = \frac{1}{3}(0.00151 + (2 \times 0.00152) + (2 \times 0.00152) + 0.00154) = 0.00304$$

$$y'_2 = 0.3128 + 0.00304 = 0.3158$$

1.1 Relating Cake resistance and permeability to porosity

By using the Happel cell model with the input parameters in Table 1, the different values for k_x are calculated as follows;

$$K_0 = \frac{0.0000085^2}{36} \frac{6 - 9(1-0.57)^{\frac{1}{3}} + 9(1-0.57)^{\frac{5}{3}} - 6(1-0.57)^2}{(1-0.57)\left(3 + 2(1-0.57)^{\frac{5}{3}}\right)} = 4.04 \times 10^{-13} m^2$$

$$K_1 = \frac{0.0000085^2}{36} \frac{6 - 9(1-0.571)^{\frac{1}{3}} + 9(1-0.571)^{\frac{5}{3}} - 6(1-0.0.571)^2}{(1-0.571)\left(3 + 2(1-0.571)^{\frac{5}{3}}\right)} = 4.08 \times 10^{-13} m^2$$

$$K_2 = \frac{0.0000085^2}{36} \frac{6 - 9(1-0.572)^{\frac{1}{3}} + 9(1-0.572)^{\frac{5}{3}} - 6(1-0.572)^2}{(1-0.572)\left(3 + 2(1-0.572)^{\frac{5}{3}}\right)} = 4.12 \times 10^{-13} m^2$$

Using Equation (5.20) with the input parameters in Table 1, the values for different α_x are calculated as follows;

$$\alpha_0 = \frac{1}{2650(1-0.570)4.04 \times 10^{-13}} = 2.17 \times 10^9 \, m \, kg^{-1}$$

$$\alpha_1 = \frac{1}{2650(1-0.571)4.08 \times 10^{-13}} = 2.16 \times 10^9 \, m \, kg^{-1}$$

$$\alpha_2 = \frac{1}{2650(1-0.572)4.12 \times 10^{-13}} = 2.14 \times 10^9 \, m \, kg^{-1}$$

using the Happel cell model with the input parameters in Table 1, the value of k_i is calculated as follows;

$$K_i = \frac{0.0000085^2}{36} \frac{6 - 9(1-0.875)^{\frac{1}{3}} + 9(1-0.875)^{\frac{5}{3}} - 6(1-0.875)^2}{(1-0.875)\left(3 + 2(1-0.875)^{\frac{5}{3}}\right)} = 8.85 \times 10^{-12} m^2$$

The value of α_i is calculated using Equation (5.21) as follows

$$\alpha_i = \frac{(1-0.57)4.04\times10^{-13}}{(1-0.889)8.85\times10^{-12}}2.17\times10^{9} = 3.83\times10^{8}\ m\ kg^{-1}$$

Appendix IV: COMPUTER CODE

```
Sub porosityloop()
   'subroutine to  minimise variance between calculated porosity and experimental
porosity
   'and experimental liquid pressure and calculated liquid pressure through nested
looping
   Dim eave As Single
   Dim eavc As Single
   Dim dedl As Single
   Dim ei As Single
   Dim afn As Single
   Dim B  As Single, C  As Single
   Dim la As Single, ua As Single, stpa As Single, stpe As Single
   Dim el As Single, ea As Single
   Dim iRowa As Long
   Dim iRowb As Long
   Dim iRowc As Long
   Dim iRowd As Long
   Dim iRowe As Long
   Dim Fname As Variant
   Dim minVar As Double  ' high value of minimum variance set
   Dim minVarp As Double 'high value of minimum variance of liquid pressure
   Dim newVar As Double  'minimisation of porosity variances
   Dim newVarp As Double 'minimisation of liquid pressure variances

   Range("F18:F19").Select
   Selection.ClearContents

   Range("AA28:AB40").Select
   Selection.ClearContents

   ' set correct folder for file opening
   ' read the fields from txt file

   Fname = Application.GetOpenFilename("Text Files (*.txt),*.txt", , _
         "Select Text Data File")
   If Fname = False Then Exit Sub
   Open Fname For Input As #1
   iRow = 28
   Do While Not EOF(1)
      Input #1, B, C
      Cells(iRow, 27) = B
      Cells(iRow, 28) = C
      iRow = iRow + 1
   Loop
   Close #1
```

```
' clear any previous output data
Columns("AQ:AV").Select
Selection.ClearContents

Application.ScreenUpdating = False

lem = 0.2
uem = 0.9
la = 2.22
ua = 2.22
el = 0.47003
ea = 0.47003
stpa = 0.01
stpe = 0.001
'Initialise
' read data from worksheet
eave = Cells(17, 6) ' experimental average porosity
minVarpp = 1000000#

iRowa = 2
iRowb = 2
iRowc = 2
iRowd = 2
iRowe = 2

For em = lem To uem Step stpe

    Cells(8, 6) = em
    Cells(iRowd, 48) = em
    iRowd = iRowd + 1
    minVarp = 1000000

        For a = la To ua Step stpa

         Cells(19, 6) = a
         dedl = Cells(4, 7) ' initial dimensionless porosity gradient, looping variable

         minVar = 1000000#
            'Do
            For dedl = el To ea
                'write data
                Cells(18, 6) = dedl

                ei = Cells(9, 11)
                Cells(iRowe, 49) = ei
                iRowe = iRowe + 1

                'If ei >= 0.991 Then Exit For
```

```
                newVar = Cells(18, 8)

                Cells(iRowa, 43) = dedl
                Cells(iRowa, 44) = newVar
                iRowa = iRowa + 1

                eavc = Cells(25, 8) ' calculated average porosity
                Cells(iRowc, 45) = eavc
                iRowc = iRowc + 1

                If newVar < minVar Then
                   minVar = newVar
                Else
                   'Exit For
                End If
                ' initialise
                dedl = dedl + 0.01  'loop, increases the value of porosity gradient
             'Loop
             Next dedl

          newVarp = Cells(28, 32)

          Cells(iRowb, 46) = a
          Cells(iRowb, 47) = newVarp
          iRowb = iRowb + 1

          If newVarp < minVarp Then
             minVarp = newVarp
          End If

       Next a

    newVarpp = Cells(28, 32)

    If newVarpp < minVarpp Then
       minVarpp = newVarpp
    End If

 Next em

 End Sub
```

Appendix V: LIQUID PRESSURE PROFILE HISTORY

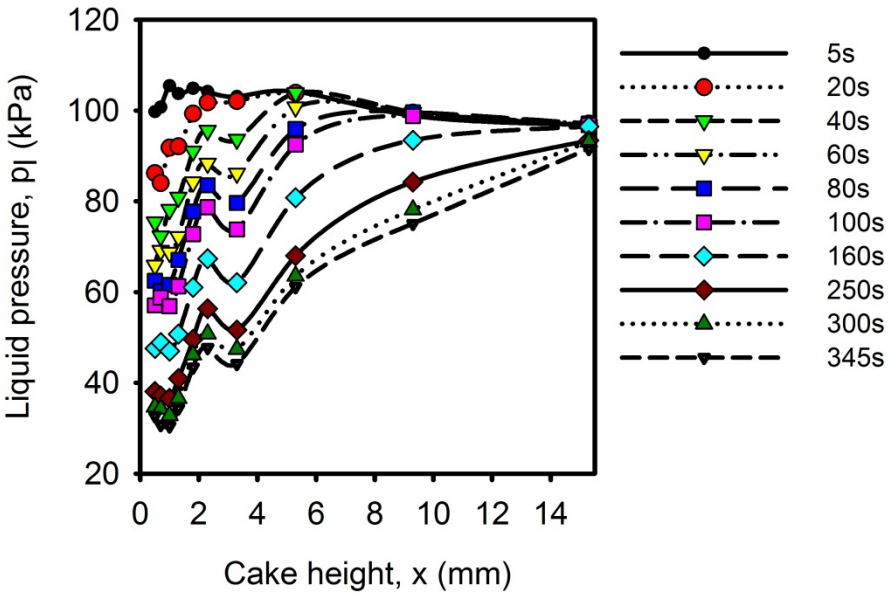

Figure 1: Hydraulic pressure history in a forming talc cake/suspension at a constant filtration pressure of 100 kPa.

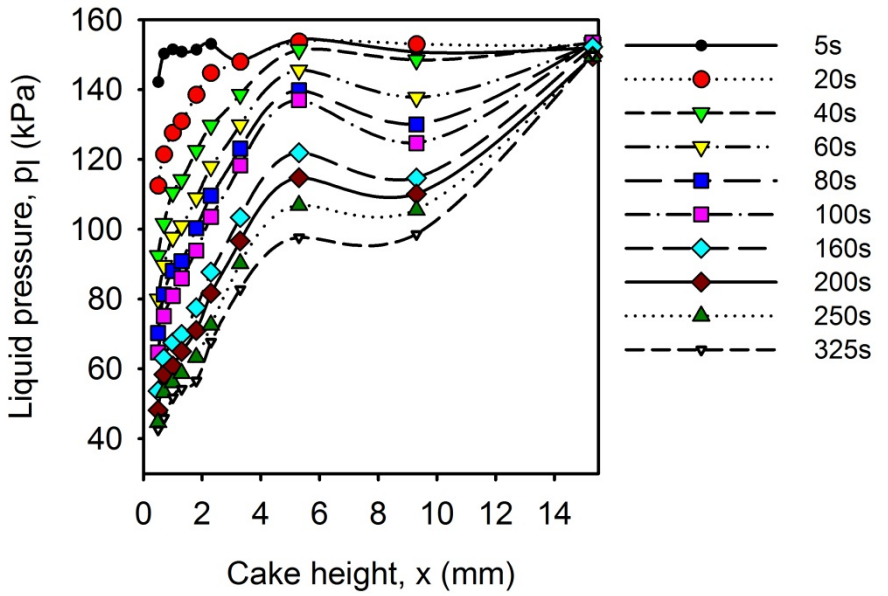

Figure 2: Hydraulic pressure history in a forming talc cake/suspension at a constant filtration pressure of 150 kPa.

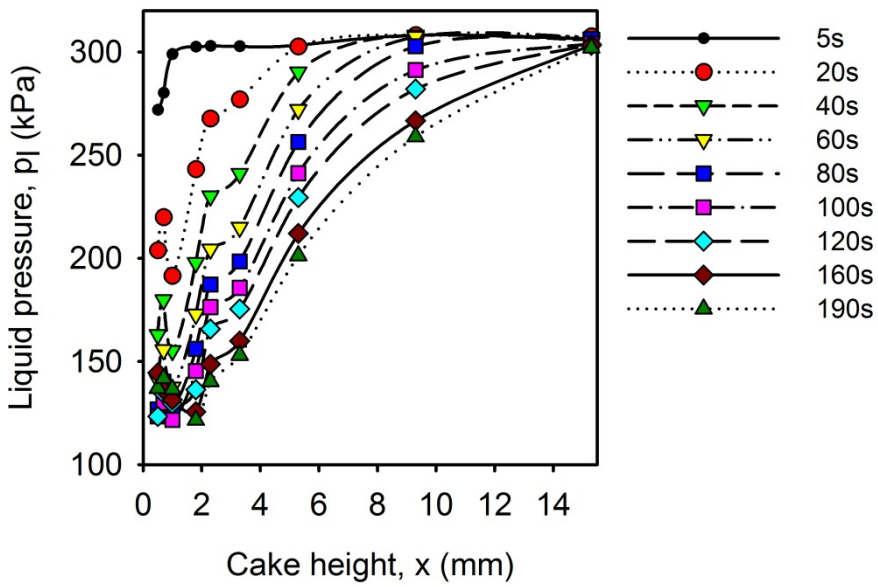

Figure 4: Hydraulic pressure history in a forming talc cake/suspension at a constant filtration pressure of 300 kPa.

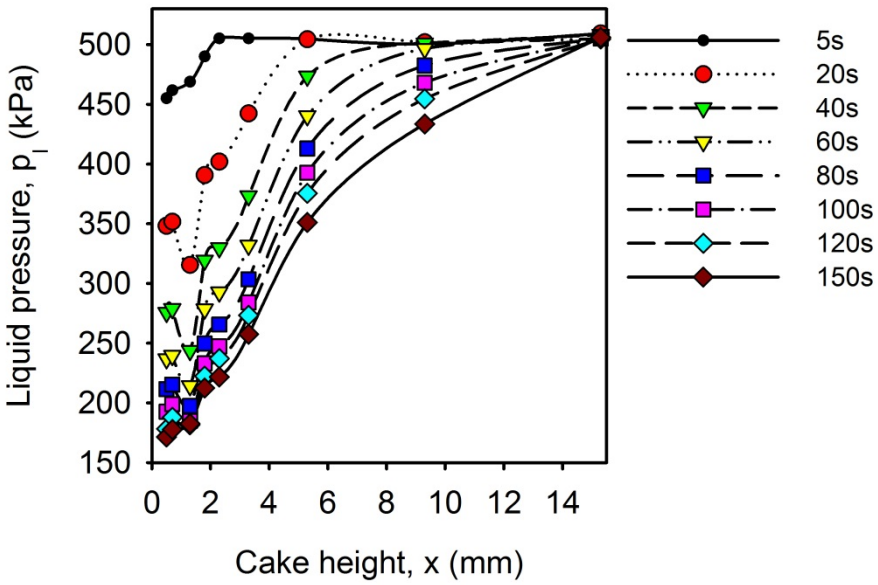

Figure 5: Hydraulic pressure history in a forming talc cake/suspension at a constant filtration pressure of 500 kPa.

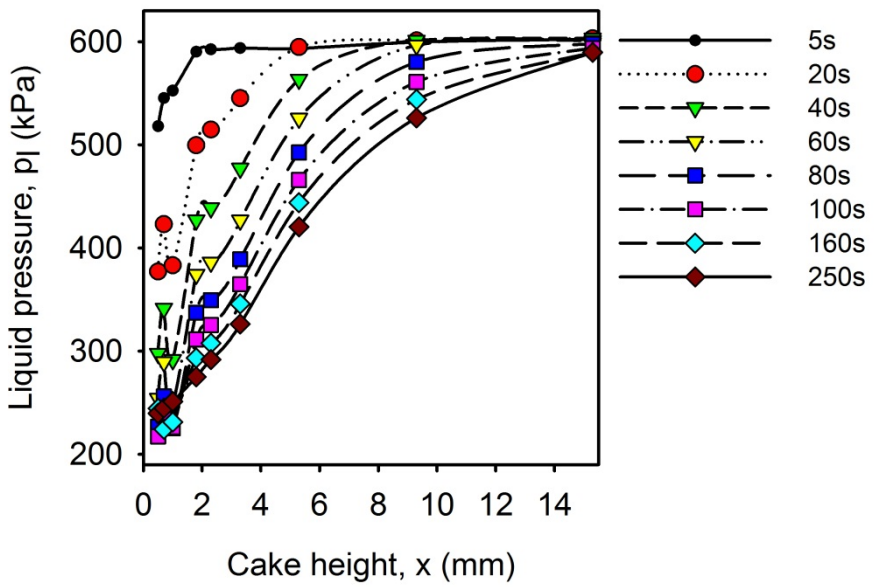

Figure 6: Hydraulic pressure history in a forming talc cake/suspension at a constant filtration pressure of 600 kPa.

Appendix VI: PLOTS OF MINIMISATION

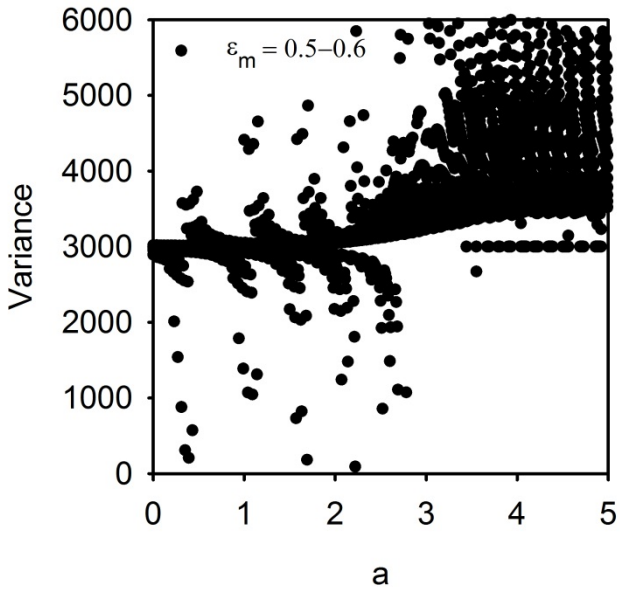

Figure 7: Graph of minimisation of variance 100 kPa, variable *a*

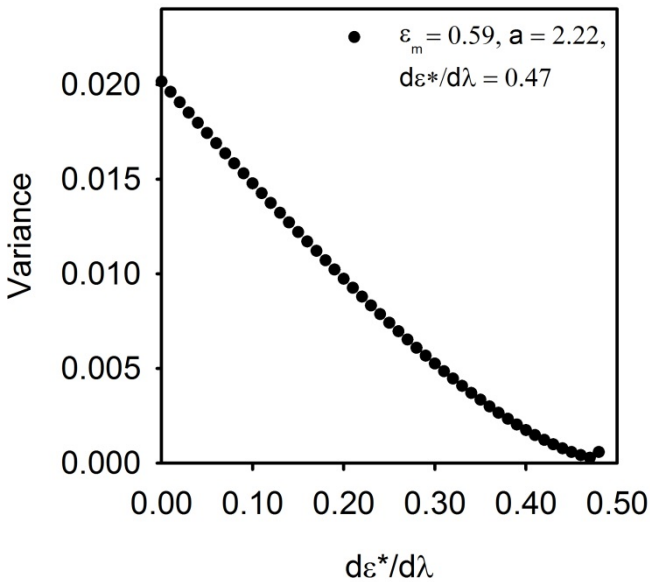

Figure 8: Graph of minimisation of variance of average porosity 100 kPa, variable $\frac{d\varepsilon*}{\partial\lambda}$

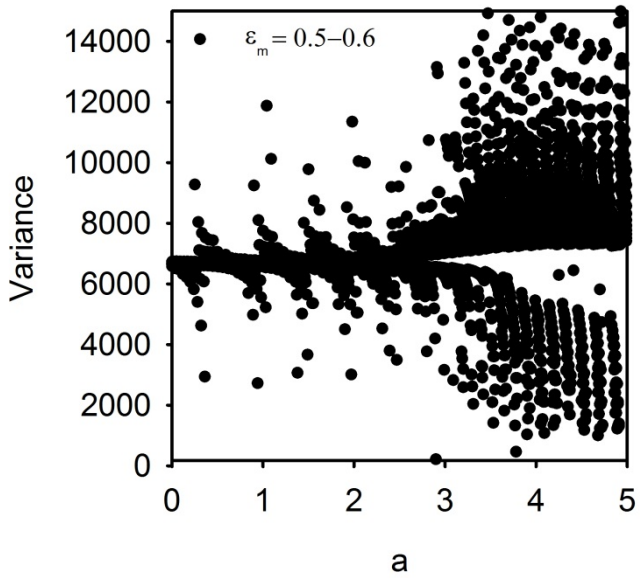

Figure 9: Graph of minimisation of variance of liquid pressures 150 kPa, variable *a*

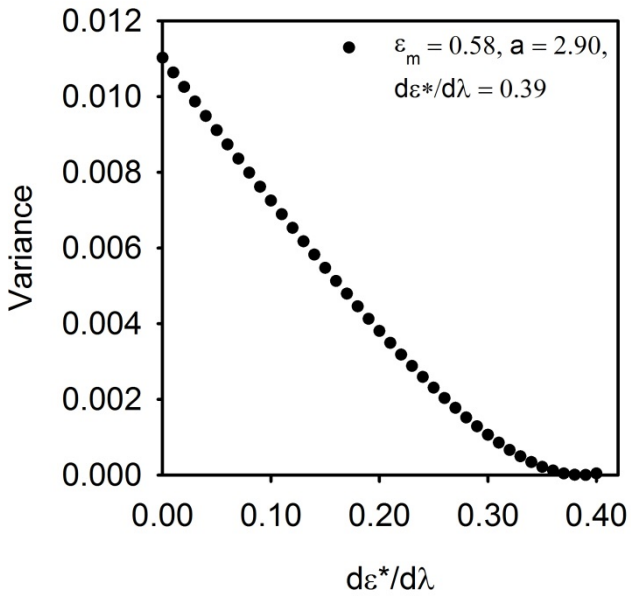

Figure 10: Graph of minimisation of variance of average porosity 150 kPa, variable $\frac{d\varepsilon*}{\partial\lambda}$

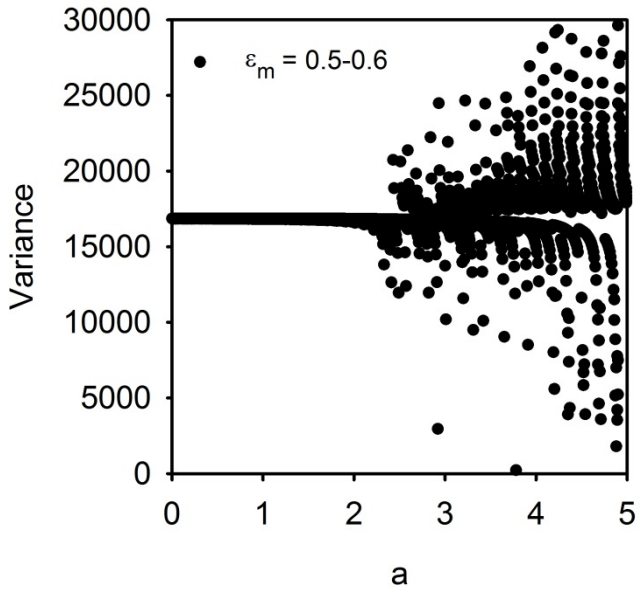

Figure 11: Graph of minimisation of variance of liquid pressures 300 kPa, variable *a*

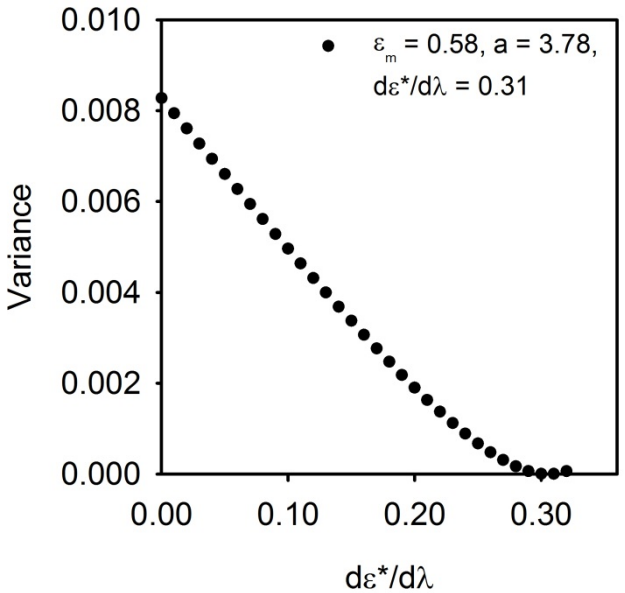

Figure 12: Graph of minimisation of variance of average porosity 300 kPa, variable $\frac{d\varepsilon*}{\partial\lambda}$

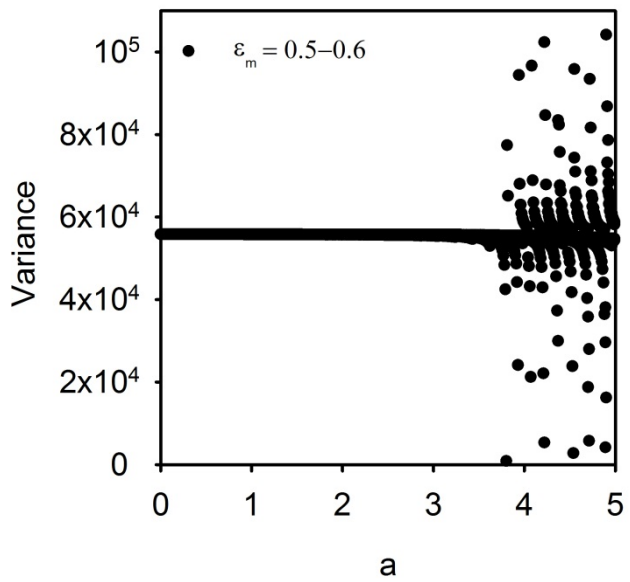

Figure 13: Graph of minimisation of variance of liquid pressures 500 kPa, variable *a*

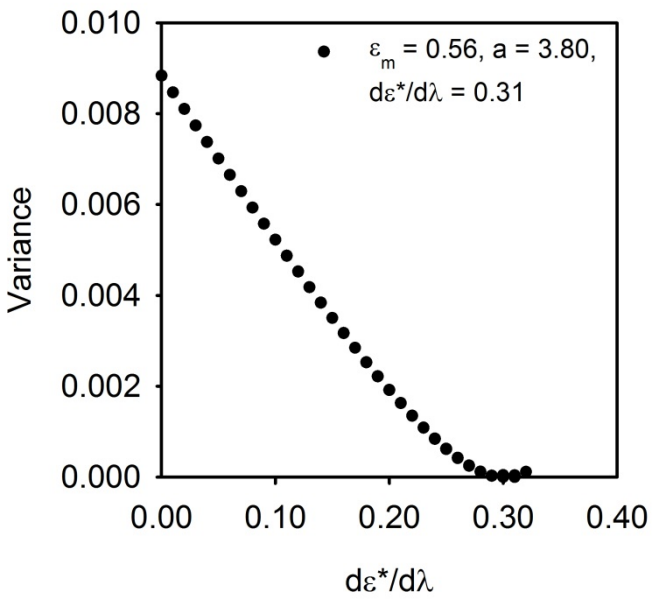

Figure 14: Graph of minimisation of variance of average porosity 500 kPa, variable $\frac{d\varepsilon*}{\partial\lambda}$

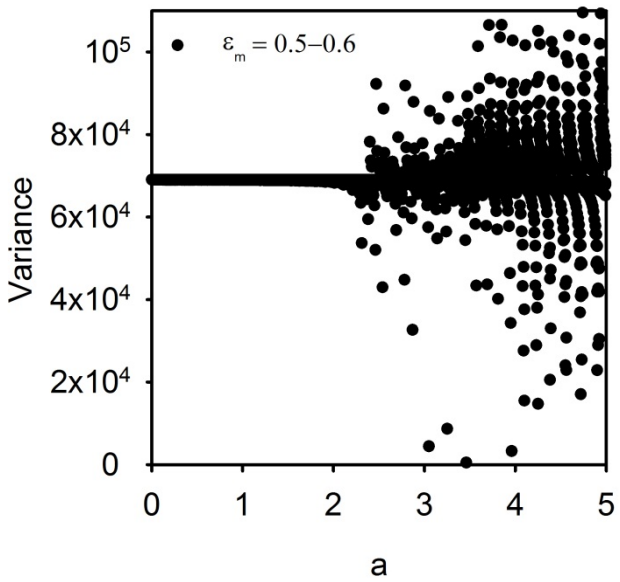

Figure 16: Graph of minimisation of variance of liquid pressures 600 kPa, variable *a*

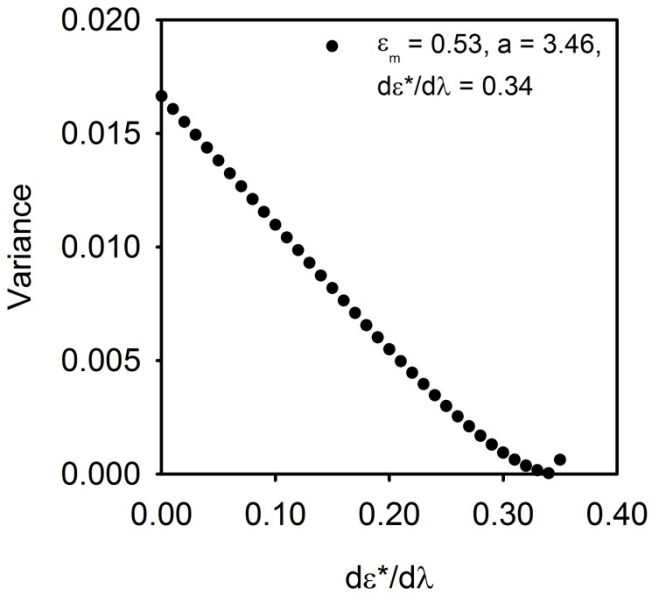

Figure 17: Graph of minimisation of variance of average porosity 600 kPa, variable $\frac{d\varepsilon*}{\partial\lambda}$

Appendix VII: CALCULATED INTERNAL CAKE PROPERTIES

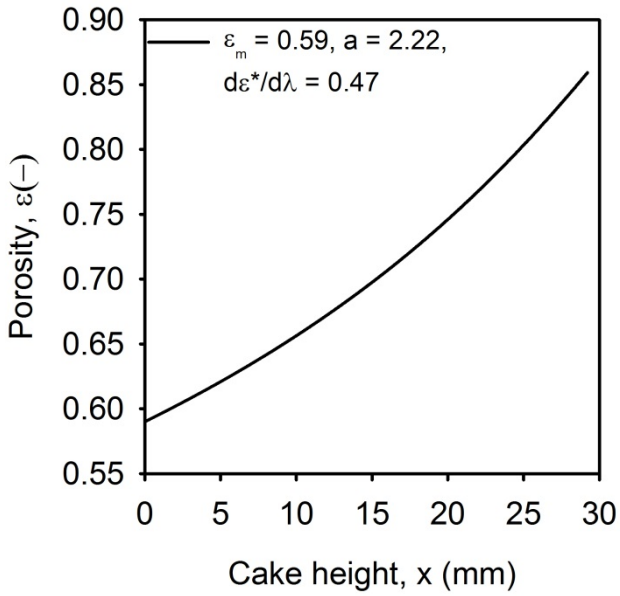

Figure 18: Porosity profile after minimisation of variance, talc 100 kPa.

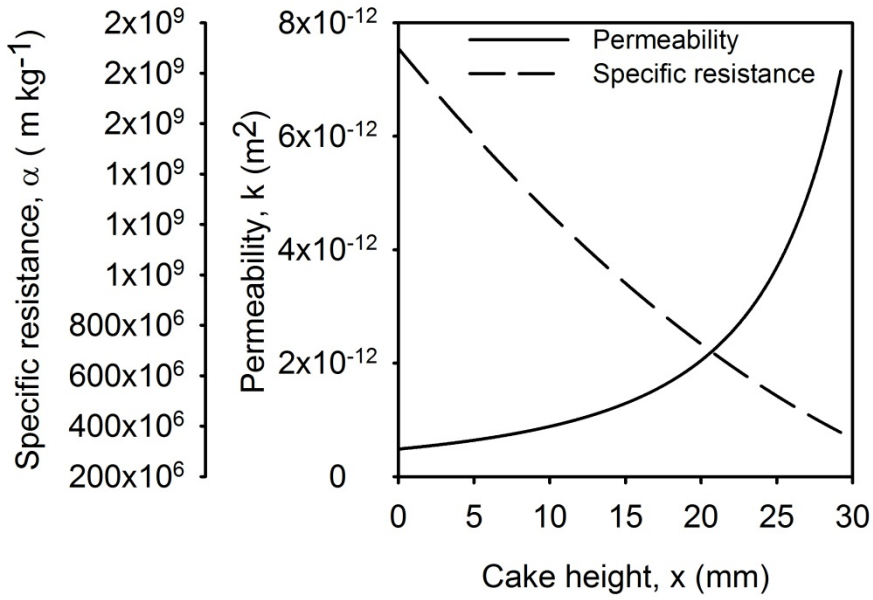

Figure 19: Specific resistance and Permeability after minimisation of variance, talc 100 kPa.

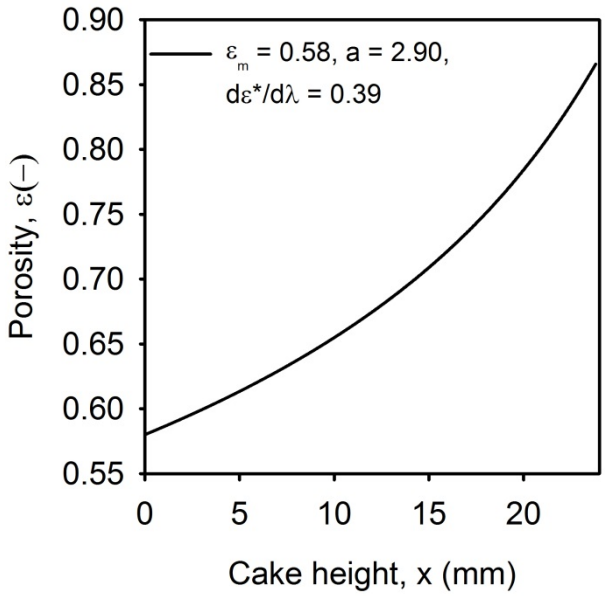

Figure 20: Porosity profile after minimisation of variance, talc 150 kPa.

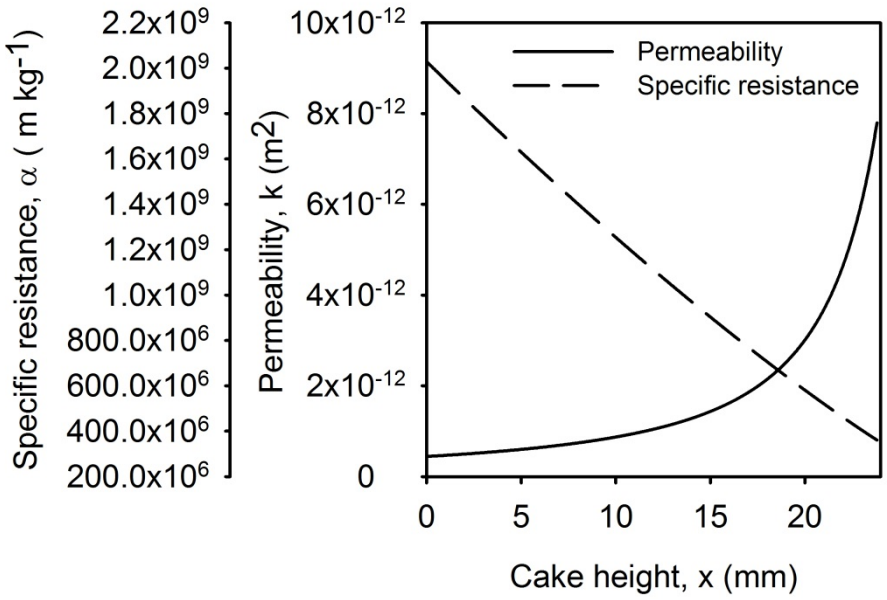

Figure 21: Specific resistance and Permeability after minimisation of variance, talc 150 kPa.

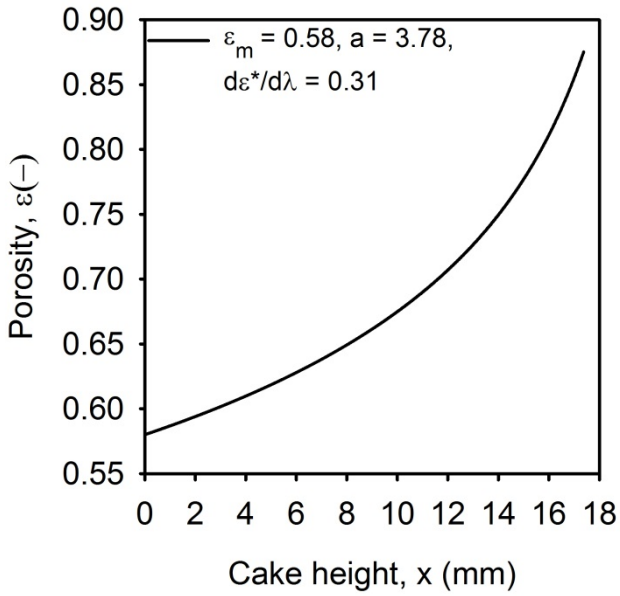

Figure 22: Porosity profile after minimisation of variance, talc 300 kPa.

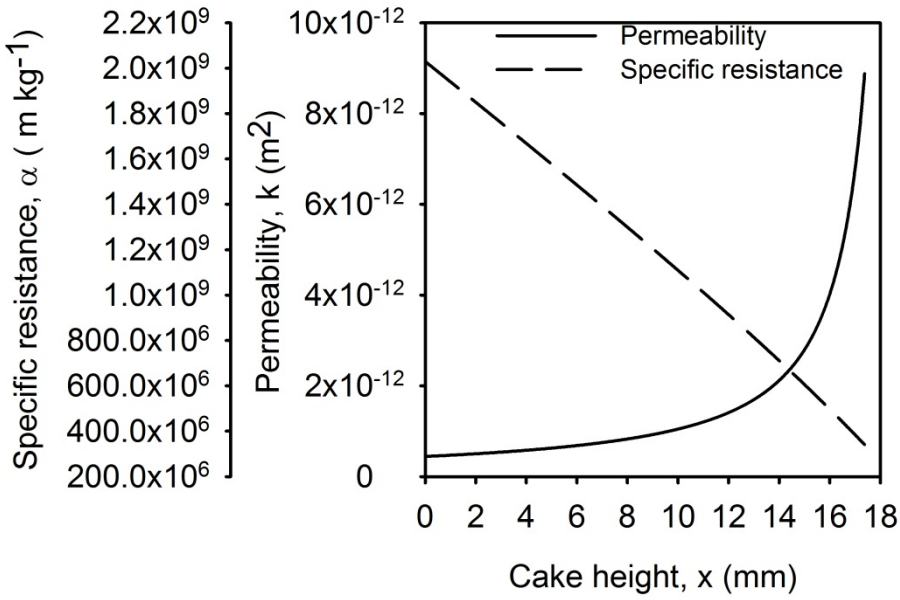

Figure 23: Specific resistance and Permeability after minimisation of variance, talc 300 kPa.

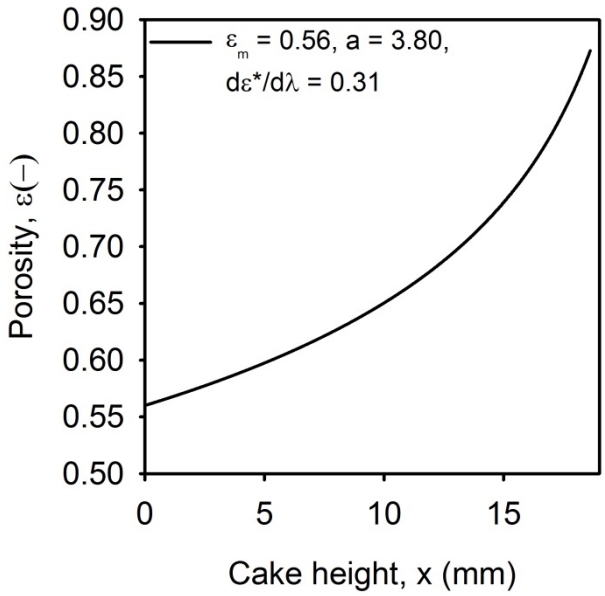

Figure 24: Porosity profile after minimisation of variance, talc 500 kPa.

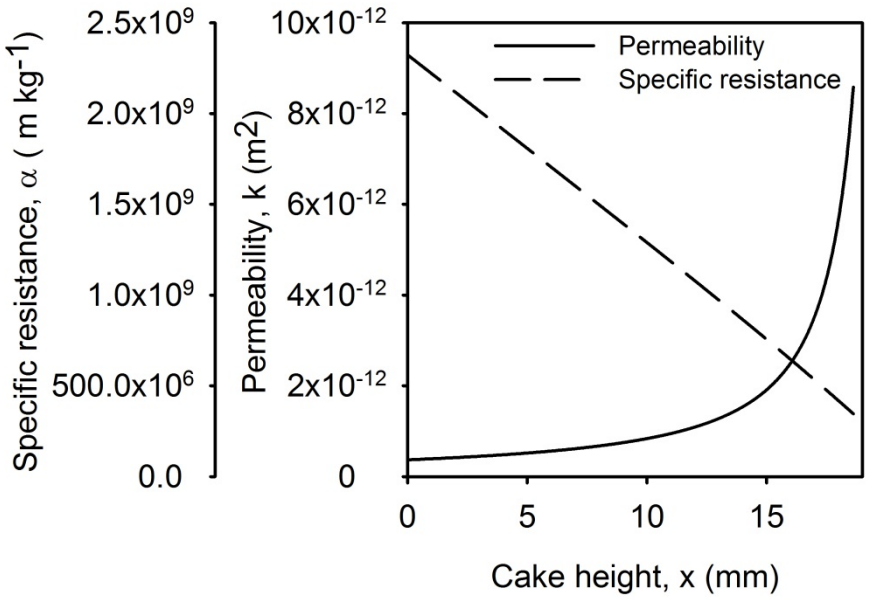

Figure 25: Specific resistance and Permeability after minimisation of variance, talc 500 kPa.

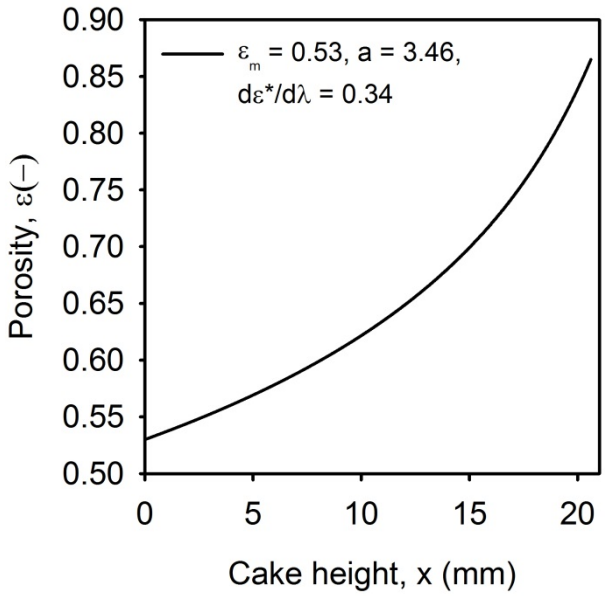

Figure 26: Porosity profile after minimisation of variance, talc 600 kPa.

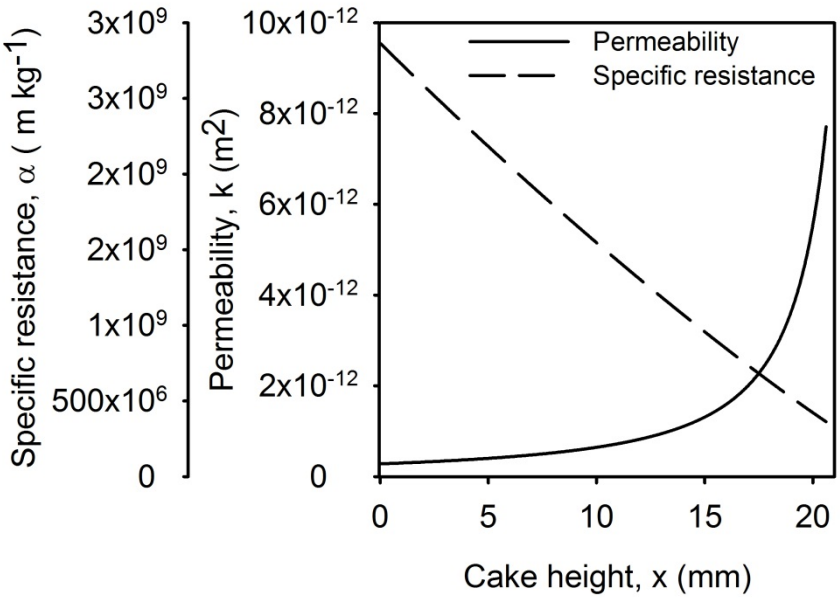

Figure 27: Specific resistance and Permeability after minimisation of variance, talc 600 kPa.

Appendix VIII: DERIVATION OF EQUATION 6.4

$$\theta = \frac{E_i t}{x_i^{\ 2}}$$

$$b = \frac{x}{x_i}$$

thus

$$\lambda = \frac{b}{\sqrt{\theta}}\text{, hence } \lambda = \frac{\frac{x}{x_i}}{\sqrt{\theta}}$$

therefore

$$\sqrt{\theta} = \frac{\frac{x}{x_i}}{\lambda} \text{ hence } \frac{x^2}{x_i^{\ 2}\lambda} = \frac{E_i t}{x_i^{\ 2}} \text{ and on rearrangement}$$

$$x = \sqrt{E_i t}\lambda$$

Appendix IX: PREDICTED LIQUID PRESSURE AND POROSITY PROFILES, POROSITY AT MEDIUM CONSTANT

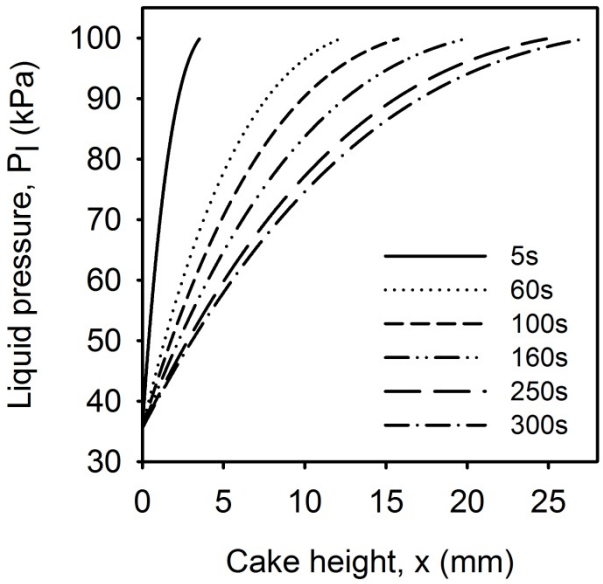

Figure 29: Predicted liquid pressure profile, talc at 100 kPa.

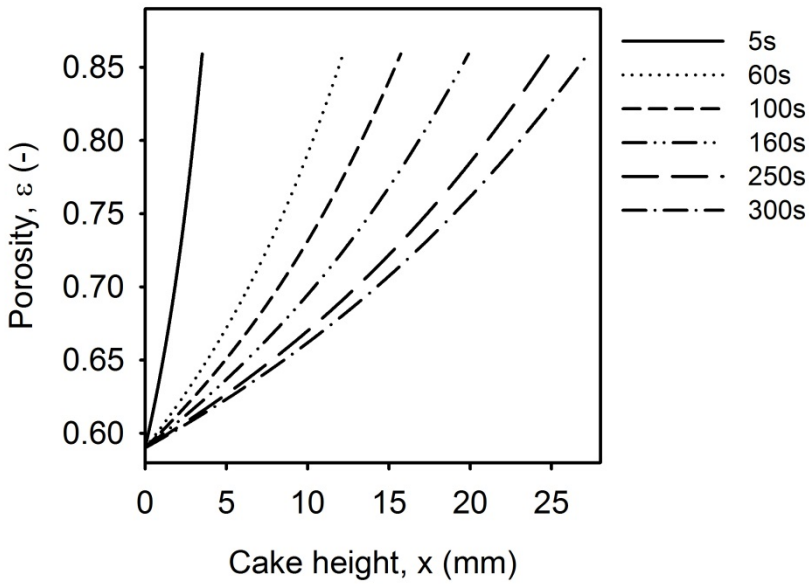

Figure 30: Predicted porosity profile, talc at 100 kPa.

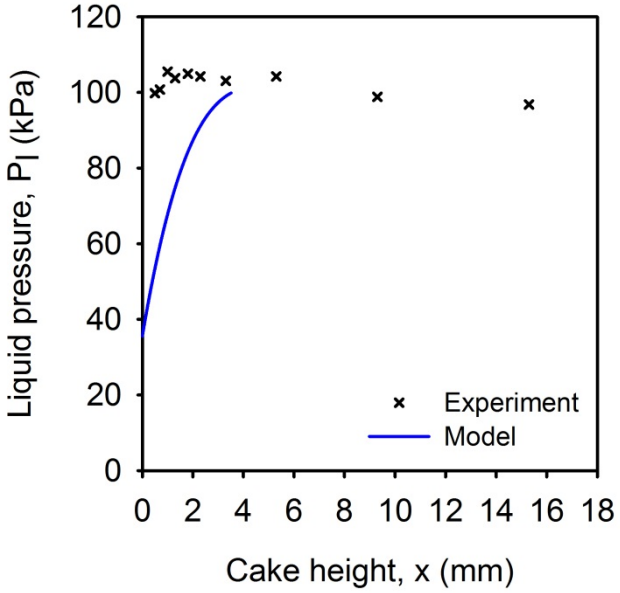

Figure 31: Predicted liquid pressure profile, talc at 100 kPa, 5s.

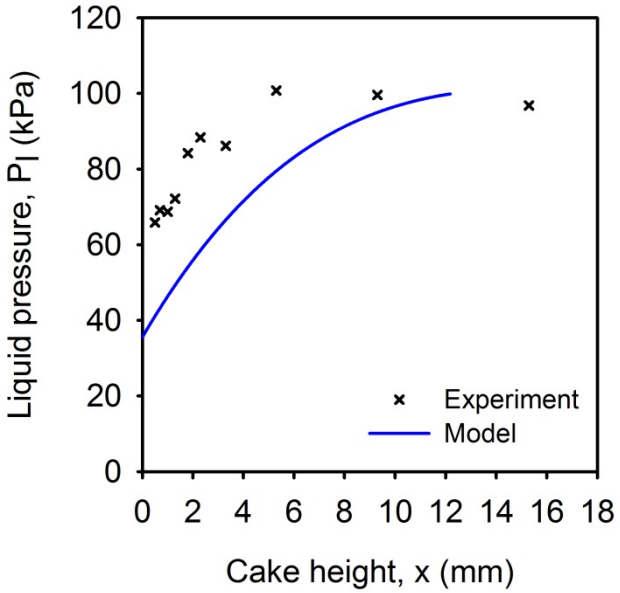

Figure 32: Predicted liquid pressure profile, talc at 100 kPa, 60s.

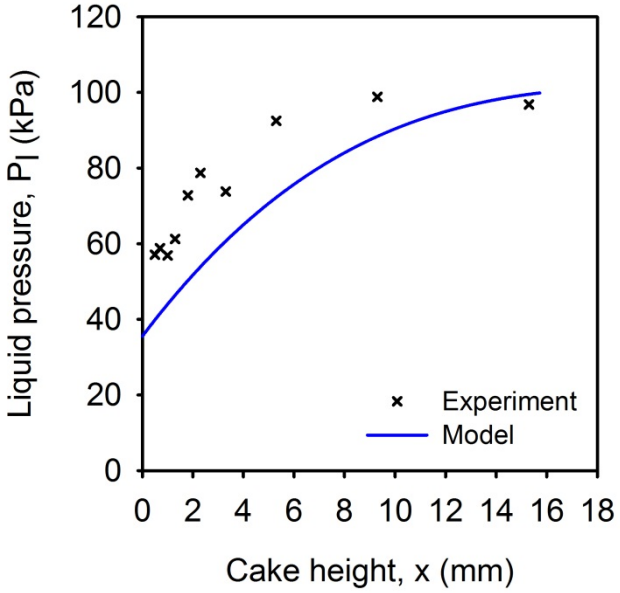

Figure 33: Predicted liquid pressure profile, talc at 100 kPa, 100s

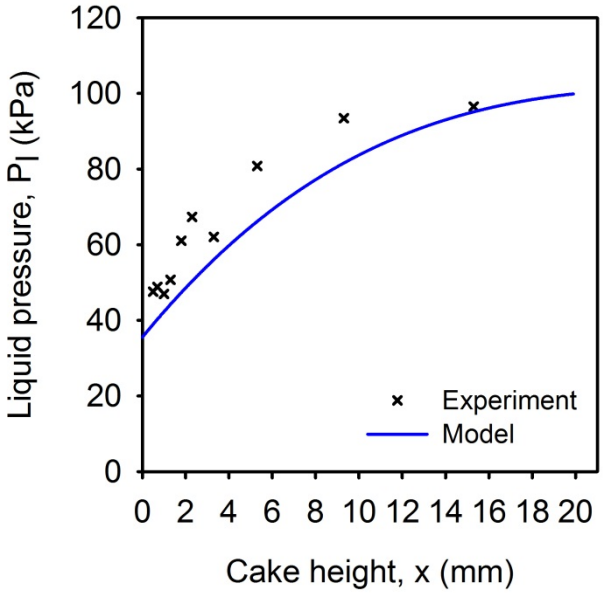

Figure 34: Predicted liquid pressure profile, talc at 100 kPa, 160s

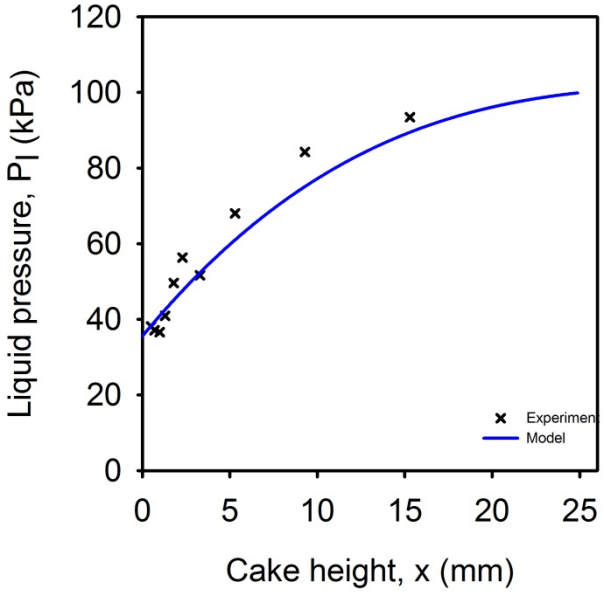

Figure 34: Predicted liquid pressure profile, talc at 100 kPa, 250s.

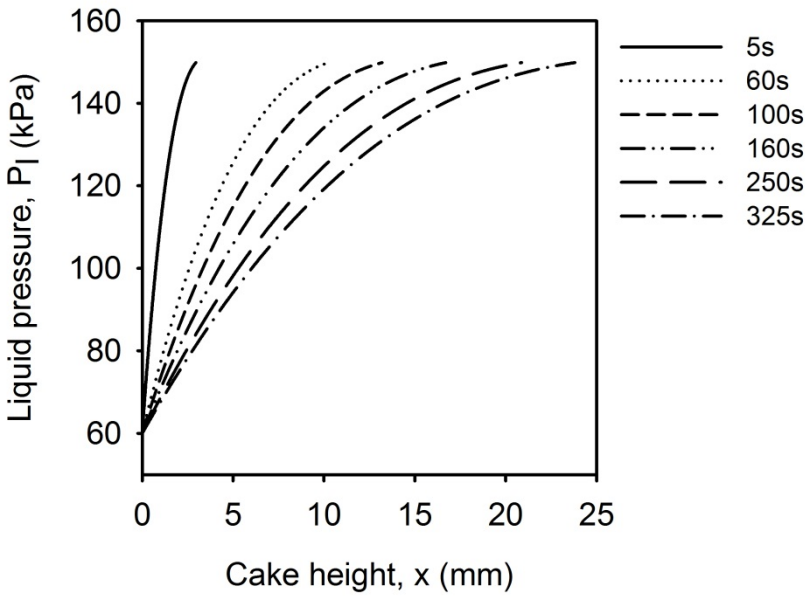

Figure 35: Predicted liquid pressure profile, talc at 150 kPa.

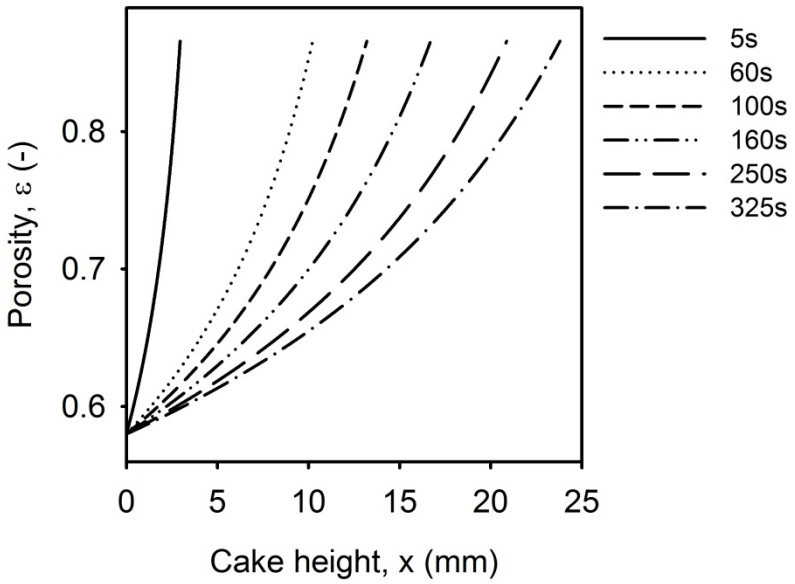

Figure 36: Predicted porosity profile, talc at 150 kPa.

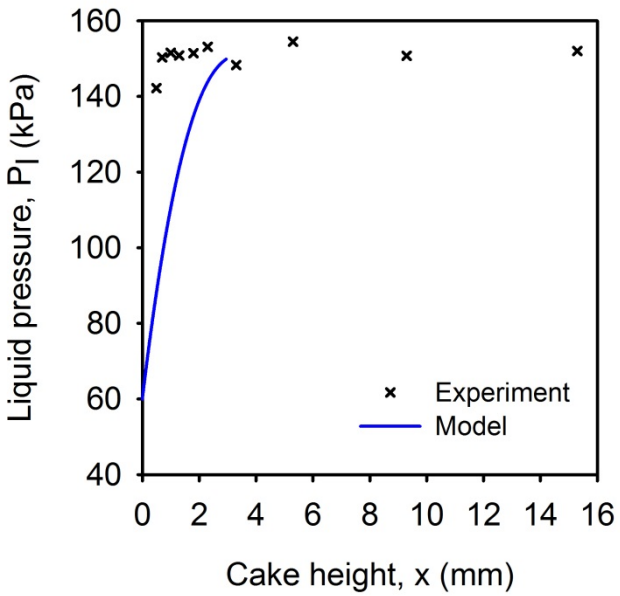

Figure 37: Predicted liquid pressure profile, talc at 150 kPa, 5s.

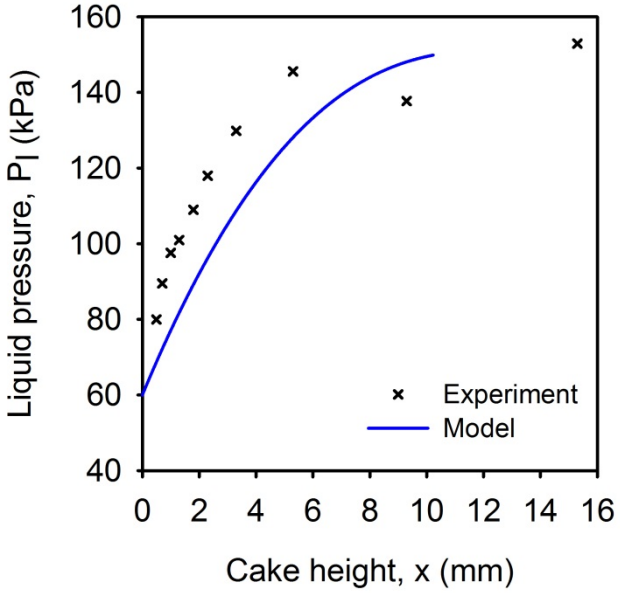

Figure 38: Predicted liquid pressure profile, talc at 150 kPa, 60s.

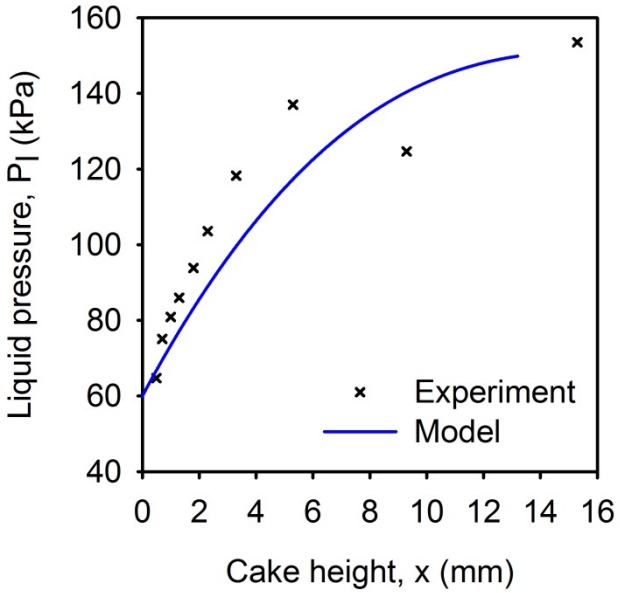

Figure 39: Predicted liquid pressure profile, talc at 150 kPa, 100s.

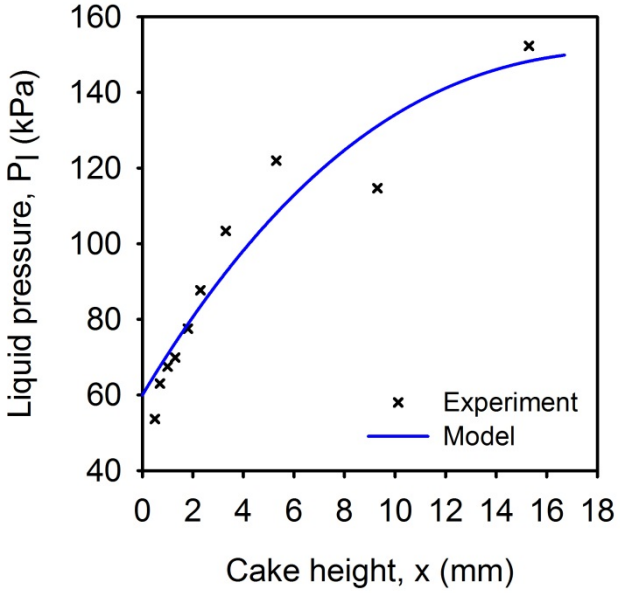

Figure 40: Predicted liquid pressure profile, talc at 150 kPa, 160s

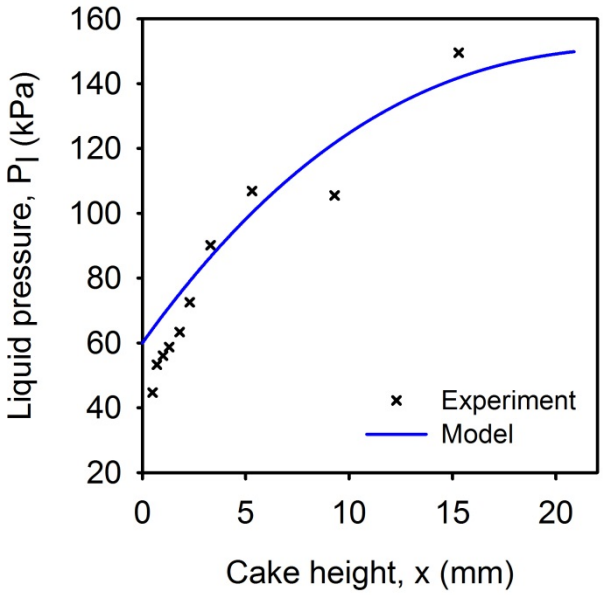

Figure 41: Predicted liquid pressure profile, talc at 150 kPa, 250s

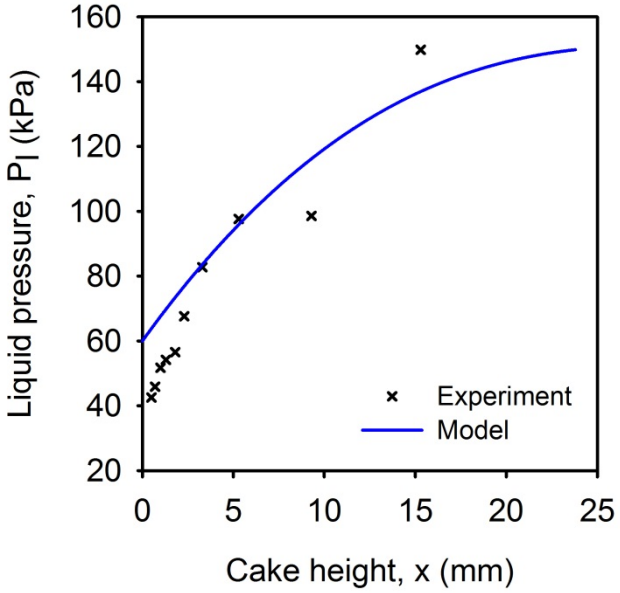

Figure 42: Predicted liquid pressure profile, talc at 150 kPa, 325s.

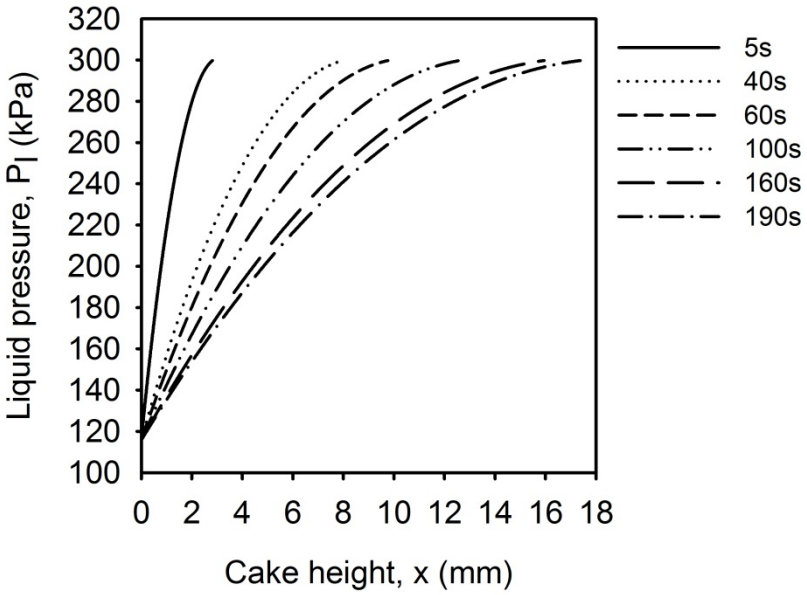

Figure 43: Predicted liquid pressure profile, talc at 300 kPa.

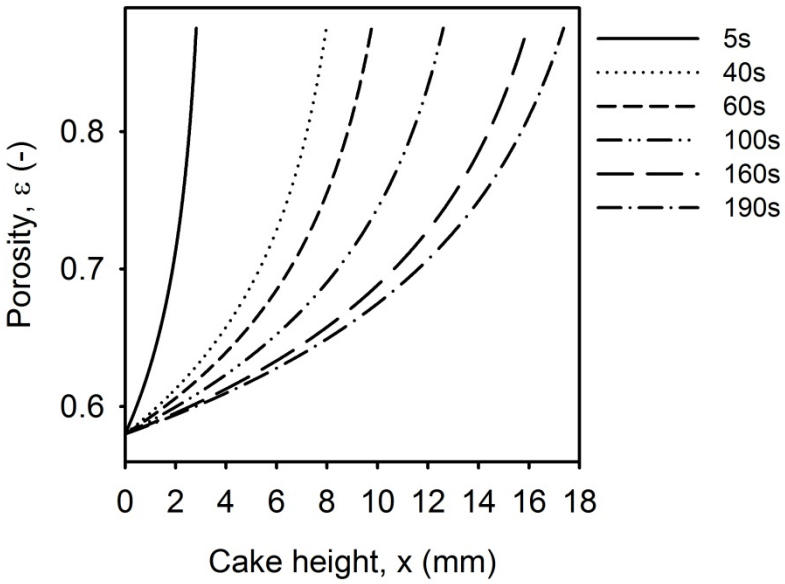

Figure 44: Predicted porosity profile, talc at 300 kPa.

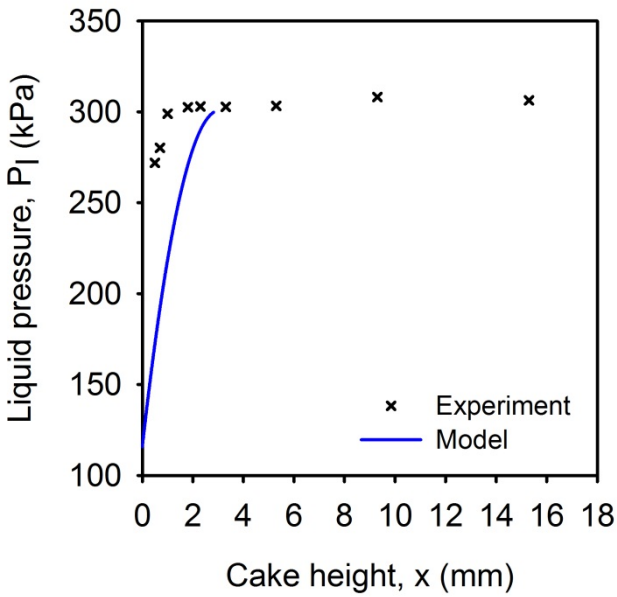

Figure 45: Predicted liquid pressure profile, talc at 300 kPa, 5s.

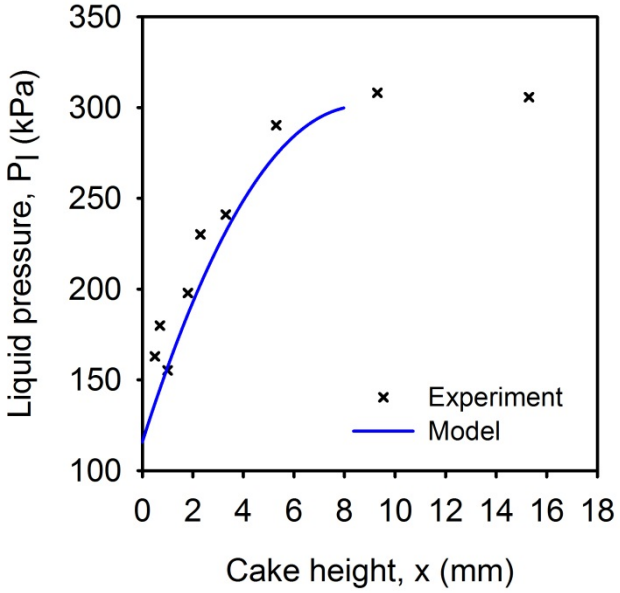

Figure 46: Predicted liquid pressure profile, talc at 300 kPa, 40s.

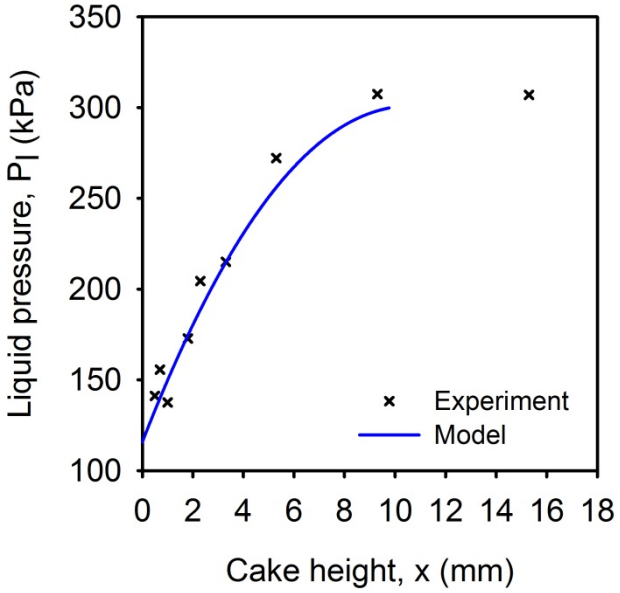

Figure 47: Predicted liquid pressure profile, talc at 300 kPa, 60s.

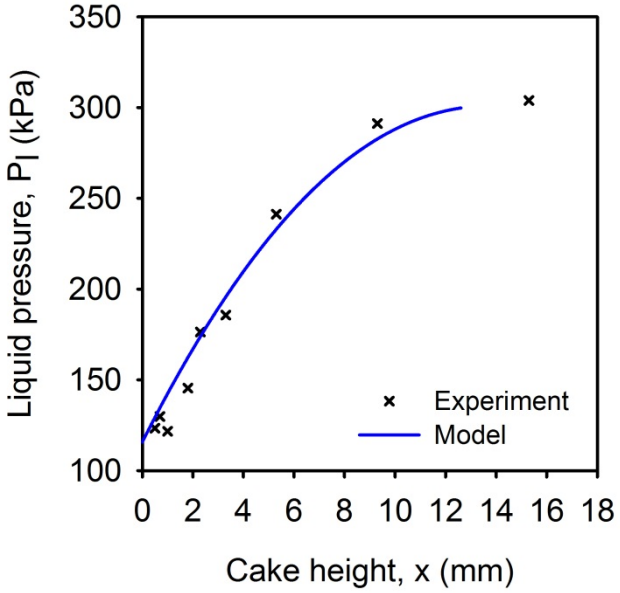

Figure 48: Predicted liquid pressure profile, talc at 300 kPa, 100s.

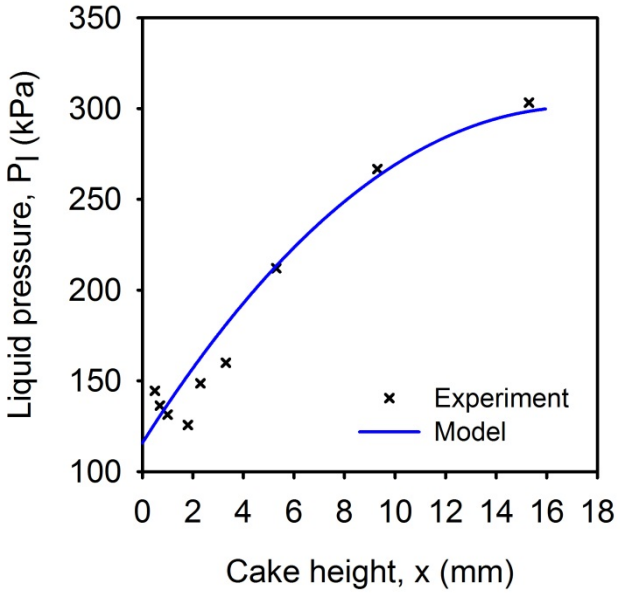

Figure 49: Predicted liquid pressure profile, talc at 300 kPa, 160s.

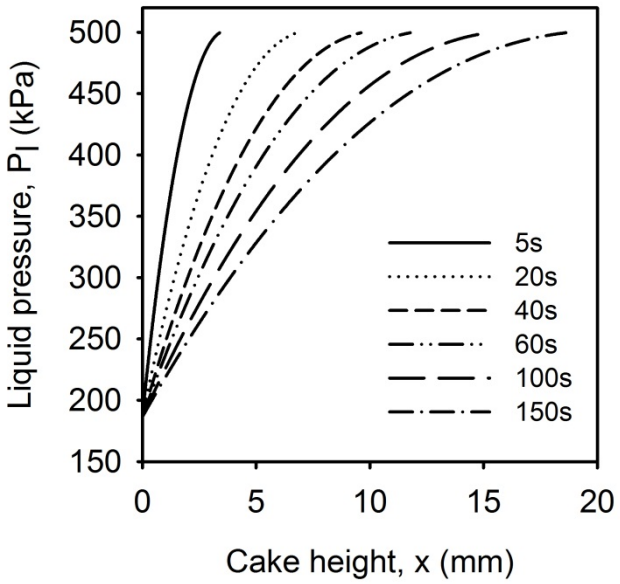

Figure 50: Predicted liquid pressure profile, talc at 500 kPa.

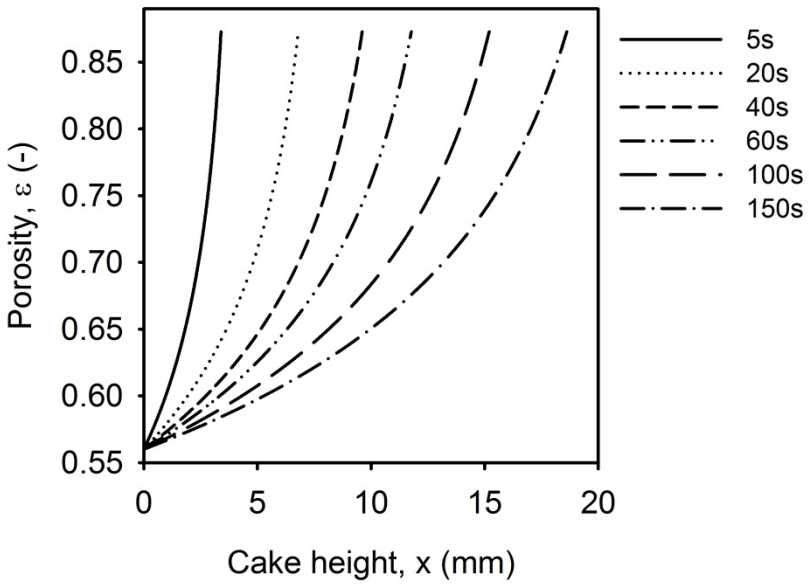

Figure 51: Predicted porosity profile, talc at 500 kPa.

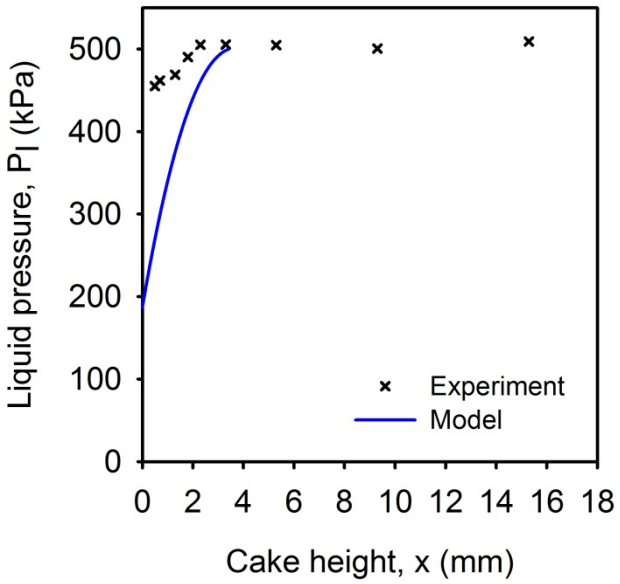

Figure 52: Predicted liquid pressure profile, talc at 500 kPa, 5s.

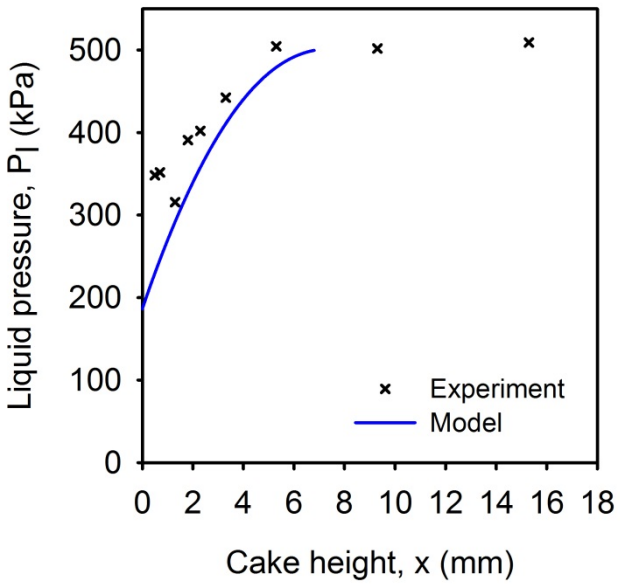

Figure 53: Predicted liquid pressure profile, talc at 500 kPa, 20s.

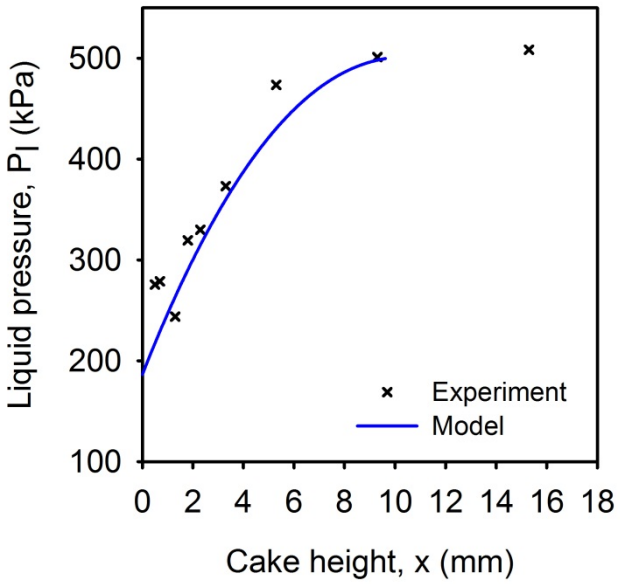

Figure 54: Predicted liquid pressure profile, talc at 500 kPa, 40s.

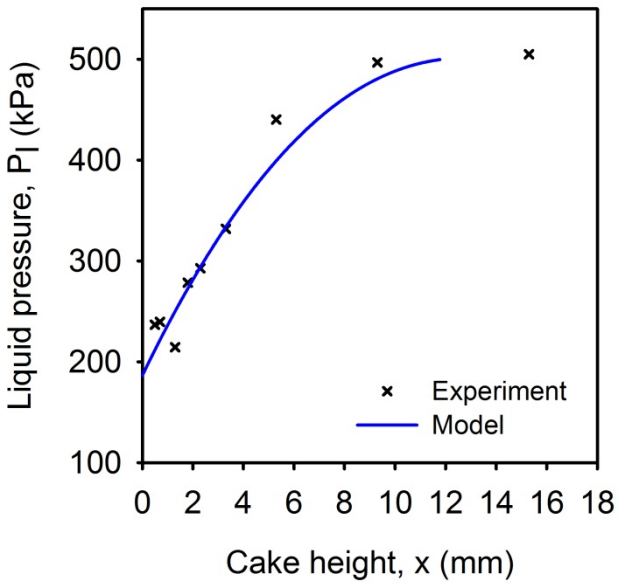

Figure 55: Predicted liquid pressure profile, talc at 500 kPa, 60s.

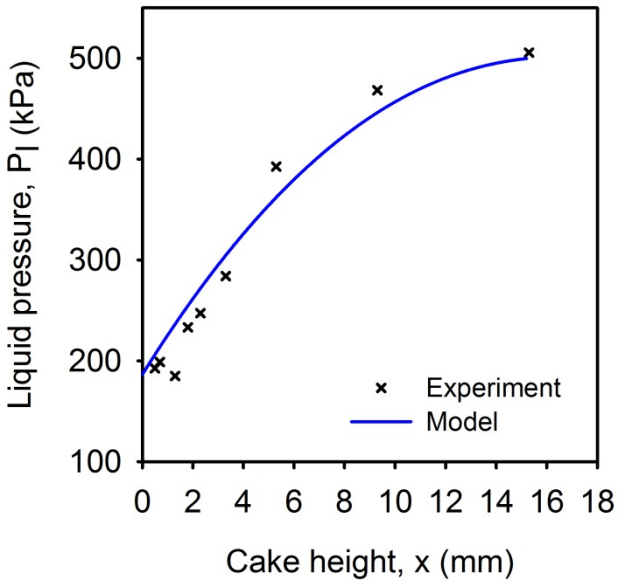

Figure 56: Predicted liquid pressure profile, talc at 500 kPa, 100s.

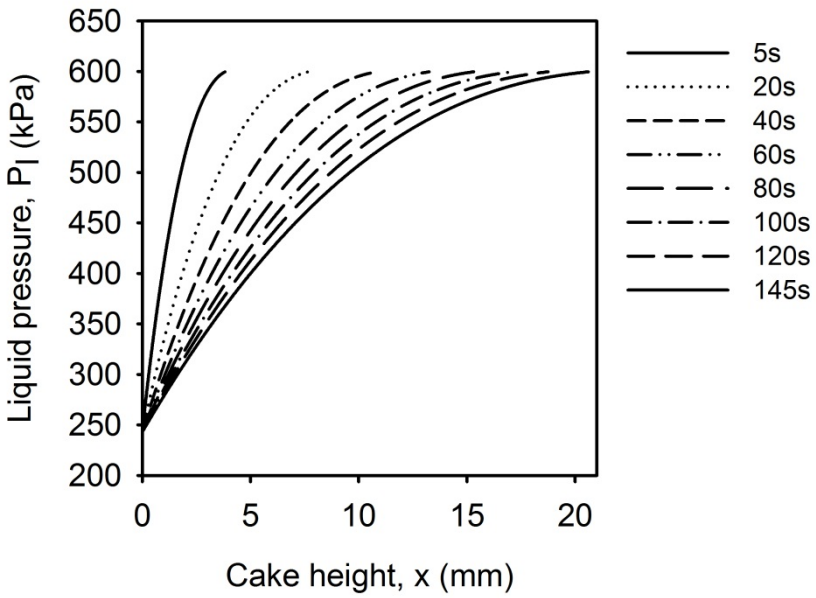

Figure 57: Predicted liquid pressure profile, talc at 600 kPa.

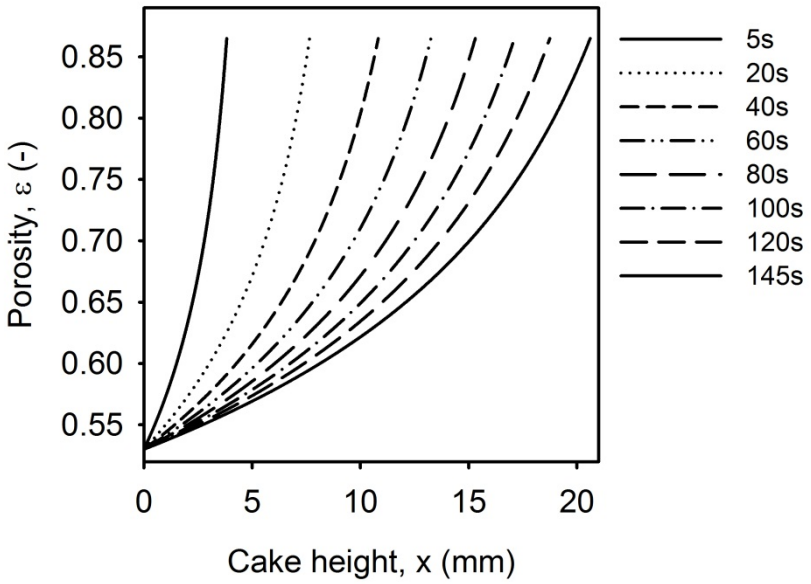

Figure 58: Predicted porosity profile, talc at 600 kPa.

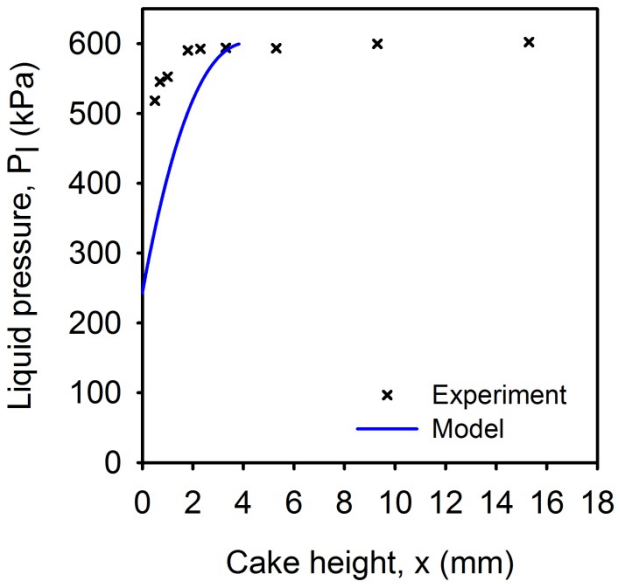

Figure 59: Predicted liquid pressure profile, talc at 600 kPa, 5s.

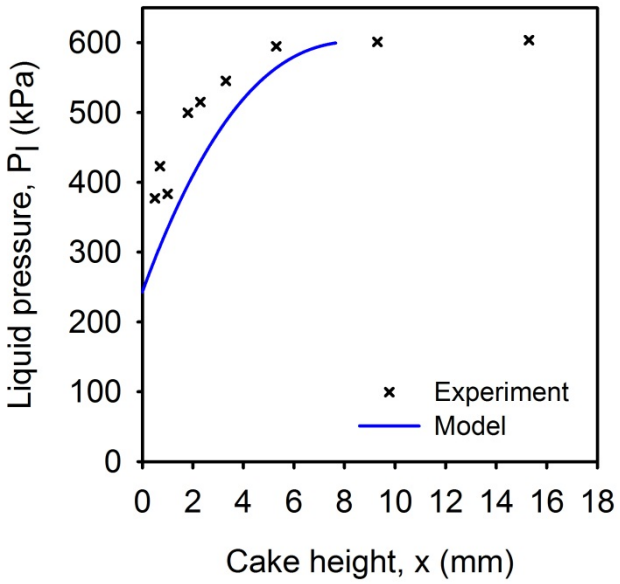

Figure 60: Predicted liquid pressure profile, talc at 600 kPa, 20s.

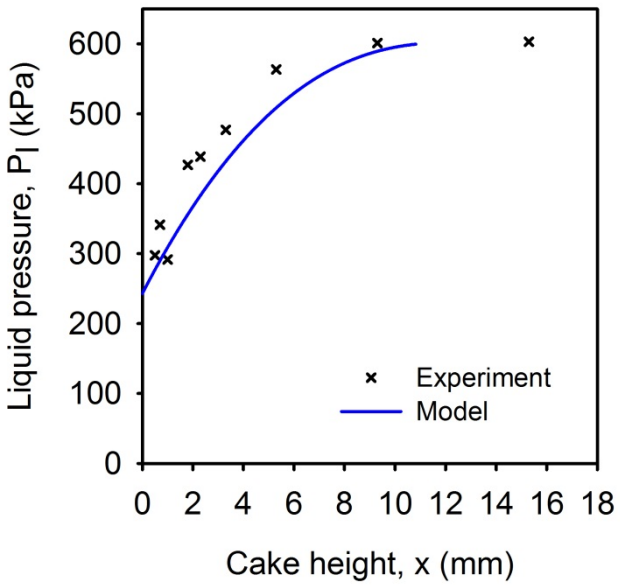

Figure 61: Predicted liquid pressure profile, talc at 600 kPa, 40s.

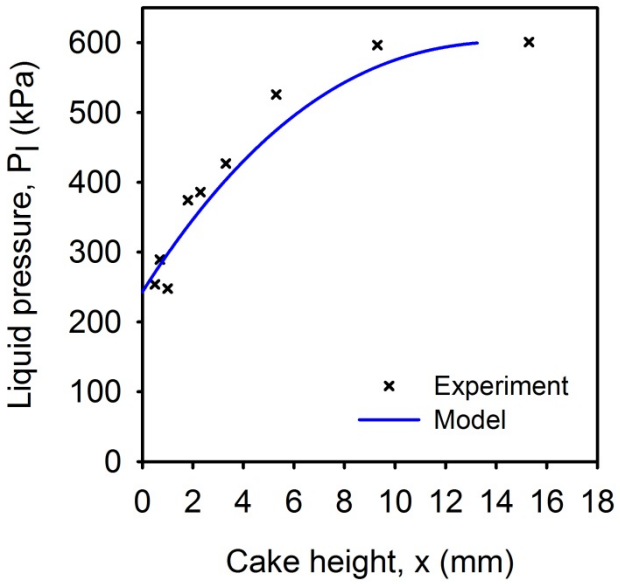

Figure 62: Predicted liquid pressure profile, talc at 600 kPa, 60s.

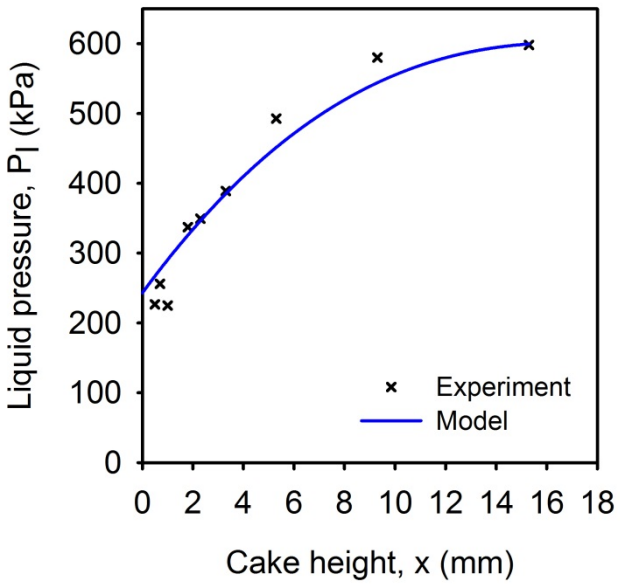

Figure 63: Predicted liquid pressure profile, talc at 600 kPa, 80s.

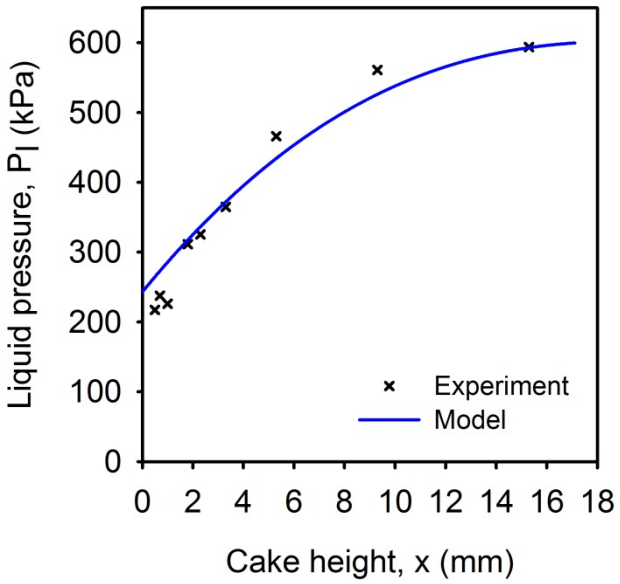

Figure 64: Predicted liquid pressure profile, talc at 600 kPa, 100s.

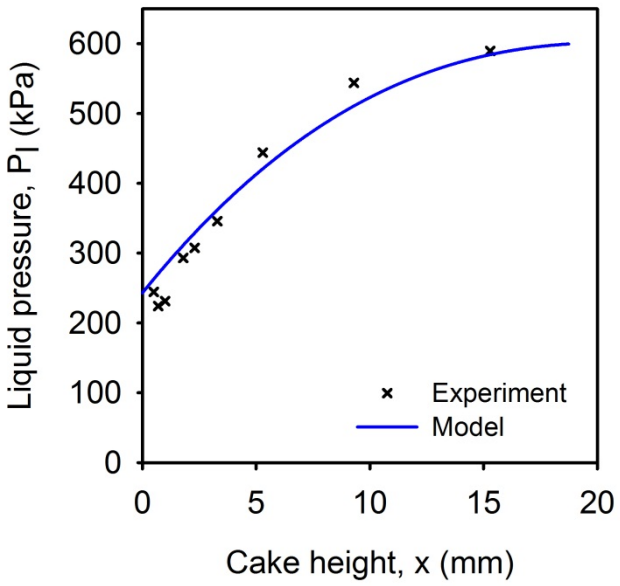

Figure 65: Predicted liquid pressure profile, talc at 600 kPa, 145s.

Appendix X: PREDICTED LIQUID PRESSURE AND POROSITY PROFILES, POROSITY VARYING AT THE MEDIUM

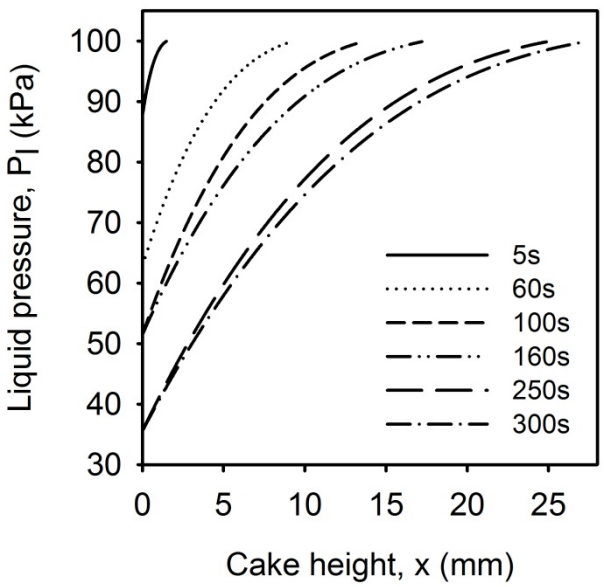

Figure 66: Predicted liquid pressure profile, talc at 100 kPa.

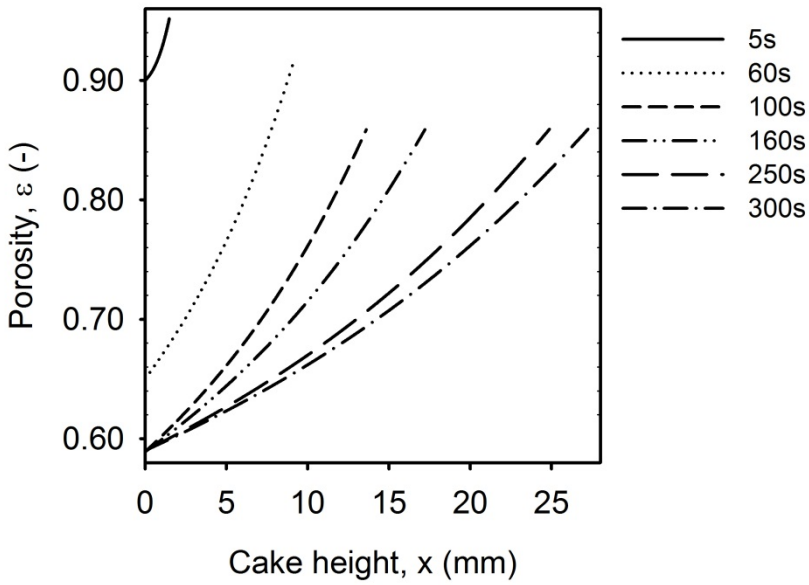

Figure 67: Predicted porosity profile, talc at 100 kPa.

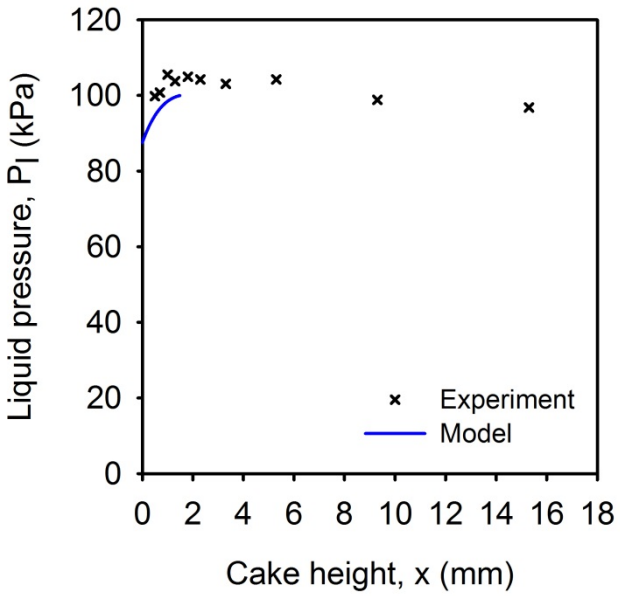

Figure 68: Predicted liquid pressure profile, talc at 100 kPa, 5s.

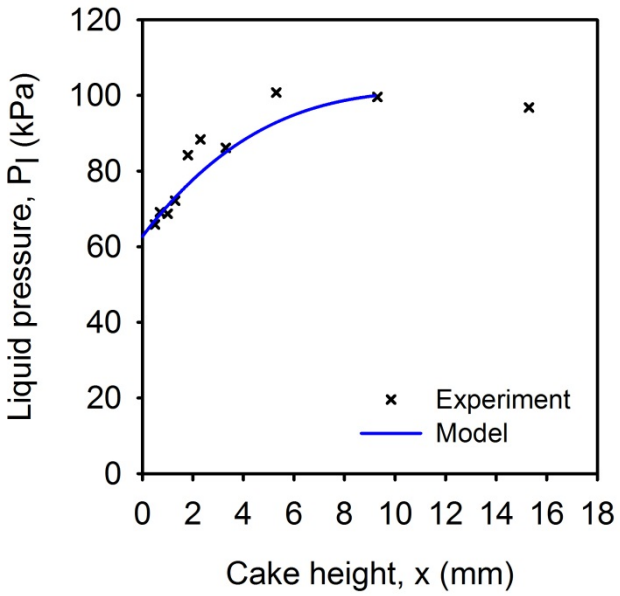

Figure 69: Predicted liquid pressure profile, talc at 100 kPa, 60s.

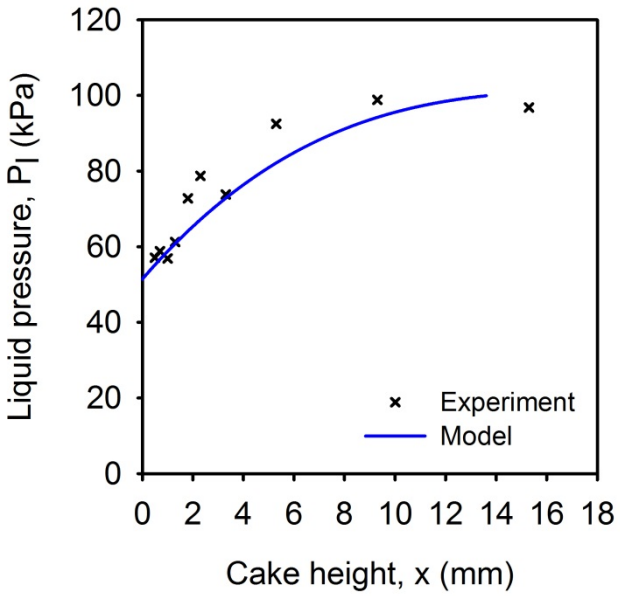

Figure 70: Predicted liquid pressure profile, talc at 100 kPa, 100s.

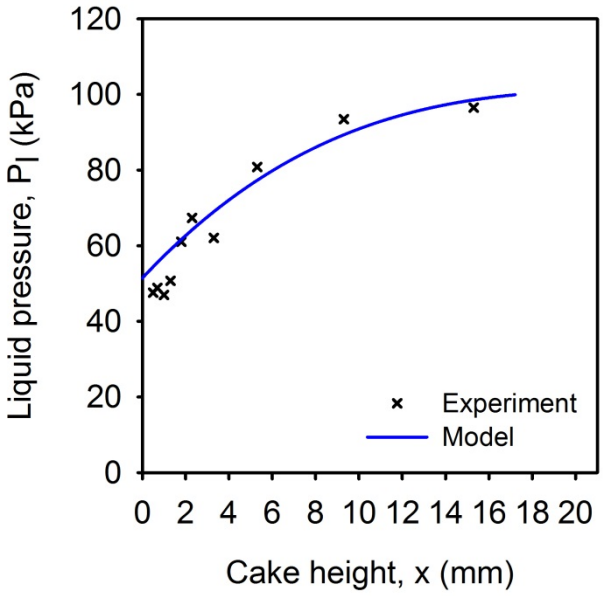

Figure 71: Predicted liquid pressure profile, talc at 100 kPa, 160s.

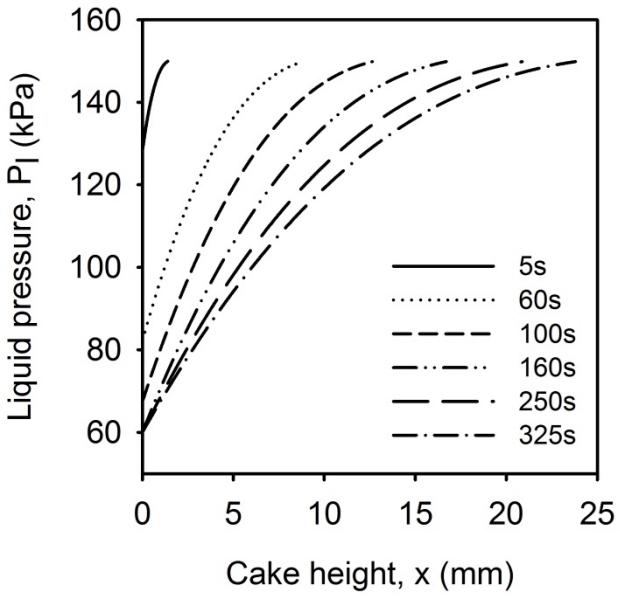

Figure 72: Predicted liquid pressure profile, talc at 150 kPa.

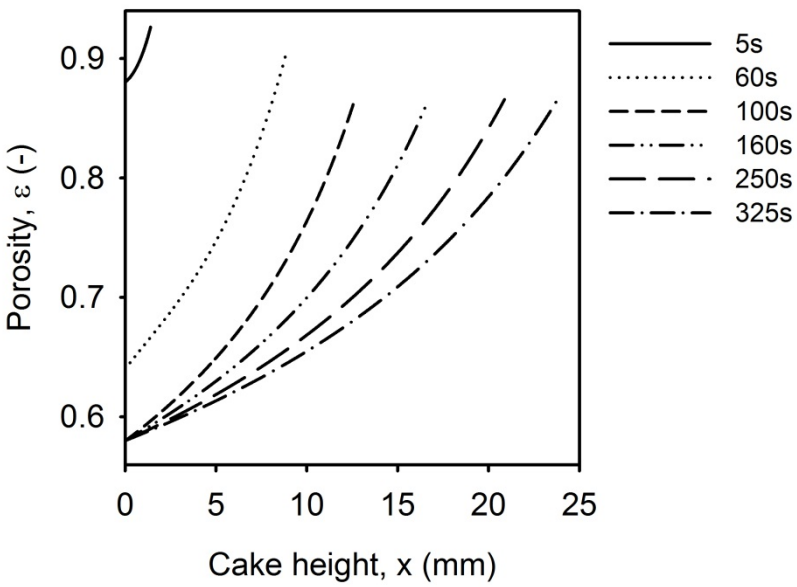

Figure 73: Predicted porosity profile, talc at 150 kPa.

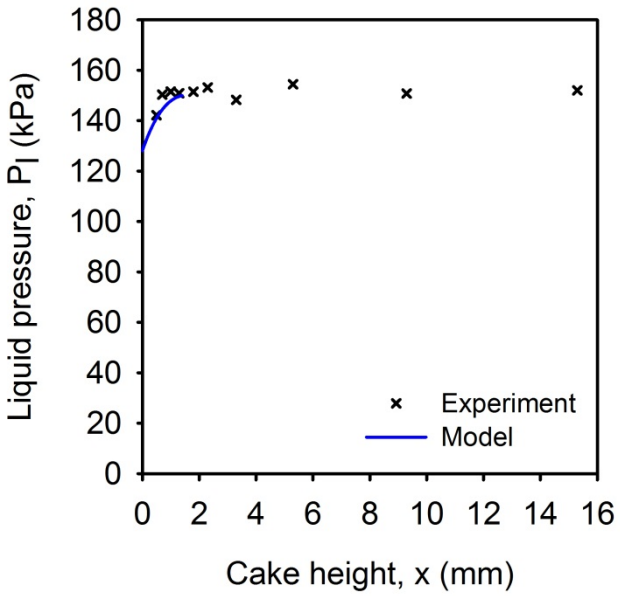

Figure 74: Predicted liquid pressure profile, talc at 150 kPa, 5s.

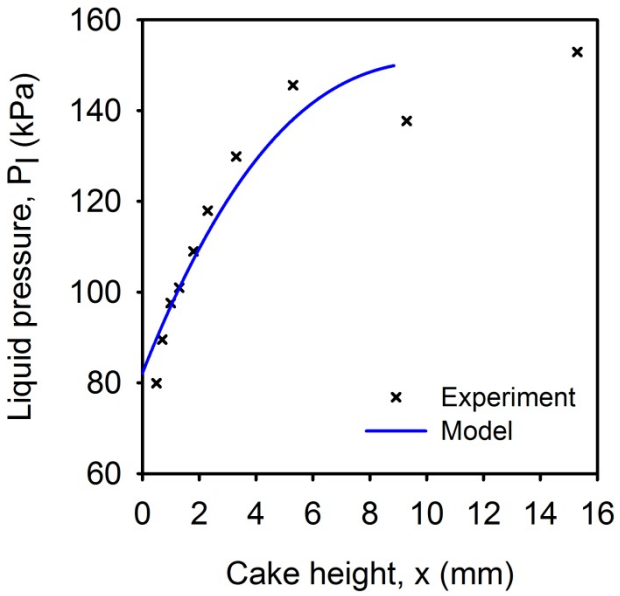

Figure 75: Predicted liquid pressure profile, talc at 150 kPa, 60s.

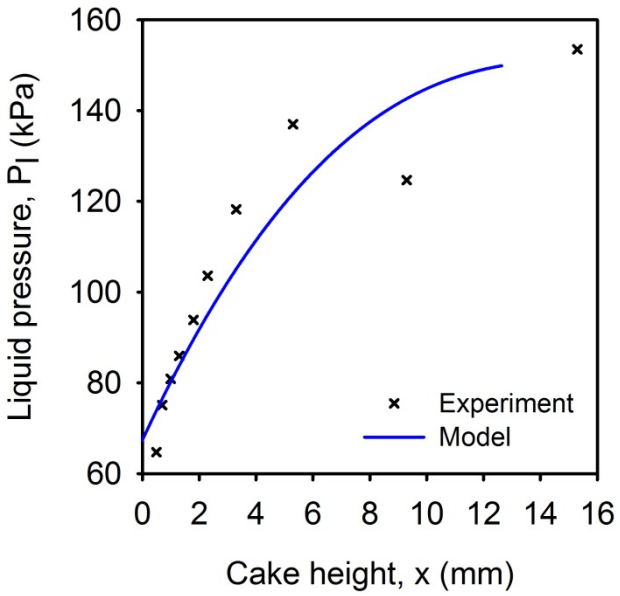

Figure 76: Predicted liquid pressure profile, talc at 100 kPa, 100s.

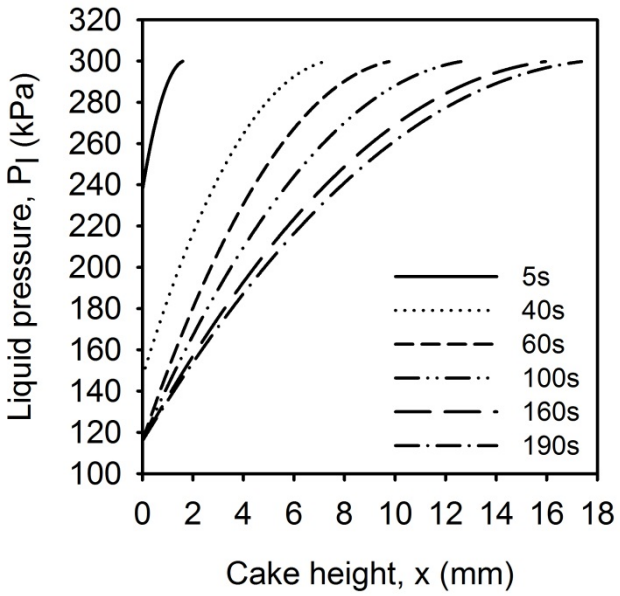

Figure 77: Predicted liquid pressure profile, talc at 300 kPa.

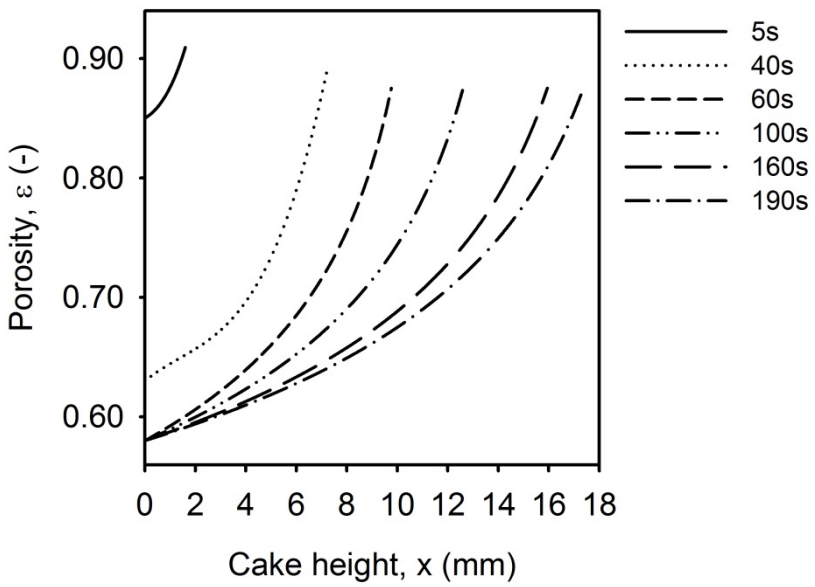

Figure 78: Predicted porosity profile, talc at 300 kPa.

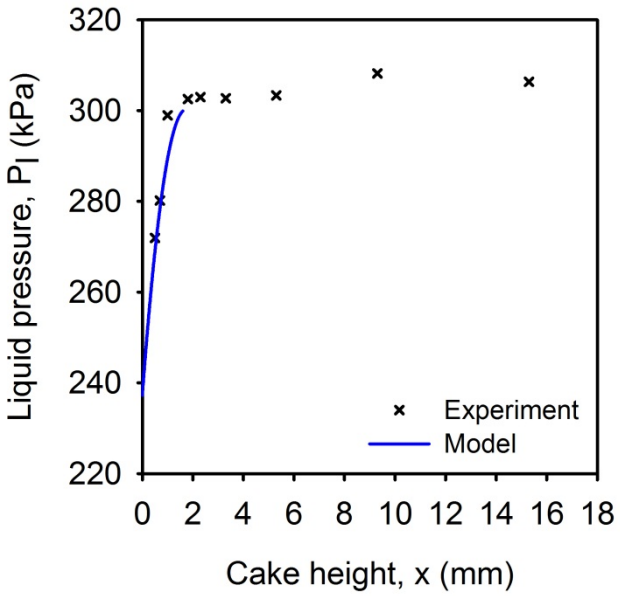

Figure 79: Predicted liquid pressure profile, talc at 300 kPa, 5s.

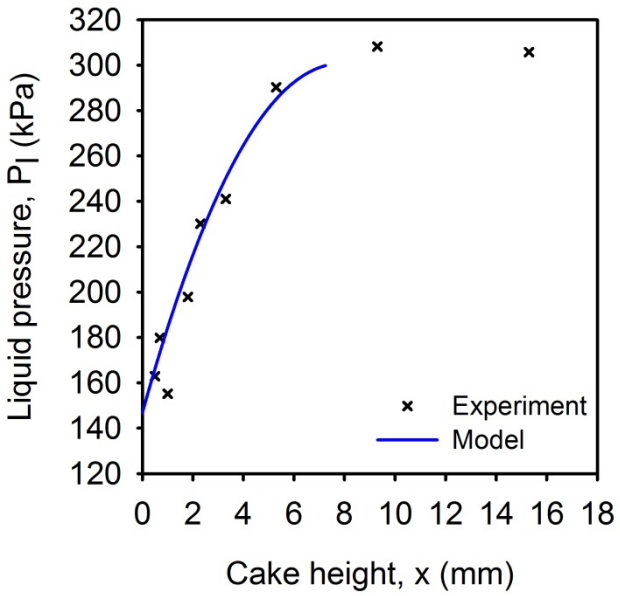

Figure 80: Predicted liquid pressure profile, talc at 300 kPa, 40s.

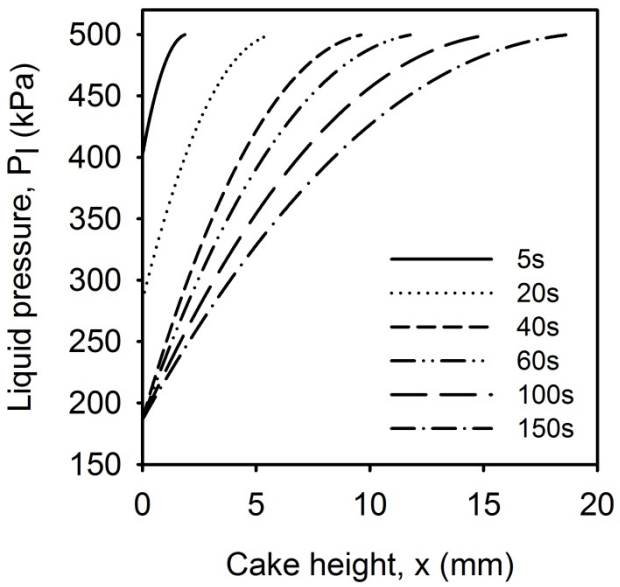

Figure 81: Predicted liquid pressure profile, talc at 500 kPa.

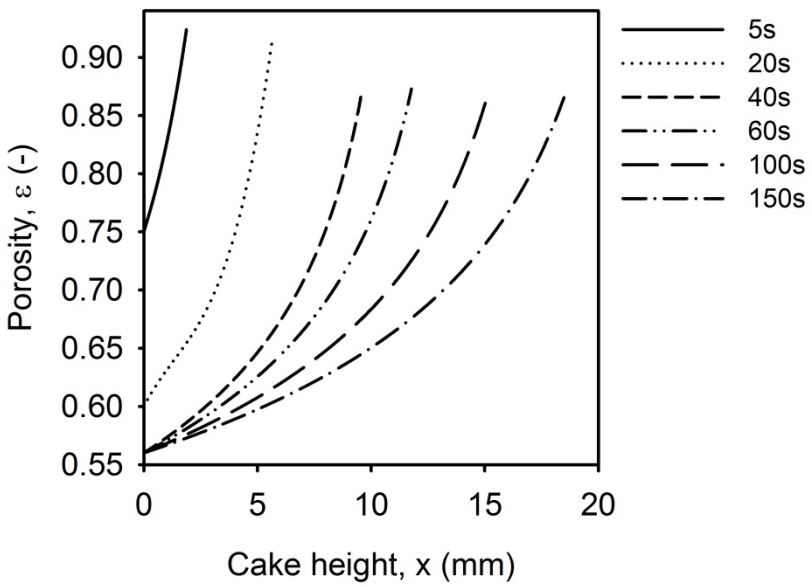

Figure 82: Predicted porosity profile, talc at 500 kPa.

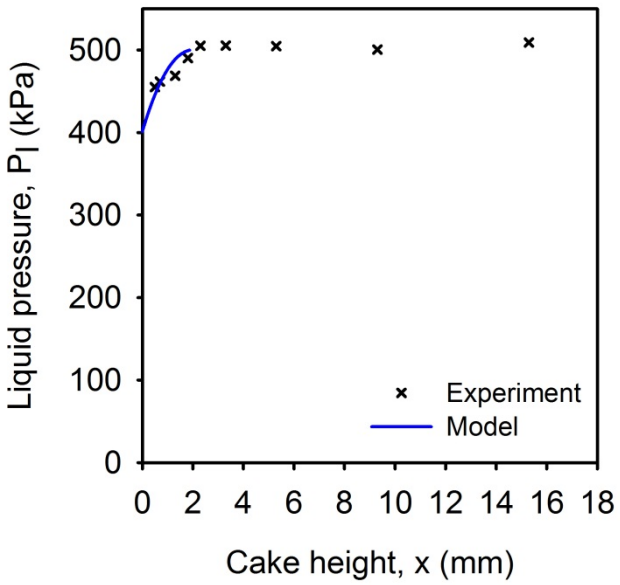

Figure 83: Predicted liquid pressure profile, talc at 500 kPa, 5s.

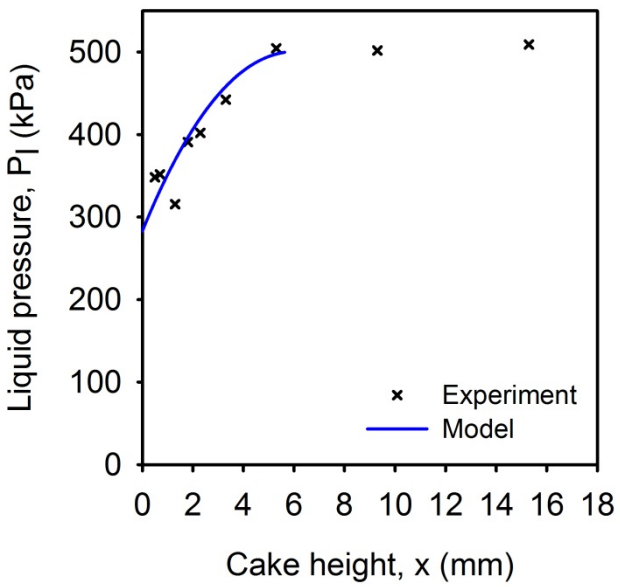

Figure 84: Predicted liquid pressure profile, talc at 500 kPa, 20s.

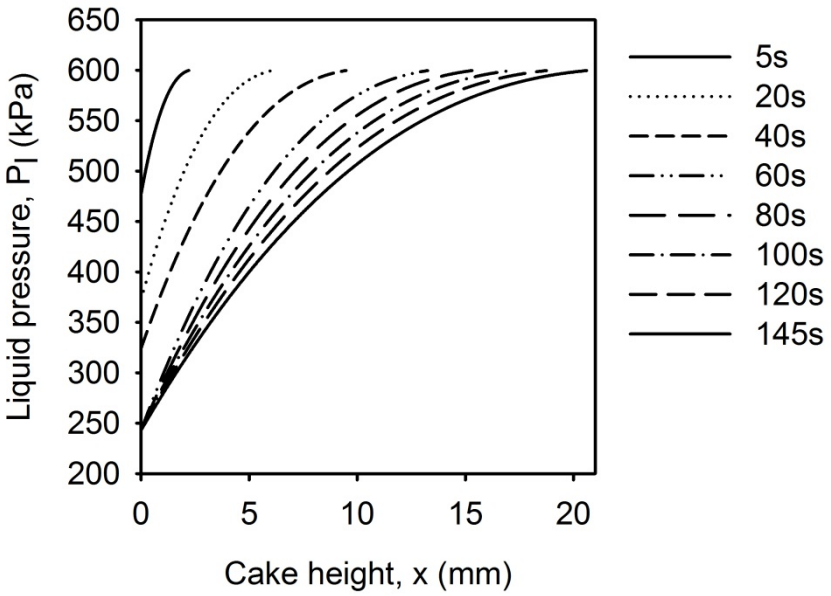

Figure 85: Predicted liquid pressure profile, talc at 600 kPa.

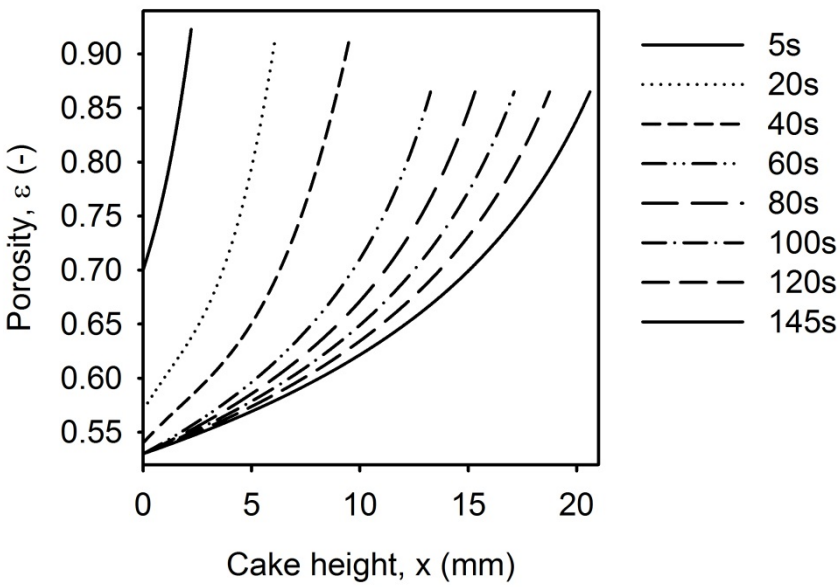

Figure 86: Predicted porosity profile, talc at 600 kPa.

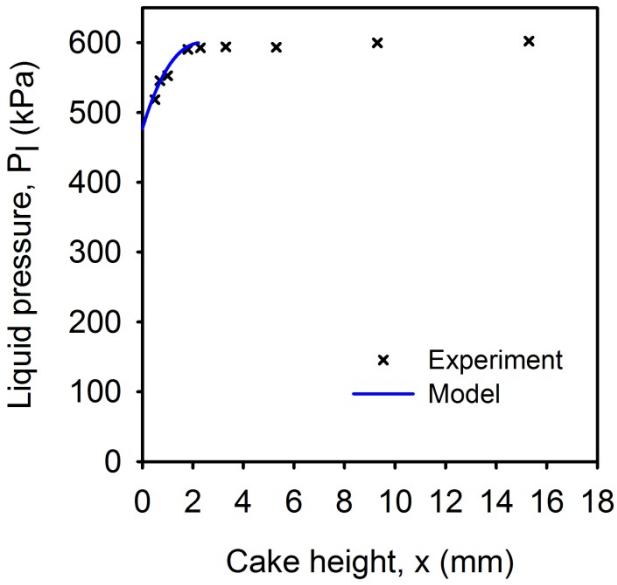

Figure 87: Predicted liquid pressure profile, talc at 600 kPa, 5s.

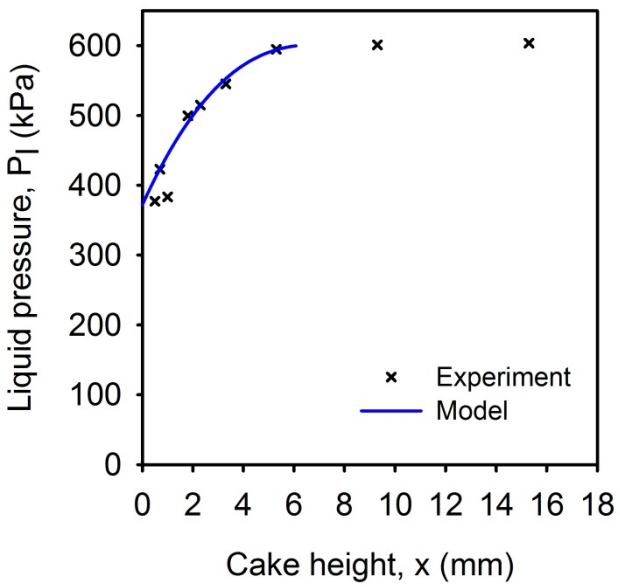

Figure 88: Predicted liquid pressure profile, talc at 600 kPa, 20s.

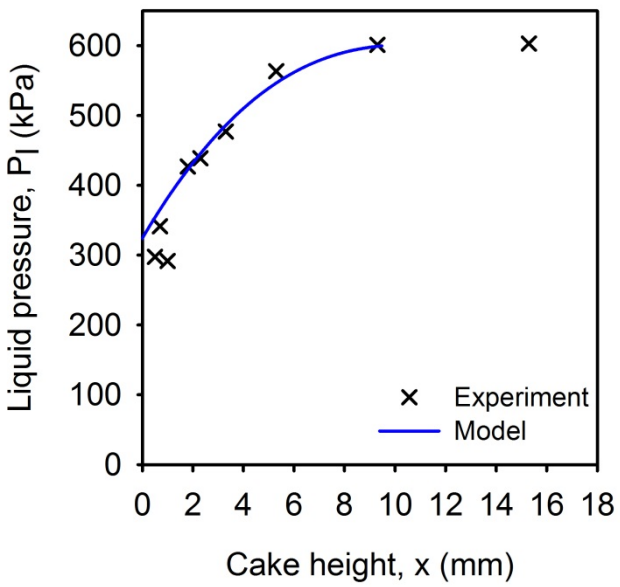

Figure 89: Predicted liquid pressure profile, talc at 600 kPa, 40s.

Appendix XI: PREDICTED CAKE HEIGHTS

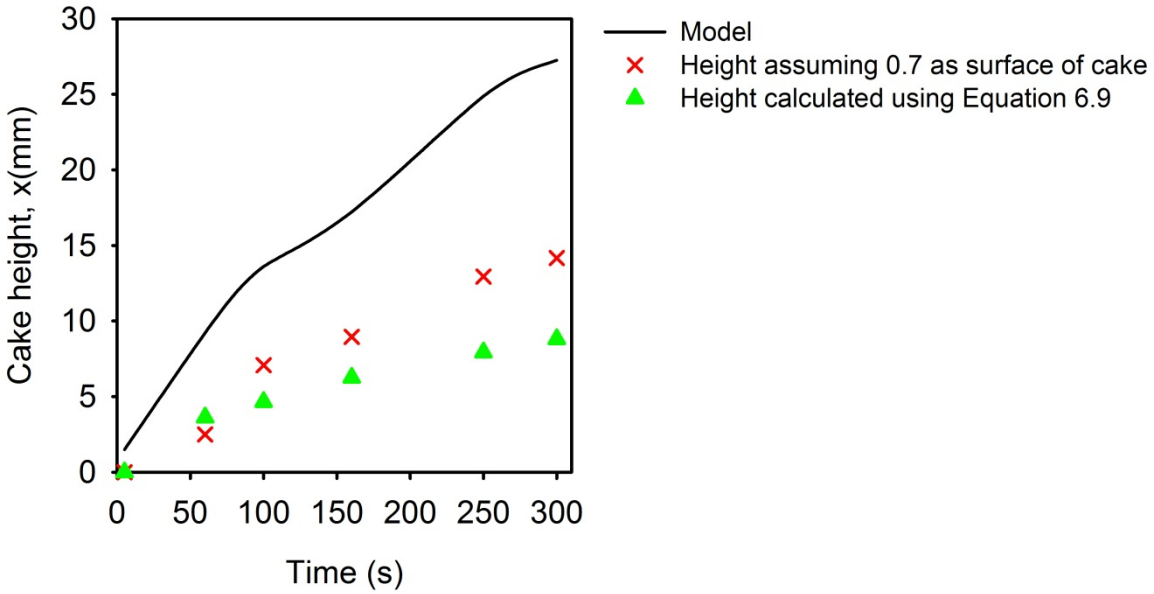

Figure 90: Predicted, theoretical and experimental cake heights with time, talc at 100 kPa.

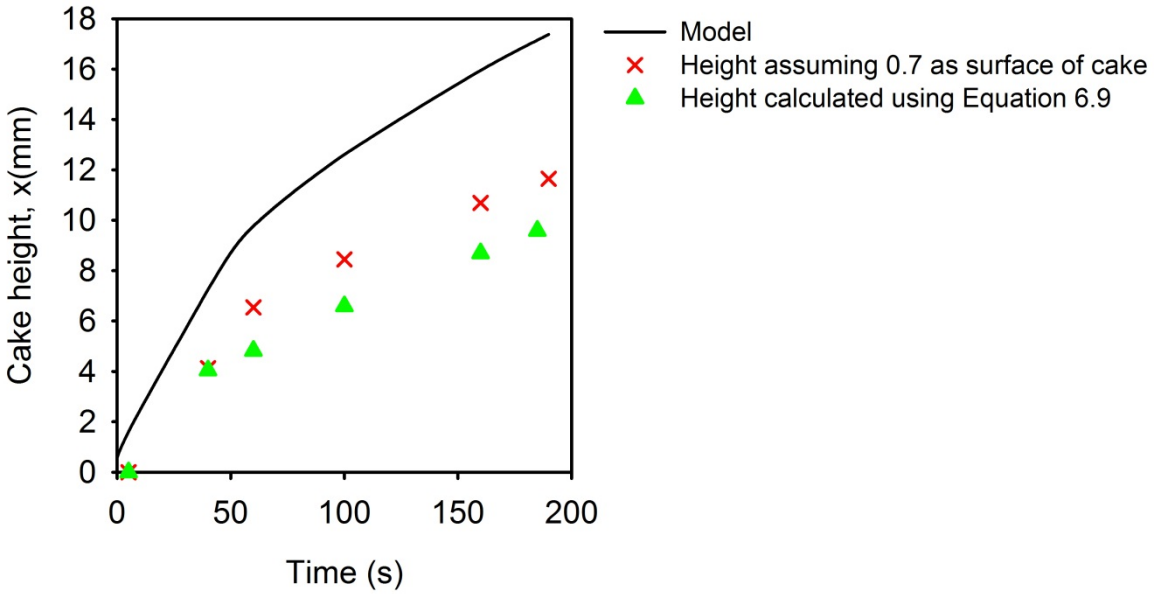

Figure 91: Predicted, theoretical and experimental cake heights with time, talc at 300 kPa.

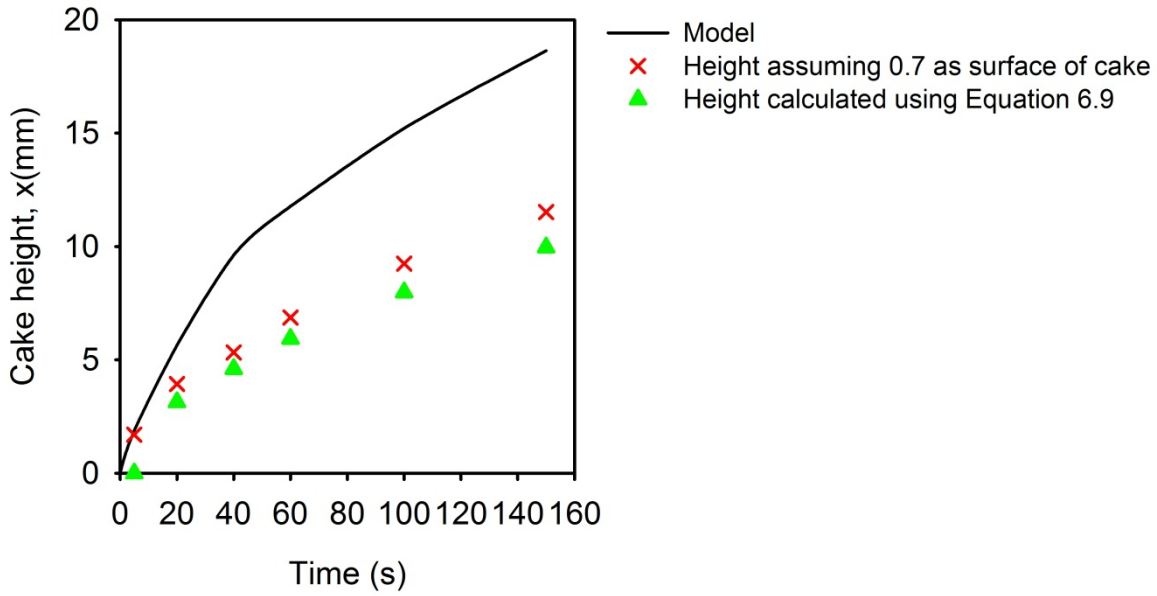

Figure 92: Predicted, theoretical and experimental cake heights with time, talc at 500 kPa.

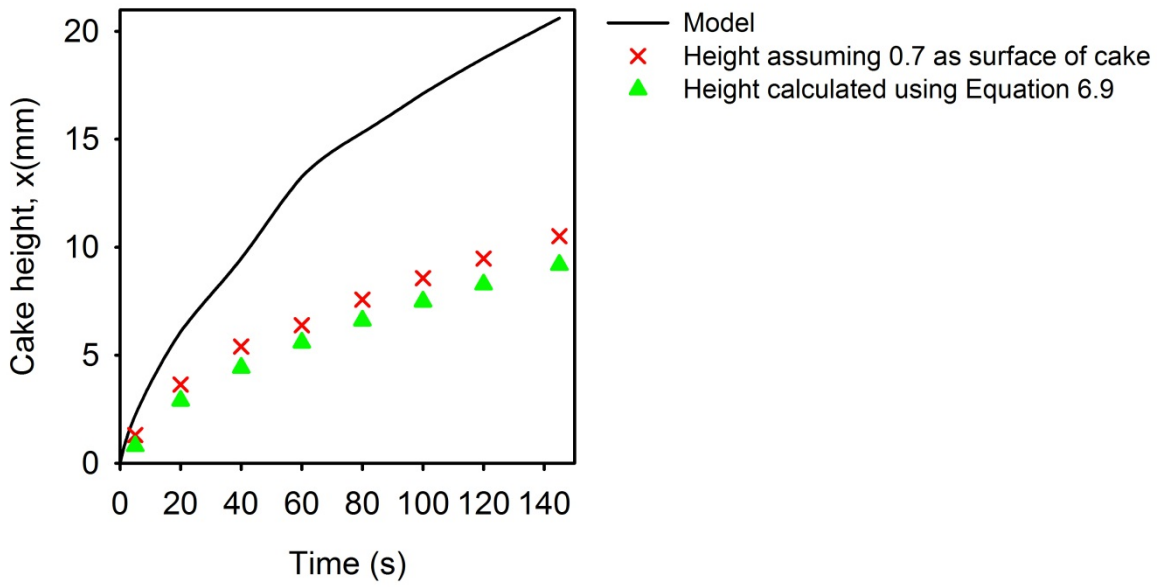

Figure 93: Predicted, theoretical and experimental cake heights with time, talc at 600 kPa